

# **Synthesis, Magnetism and Redox Properties of Verdazyl Radicals, Diradicals and Related Coordination Compounds**

by

Kevin James Anderson  
B.Sc, University of Guelph, 2003

A Dissertation Submitted in Partial Fulfillment  
of the Requirements for the Degree of

DOCTOR OF PHILOSOPHY

in the Department of Chemistry

© Kevin James Anderson, 2010  
University of Victoria

All rights reserved. This dissertation may not be reproduced in whole or in part, by photocopy or other means, without the permission of the author.

## **Supervisory Committee**

# **Synthesis, Magnetism and Redox Properties of Verdazyl Radicals, Diradicals and Related Coordination Compounds**

by

Kevin James Anderson  
B.Sc, University of Guelph, 2003

## **Supervisory Committee**

Dr. Robin G. Hicks, (Department of Chemistry)  
**Supervisor**

Dr. Lisa Rosenberg, (Department of Chemistry)  
**Departmental Member**

Dr. Peter Wan, (Department of Chemistry)  
**Departmental Member**

Dr. Terry Pearson, (Department of Biochemistry and Microbiology)  
**Outside Member**

**Supervisory Committee**

Dr. Robin G. Hicks, (Department of Chemistry)  
**Supervisor**

Dr. Lisa Rosenberg, (Department of Chemistry)  
**Departmental Member**

Dr. Peter Wan, (Department of Chemistry)  
**Departmental Member**

Dr. Terry Pearson, (Department of Biochemistry and Microbiology)  
**Outside Member**

**Abstract**

Coordination compounds involving stable radicals represent a promising avenue toward the design of new magnetic materials. In this respect, a series of new metal-verdazyl radical complexes has been prepared and their magnetic properties reported. These systems can be envisioned as model systems designed to help elucidate the fundamental electronic interactions between one paramagnetic metal ion and one verdazyl radical that lead to magnetic exchange.

A new chelating verdazyl diradical has also been prepared and fully characterised. The electronic ground state of this diradical species has been established through magnetic and variable temperature electron paramagnetic resonance (VT-EPR) studies. In an effort to expand the metal-radical model systems beyond simple 1:1 metal:radical complexes, this verdazyl diradical was employed as a ligand to prepare a succession of first row transition metal complexes. The magnetic properties of the resulting

coordination compounds have been studied in an effort to understand how the nature of the metal-diradical magnetic exchange changes with the metal used.

In addition to the wide-spread interest in the magnetic properties of stable organic radicals, there is a growing awareness of the redox properties of this class of compounds. Electrochemical and spectroelectrochemical techniques were utilised to probe the redox properties of a verdazyl diradical and a structurally similar verdazyl monoradical. Coordination compounds involving the redox-inert metal zinc were also prepared and their redox properties investigated. While the addition of zinc to the verdazyl diradical had no significant impact on the magnetic properties of the diradical, there is a distinct difference between the redox properties of the diradical itself and its zinc complex. Coordination to zinc also affected the redox properties of the verdazyl monoradical, although to a lesser extent than what was observed for the diradical.

## Table of Contents

<b>Supervisory Committee.....</b>	<b>ii</b>
<b>Abstract.....</b>	<b>iii</b>
<b>Table of Contents.....</b>	<b>v</b>
<b>List of Figures.....</b>	<b>ix</b>
<b>List of Schemes.....</b>	<b>xv</b>
<b>List of Tables.....</b>	<b>xvii</b>
<b>List of Numbered Compounds.....</b>	<b>xix</b>
<b>List of Abbreviations.....</b>	<b>xxvii</b>
<b>Acknowledgements.....</b>	<b>xxxii</b>
<b>Dedication.....</b>	<b>xxxiii</b>
<b>Chapter 1: Introduction and background.....</b>	<b>1</b>
1.1 Stable radicals.....	1
1.2 Stable radical coordination chemistry.....	3
1.2.1 Nitroxide coordination compounds.....	4
1.2.2 Phenoxyl radical coordination compounds.....	9
1.2.3 Thiazyl radical coordination chemistry.....	13
1.2.4 Aminyl radical coordination compounds.....	16
1.2.5 Metal-verdazyl complexes.....	18
1.3 Thesis objectives.....	23
<b>Chapter 2: Structural and magnetic properties of a series of coordination compounds based on verdazyl radicals and diradicals.....</b>	<b>27</b>
2.1 New magnetic materials.....	27
2.2 The metal-radical approach to magnetic materials.....	28
2.3 Metal-radical complexes as model systems in magnetic materials design.....	31

2.3.1 Verdazyl radical systems as model complexes for magnetic materials design.....	33
2.3.2 General syntheses of 6-oxoverdazyl radicals.....	34
2.4 1:1 metal-verdazyl complexes.....	37
2.4.1 Synthesis and characterisation of 1:1 metal-verdazyl complexes.....	37
2.4.2 Structural characterisation of nickel-verdazyl complex <b>2.14</b> .....	39
2.4.3 Magnetic properties of nickel-verdazyl complex <b>2.14</b> .....	41
2.4.4 Structural characterisation of cobalt-verdazyl complex <b>2.15</b> .....	43
2.4.5 Magnetic properties of <b>2.15</b> .....	45
2.4.6 Structural characterisation of manganese-verdazyl complex <b>2.16</b> .....	46
2.5 Synthesis and magnetic characterisation of a verdazyl-based diradical and associated coordination compounds.....	49
2.5.1 Synthesis of verdazyl diradical <b>2.18</b> .....	49
2.5.2 Structural characterisation of diradical <b>2.18</b> .....	50
2.5.3 Solution-phase electronic properties of diradical <b>2.18</b> .....	53
2.5.4 Magnetic properties of diradical <b>2.18</b> .....	57
2.6 Coordination complexes of diradical <b>2.18</b> .....	62
2.6.1 Structural characterisation of zinc-diradical complex <b>2.19</b> .....	64
2.6.2 Magnetic properties of <b>2.19</b> .....	66
2.6.3 Structural characterisation of manganese-diradical complex <b>2.20</b> .....	68
2.6.4 Magnetic properties of <b>2.20</b> .....	69
2.6.5 Structural characterisation of iron-diradical complex <b>2.21</b> .....	73
2.6.6 Magnetic properties of <b>2.21</b> .....	74
2.6.7 Structural characterisation of cobalt-diradical complex <b>2.22</b> .....	76
2.6.8 Magnetic properties of <b>2.22</b> .....	77
2.6.9 Structural characterisation of nickel-diradical complex <b>2.23</b> .....	79
2.6.10 Magnetic properties of <b>2.23</b> .....	81
2.7 Synthesis and characterisation of other coordination compounds involving <b>2.18</b> ..	83
2.7.1 Synthesis and characterisation of chromium complex <b>2.28</b> .....	83
2.7.2 Magnetic properties of chromium complex <b>2.28b</b> .....	88
2.7.3 Synthesis and characterisation of copper complex <b>2.29</b> .....	90
2.8 Summary.....	94
2.9 Experimental.....	97
2.9.1 General considerations.....	97
2.9.2 Synthesis and characterisation of <b>2.13M(hfac)<sub>2</sub></b> coordination compounds.....	98

2.9.3 Synthesis and characterisation of diradical <b>2.18</b> .....	100
2.9.4 Synthesis and characterisation of <b>2.18</b> MCl <sub>2</sub> coordination compounds.....	102
<b>Chapter 3: Redox properties of verdazyl radicals, diradicals and derived coordination compounds</b> .....	<b>107</b>
3.1 Redox properties of stable radicals and their coordination compounds.....	107
3.1.1 Redox-based applications of stable radicals.....	107
3.1.2 Stable radicals as redox-active ligands.....	110
3.2 Redox properties of verdazyl radicals and coordination compounds.....	111
3.3 Synthesis of verdazyl radical <b>3.9</b> .....	113
3.4 Structural characterisation of verdazyl radical <b>3.9</b> .....	114
3.5 Synthesis of zinc complex <b>3.10</b> .....	115
3.6 Structural characterisation of zinc complex <b>3.10</b> .....	116
3.7 Solution-phase electronic properties of <b>3.9</b> and <b>3.10</b> .....	117
3.8 Redox properties of verdazyl radical <b>3.9</b> and zinc complex <b>3.10</b> .....	120
3.9 Redox properties of diradical <b>2.18</b> and zinc complex <b>2.19</b> .....	123
3.10 Reduction of zinc diradical complex <b>2.19</b> .....	127
3.11 Oxidation of zinc diradical complex <b>2.19</b> .....	128
3.12 Redox-induced structural changes in coordination compounds.....	131
3.13 Potential-dependent spectroscopy of verdazyl ligands and metal complexes....	135
3.13.1 Potential-dependent spectroscopy of radical <b>3.9</b> and zinc complex <b>3.10</b> ....	135
3.13.2 Chemical titration of monoradical <b>3.9</b> .....	136
3.13.3 Spectroelectrochemical studies of diradical <b>2.18</b> and zinc complex <b>2.19</b> ...	137
3.14 Chemical oxidations of verdazyl radical and diradical compounds.....	138
3.14.1 Synthetic efforts towards verdazyl-derived cationic and dicationic species.....	139
3.14.2 Electronic nature of amide moiety in 6-oxoverdazyl radical species.....	140
3.14.3 Infrared spectra of verdazyl monoradical and monocationic species.....	141
3.14.4 Infrared spectra of verdazyl diradical and dicationic species.....	142

3.15 Summary.....	144
3.16 Experimental.....	146
3.16.1 General Electrochemical Considerations.....	146
3.16.2 Synthesis of verdazyl <b>3.9</b> and zinc complex <b>3.10</b> .....	147
3.16.3 Chemical oxidations of <b>2.18</b> , <b>2.19</b> , <b>3.9</b> and <b>3.10</b> .....	149
<b>Chapter 4: Conclusions and future work.....</b>	<b>152</b>
<b>References.....</b>	<b>159</b>
<b>Appendix A: <sup>1</sup>H NMR Spectrum of tetrazane precursor of 3.9.....</b>	<b>176</b>
<b>Appendix B: Crystallographic parameters.....</b>	<b>177</b>
<b>Appendix C: Complete list of bond lengths and angles.....</b>	<b>181</b>
<b>Appendix D: Raw magnetic data and derivation of magnetic models.....</b>	<b>233</b>



## List of Figures

Figure 2.1: Schematic depiction of a coordination network composed of paramagnetic metals (circles) and organic radical ligands (rectangles) with ferromagnetically coupled magnetic moments.....	29
Figure 2.2: Hypothetical coordination network where antiferromagnetic interactions between metal centres (circles) and radical ligands (rectangles) with unequal magnetic moments leads to ferrimagnetism.....	30
Figure 2.3: Schematic representation of potential model systems to investigate (a) metal-radical coupling, (b) metal-radical-metal coupling and (c) radical-metal-radical coupling.....	32
Figure 2.4: Electronic spectra of radical <b>2.13</b> and coordination compounds <b>2.14</b> and <b>2.15</b> in dichloromethane.....	39
Figure 2.5: Molecular structure of <b>2.14</b> . Thermal ellipsoids displayed at 50% probability level. Fluorine and hydrogen atoms removed for clarity.....	41
Figure 2.6: $\chi T$ vs. $T$ for <b>2.14</b> between 300 and 2 K. Experimental data ( $\circ$ ) and calculated model fit (—).....	42
Figure 2.7: Molecular structure of <b>2.15</b> . Thermal ellipsoids displayed at 50% probability level. Fluorine and hydrogen atoms removed for clarity.....	44
Figure 2.8: $\chi T$ vs. $T$ for <b>2.15</b> between 300 and 2 K. Experimental data ( $\circ$ ) and calculated model fit (—).....	45
Figure 2.9: Molecular structure of manganese complex <b>2.16</b> . Thermal ellipsoids displayed at the 50% probability level. Fluorine and hydrogen atoms removed for clarity. Atoms associated with <i>n</i> -pentane and <i>o</i> -hydroquinone have also been removed.....	47
Figure 2.10: Infrared spectra of (a) tetrazane <b>2.17</b> and (b) diradical <b>2.18</b> recorded as pressed KBr disks with air background. Carbonyl band in both (a) and (b) indicated by ‡; N-H band in (a) indicated by †.....	51
Figure 2.11: Face-on (top) and edge-on (bottom) view of the molecular structure of <b>2.18</b> . Thermal ellipsoids displayed at 50% probability level. Hydrogen atoms removed for clarity.....	52
Figure 2.12: Partial view of the crystal packing of <b>2.18</b> showing close contact points between selected atoms with non-zero spin density.....	53

Figure 2.13: Experimental (solid line) and simulated (dashed red line) X-band EPR spectra of diradical <b>2.18</b> in frozen toluene (77 K). Highlighted (green box) signal in experimental spectrum is due to $S = \frac{1}{2}$ impurity in the sample.....	55
Figure 2.14: Curie plot of the intensity of $\Delta m_s = 2$ signal for <b>2.18</b> between 4.5 and 90 K. Inset: $\Delta m_s$ signal centred at 1667 G.....	56
Figure 2.15: UV-Vis spectra of monoradical <b>2.13</b> (dashed line) and diradical <b>2.18</b> (solid line) in dichloromethane.....	57
Figure 2.16: $\chi T$ vs. $T$ data ( $\circ$ ) and model fit (—) of diradical <b>2.18</b> from 300 – 2 K. Diamagnetic corrections made using the slope method.....	58
Figure 2.17: $\chi T$ vs. $T$ data ( $\circ$ ) and model fit (—) of diradical <b>2.18</b> from 300 – 2 K. Diamagnetic corrections made using Pascal's constants.....	60
Figure 2.18: The presence of a radical polarises the $\pi$ -electrons in an aromatic ring (a). This spin polarisation mechanism favours ferromagnetic coupling in <i>meta</i> -substituted diradicals (b) and antiferromagnetic exchange in a <i>para</i> -substituted diradicals (c).....	62
Figure 2.19: UV-Vis spectra of diradical <b>2.18</b> and related coordination compounds <b>2.19</b> – <b>2.23</b> in dichloromethane.....	63
Figure 2.20: Molecular structure of zinc-diradical complex <b>2.19</b> . Thermal ellipsoids displayed at 50% probability level. Hydrogen atoms removed for clarity.....	65
Figure 2.21: $\chi T$ vs. $T$ data ( $\circ$ ) and model fit (—) of complex <b>2.19</b> from 300 – 2 K.....	67
Figure 2.22: Molecular structure of manganese-diradical complex <b>2.20</b> . Thermal ellipsoids displayed at 50% probability level. Hydrogen atoms removed for clarity.....	69
Figure 2.23: $\chi T$ vs. $T$ data ( $\circ$ ) and model fit (—) of complex <b>2.20</b> from 300 – 2 K.....	70
Figure 2.24: Simplified antiferromagnetic coupling relationship between $S = 5/2$ $Mn^{2+}$ ion and two $S = \frac{1}{2}$ verdazyl (Vd) radicals.....	71
Figure 2.25: Metal-based $d$ -orbitals in order of relative energies in trigonal bipyramidal coordination geometry. $p$ -Orbitals represent $\pi$ -SOMO of verdazyl radicals to show relationship with $d$ -orbitals (6-oxoverdazyl rings omitted in some cases for clarity).....	73
Figure 2.26: Molecular structure of iron-diradical complex <b>2.21</b> . Thermal ellipsoids displayed at 50% probability level. Hydrogen atoms removed for clarity.....	74
Figure 2.27: $\chi T$ vs. $T$ data ( $\circ$ ) and model fit (—) of complex <b>2.21</b> from 300 – 2 K.....	75

Figure 2.28: Molecular structure of cobalt-diradical complex <b>2.22</b> . Thermal ellipsoids displayed at 50% probability level.....	77
Figure 2.29: $\chi T$ vs. T data ( $\circ$ ) and model fit (—) of complex <b>2.22</b> from 2 – 300 K.....	78
Figure 2.30: Molecular structure of nickel-diradical complex <b>2.23</b> . Thermal ellipsoids displayed at 50% probability level. Hydrogen atoms removed for clarity.....	80
Figure 2.31: $\chi T$ vs. T data ( $\circ$ ) and model fit (—) for complex <b>2.23</b> from 2 – 300 K.....	82
Figure 2.32: Molecular structure of <b>2.28b</b> . Thermal ellipsoids displayed at 50% probability level. Calculated hydrogen atoms removed for clarity.....	85
Figure 2.33: Infrared spectra of (a) diradical <b>2.18</b> and (b) chromium complex <b>2.28b</b> recorded as pressed KBr disks with air background. N-H band in <b>2.28b</b> indicated by $\dagger$ .....	87
Figure 2.34: UV-Vis spectra of diradical <b>2.18</b> (dashed line) and chromium complex <b>2.28b</b> (solid line) in dichloromethane.....	88
Figure 2.35: $\chi T$ vs. T data ( $\circ$ ) and model fit (—) of complex <b>2.28b</b> from 2 – 300 K.....	89
Figure 2.36: Molecular structure of <b>2.29</b> showing structure of repeat unit (top) and extended structure (bottom). Thermal ellipsoids displayed at 50% probability level. Hydrogen atoms removed for clarity.....	92
Figure 2.37: UV-Vis spectra of diradical <b>2.18</b> (dashed line) and copper complex <b>2.29</b> (solid line) in dichloromethane.....	94
Figure 3.1: Molecular structure of <b>3.9</b> . Thermal ellipsoids displayed at 50% probability level. Hydrogen atoms removed for clarity.....	114
Figure 3.2: Molecular structure of <b>3.10</b> . Thermal ellipsoids displayed at 50% probability level. Hydrogen atoms removed for clarity.....	117
Figure 3.3: UV-Vis spectra of radical <b>3.9</b> (black) and zinc complex <b>3.10</b> (red) in dichloromethane.....	118
Figure 3.4: Experimental (black) and simulated (red) X-band EPR spectra of <b>3.9</b> ( $5.0 \times 10^{-4}$ M in toluene).....	119
Figure 3.5: Experimental (black) and simulated (red) X-band EPR spectra of <b>3.10</b> ( $9.5 \times 10^{-6}$ M in $\text{CH}_2\text{Cl}_2$ ).....	120
Figure 3.6: Cyclic voltammograms of <b>3.9</b> (a, 1.1 mM) and <b>3.10</b> (b, 1.0 mM). Both CVs recorded in $\text{CH}_3\text{CN}$ with 0.1 M $\text{Bu}_4\text{NBF}_4$ as supporting electrolyte.....	121

Figure 3.7: Cyclic voltammograms of (a) <b>2.18</b> and (b) <b>2.19</b> . Both CVs recorded on 1.0 mM solutions in CH <sub>3</sub> CN with 0.1 M Bu <sub>4</sub> NBF <sub>4</sub> as supporting electrolyte.....	124
Figure 3.8: Osteryoung square wave voltammograms showing reduction (left) and oxidation (right) of <b>2.18</b> (0.997 mM solution in CH <sub>3</sub> CN with 0.1 M Bu <sub>4</sub> NBF <sub>4</sub> as supporting electrolyte). Peak centred at 160 mV is due to ocatmethylferrocene (added as internal standard, 0.972 mM).....	126
Figure 3.9: Cyclic voltammograms of reduction process for <b>2.19</b> (1.0 mM solution in CH <sub>3</sub> CN with 0.1 M Bu <sub>4</sub> NBF <sub>4</sub> as supporting electrolyte) showing scan-rate dependence (left) and multiple scan reproducibility at 100 mV/s (right).....	127
Figure 3.10: Cyclic voltammogram of <b>2.19</b> (1.0 mM solution in CH <sub>3</sub> CN with 0.1 M Bu <sub>4</sub> NBF <sub>4</sub> as supporting electrolyte) showing a reversible one-electron reduction at -0.74 V (solid line) and a second irreversible reduction at more negative potential (dashed line).....	128
Figure 3.11: Cyclic voltammograms of oxidation process for <b>2.19</b> (1.0 mM solution in CH <sub>3</sub> CN with 0.1 M Bu <sub>4</sub> NBF <sub>4</sub> as supporting electrolyte) showing scan-rate dependence (left) and multiple scan reproducibility at 100 mV/s (right).....	129
Figure 3.12: Potential-dependent UV-Vis spectra for <b>3.9</b> (left) and <b>3.10</b> (right). Successive coloured lines correspond to spectra recorded at different potentials. Potentials listed represent actual applied potential and are not corrected to the Fc/Fc <sup>+</sup> redox couple.....	136
Figure 3.13: UV-Vis spectra for the chemical titration of <b>3.9</b> with NOPF <sub>6</sub> as the oxidant.....	137
Figure 3.14: Potential-dependent UV-Vis spectra for <b>2.18</b> (left) and <b>2.19</b> (right). Successive coloured lines correspond to spectra recorded at different potentials. Potentials listed represent actual applied potential and are not corrected to the Fc/Fc <sup>+</sup> redox couple.....	138
Figure A-1: Raw <sup>1</sup> H NMR Spectrum of tetrazane precursor of <b>3.9</b> .....	176
Figure C-1: ORTEP view of <b>2.14</b> . Thermal ellipsoids displayed at 50% probability level. Hydrogen atoms removed for clarity.....	181
Figure C-2: ORTEP view of <b>2.15</b> . Thermal ellipsoids displayed at 50% probability level. Hydrogen atoms removed for clarity.....	187
Figure C-3: ORTEP view of <b>2.16</b> . Thermal ellipsoids displayed at 50% probability level. Hydrogen atoms removed for clarity.....	192

Figure C-4: ORTEP view of <b>2.18</b> . Thermal ellipsoids displayed at 50% probability level. Hydrogen atoms removed for clarity.....	199
Figure C-5: ORTEP view of <b>2.19</b> . Thermal ellipsoids displayed at 20% probability level. Hydrogen atoms removed for clarity.....	202
Figure C-6: ORTEP view of <b>2.20</b> . Thermal ellipsoids displayed at 20% probability level. Hydrogen atoms removed for clarity.....	204
Figure C-7: ORTEP view of <b>2.21</b> . Thermal ellipsoids displayed at 20% probability level. Hydrogen atoms removed for clarity.....	206
Figure C-8: ORTEP view of <b>2.22</b> . Thermal ellipsoids displayed at 50% probability level. Hydrogen atoms removed for clarity.....	208
Figure C-9: ORTEP view of <b>2.23</b> . Thermal ellipsoids displayed at 50% probability level. Hydrogen atoms removed for clarity.....	211
Figure C-10: ORTEP view of <b>2.28b</b> . Thermal ellipsoids displayed at 50% probability level. Calculated hydrogen atoms removed for clarity.....	216
Figure C-11: ORTEP view of <b>2.29</b> . Thermal ellipsoids displayed at 50% probability level.....	221
Figure C-12: ORTEP view of <b>3.9</b> . Thermal ellipsoids displayed at 50% probability level. Hydrogen atoms removed for clarity.....	225
Figure C-13: ORTEP view of <b>3.10</b> . Thermal ellipsoids displayed at 50% probability level. Hydrogen atoms removed for clarity.....	228
Figure D-1: Raw $\chi T$ vs. T magnetic data for nickel-verdazyl complex <b>2.14</b> .....	233
Figure D-2: Raw $\chi T$ vs. T magnetic data for cobalt-verdazyl complex <b>2.15</b> .....	233
Figure D-3: Raw $\chi T$ vs. T magnetic data for diradical <b>2.18</b> .....	234
Figure D-4: Raw $\chi T$ vs. T magnetic data for zinc-diradical complex <b>2.19</b> .....	234
Figure D-5: Raw $\chi T$ vs. T magnetic data for manganese-diradical complex <b>2.20</b> .....	235
Figure D-6: Raw $\chi T$ vs. T magnetic data for iron-diradical complex <b>2.21</b> .....	235
Figure D-7: Raw $\chi T$ vs. T magnetic data for cobalt-diradical complex <b>2.22</b> .....	236
Figure D-8: Raw $\chi T$ vs. T magnetic data for nickel-diradical complex <b>2.23</b> .....	236

Figure D-9: Raw  $\chi T$  vs. T magnetic data for chromium-diradical complex **2.28b**.....237

## List of Schemes

Scheme 1.1: Spin trapping mechanism whereby DMPO <b>1.2</b> is added to a reactive organic radical to form a stable nitroxide radical <b>1.3</b> .....	3
Scheme 1.2: The active site of galactose oxidase has three redox-accessible stable states: (a) Catalytically active phenoxyl-copper(II) complex; (b) catalytically inactive form representative of the first crystallographic characterisation of the active site; (c) catalytically active phenolate-copper(I) complex.....	11
Scheme 2.1: General synthesis of 1,5-dimethyl-3-substituted-6-oxoverdazyls <b>2.4</b> .....	35
Scheme 2.2: Synthesis of 1,5-diisopropyl-3-substituted-6-oxoverdazyls.....	36
Scheme 2.3: Synthesis of verdazyl coordination compounds <b>2.14</b> and <b>2.15</b> .....	38
Scheme 2.4: Synthesis of compound <b>2.16</b> , crystallised with hydroquinone.....	47
Scheme 2.5: Synthesis of diradical <b>2.18</b> .....	50
Scheme 2.6: Synthesis of complexes with the general structure <b>2.18</b> MCl <sub>2</sub> .....	62
Scheme 2.7: Synthesis of the chromium(III) coordination compound <b>2.28</b> .....	84
Scheme 2.8: Synthesis of the copper(II) coordination compound <b>2.29</b> .....	91
Scheme 3.1: Redox properties of nitroxide radicals.....	108
Scheme 3.2: Redox properties of verdazyl radicals.....	112
Scheme 3.3: Synthesis of radical <b>3.9</b> .....	113
Scheme 3.4: Synthesis of zinc complex <b>3.10</b> .....	115
Scheme 3.5: <b>2.19</b> undergoes two electron-transfer processes (E, E) to give the dicationic species <b>2.19</b> <sup>++</sup> . This species undergoes a chemical change with respect to each of the verdazyl rings (C, C) to yield the uncoordinated dication <b>2.19b</b> <sup>++</sup> . Two-electron reduction of this species (E, E) gives an uncoordinated diradical <b>2.19b</b> , which undergoes a chemical change whereby the verdazyl rings recoordinate to zinc to regenerate the original species <b>2.19</b> .....	130
Scheme 3.6: Redox-induced structural changes in the ruthenium sandwich complex <b>3.12a</b> whereby ligand hapticity changes upon reduction. Boxed structures represent isolated and characterised species.....	132

Scheme 3.7: Ligand-based redox-induced structural changes in <b>3.13a</b> rely on redox-activity of appended ferrocene groups.....	134
Scheme 3.8: Chemical oxidation of <b>3.9</b> using NOPF <sub>6</sub> as oxidant.....	140
Scheme 3.9: Resonance contributions to the amide moiety in the verdazyl ring that dictates the sensitivity of the carbonyl stretch in the infrared spectrum.....	140

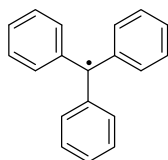
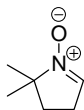
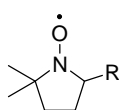
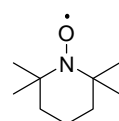
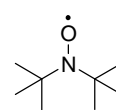
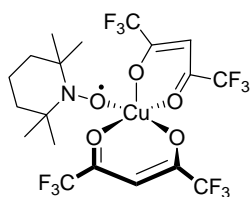
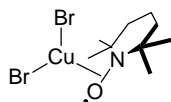
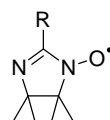
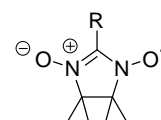
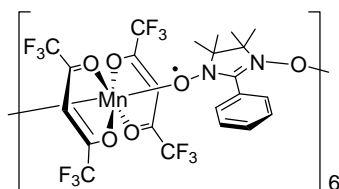
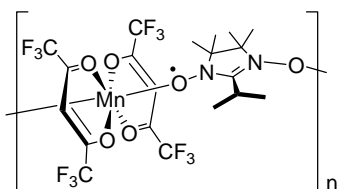
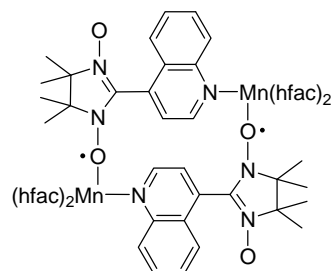
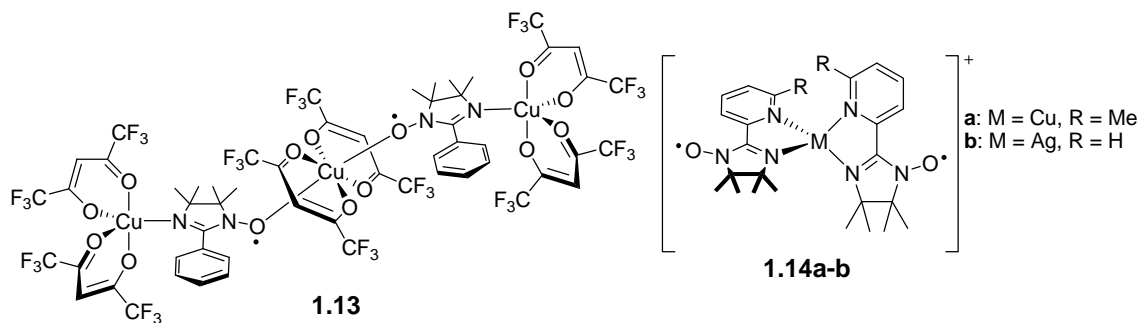
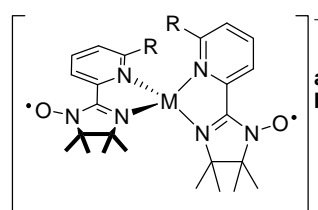


## List of Tables

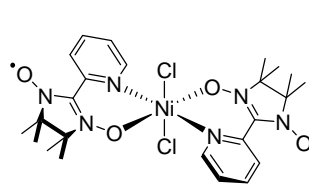
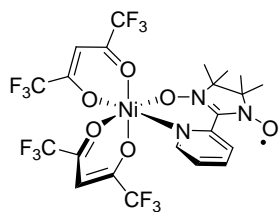
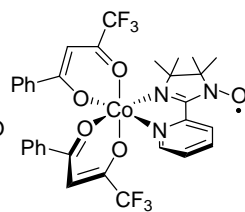
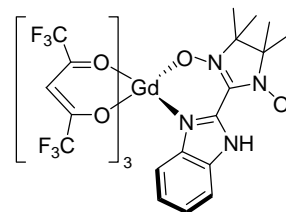
Table 2.1: Selected bond lengths (Å) and angles (degrees) for <b>2.14</b> .....	41
Table 2.2: Selected bond lengths (Å) and angles (degrees) for <b>2.15</b> .....	44
Table 2.3: Selected bond lengths (Å) and angles (degrees) for <b>2.16</b> .....	48
Table 2.4: Selected bond lengths (Å) and angles (degrees) for <b>2.18</b> .....	52
Table 2.5: Selected bond lengths (Å) and angles (degrees) for <b>2.19</b> .....	66
Table 2.6: Selected bond lengths (Å) and angles (degrees) for <b>2.20</b> .....	69
Table 2.7: Selected bond lengths (Å) and angles (degrees) for <b>2.21</b> .....	74
Table 2.8: Selected bond lengths (Å) and angles (degrees) for <b>2.22</b> .....	77
Table 2.9: Selected bond lengths (Å) and angles (degrees) for <b>2.23</b> .....	81
Table 2.10: Selected bond lengths (Å) and angles (degrees) for <b>2.28b</b> .....	86
Table 2.11: Selected bond lengths (Å) and angles (degrees) for <b>2.29</b> .....	93
Table 3.1: Selected bond lengths (Å) and angles (degrees) for <b>3.9</b> .....	115
Table 3.2: Selected bond lengths (Å) and angles (degrees) for <b>3.10</b> .....	117
Table 3.3: Calculated hyperfine coupling parameters for <b>3.9</b> and <b>3.10</b> .....	120
Table 3.4: Electrochemical parameters for <b>3.9</b> and <b>3.10</b> .....	121
Table 3.5: Electrochemical parameters for <b>2.18</b> and <b>2.19</b> .....	124
Table 3.6: Infrared frequency of the carbonyl group in diradicals <b>3.9</b> and <b>3.10</b> and dications <b>3.9<sup>+</sup>PF<sub>6</sub><sup>-</sup></b> and <b>3.10<sup>+</sup>PF<sub>6</sub><sup>-</sup></b> .....	142
Table 3.7: Infrared frequency of the carbonyl group in diradicals <b>2.18</b> and <b>2.19</b> and dications <b>2.18<sup>2+</sup>(PF<sub>6</sub><sup>-</sup>)<sub>2</sub></b> and <b>2.19<sup>2+</sup>(PF<sub>6</sub><sup>-</sup>)<sub>2</sub></b> .....	143
Table B-1: Crystallographic parameters.....	177
Table C-1: Bond lengths(Å) and angles(°) for <b>2.14</b> .....	181
Table C-2: Bond lengths(Å) and angles(°) for <b>2.15</b> .....	187

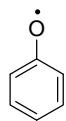
Table C-3: Bond lengths(Å) and angles(°) for <b>2.16</b> .....	193
Table C-4: Bond lengths(Å) and angles(°) for <b>2.18</b> .....	199
Table C-5: Bond lengths(Å) and angles(°) for <b>2.19</b> .....	202
Table C-6: Bond lengths(Å) and angles(°) for <b>2.20</b> .....	204
Table C-7: Bond lengths(Å) and angles(°) for <b>2.21</b> .....	206
Table C-8: Bond lengths(Å) and angles(°) for <b>2.22</b> .....	208
Table C-9: Bond lengths(Å) and angles(°) for <b>2.23</b> .....	211
Table C-10: Bond lengths(Å) and angles(°) for <b>2.28b</b> .....	216
Table C-11: Bond lengths(Å) and angles(°) for <b>2.29</b> .....	221
Table C-12: Bond lengths(Å) and angles(°) for <b>3.9</b> .....	225
Table C-13: Bond lengths(Å) and angles(°) for <b>3.10</b> .....	228

## List of Numbered Compounds

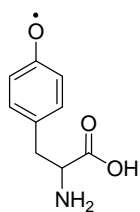
**1.1****1.2****1.3****1.4****1.5****1.6****1.7****1.8****1.9****1.10****1.11****1.12****1.13****1.14a-b**

**a:** M = Cu, R = Me  
**b:** M = Ag, R = H

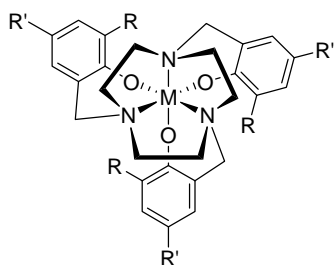
**1.15****1.16****1.17****1.18**



1.19

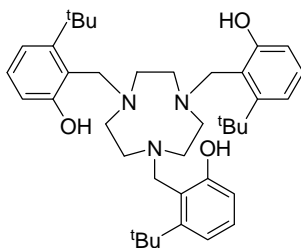


1.20

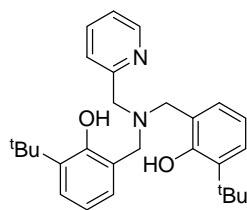


1.21a-d

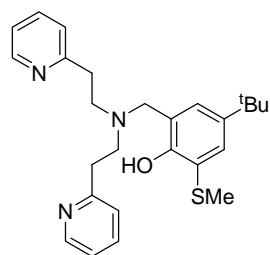
- a: R = <sup>t</sup>Bu, R' = <sup>t</sup>Bu, M = Ga  
 b: R = <sup>t</sup>Bu, R' = OMe, M = Ga  
 c: R = <sup>t</sup>Bu, R' = <sup>t</sup>Bu, M = Sc  
 d: R = <sup>t</sup>Bu, R' = OMe, M = Sc



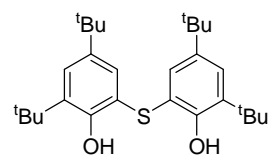
1.22



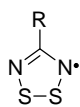
1.23



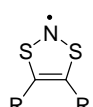
1.24



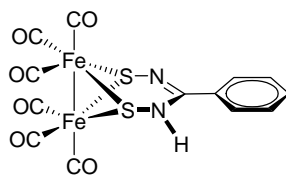
1.25



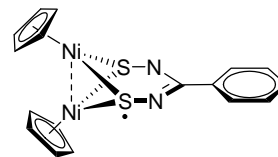
1.26



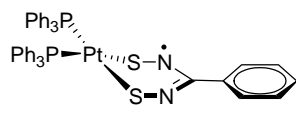
1.27



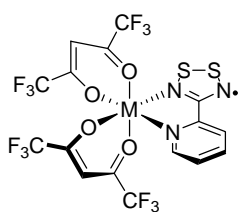
1.28



1.29

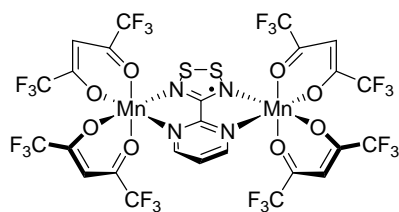


1.30

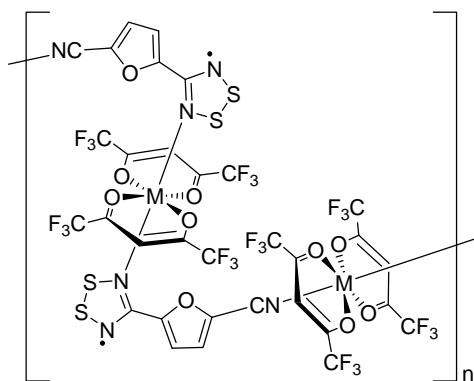


1.31a-c

- a: M = Mn  
 b: M = Cu  
 c: M = Co

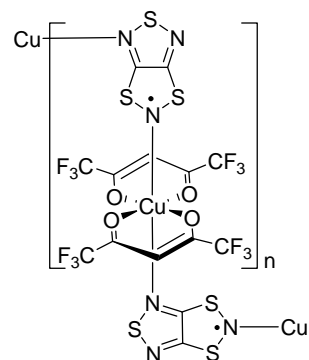


1.32

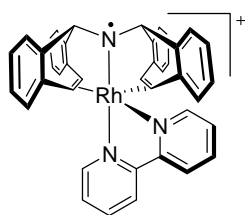


1.33a-c

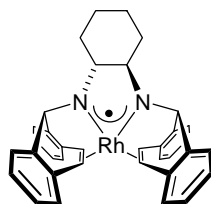
a: M = Mn  
b: M = Ni  
c: M = Co



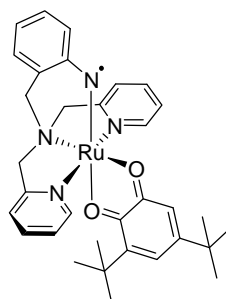
1.34



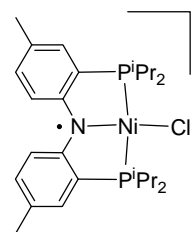
1.35



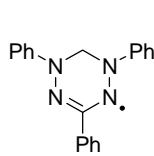
1.36



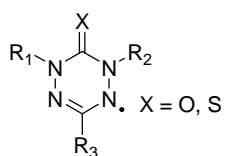
1.37



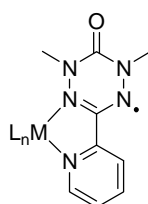
1.38



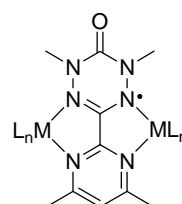
1.39



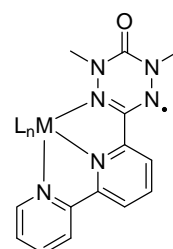
1.40



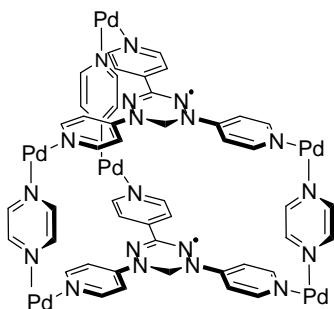
1.41



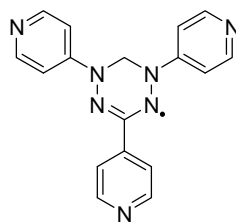
1.42



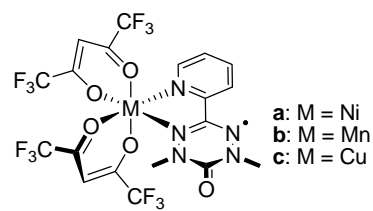
1.43



1.44

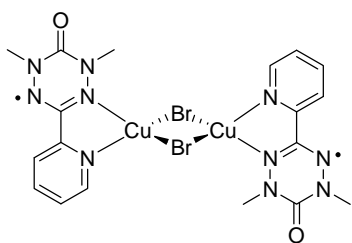
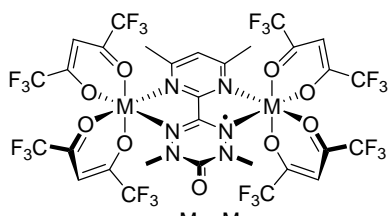


1.45

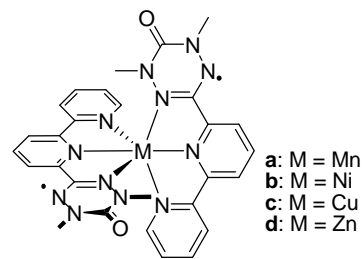


1.46a-c

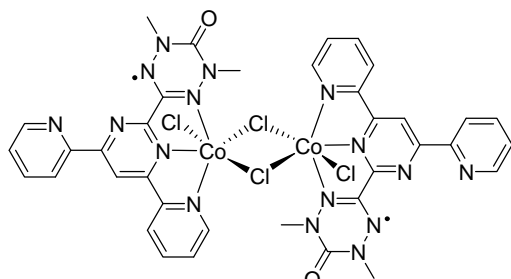
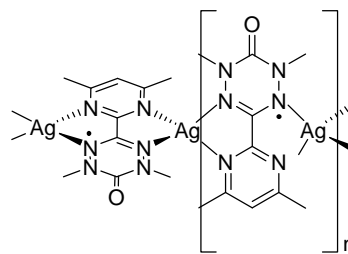
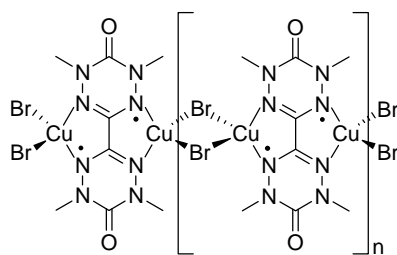
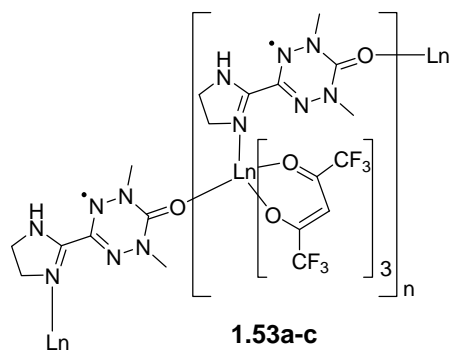
a: M = Ni  
b: M = Mn  
c: M = Cu

**1.47**

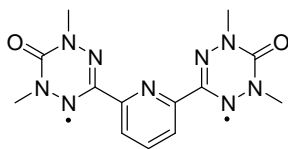
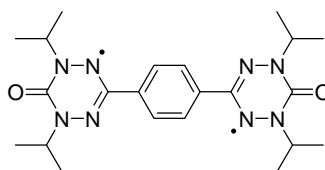
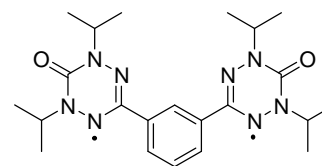
a: M = Mn  
b: M = Ni

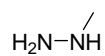
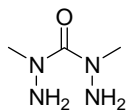
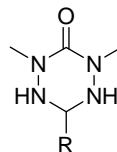
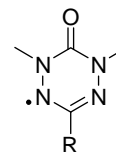
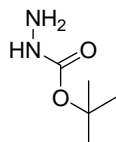
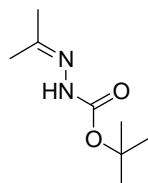
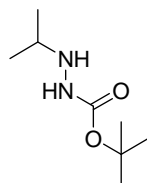
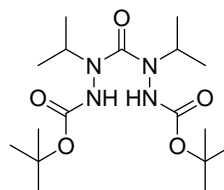
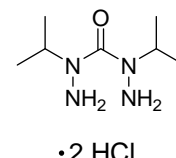
**1.48a-b**

a: M = Mn  
b: M = Ni  
c: M = Cu  
d: M = Zn

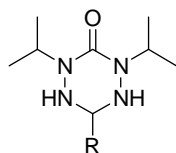
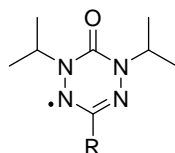
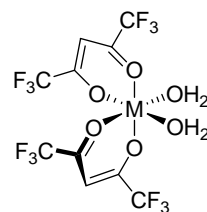
**1.49a-d****1.50****1.51****1.52**

a: Ln = Gd  
b: Ln = Tb  
c: Ln = Dy

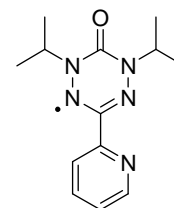
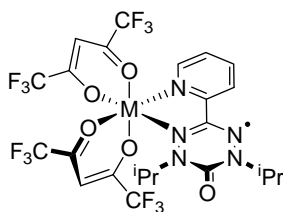
**1.53a-c****1.54****1.55****1.56**

**2.1****2.2****2.3****2.4****2.5****2.6****2.7****2.8**

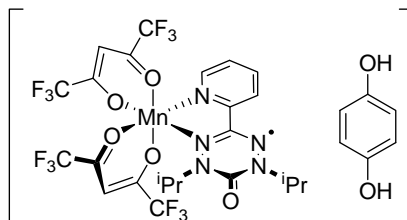
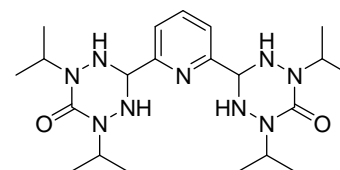
• 2 HCl

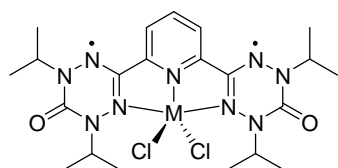
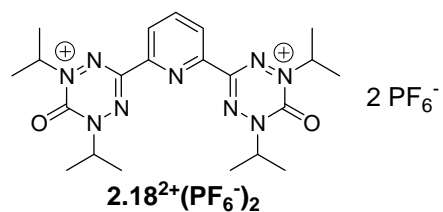
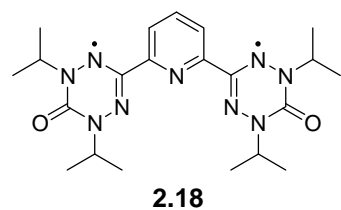
**2.9****2.10****2.11**

**2.12a:** M = Ni  
**2.12b:** M = Co  
**2.12c:** M = Mn

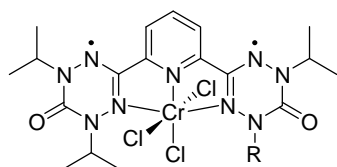
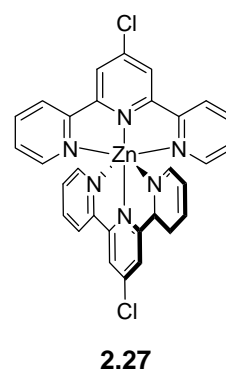
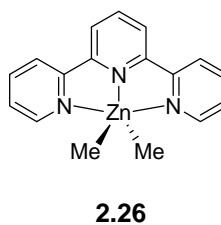
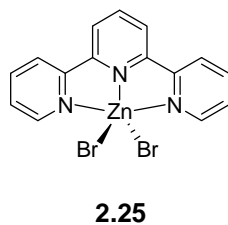
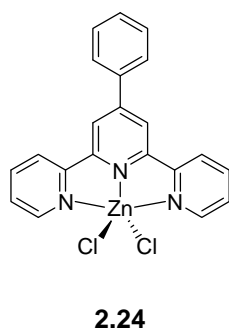
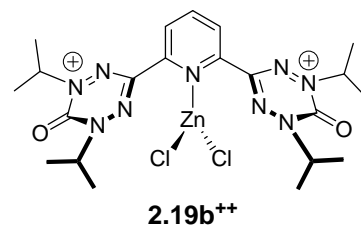
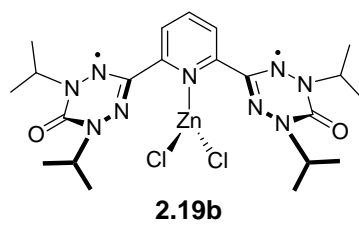
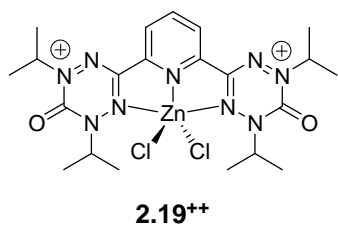
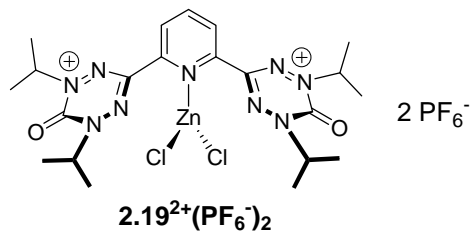
**2.13**

**2.14:** M = Ni  
**2.15:** M = Co

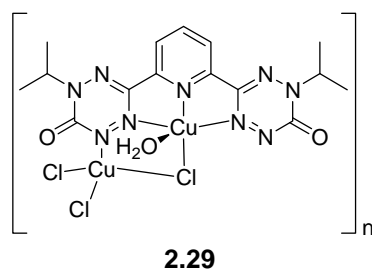
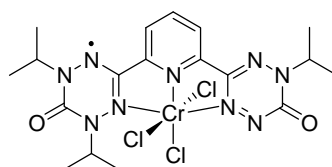
**2.16****2.17**



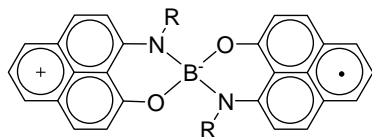
**2.19:** M = Zn  
**2.20:** M = Mn  
**2.21:** M = Fe  
**2.22:** M = Co  
**2.23:** M = Ni



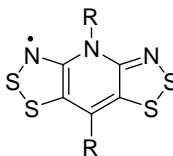
**2.28b:** R = H



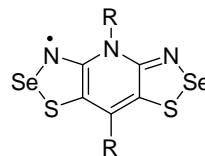




3.1



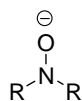
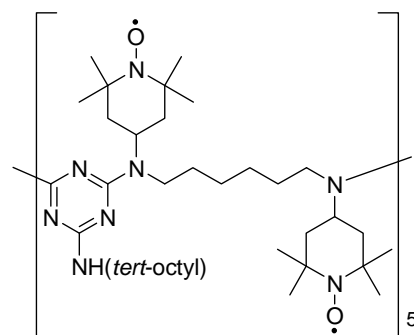
3.2



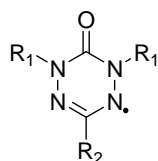
3.3



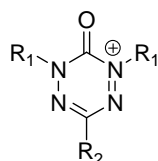
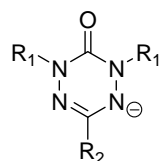
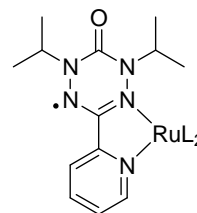
3.4

3.4<sup>+</sup>3.4<sup>-</sup>

3.5

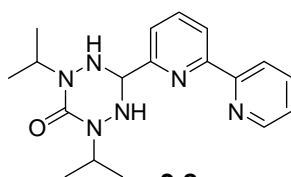


3.6

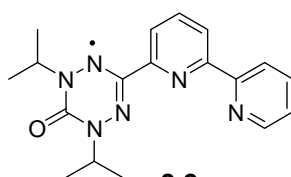
3.6<sup>+</sup>3.6<sup>-</sup>

3.7a: L = acac

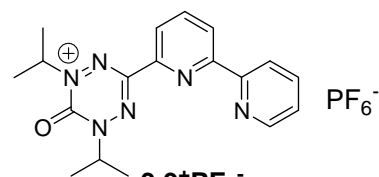
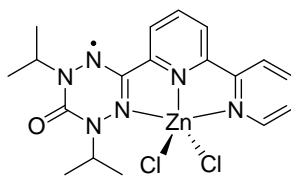
3.7b: L = hfac



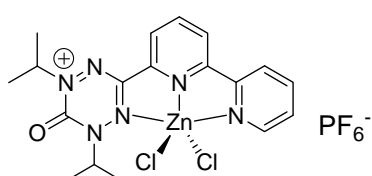
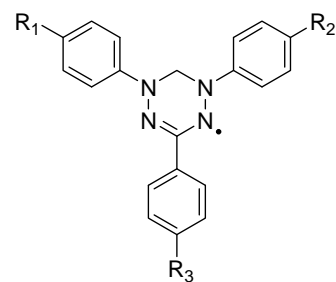
3.8



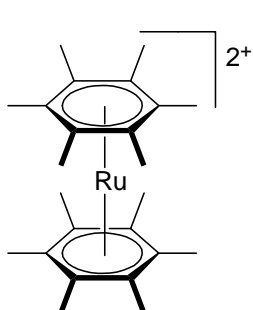
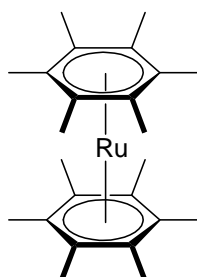
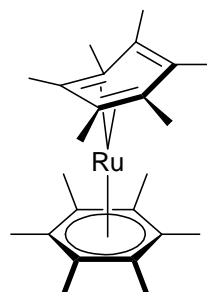
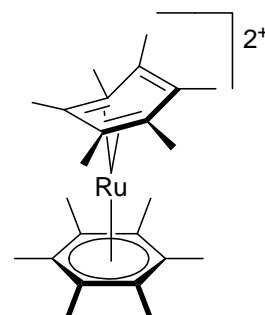
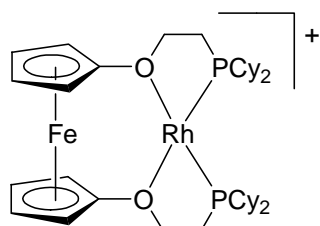
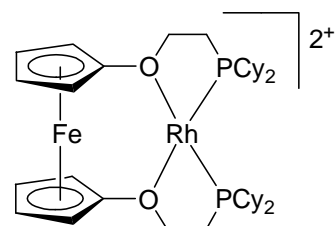
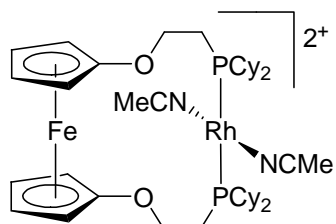
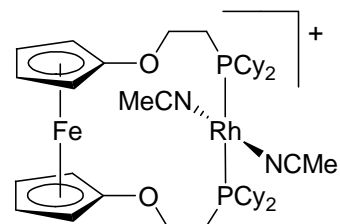
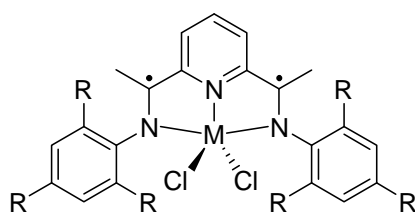
3.9

3.9<sup>+</sup>PF<sub>6</sub><sup>-</sup>

3.10

3.10<sup>+</sup>PF<sub>6</sub><sup>-</sup>

3.11

**3.12a****3.12b****3.12c****3.12d****3.13a****3.13b****3.13c****3.13d****4.1:** M = Fe**4.2:** M = Co

## List of Abbreviations

A	Ampere(s)
Å	Angstrom(s)
<i>a</i>	hyperfine coupling constant
acac	acetylacetonato
Anal. Calcd.	analytical calculated
br	broad
Bu	butyl
C	Celsius or chemical change step
<i>c</i>	speed of light
cm	centimetre(s)
cm <sup>-1</sup>	wavenumber(s)
CV	cyclic voltammetry or cyclic voltammogram
Cy	cyclohexyl
d	inter-electron distance or doublet
DFT	density functional theory
DMPO	5,5-dimethyl-1-pyrroline- <i>N</i> -oxide
DMSO	dimethyl sulfoxide
DMSO-d <sub>6</sub>	deuterated dimethyl sulfoxide
E	electron-transfer step
E <sub>cell</sub>	cell potential
E <sup>o</sup> <sub>ox</sub>	oxidation potential
E <sup>o</sup> <sub>red</sub>	reduction potential

$e^-$	electron
EI-MS	electron impact mass spectrometry
emu	electromagnetic units
EPR	electron paramagnetic resonance
ESI-MS	electrospray ionisation mass spectrometry
Fc	ferrocene
$Fc^+$	ferrocenium
FT-IR	Fourier-transform infrared
$g$	Lande factor or gram(s)
GO	galactose oxidase
$H$	Hamiltonian operator
$h$	hour(s) or Planck's constant
hfac	hexafluoroacetato
Hz	Hertz
$I$	nuclear spin number
$iPr$	isopropyl
IR	infrared
$J$	coupling constant (NMR or magnetic exchange)
K	Kelvin(s)
$k$	Boltzmann constant
L	litre(s)
LSI-MS	liquid secondary ionisation mass spectrometry
M	molar or transition metal

<i>m</i>	meta
m	medium, metre or multiplet
$m_s$	spin quantum number
mg	milligram(s)
MHz	megahertz
mL	millilitre(s)
mM	millimolar
mm	millimetre(s)
mmol	millimole(s)
mol	mole(s)
MPMS	magnetic property measurement system
Mp.	melting point
MS	mass spectrometry or mass spectrum
mT	milliTesla(s)
mV	millivolt(s)
$m/z$	mass-to-charge ratio
N	Avogadro's number
nm	nanometre(s)
NMR	nuclear magnetic resonance
<i>o</i>	ortho
OSWV	Osteryoung square wave voltammetry
<i>p</i>	para
PIPO	polymer-immobilised piperidinyI oxyl

ppm	parts per million
R	generic organic functional group or goodness of fit factor
RNR	ribonucleotide reductase
S	spin number
s	second(s) or strong
sh	shoulder
SMMs	single molecule magnets
SOMO	singly occupied molecular orbital
SQUID	superconducting quantum interference device
T	temperature or Tesla
t	triplet
TCNE	tetracyanoethylene
TCNQ	tetracyanoquinodimethane
TEMPO	2,2,6,6-tetramethylpiperidine-1-oxyl
tert	tertiary
tfac	trifluoroacetato
THF	tetrahydrofuran
UV	ultraviolet
V	Volt(s)
Vd	verdazyl radical
Vis	visible
vs	very strong
VT-EPR	variable temperature electron paramagnetic resonance

w	weak
$\beta$	Bohr magneton
$\Delta$	difference (delta)
$\Delta E_p$	peak-to-peak potential difference
$\delta$	chemical shift (delta)
$\varepsilon$	extinction coefficient
$\eta$	hapticity (eta)
$\theta$	Weiss constant
$\lambda$	wavelength (lamda)
$\lambda_{\max}$	wavelength of maximum absorption
$\mu A$	microamperes
$\mu_0$	permeability of free space
$\rho$	spin density or purity factor
$\chi$	magnetic susceptibility
$^\circ$	degrees

## Acknowledgments

First of all, I must thank my family; mom, dad, Scott and Shaundra, for supporting and encouraging me in my academic endeavours. You have always been there to help me out in whatever way was needed. I could never have accomplished this without all of you.

Thank you to my supervisor, Dr. Robin “Sugs” Hicks. Your guidance, support and patience have been an integral part of my success. You have taught me how to keep the pace, academically and otherwise. Thanks also to past and present Hicks Park members. The daily grind of lab work was always made more enjoyable when it was shared with friends. A special thank you goes out to all of my friends and fellow grad students at UVic. It was always nice to be able to share the grad student experience with a close group.

Thanks to UVic chemistry staff and faculty, without whose support and expertise none of this work would have been achievable. A special thank you to Dave Berry, my teaching supervisor during my time at UVic. Teaching was an important aspect of grad school for me, and your advice and guidance has been a strong and positive influence on my teaching career.

Finally, thanks to my best friend and teammate, Brynn. You have always been there for me through the ups and downs. In many ways, I owe this accomplishment to you.



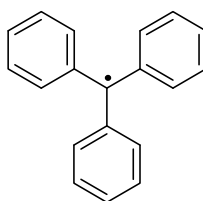
## **Dedication**

To my parents, whose love and support have helped me become the person I am today. And to my high school chemistry teacher, Mr. Dudgeon, who inspired my original fascination with chemistry.

# Chapter 1: Introduction and background

## 1.1 Stable radicals

Science progresses when discoveries are made that inspire others to take up the same line of research. Further experiments are carried out, which either support or refute the original results. Sometimes new findings follow rather intuitively from the existing body of knowledge and quietly make their way into the literature. Occasionally, however, a controversial proposal is put forward that attracts the attention of the cream of the scientific crop. In 1900, Moses Gomberg's discovery of the triphenylmethyl radical<sup>1</sup> shed light on a new class of compounds and the study of radicals was born. At the turn of the 20<sup>th</sup> century this discovery sparked intense debate among leading researchers of the time and would ultimately lead to a change in the fundamental understanding of electronic interactions in molecules. Gomberg's work, and the debate that filled the chemical literature in the ensuing years,<sup>2</sup> established the existence of unpaired electrons in stable organic molecules.



### 1.1

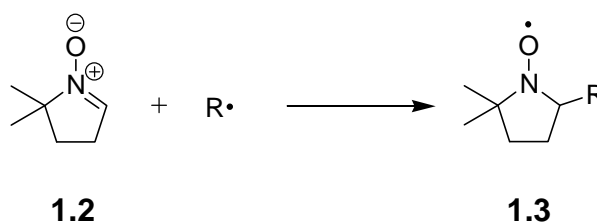
In the intervening century-plus since Gomberg's seminal paper, significant progress has been made in the field of radical chemistry. Many new families of stable organic radicals, incorporating structural motifs beyond the original triphenylmethyl framework, have been developed and examples of both charged and neutral stable

radicals are now known.<sup>3, 4</sup> Because the research presented in this thesis deals exclusively with neutral radicals the remainder of the introductory section will focus on this class of compounds.

Although the existence of radicals is now universally accepted, an exact definition of stability, as it applies to organic radicals, has proven to be elusive. The term *persistent* is often applied to radicals whose lifetime is highly environment-specific; for example radicals that last long enough to be characterised under a given set of conditions.<sup>4</sup> The classification of *stable* is generally reserved for radicals that can actually be isolated and stored for an indefinite period. Ingold's definition of a stable radical as one that can be handled using "no more precautions than would be used for the majority of commercially available organic chemicals"<sup>5</sup> serves as a practical distinction between stable and persistent for the purposes of this thesis.

The desire to design radicals with predictable and tuneable properties has precipitated a proliferation of new families of stable radicals and the synthesis and characterisation of new stable radicals continues to be an important area of research in this domain.<sup>3</sup> Beyond these fundamental studies, stable radicals are being used in an increasing number of direct applications. Various spin trapping agents – organic compounds that can combine with a reactive radical to produce a stable radical adduct – have been known for more than 40 years.<sup>6-9</sup> A classic mechanism of spin trapping, which uses 5,5-dimethyl-1-pyrroline-*N*-oxide (DMPO **1.2**) to yield a stable nitroxide radical **1.3**, is presented in Scheme 1.1. The use of spin labels, whereby a stable radical is appended to a molecular fragment to allow characterisation of the species by electron paramagnetic resonance spectroscopy, can be used *in vivo* for biological and biochemical studies.<sup>10</sup>

Other nitroxides have been thoroughly investigated as oxidation catalysts to effect the transformation of alcohols to aldehydes.<sup>11</sup> Stable radicals have factored heavily in the development of molecule-based magnetic materials; the first strictly organic radical to show bulk magnetic ordering was reported in 1991.<sup>12, 13</sup> Since that time, many more stable radicals have been discovered that show bulk magnetic ordering.<sup>14</sup>



**Scheme 1.1:** Spin trapping mechanism whereby DMPO **1.2** is added to a reactive organic radical to form a stable nitroxide radical **1.3**.

In addition to the applications that have been previously described in this chapter, certain families of radicals have more recently been cultivated as ligands in coordination chemistry. Metal-radical complexes offer a unique opportunity to study the relationship between unpaired electrons on a metal centre with those on an open-shell organic ligand. The following sections will give an overview of some well-known classes of neutral radical coordination compounds, which will serve as an introduction to the research to be presented in the balance of this thesis.

## 1.2 Stable radical coordination chemistry

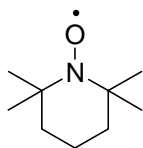
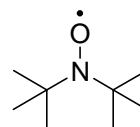
Coordination chemistry is an important aspect of the study of stable radicals. Many organic compounds have been developed as ligands and a similar trend is continually evolving with stable radicals. Radical coordination chemistry comprises a

number of different avenues, from the biological importance of naturally-occurring metal-radical interactions to the rational design of stable radical coordination complexes directed at materials and synthetic applications.

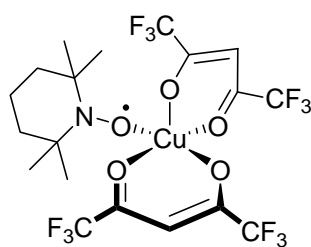
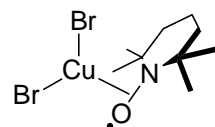
Nitric oxide and dioxygen are two open-shell species that are vitally important in biology and biochemistry. Both compounds coordinate to metals in proteins and much effort has been devoted to elucidating the structure of these complexes and the nature of the metal-ligand interactions *in vivo*.<sup>15-19</sup> Molecular oxygen coordination has also been studied with respect to oxidation catalysts for organic substrates.<sup>20</sup> Notwithstanding the significance of nitric oxide and dioxygen as ligands, they are quite distinct from the coordinating stable radicals at the hub of this thesis, as neither NO nor O<sub>2</sub> can be derivatised or “tuned” as a ligand. The focus here will be on stable neutral radicals whose organic framework allows for synthetic modification of the spin-bearing unit. In this way so-called “designer” radical ligands can be adapted to a variety of coordination environments.

### 1.2.1 Nitroxide coordination compounds

Nitroxides are the most well known classes of stable organic radicals. They are generally inert towards dimerisation, disproportionation and reaction with oxygen. A large number of nitroxide radicals have been isolated and characterised.<sup>21-26</sup> The inherent stability of nitroxides is attributed to two factors; delocalisation of spin density and steric protection. In nitroxide radicals such as TEMPO **1.4** and di-*tert*-butylnitroxide **1.5**, the singly occupied molecular orbital (SOMO) is a  $\pi^*$ -orbital, delocalised over the nitrogen and oxygen atoms.<sup>27</sup> The radical is further stabilised by the incorporation of significant steric bulk around the nitroxyl moiety.

**1.4****1.5**

Nitroxide coordination compounds were first reported in the 1960s.<sup>27</sup> The earliest examples were complexes of di-*tert*-butylnitroxide with cobalt halides<sup>28</sup> (**1.5**CoX<sub>2</sub>, X = Br, Cl) and copper  $\beta$ -diketonates<sup>29</sup> (**1.5**Cu(hfac)<sub>2</sub> and **1.5**Cu(tfac)<sub>2</sub>). Although none of these complexes were structurally characterised, the radical nature of the nitroxide ligand was confirmed by spectroscopic techniques. The first example of a nitroxide-metal complex whose structure was determined by X-ray crystallography was compound **1.6**.<sup>30</sup> Here, the TEMPO radical binds as a  $\sigma$ -donor ligand through the oxygen atom, which is the normal coordination mode for simple nitroxide derivatives. Nitroxide coordination has also been reported where the binding mode is side-on, as in **1.7**, with the N-O $\cdot$  moiety of the TEMPO radical acting as a  $\pi$ -donor.<sup>31</sup>

**1.6****1.7**

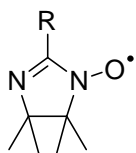
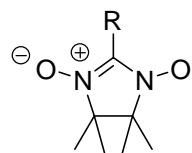
Nitroxide radicals have been investigated as oxidation co-catalysts, used in conjunction with transition metals. In particular, mixtures of TEMPO with Ru and Cu complexes have been found to be active in the oxidation of a variety of alcohols.<sup>32</sup> Catalytic activity can be tuned depending on the metal and ancillary ligands used, and many of these systems use atmospheric oxygen as the oxidising agent.<sup>11</sup> Although the

exact nature of the catalytically active species remains uncharacterised, the electronic interactions among metal, radical and organic substrate are clearly central to the activity of these systems.

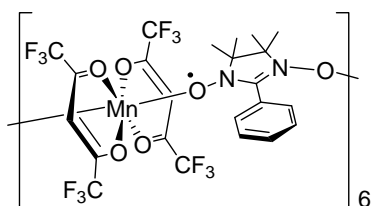
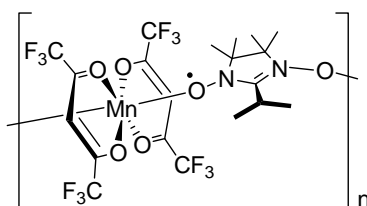
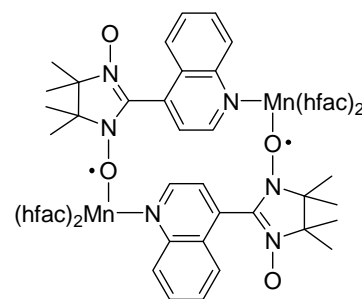
In addition to the catalytic activity of these radicals, the progress of molecular magnetism has factored even more heavily in the growth of nitroxide coordination chemistry.<sup>33</sup> One approach to the design of new magnetic materials requires paramagnetic ligands that can bridge multiple metal centres, thus mediating extended magnetic communication. Coordination polymers involving various bridging nitroxide radicals have been reported and some of these exhibit bulk magnetic ordering.<sup>34-36</sup> However, these examples are rare and the temperatures below which these complexes magnetically order are extremely low. For these reasons, pertinent model systems designed to investigate fundamental electronic interactions among metals and radicals are still highly sought-after synthetic targets.

In general, TEMPO and other simple nitroxides are not the best candidates to be magnetic building blocks. They have only one spin-bearing binding site and, as such, do not lend themselves to the development of extended structures. Imino nitroxides **1.8** and nitronyl nitroxides **1.9** provide a solution to this problem; having two donor sites inherent in the molecular framework allows coordination of one radical ligand to multiple metal centres. Moreover, both imino and nitronyl nitroxides are amenable to synthetic modification. The incorporation of substituents that contain other donor atoms provides a means to enhance the binding affinity of the ligand beyond the relatively weak donor strength of the nitroxyl moiety. Imino and nitronyl nitroxides also exhibit increased delocalisation of the unpaired electron, compared to that in the simple nitroxide

derivatives discussed previously. Imino nitroxides show positive spin density on the imine nitrogen as well as the nitroxyl group, while an equal distribution of spin density over both nitroxyl groups is seen in nitronyl nitroxides.<sup>37</sup>

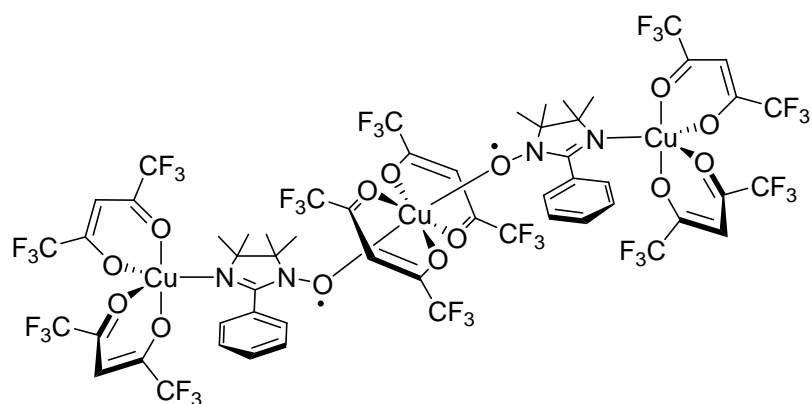
**1.8****1.9**

Nitronyl nitroxide coordination compounds have been reported where the nature of the R-substituent has a pronounced affect on the ultimate structure of the metal-radical complex. A phenyl-substituted nitronyl nitroxide has been shown to form rings consisting of six repeating metal-radical units with Mn(II) as the metal centre and hexafluoroacetylacetonato ancillary ligands **1.10**.<sup>38</sup> The formation of the macrocyclic structure was attributed to  $\pi$  interactions between the phenyl rings of the radical and the hfac ancillary ligands. Complexes involving the same metal and ancillary ligands, but with isopropyl **1.11** and ethyl groups in place of the phenyl substituent formed chains, rather than a discrete ring structure.<sup>39</sup> Incorporation of a coordinating quinoline moiety resulted in a different macrocyclic structure **1.12** consisting of two Mn(hfac)<sub>2</sub> units and two quinoline-substituted nitronyl nitroxide radicals.<sup>40</sup>

**1.10****1.11****1.12**



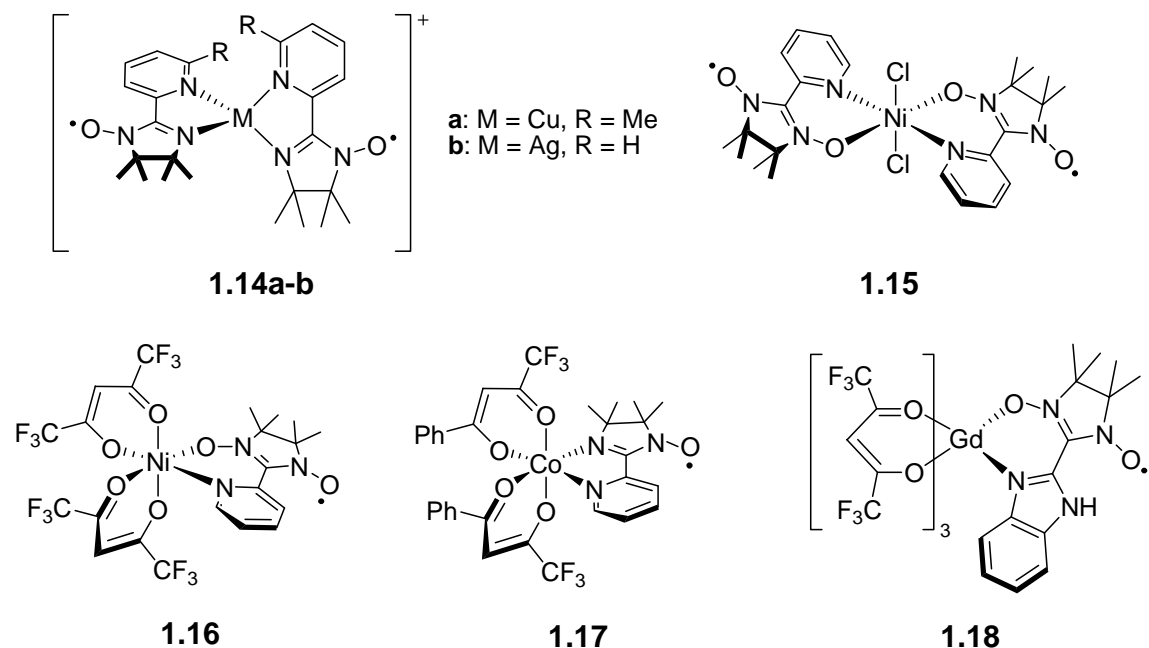
There is a pronounced difference in the fundamental coordination chemistry of imino and nitronyl nitroxides. Nitronyl nitroxides coordinate exclusively through oxygen atoms, while imino nitroxides are capable of binding metals via oxygen or nitrogen coordination. Luneau et al. demonstrated that a phenyl-substituted imino nitroxide ligand can bind copper(II) through both oxygen and nitrogen simultaneously.<sup>41</sup> Furthermore, this group reported that the magnetic coupling in the metal-radical oligomer **1.13** depends on both the binding mode of the ligand (axial vs. equatorial coordination) and the nature of the metal-radical bond (NO-M vs. N-M).



**1.13**

Examples of 1:1 metal:radical complexes involving both nitronyl nitroxide and imino nitroxide ligands have been used as model systems to investigate discrete electronic interactions between these radicals and a variety of metal centres.<sup>27</sup> Chelating nitroxides have also been used to prepare 2:1 radical:metal complexes **1.14a-b**<sup>42, 43</sup>, **1.15**<sup>44</sup> extending these model systems to allow the investigation of radical-metal-radical spin communication. To overcome the weak Lewis basicity of the nitroxyl moiety, substituents containing donor atoms are routinely employed to make a bidentate nitroxide ligand. Strongly withdrawing ancillary ligands are also common in nitroxide coordination compounds for the same reason. Lanthanide coordination compounds

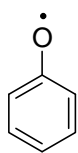
involving bidentate imino and nitronyl nitroxide ligands have recently been investigated for their luminescent properties.<sup>45-47</sup> Compounds **1.16**<sup>44</sup>, **1.17**<sup>48</sup> and **1.18**<sup>46</sup> are presented as representative examples of bidentate imino and nitronyl nitroxide complexes involving electron-withdrawing ancillary ligands.



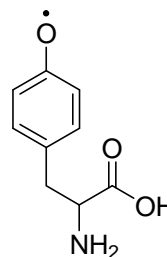
### 1.2.2 Phenoxyl radical coordination compounds

The coordination chemistry of phenoxyl radicals **1.19** has been developed tangentially to that of most other classes of stable radicals. The roots of this chemistry are in biological systems, far removed from the modern materials development trend that has driven the proliferation of nitroxide coordination chemistry. In fact, the breadth of known phenoxyl-metal compounds can be traced to two biologically important enzymes; ribonucleotide reductase (RNR) and galactose oxidase (GO).<sup>49, 50</sup> Ribonucleotide reductase, specifically the R2 subunit of this enzyme, has at its active site a tyrosyl radical (**1.20**, derived from the amino acid tyrosine) in close proximity to an iron centre.

Although X-ray diffraction studies have indicated that the radical is not actually coordinated to iron in this system (the phenoxyl oxygen sits 5.3 Å from the closest iron site<sup>51</sup>), the electronic interactions between the metal centre and the radical are fundamental to the activity of this enzyme.<sup>50</sup> Galactose oxidase, on the other hand, includes a tyrosyl radical directly coordinated to a copper(II) centre, making this complex more germane to a discussion of phenoxyl coordination compounds.

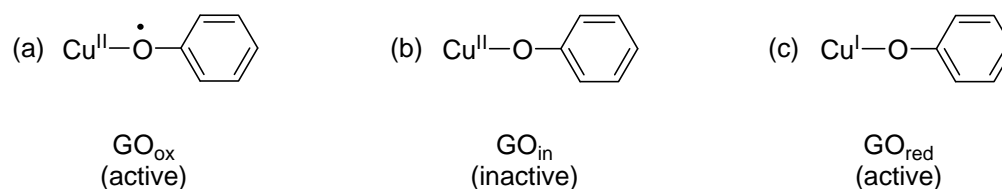


1.19



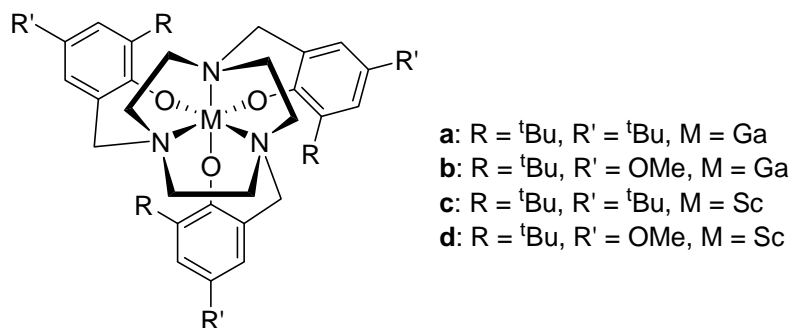
1.20

Galactose oxidase provides an interesting example of a coordination compound where both the metal and ligand are paramagnetic. However the significance of this protein is not related to any magnetic coupling between metal and ligand electrons, but rather to the unique redox properties that this motif imparts on the enzyme.<sup>52</sup> Galactose oxidase is involved in the catalytic oxidation of primary alcohols *in vivo*. The electronic interplay between the metal centre and the tyrosyl ligand lead to three distinct, stable oxidation states of the active site (shown in Scheme 1.2). While an inactive form of the enzyme was characterised by X-ray crystallography in 1991,<sup>53</sup> detailed spectroscopic investigations by Whittaker et al. were the first studies aimed at elucidating the electronic nature of both the copper centre and the tyrosyl ligand in the active enzyme.<sup>54, 55</sup>

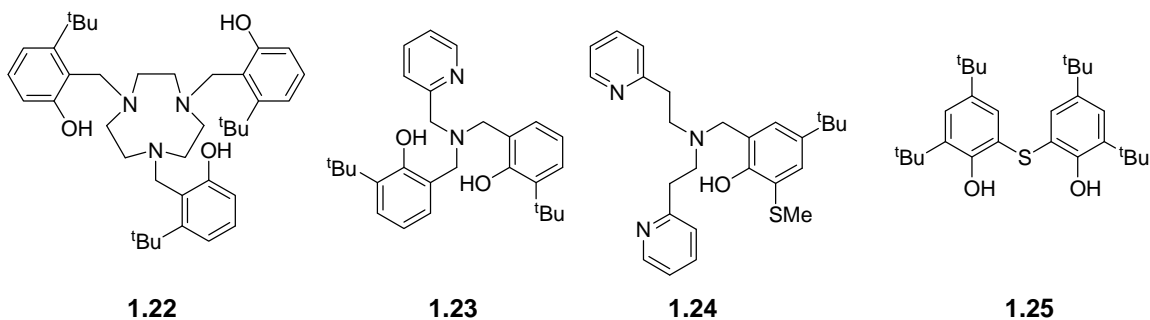


**Scheme 1.2:** The site of galactose oxidase has three redox-accessible stable states: (a) Catalytically active phenoxyl-copper(II) complex; (b) catalytically inactive form representative of the first crystallographic characterisation of the active site; (c) catalytically active phenolate-copper(I) complex.

The catalytic oxidation process involving galactose oxidase is compatible with a range of primary alcohols yet the enzyme is inert toward secondary alcohols.<sup>56</sup> This has spurred a great interest in developing phenoxyl coordination compounds that mimic the oxidative activity of GO.<sup>57</sup> Much of the early research in this area involved the synthesis of complexes with redox-inert metals. In these systems, any redox processes must be strictly ligand-based. Model complexes have been prepared comprising Ga(III) and Sc(III) with coordinated phenolate ligands **1.21a-d**.<sup>58</sup> Analogous complexes where the macrocyclic ligand has both appended phenol and phenolate derivatives coordinated to Zn(II) have also been reported.<sup>59</sup> In all cases the ligands were oxidised to give complexes where the phenoxyl ligand is unambiguously coordinated to the metal centre. Cyclic voltammetry studies on these systems have shown that depending on the nature of the R and R' substituents on the phenoxyl moiety, mono-, di- and tri-radicals are electrochemically accessible.

**1.21a-d**

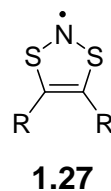
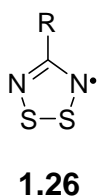
Complexes involving the phenolate/phenoxy moiety and containing redox-active metals have also been reported. Redox activity can be mainly ligand-based or metal-based, depending on the metal involved; a good deal of research has been dedicated to identifying the origin of the electrochemistry in GO-type systems.<sup>60</sup> Of the first-row transition metal complexes reported, those involving copper(II) are the most heavily studied.<sup>57</sup> A variety of ligand systems have also been studied in an effort to replicate the amino acid residues surrounding the copper(II) centre in galactose oxidase. Nitrogen-based macrocycles with phenol-derivatives **1.22**, similar to those used in the Zn, Ga and Sc complexes described earlier, are featured prominently in the work of Wieghardt and co-workers.<sup>61</sup> Substituted amine ligands **1.23**, **1.24** where the three N-substituents are a mixture of pyridine and phenol derivatives have also been used.<sup>62, 63</sup> Sulfur-bridged phenol derivatives **1.25** have recently been used to give phenoxy-copper(II) complexes that are stable in air.<sup>64</sup> The coordinated phenol ligands undergo one-electron oxidation to give a coordinated phenoxy moiety. Ultimately, the redox activity and spectroscopic properties of a variety of galactose oxidase models have been thoroughly investigated.<sup>60</sup> Catalytic activity of certain systems towards alcohol oxidation has also been examined.<sup>64</sup>



### 1.2.3 Thiazyl radical coordination chemistry

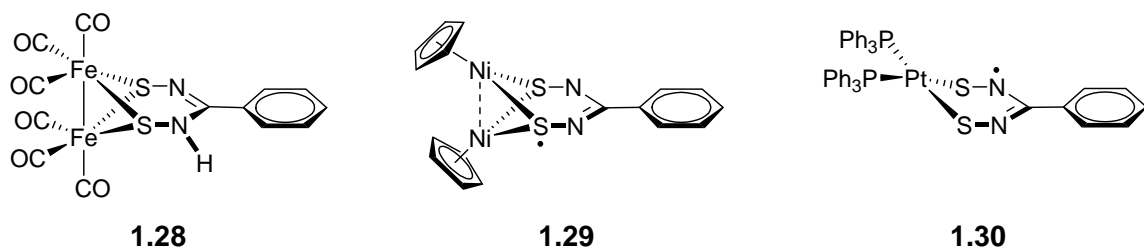
A class of radicals that continues to show promise as a potential building block for various materials applications is the thiazyl family.<sup>65</sup> Thiazyl radicals are open-shell species containing the  $-S-N^{\bullet}-$  moiety. Examples of thiazyl radicals encompassing a variety of molecular frameworks are known; linear species and cyclic radicals of varying ring size have been reported.<sup>66, 67</sup>

While the number of thiazyl radical derivatives is diverse, the family of known thiazyl radical coordination compounds is much smaller. In fact, thiazyl-based metal-radical complexes primarily involve only two main categories of this radical family; namely, 1,2,3,5-dithiadiazolyl **1.26** and 1,3,2-dithiazolyl radicals **1.27**.

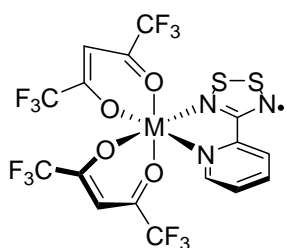


Many of the early examples of 1,2,3,5-dithiadiazolyl coordination compounds feature a number of structural similarities. The radical ligands are bound through the sulfur atoms and, in many cases, contain a phenyl substituent on the 1,2,3,5-dithiadiazolyl ring. What differentiates these preliminary thiazyl coordination

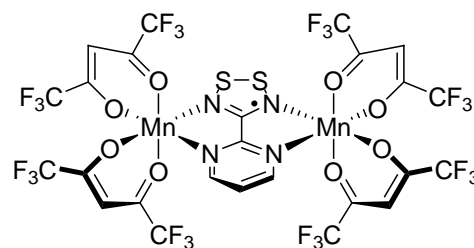
compounds is the nature of the coordinated radical. Banister et al. reported what was believed to be the first 1,2,3,5-dithiadiazolyl complex **1.28** in 1989.<sup>68</sup> However, subsequent analysis of this compound revealed the presence of an N-H bond, indicating that the thiazyl ligand was not actually a radical.<sup>69, 70</sup> The same group later reported an analogous dimetallic complex **1.29** involving nickel.<sup>71</sup> The structure was characterised by X-ray crystallography and magnetic measurements indicated that this complex was paramagnetic. Extended-Hückel calculations imply that the unpaired electron is delocalised over the nickel, sulfur and carbon atoms of the metallacycle framework. A monometallic platinum complex **1.30** was reported in which the ligand also retained its radical nature upon coordination to the metal centre.<sup>72</sup> Again in this case, the sulfur-sulfur bond of the original dithiadiazolyl radical is broken and the platinum centre is incorporated into a six-membered metallacycle.



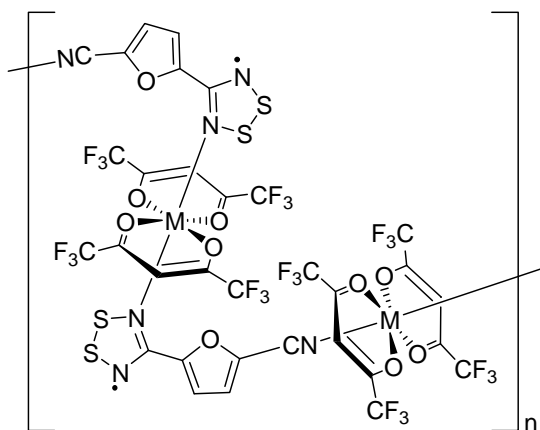
Similarly to what has been demonstrated in nitroxide coordination chemistry, recent research has shown that inclusion of R-groups containing donor atoms can modify the coordination mode of the dithiadiazolyl ligand. The use of chelating ligands leads to the formation of discrete N-bound complexes **1.31a-c**.<sup>73, 74</sup> Since there is significant spin density on the nitrogen atoms of the dithiadiazolyl ring, these complexes can act as model systems to investigate magnetic coupling between the radical ligand and paramagnetic metal centres. Complexes involving bis-bidentate ligands **1.32** extend this model system to investigate metal-radical-metal communication.<sup>75</sup>

**1.31a-c**

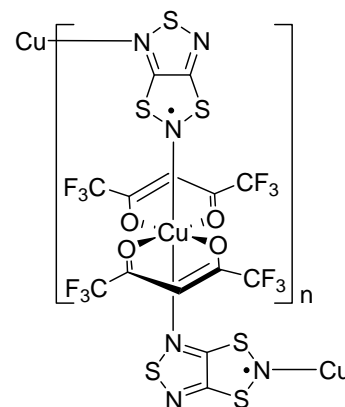
a: M = Mn  
b: M = Cu  
c: M = Co

**1.32**

Extended chain-like structures have also been reported for both 1,2,3,5-dithiadiazolyl and 1,3,2-dithiazolyl radicals. Formation of a polymeric arrangement **1.33a-c** involving monodentate N-coordination of the radical ligand results from the incorporation of a cyanofuran derivative on a 1,2,3,5-dithiadiazolyl ring.<sup>76</sup> Another coordination polymer involving Cu(hfac)<sub>2</sub> and a bicyclic 1,3,2-dithiazolyl radical **1.34** has also been reported and the magnetic properties of the chain have been characterised.<sup>77</sup> Here, the ligand bridges Cu(hfac)<sub>2</sub> moieties using two electronically distinct nitrogen atoms, only one of which bears significant spin density. Because of this binding mode, there is no propagation of magnetic communication through the chain.

**1.33a-c**

a: M = Mn  
b: M = Ni  
c: M = Co

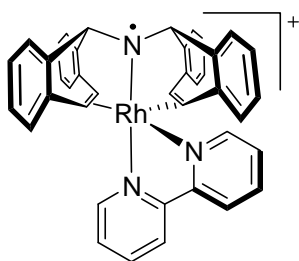
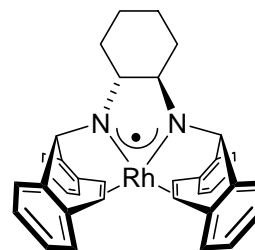
**1.34**



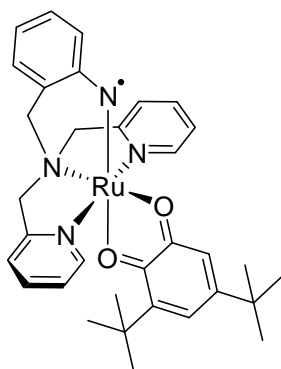
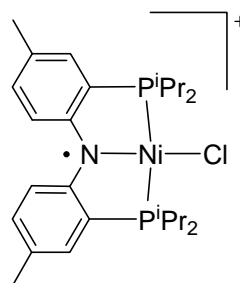
#### 1.2.4 Aminyl radical coordination compounds

Aminyl radicals ( $R_2N^\bullet$ ) differ from those discussed to this point in that the majority of the spin density associated with these radicals resides on a lone nitrogen atom. As a result, these radicals do not enjoy the same level of stability as the nitroxide or thiazyl family, where the unpaired electron is delocalised over multiple atoms. A variety of aminyl radicals have been generated in thermolysis and photolysis reactions and characterised by EPR spectroscopy.<sup>78</sup> However, most of these aminyl radicals have very limited lifetimes and are far from isolable. The few examples that are stable enough to be isolated and characterised require the presence of bulky substituents on nitrogen.<sup>79</sup>

Aminyl coordination compounds had been proposed in the early 1980s,<sup>80</sup> however it was not until 2005 that the first metal-aminyl complex was fully characterised.<sup>81</sup> The cationic complex **1.35** was proposed as an aminyl radical coordinated to a rhodium(I) centre, in contrast to an amide ligand coordinated to rhodium(II). This suggestion was corroborated by EPR spectroscopy and DFT calculations, both of which indicate that the majority of the spin density for this structure resides on the nitrogen atom. An analogous complex was reported in which a diamine ligand is oxidised to give a coordinated aminyl **1.36** where the unpaired electron is delocalised over two nitrogen atoms, with significant spin density also on the metal centre.<sup>82</sup>

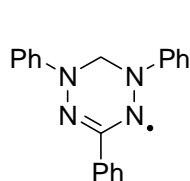
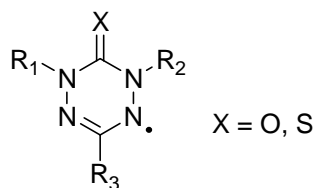
**1.35****1.36**

Aminyl complexes **1.37**, **1.38** have also been reported where a significant amount of spin density is delocalised over other parts of the ligand framework, rather than on the metal centre.<sup>83, 84</sup> These compounds involve aromatic groups directly bound to the spin-bearing nitrogen atom. Compound **1.37** presents an interesting case where there exist multiple redox-active sites within the complex; the aminyl and semiquinone ligands and the metal centre itself can all undergo redox chemistry. In fact, the authors of this paper present spectroscopic evidence for the existence of analogues in which the ligands and metal are in various oxidation states.<sup>84</sup> Compound **1.38** was structurally characterised by X-ray crystallography, and EPR studies of this complex indicate that the unpaired electron is mostly ligand-based.<sup>83</sup> The non-innocent nature of aminyl ligands provides a motivating source of academic inquiry. Furthermore, some aminyl coordination compounds are being investigated as potential oxidation catalysts, stemming from their appealing redox activity.<sup>85, 86</sup>

**1.37****1.38**

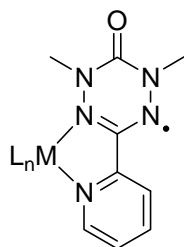
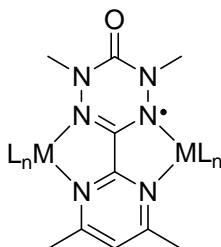
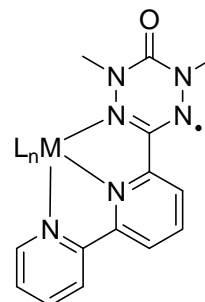
### 1.2.5 Metal-verdazyl complexes

Verdazyls are resonance-stabilised radicals in which the bulk of the spin density is delocalised over the four nitrogen atoms in the heterocyclic framework.<sup>87</sup> This leads to stability that compares favourably with what is seen in the nitroxide family. The earliest verdazyls **1.39** contain a saturated carbon<sup>88</sup> within the heterocyclic framework. 6-Oxoverdazyls and related derivatives **1.40** were developed in the 1980s and are distinguished from **1.39** by the presence of a carbonyl or thiocarbonyl group.<sup>89, 90</sup>

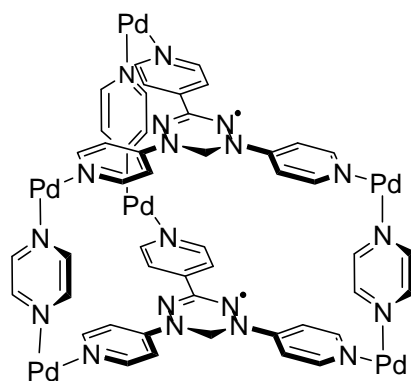
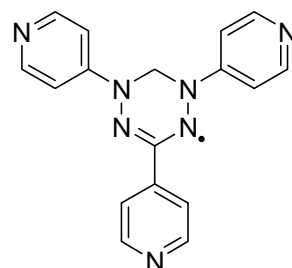
**1.39****1.40**

The synthetic approach to 6-oxoverdazyls (**1.40**, X=O) allows for the relatively straightforward incorporation of a variety of substituents at the R<sub>3</sub> position.<sup>90</sup> This, in turn, gives a facile route to an array of multidentate ligands based on the verdazyl framework. Ligand motifs based on pyridine **1.41**, pyrimidine **1.42** and bipyridine **1.43**

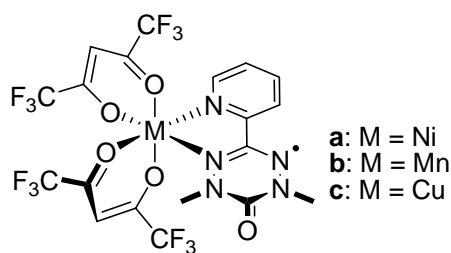
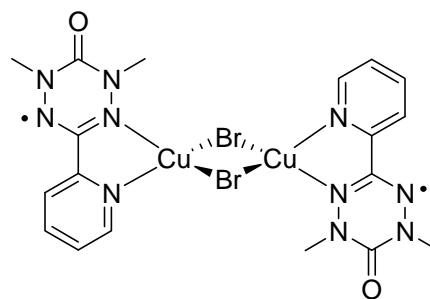
are examples of the bidentate, bis-bidentate and tridentate binding capacity of verdazyl-based radicals, respectively.

**1.41****1.42****1.43**

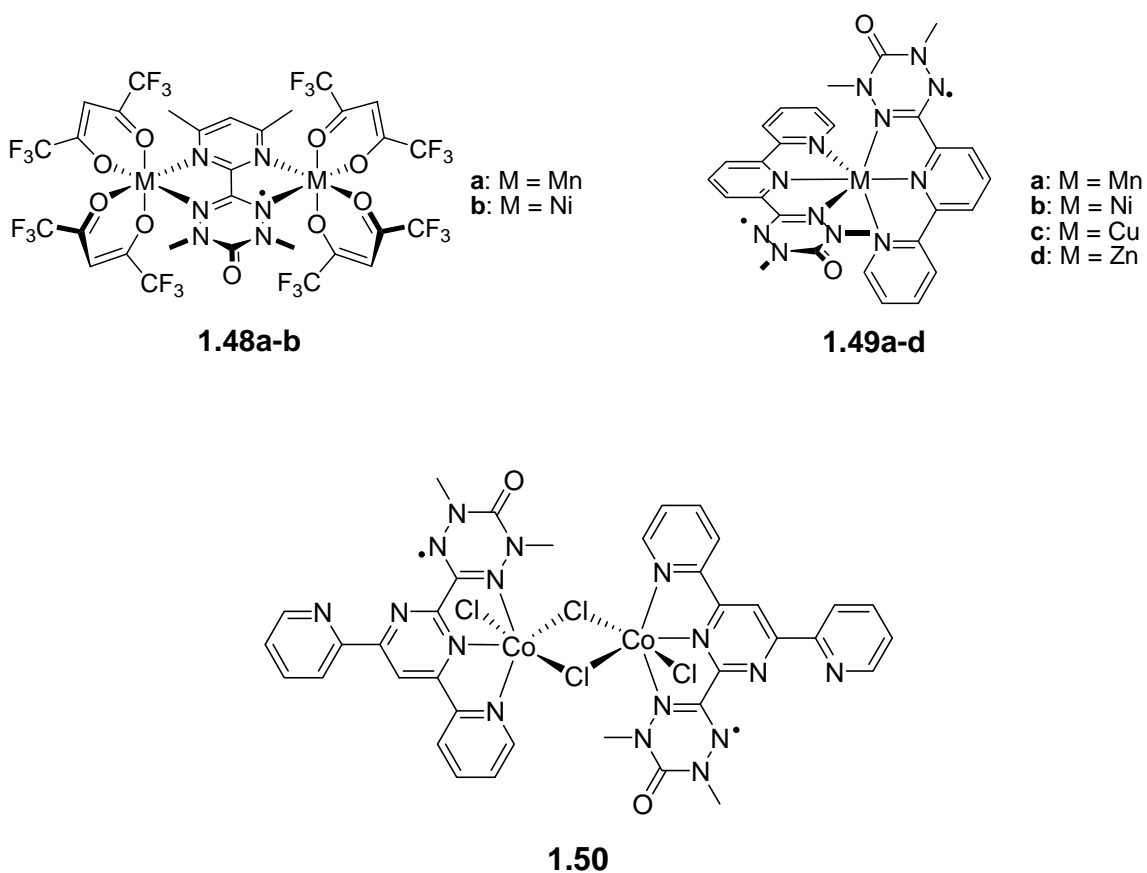
The binding modes presented above allow for the examination of direct electronic communication between the verdazyl moiety and a metal centre. This mode of direct coordination of the verdazyl nitrogen to a metal centre is found in the majority of verdazyl coordination compounds. A notable exception to this binding mode in verdazyl coordination compounds was recently reported by Fujita et al.<sup>91</sup> The 3-dimensional cage compound **1.44** features a 4-pyridyl-substituted verdazyl radical **1.45** coordinated to three Pd centres through the pyridine nitrogen atoms. This cage complex is a unique example of verdazyl coordination where the binding mode does not directly involve the verdazyl heterocycle. It also differs from the majority of verdazyl coordination compounds in that the ligand itself contains the saturated ring carbon in place of the more common carbonyl group at that position. The cage compound **1.44**, and another prepared by the same group,<sup>92</sup> were shown to enclathrate a variety of guests, including nitroxide radicals and various copper(II) complexes.

**1.44****1.45**

6-Oxoverdazyl coordination compounds involving both paramagnetic and diamagnetic metal centres have been investigated. Simple metal-radical complexes **1.46a-c** have been studied in an effort to better understand the magnetic coupling between the radical  $\pi$ -SOMO and the relevant metal  $d$ -orbitals.<sup>93, 94</sup> The nature of the magnetic exchange (ferromagnetic or antiferromagnetic) in these complexes has been shown to be highly dependent on the character of the magnetic orbital on the metal.<sup>95</sup> Diamagnetic metals have been shown to affect the spatial arrangement, and hence the magnetic coupling, between verdazyl units in compound **1.47**,<sup>96</sup> although no metal-radical coupling is possible in such systems.

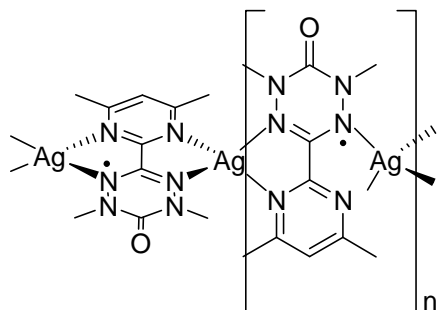
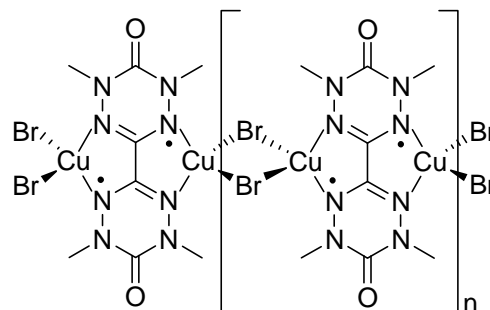
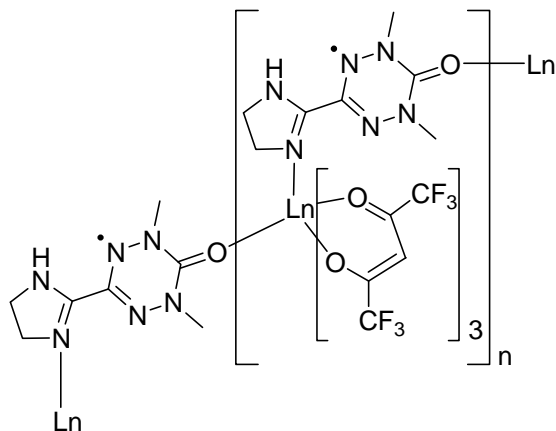
**1.46a-c****1.47**

Other examples of verdazyl coordination compounds involving more than one metal and radical have also been reported.<sup>97-99</sup> Various combinations of metals and substituted verdazyls have been employed to study magnetic interactions within the metal-radical-metal **1.48a-b**<sup>99</sup> and radical-metal-radical **1.49a-d** motifs<sup>98</sup>. Additionally, the  $\mu$ -halide bridging motif (similar to that seen in **1.47**) has been further explored using a paramagnetic metal **1.50**.<sup>97</sup>



As noted above, the main driving force behind this research has so far been to develop building blocks for new magnetic materials. However, discovering new materials requires systems that exhibit long-range magnetic ordering. To this end, a one-dimensional coordination polymer **1.51** has been reported that incorporates a

bis-bidentate pyrimidine-substituted verdazyl radical coordinated to silver(I) ions.<sup>100</sup> The diamagnetic silver ions mediate antiferromagnetic coupling between the verdazyl radicals, which is propagated along the length of the chain. Another coordination polymer **1.52** has been reported that incorporates a verdazyl diradical combined with copper(I) ions and bridging bromides.<sup>101</sup> This chain exhibits antiferromagnetic coupling between the discrete spin centres of each diradical, and also antiferromagnetic interactions among the diradical units along the chain. The first verdazyl coordination compound involving lanthanides **1.53** was recently reported.<sup>102</sup> The compound is best described as a ferrimagnetic chain that is unique because of both the metals involved and the radical coordination mode. This is the first example of 6-oxoverdazyl coordination through the carbonyl oxygen. Additionally, **1.53** represents a rare example of a verdazyl ligand that does not form a chelate ring with the metal centre, despite having another donor atom (nitrogen) in the substituent at the 3-position of the verdazyl ring.

**1.51****1.52****1.53a-c**

**a:** Ln = Gd  
**b:** Ln = Tb  
**c:** Ln = Dy

### 1.3 Thesis objectives

A great deal of the known coordination chemistry of stable radicals has been developed with an eye towards molecular magnetism. Much of the work in this area has focussed on finding suitable pairings between metals and radicals to give the best combination of strong magnetic exchange with the possibility to extend this electronic communication beyond discrete complexes. To this end, most of the work done by previous members of the Hicks research group has been aimed at studying verdazyl-metal model complexes. One of the primary goals of these studies has been to better understand the nature of the metal-verdazyl electronic communication across a range of metals.

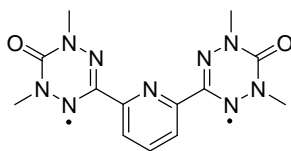
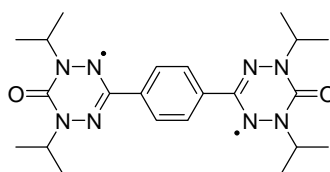
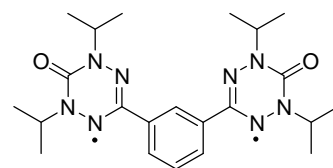


The choice to use the verdazyl radical as the basis of our research was made because of the inherent stability associated with this radical and the ease of synthetic modification, as previously discussed. At the outset of the research described herein, the 1,5-dimethyl-substituted oxoverdazyl framework (**1.40**, X=O; R<sub>1</sub>=R<sub>2</sub>=CH<sub>3</sub>) was the most familiar structural motif within our research group. Despite the stability associated with the verdazyl heterocycle, early results indicated that not all of these methyl-substituted radicals were equally stable. Furthermore, it was impossible to predict which derivatives would have great enough stability to allow for complete structural characterisation, physical property determination and a systematic study of the coordination chemistry. Georges et al. have recently established that the methyl-substituted verdazyls are prone to disproportionation reactions involving the methyl hydrogens.<sup>103</sup> These compounds are currently being investigated as potential living-radical polymerisation catalysts.<sup>104, 105</sup>

In 2005, Brook *et al.* published a synthesis of new verdazyl derivatives with isopropyl substituents in place of the methyl groups.<sup>106</sup> This modification imparts enhanced stability over the methyl-verdazyls and allowed us to revisit a number of target complexes that were otherwise too unstable for thorough investigation. The primary goal of this thesis was to employ the new synthetic methodology to create a series of N-isopropyl-substituted 6-oxoverdazyl radicals and diradicals. The superior stability of these ligands would then enable the generation of a corresponding series of metal complexes in a more predictable fashion. Ultimately, these compounds would be utilised to complete a systematic examination of the fundamental electronic relationships between the radical moieties and various metals.

The first goal of this work was to investigate the coordination chemistry and magnetism of metal-verdazyl complexes using N-isopropyl substituted 6-oxoverdazyl ligands. Early work included the synthesis and characterisation of coordination compounds involving an isopropyl derivative of the pyridine-substituted verdazyl monoradical **1.40** ( $X=O$ ,  $R_1=R_2=iPr$ ;  $R_3=2$ -pyridyl). Magnetic studies were conducted and compared with those previously reported for complexes involving the N-methyl substituted variety of this radical.<sup>94</sup>

Another highly sought-after target was the pyridine-bridged verdazyl diradical **1.54**. Exhaustive attempts (by a former graduate student in our research group) to synthesise **1.54** proved futile when working with the N-methyl based verdazyl. More recent attempts by another former group member to make phenyl-bridged N-isopropyl derivatives of this compound led to stable diradicals **1.55** and **1.56** that showed a variation in the magnetic coupling with the nature of the phenyl bridge (*meta* vs. *para*).<sup>107</sup> However, the presence of a phenyl linker limits the utility of **1.56** as a ligand in coordination chemistry. In light of this, we desired an N-isopropyl substituted version of **1.54** that would act as a stable tridentate diradical ligand. Chapter 2 details the synthesis and characterisation of the 1,5-diisopropyl-3-pyridyl-substituted verdazyl radical and diradical, and a series of related coordination compounds. Additionally, structural characterisation and magnetic studies were performed on metal complexes of both the monoradical and diradical ligands.

**1.54****1.55****1.56**

Recently our group has also become interested in the redox properties of verdazyl radicals.<sup>108</sup> Redox activity of metal complexes involving non-innocent ligands represents a growing area of research in the field of general coordination chemistry.<sup>109, 110</sup> One aspect of the current research in our group focuses on the role of verdazyls as non-innocent ligands and a number of ruthenium-verdazyl complexes have been investigated in this light.<sup>111</sup> In the course of studying magnetic coupling in the isopropyl-derivative of **1.54**, we also became interested in exploring the redox properties of this compound. Chapter 3 describes a variety of electrochemical and spectroelectrochemical studies carried out on the pyridine-bridged isopropyl diradical and the related zinc complex. In an effort to better appreciate the differences in electrochemical behaviour between mono- and diradicals, a bipyridine-substituted verdazyl monoradical was also prepared. This compound mimics the coordination environment of the diradical, but has only one unpaired electron. Analogous coordination chemistry and electrochemical studies were performed and the results compared with those from the diradical analyses.

## **Chapter 2: Structural and magnetic properties of a series of coordination compounds based on verdazyl radicals and diradicals**

### **2.1 New magnetic materials**

Magnetic components have played an important role in the evolution of device-based technology over the last 50 years. Despite the growth in the number of materials and devices that make use of this property, the actual magnetic components have not changed significantly. Today's magnets are predominantly based on metals and metal oxides.<sup>112</sup> The synthetic routes to these materials are expensive and energy-intensive. Additionally, metals are intrinsically heavier than carbon-based materials. In an age where the trend in materials and devices is to pack more technology into smaller and lighter packages, an organic approach to magnetic materials represents a new paradigm in the field.<sup>113, 114</sup>

A number of different approaches towards the design of molecule-based magnets have been established with the goal of developing new magnetic materials.<sup>115-119</sup> Purely organic strategies have focussed on organic radical polymers and crystal engineering.<sup>14, 120, 121</sup> Metal-organic hybrid materials have utilised diamagnetic bridging ligands to optimise magnetic exchange among paramagnetic metals.<sup>122-125</sup> The metal-radical approach has been developed in a similar fashion to the metal-organic hybrid framework described above, with the notable exception that the ligands in this case are also paramagnetic.<sup>126</sup> This design strategy offers further opportunities for exchange coupling among spin centres, owing to the unpaired electrons on the organic ligands. Each of these archetypes has its own inherent benefits and detracts. Exclusive use of organic

radicals offers the potential to achieve magnetic materials that could be manufactured and processed in a similar manner to commercial plastics. However, the use of organic radicals (where  $S = \frac{1}{2}$ ) as the primary building blocks limits the overall number of spins available for magnetic coupling in the ultimate material. Within the coordination network paradigm, research based on cyanide-bridged metal networks has yielded materials that show magnetic ordering at or above room temperature.<sup>127-130</sup> Although these systems have shown considerable promise in terms of utility as room temperature magnetic materials, no other organic bridging ligands have so far been shown to mediate strong inter-metal magnetic exchange. The metal-radical approach combines the benefits of carbon-based materials with the potential for enhanced magnetic exchange between paramagnetic metals and organic radical ligands. Of the various research avenues currently being explored, the metal-radical approach is the most germane to the research presented in this thesis.

## **2.2 The metal-radical approach to magnetic materials**

The metal-radical approach to designing new magnetic materials relies on magnetic coupling interactions between organic radical ligands and paramagnetic metals.<sup>126</sup> It is this use of paramagnetic organic ligands to better mediate magnetic exchange among metal centres that offers a great advantage over the diamagnetic ligands discussed in the previous section. The construction of multidimensional polymeric networks of metals and radicals (Figure 2.1) that exhibit bulk magnetic ordering represents the ultimate goal in this line of research.

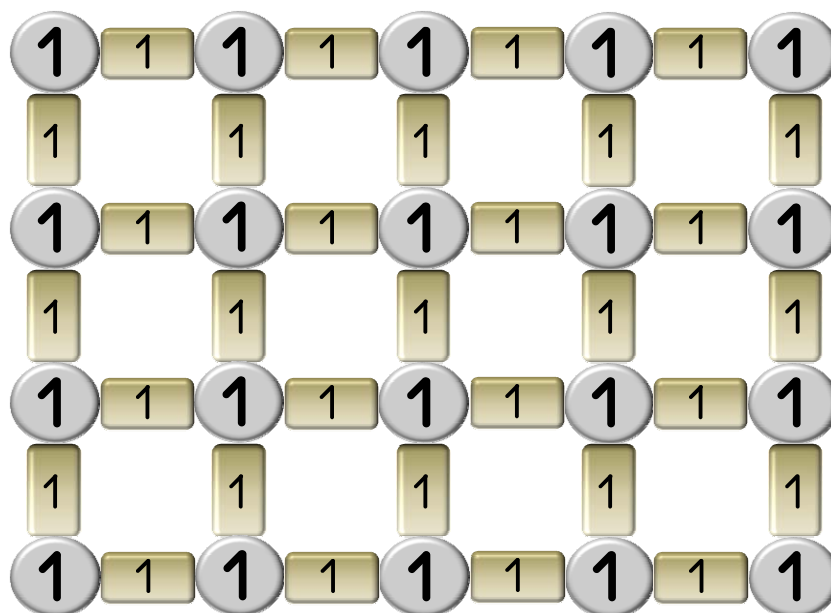


**Figure 2.1:** Schematic depiction of a coordination network composed of paramagnetic metals (circles) and organic radical ligands (rectangles) with ferromagnetically coupled magnetic moments.

Figure 2.1 is a schematic representation of an ideal metal-radical network in which all of the spins are coupled ferromagnetically, which can lead to bulk magnetic ordering. However, antiferromagnetic metal-radical interactions are also possible, and this does not necessarily preclude magnetic ordering in the bulk sample. Two factors are critical to the overall bulk magnetic properties in systems where the primary exchange mechanism is antiferromagnetic coupling: The overall topology of the coordination network, as well as the difference between spin states of the radical ligands (typically  $S = \frac{1}{2}$ ) and metal centres (typically  $S \geq \frac{1}{2}$ ) can both lead to scenarios wherein the metal spins are not fully compensated by antiferromagnetically coupled radical spins. This results in ferrimagnetism – a situation where the metal magnetic moments are coupled ferromagnetically with respect to each other – which can also give rise to bulk ordering.

Figure 2.2 presents a coordination network where antiferromagnetic coupling between metals and radicals with inequivalent magnetic moments leads to ferrimagnetism.

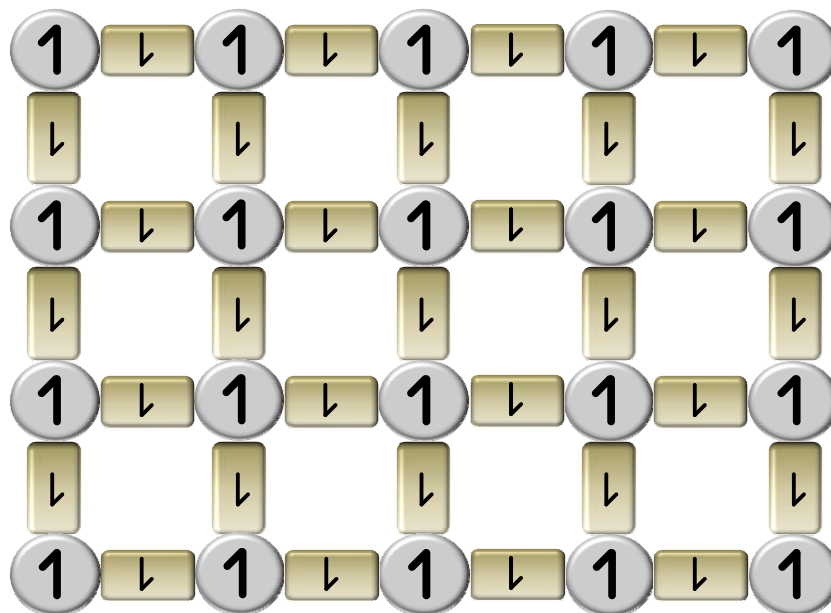


**Figure 2.2:** Hypothetical coordination network where antiferromagnetic interactions between metal centres (circles) and radical ligands (rectangles) with unequal magnetic moments leads to ferrimagnetism.

Much effort has been devoted to developing metal-radical coordination polymers and multi-dimensional networks that show magnetic ordering. The most successful ligands are based on tetracyanoethylene (TCNE) and tetracyanoquinodimethane (TCNQ) radical anions.<sup>131-133</sup> Although there are examples of TCNE-based networks that magnetically order at or above room temperature, until very recently the exact structures of such coordination networks have been poorly characterised.<sup>134</sup> This lack of structural information inhibits the ability to derive direct structure-property relationships, which is crucial in the design of new materials.

By comparison, there are relatively few examples of coordination polymers involving *neutral* organic radicals that demonstrate magnetic ordering at any temperature. To this point, the most extensively-used ligands in such complexes are based on nitroxide radicals.<sup>135-139</sup> Although certain nitroxide-based coordination compounds do show magnetic ordering, making them viable candidates for materials development, the critical temperatures are still far too low to be practically useful. Coordination polymers involving other families of radicals have been reported, but so far none have been shown to exhibit magnetic ordering.<sup>100, 102, 140</sup>

### **2.3 Metal-radical complexes as model systems in magnetic materials design**

Despite the abundance of reports on the subjects of organic ferromagnets and metal-radical coordination compounds, there remains a dearth of molecular systems whose magnetic ordering temperatures are high enough to be functionally useful. Clearly there is still a lot of room to optimise the fundamental electronic interactions between metals and radicals that lead to magnetic coupling and ultimately, magnetic ordering. A “bottom-up” approach to resolving this challenge involves the preparation and study of model compounds; small-molecules that allow the study of discrete metal-radical electronic interactions. The imminent goal of this line of attack is then to discover combinations of metals and radicals that will give strong magnetic coupling. As suitable metal-radical combinations are realised, they can be exploited to prepare systems that can be expanded into coordination polymers or multi-dimensional networks.



Model compounds of varying degrees of complexity can be envisioned that would facilitate the study of metal-radical coupling. The simplest systems are those comprising one metal and one radical (Figure 2.3a). A direct determination of the orbitals involved in magnetic exchange is then facilitated by having only one coupling interaction to consider. Larger, yet still discrete, molecular prototypes provide an opportunity to probe the coupling interactions that arise when multiple metal and radical sites are introduced. A bridging radical could be combined with two metal centres to explore metal-radical-metal coupling interactions (Figure 2.3b). Similarly, diradical coordination compounds can be used to study radical-metal-radical magnetic exchange (Figure 2.3c).

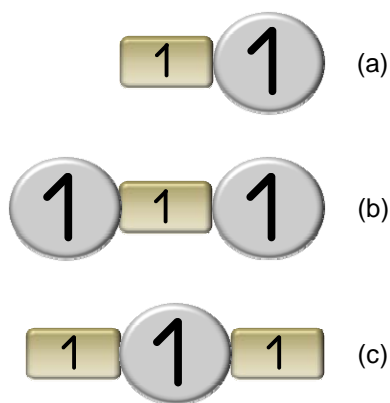


**Figure 2.3:** Schematic representation of potential model systems to investigate (a) metal-radical coupling, (b) metal-radical-metal coupling and (c) radical-metal-radical coupling.

For the purposes of model systems, an organic radical framework that is robust and amenable to synthetic modification is desirable. In this way, it is straightforward to prepare and scan a library of different radicals with the aim to tune the binding properties of the radical and enhance the electronic communication between metal and radical. Finding suitable building blocks may then greatly facilitate the pursuit of

multidimensional coordination networks that exhibit magnetic ordering at high temperatures.

The compounds presented in this chapter were designed to act as model systems to study discrete magnetic coupling interactions between different metal-radical combinations. These complexes are not meant to be expanded into coordination polymers or grids because the radicals employed are simply not bridging ligands. At this point, it is worthwhile to introduce the concept of single molecule magnetism. This phenomenon can arise in discrete molecular entities with high intrinsic spin values whereby the individual molecular entity exhibits the physical properties associated with magnetic ordering.<sup>141-144</sup> Single molecule magnets (SMMs) represent another intensely studied avenue toward the design of new magnetic materials.<sup>145</sup> While the explicit design of new SMMs is not the primary focus of this work, the fundamental knowledge gained from this study of metal-radical interactions nonetheless has the potential to be applied to a variety of purposes.

### **2.3.1 Verdazyl radical systems as model complexes for magnetic materials design**

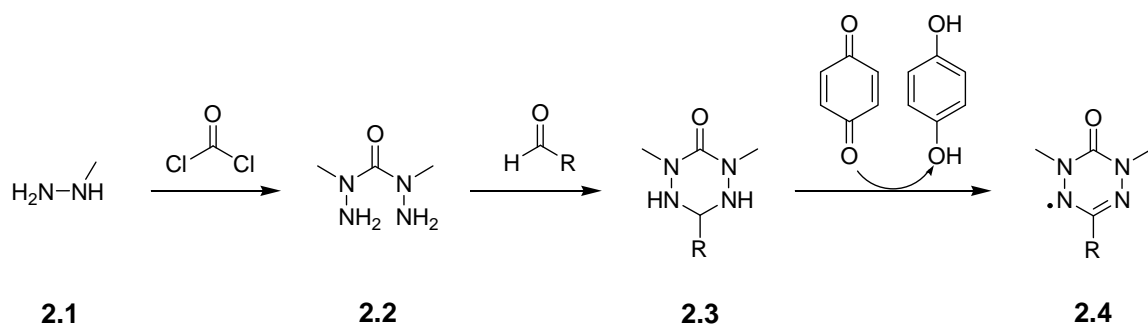
Radical stability is of paramount importance in the pursuit of new processes to design magnetic materials. Reactions that lead to the loss of unpaired electrons necessarily result in decreased magnetic character in the end material. Verdazyls, along with nitronyl nitroxides, are the most stable general family of radicals. Furthermore, the synthetic methodology used to prepare verdazyls lends itself to straightforward modification of the radical. The inherent stability and ease of synthetic variation make

this family of compounds an attractive target for use in expanding the realm of metal-radical model systems.

Verdazyl-based complexes have been the basis of metal-radical magnetic coupling studies by our group<sup>93, 94, 97-99, 146, 147</sup> and others.<sup>96, 148-150</sup> Examples of both ferromagnetic and antiferromagnetic metal-verdazyl coupling have been reported, with the nature of the magnetic exchange being dependent on the metal used. Verdazyl-based diradicals have been the subject of both theoretical<sup>151, 152</sup> and practical analyses,<sup>107, 153</sup> although so far few have been employed as ligands in coordination chemistry.<sup>101</sup>

### 2.3.2 General syntheses of 6-oxoverdazyl radicals

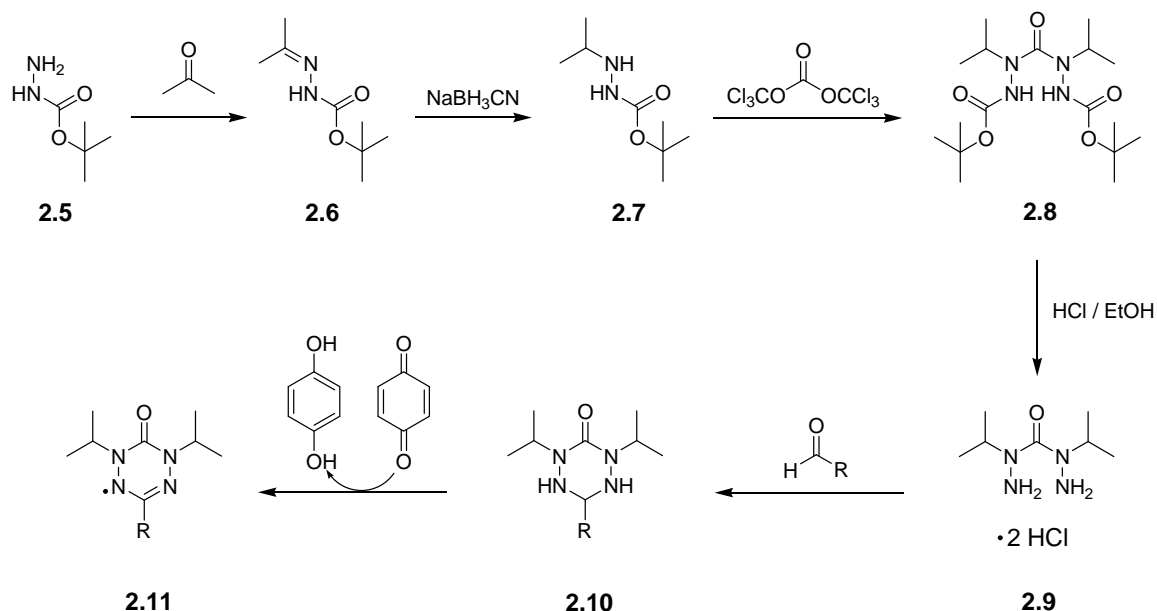
Although various sub-classes of verdazyl radicals are known (see Chapter 1), research in our group has focussed on the 6-oxoverdazyl family. At the outset of this project, all of the verdazyl radicals and associated coordination compounds studied by former group members were 1,5-dimethyl-3-substituted-6-oxoverdazyls **2.4**. A typical synthesis of 1,5-dimethyl-substituted-6-oxoverdazyls<sup>89, 90</sup> comprises the condensation of two equivalents of methylhydrazine **2.1** with one equivalent of phosgene. The resulting bis(methylhydrazide) **2.2** is then condensed with an aldehyde to give a tetrazane **2.3**, which is subsequently oxidised with *p*-benzoquinone or another suitable oxidant to give the desired verdazyl radical **2.4**. This synthetic pathway is shown in Scheme 2.1. One of the most attractive features of this synthetic scheme is that a diverse array of radicals is attainable in only a few steps from virtually any commercially available aldehyde.<sup>154-156</sup>



**Scheme 2.1:** General synthesis of 1,5-dimethyl-3-substituted-6-oxoverdazyls **2.4**.

Although the synthesis presented in Scheme 2.1 provides an efficient route to a diverse array of 6-oxoverdazyl radicals, certain limitations associated with this methodology and the resulting radicals began to arise early in this project, as has been noted by others.<sup>106, 157</sup> The primary obstacle is related to the stability of the radical. As noted in Chapter 1, N-methyl-substituted verdazyls are prone to disproportionation via a hydrogen-abstraction pathway.<sup>103, 105</sup> This reaction limits the stability of the radical building block and, as such, impedes subsequent studies of verdazyl-metal magnetic coupling. A secondary challenge is related to the availability of starting materials for this synthesis; namely, that methylhydrazine is now exceedingly difficult to purchase.

Brook's synthesis of 1,5-diisopropyl-substituted verdazyls<sup>106</sup> **2.11** presents a means to circumvent both of these problems. The route presented in Scheme 2.2 involves readily available starting materials and ultimately leads to verdazyl radicals whose stability is greatly enhanced over the 1,5-dimethyl-substituted generation. Furthermore, since the steps involved in the preparation of the tetrazane precursor and the subsequent oxidation to the radical remain intact, there is no loss in the variety of R-substituents that can be installed onto the C3-position of the verdazyl framework.



**Scheme 2.2:** Synthesis of 1,5-diisopropyl-3-substituted-6-oxoverdazyls.

The results presented in the balance of this chapter focus on the use of 1,5-diisopropyl-substituted verdazyl radicals in the synthesis and study of metal-radical model complexes. A succession of 1:1 metal:verdazyl complexes was prepared and used to investigate the magnetic coupling interactions within the series. A study of the effects of different R-substituents on magnetic coupling was achieved by comparing the N-isopropyl-substituted coordination compounds to previously reported N-methyl-substituted analogues. The general synthesis presented in Scheme 2.2 was also used to prepare a verdazyl-based diradical ligand and a corresponding series of metal complexes. Magnetic studies of the diradical and associated complexes served to extend the model system beyond the realm of discrete 1:1 metal:radical interactions.

## Results and Discussion

### 2.4 1:1 metal-verdazyl complexes

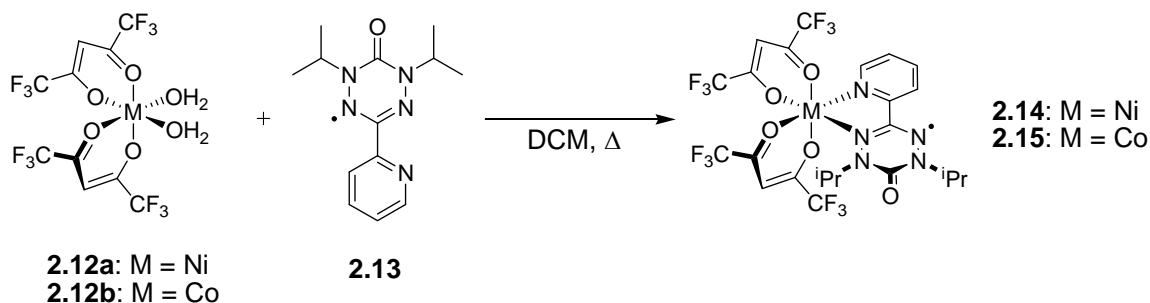
#### 2.4.1 Synthesis and characterisation of 1:1 metal-verdazyl complexes

As outlined in Chapter 1, one goal of this project was to use the new synthetic methodology outlined above to explore the coordination chemistry of N-isopropyl-substituted analogues of previously prepared verdazyl radical ligands. Specifically, the first target was the bidentate pyridine-substituted ligand **2.13**. Carbonic acid bis(1-isopropylhydrazide) **2.9** was condensed with 2-pyridinecarboxaldehyde to give the pyridine-substituted tetrazane (**2.10**, R = 2-pyridyl), as shown in Scheme 2.2. Oxidation with *p*-benzoquinone followed by purification on a column of neutral alumina (to remove any hydroquinone by-product) gave the desired pyridine-substituted verdazyl radical **2.13**. Specific synthetic details and structural characterisation of verdazyl **2.13** have been reported previously.<sup>93, 106</sup>

Radical **2.13** was used to synthesise a succession of coordination compounds according to the general methodology presented in Scheme 2.3. One equivalent each of the appropriate aquated metal bis(hexafluoroacetylacetonate) salt and **2.13** were heated together in refluxing dichloromethane to give the resulting metal-verdazyl complexes **2.14** – **2.16**. Crystallisation of **2.14** was straightforward and was accomplished by slow cooling of a saturated hexanes solution of the crude reaction product. This same method resulted in crystalline material of **2.15** only at sub-zero degree Celsius temperatures. Attempts to isolate the product at room temperature resulted in the crystals reverting to a

thick, tarry mixture. Suitable crystalline samples of **2.15** were ultimately realised using vapour diffusion methods with ethyl acetate as solvent and n-pentane as counter-solvent.

Vapour diffusion techniques yielded an exceedingly small sample of the manganese complex **2.16**, which crystallised in an anomalous manner to the nickel and cobalt compounds, **2.14** and **2.15**, respectively. The synthesis and structure of **2.16** is discussed in further detail in Section 2.4.6. The original yield of **2.16** was insufficient to allow the electronic and magnetic characterisation that is presented for **2.14** and **2.15**. Subsequent attempts to synthesise suitable samples of **2.16** were unsuccessful.



**Scheme 2.3:** Synthesis of verdazyl coordination compounds **2.14** and **2.15**.

Coordination of 6-oxoverdazyl radicals to a metal centre can be conveniently monitored by infrared spectroscopy.<sup>157, 158</sup> The stretching frequency of the carbonyl group in the radical ligand is sensitive to the electronic structure of the verdazyl heterocycle. Typically, this signal shifts to higher energy upon coordination. This trend is evident in both coordination compounds **2.14** and **2.15**. The C=O stretch is seen at  $1686\text{ cm}^{-1}$  in the free ligand **2.13**, but upon coordination the band shifts to  $1711\text{ cm}^{-1}$  in **2.14** and  $1709\text{ cm}^{-1}$  in **2.15**.

Electronic spectra for complexes **2.14** and **2.15** and radical **2.13** are compared in Figure 2.4. The absorption maximum at 410 nm in the spectrum of **2.13** represents a transition associated with the verdazyl SOMO.<sup>159</sup> For the metal complexes **2.14** and **2.15**, this absorption is red-shifted by about 20 nm. This is consistent with radical coordination to the metal centre that has been reported for analogous methyl-substituted verdazyl M(hfac)<sub>2</sub> compounds.<sup>94</sup>

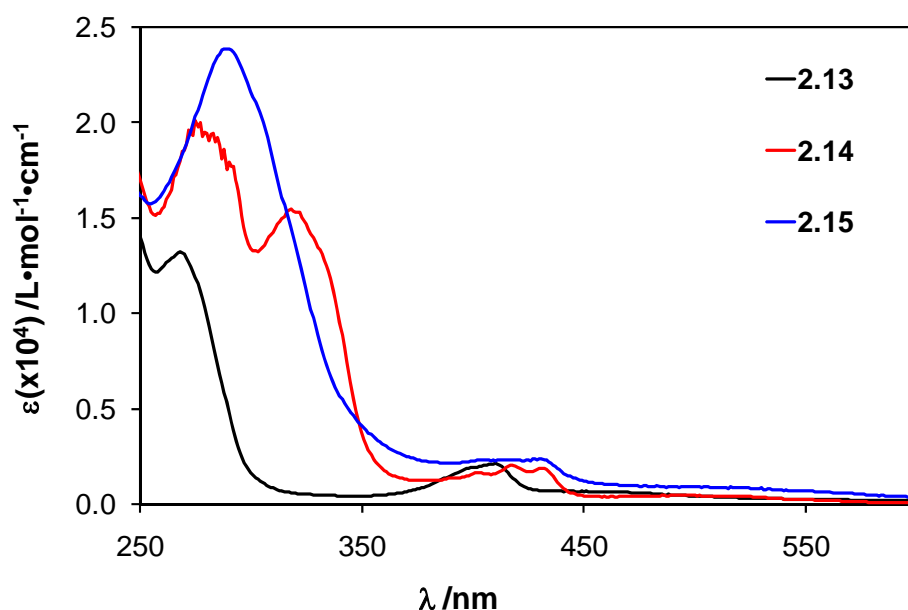


**Figure 2.4:** Electronic spectra of radical **2.13** and coordination compounds **2.14** and **2.15** in dichloromethane.

#### 2.4.2 Structural characterisation of nickel-verdazyl complex **2.14**

The molecular structure of **2.14** is shown in Figure 2.5 with selected bond lengths and angles highlighted in Table 2.1. The verdazyl heterocycle and its substituent pyridine ring are mutually coplanar. The geometry around the central nickel(II) ion is *pseudo*-octahedral and the verdazyl ligand forms a 5-membered chelate ring with the



metal centre. Bond lengths and angles around the verdazyl ligand are consistent with those reported for 1,5-dimethyl-substituted analogues of this complex,<sup>94</sup> as well as with the other metal coordination compounds reported in this section. Furthermore, the verdazyl bond lengths and angles are not significantly different from those reported for radical **2.13**.<sup>93</sup> The N4-isopropyl group (distal to the Ni<sup>2+</sup> centre) is positioned with the C5-proton aligned *syn* to the carbonyl group in the verdazyl ring, which coincides with the arrangement of these bonds in the radical itself.<sup>93, 106</sup> Conversely, the N3-isopropyl group is positioned such that the analogous methine-proton (located on C1) is *anti* to the carbonyl group to minimise steric interactions of the isopropyl group with the hexafluoroacetylacetonate ancillary ligands. With respect to the coordinative bonds in **2.14**, the pyridine nitrogen is located closer to the metal centre [Ni1-N1 = 2.040(3) Å] than the verdazyl nitrogen [Ni1-N2 = 2.120(3) Å]. This difference is common to other chelating verdazyl ligands with nitrogen-containing substituents<sup>98, 99</sup> and it underscores the difference in  $\sigma$ -donor strength between the verdazyl and pyridine nitrogen atoms.

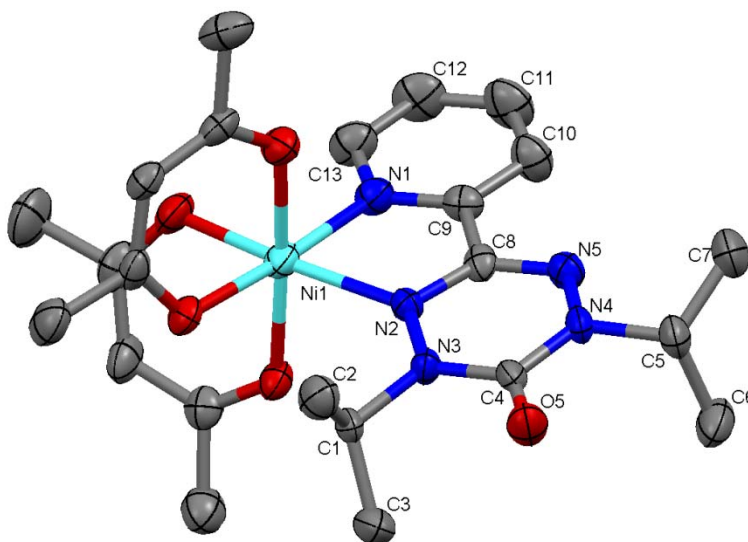


**Figure 2.5:** Molecular structure of **2.14**. Thermal ellipsoids displayed at 50% probability level. Fluorine and hydrogen atoms removed for clarity.

**Table 2.1:** Selected bond lengths (Å) and angles (degrees) for **2.14**.

Atoms	Length (Å)	Atoms	Angle (°)
C4-O5	1.219(5)	N3-C4-N4	114.7(4)
C4-N3	1.378(5)	N2-C8-N5	127.5(4)
C4-N4	1.382(5)	Ni1-N1-C9	116.5(3)
C8-C9	1.480(5)	Ni1-N2-C8	112.8(3)
C8-N2	1.341(5)	N3-N2-C8	115.3(3)
C8-N5	1.316(5)	N2-N3-C4	122.9(4)
N2-N3	1.370(4)	N5-N4-C4	124.5(4)
N4-N5	1.367(4)	N4-N5-C8	114.5(4)
Ni1-N1	2.040(3)	N1-Ni1-N2	78.78(14)
Ni1-N2	2.120(3)		

### 2.4.3 Magnetic properties of nickel-verdazyl complex **2.14**

Magnetic properties of **2.14** were measured from 300 – 2 K and the results are displayed in Figure 2.6. The product of magnetic susceptibility and temperature ( $\chi T$ ) at 300 K is 1.76 emu•K•mol<sup>-1</sup>. This value is higher than the expected spin-only value of 1.38 emu•K•mol<sup>-1</sup> for two uncoupled spins of  $S = 1$  and  $S = \frac{1}{2}$  (with the spin-only value

calculated assuming a g-value of 2.00). As temperature is lowered from 300 to 68 K,  $\chi T$  gradually increases. Between 68 and 25 K, the data plateaus at a maximum value of  $1.98 \text{ emu}\cdot\text{K}\cdot\text{mol}^{-1}$ . Below 25 K,  $\chi T$  decreases rapidly. The observed magnetic behaviour is qualitatively consistent with a previous report for the 1,5-dimethyl-substituted analogue of this complex.<sup>94</sup>

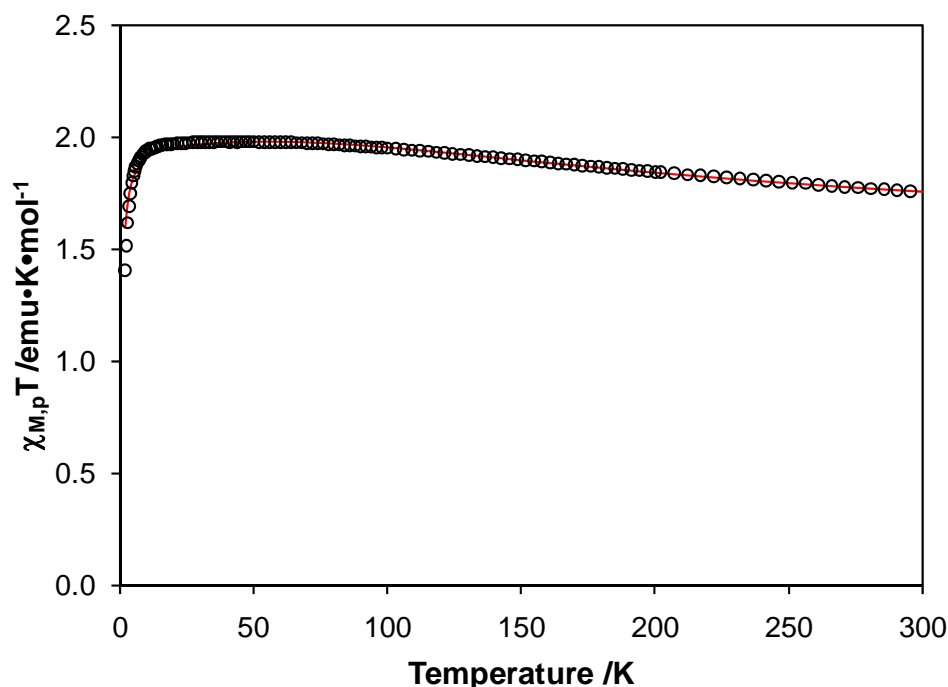


**Figure 2.6:**  $\chi T$  vs.  $T$  for **2.14** between 300 and 2 K. Experimental data ( $\circ$ ) and calculated model fit ( $-$ ).

The solid red line in Figure 2.6 represents the curve calculated from Equation 2.1 (see Appendix D for raw magnetic data and derivation of magnetic models) with the following parameters:  $g_{\text{vd}} = 2.00$ ,  $g_{\text{Ni}} = 2.10$ ,  $J = +140 \text{ cm}^{-1}$  and  $\theta = -0.5 \text{ K}$ . The model gave a goodness of fit factor of  $R = 0.014$  (with goodness of fit calculated as  $R = [\Sigma(\chi_{\text{obs}} - \chi_{\text{calc}})^2 / \Sigma\chi_{\text{obs}}^2]^{1/2}$ ). At 300 K, the  $\chi T$  value of  $1.76 \text{ emu}\cdot\text{K}\cdot\text{mol}^{-1}$  is slightly lower than the spin-only value for an  $S = 3/2$  system ( $1.88 \text{ emu}\cdot\text{K}\cdot\text{mol}^{-1}$ ), which would

result from ferromagnetic coupling of the  $S = 1$   $\text{Ni}^{2+}$  ion with the  $S = \frac{1}{2}$  verdazyl radical. This  $\chi T$  value implies that at 300 K there is some population of uncoupled excited states. On lowering the temperature, these states become depopulated, and the ferromagnetically coupled ground state becomes the predominant intramolecular magnetic interaction. The sharp decrease in  $\chi T$  observed in the low temperature regime can be explained by intermolecular antiferromagnetic interactions and/or zero-field splitting of the nickel  $d$ -orbitals. These interactions were modelled by introducing a Weiss constant,  $\theta$ , in Equation 2.1.

$$\chi = \frac{N\beta^2}{4k(T-\theta)} \frac{10g_1^2 \exp\left(\frac{15J}{8kT}\right) + g_2^2 \exp\left(\frac{3J}{8kT}\right)}{2\exp\left(\frac{15J}{8kT}\right) + \exp\left(\frac{3J}{8kT}\right)} \quad (2.1)$$

$$g_1 = \frac{g_{\text{Vd}} + 2g_{\text{Ni}}}{3} \quad g_2 = \frac{-g_{\text{Vd}} + 4g_{\text{Ni}}}{3}$$

#### 2.4.4 Structural characterisation of cobalt-verdazyl complex **2.15**

The molecular structure of **2.15** is shown in Figure 2.7, with selected bond lengths and angles presented in Table 2.2. Compound **2.15** shares many of the same structural characteristics with its  $\text{Ni(II)}$  analogue **2.14**. The two six-membered rings comprising the radical ligand are again mutually coplanar. The geometry around the central cobalt(II) ion is *pseudo*-octahedral, with the metal ion sitting just above the plane of the verdazyl radical. A 5-membered chelate ring incorporates Co1 and the N1-C9-C8-N2 fragment of the verdazyl ligand. Alternation of the positioning of the N-substituted isopropyl groups (with H1C *anti* to the C4-O5 carbonyl group and H5C *syn* to this group) is also seen in **2.15**. The difference in bond lengths between the two N-N bonds of the verdazyl ring is slightly more pronounced in **2.15** [ $\text{N2-N3} = 1.365(4) \text{ \AA}$ ;  $\text{N4-N5} = 1.347(5) \text{ \AA}$ ] than what

is seen in nickel complex **2.14**. A similar discrepancy in the coordinative bonds to the metal centre is seen with cobalt complex **2.15** [Co1-N1 = 2.092(3) Å; Co1-N2 = 2.163(3) Å] as was evident with nickel complex **2.14**; again this highlights the difference in  $\sigma$ -donor strength between the two different coordinating nitrogen atoms in the ligand.

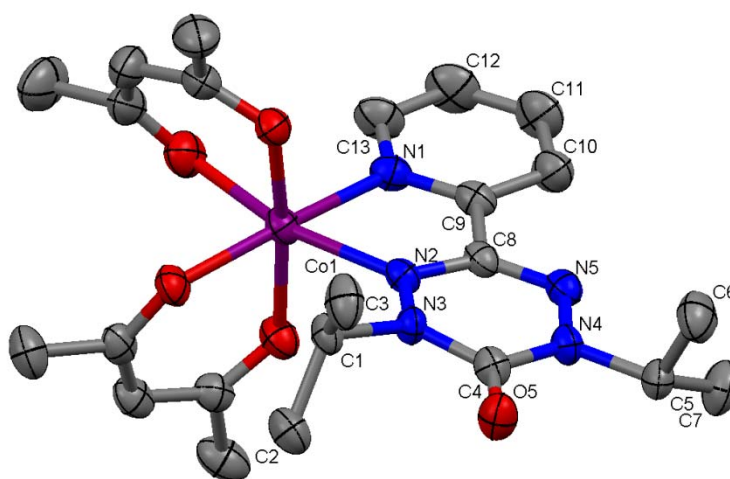


**Figure 2.7:** Molecular structure of **2.15**. Thermal ellipsoids displayed at 50% probability level. Fluorine and hydrogen atoms removed for clarity.

**Table 2.2:** Selected bond lengths (Å) and angles (degrees) for **2.15**

Atoms	Length (Å)	Atoms	Angle (°)
C4-O5	1.209(5)	N3-C4-N4	113.8(3)
C4-N3	1.387(5)	N2-C8-N5	127.4(4)
C4-N4	1.389(5)	Co1-N1-C9	117.5(3)
C8-C9	1.485(6)	Co1-N2-C8	114.4(3)
C8-N2	1.339(5)	N3-N2-C8	114.9(3)
C8-N5	1.308(5)	N2-N3-C4	123.2(3)
N2-N3	1.365(4)	N5-N4-C4	124.5(3)
N4-N5	1.347(5)	N4-N5-C8	115.3(3)
Co1-N1	2.092(3)	N1-Co1-N2	76.52(12)
Co1-N2	2.163(3)		

### 2.4.5 Magnetic properties of **2.15**

Magnetic properties of **2.15** were measured from 300 – 2 K and the results are displayed in Figure 2.8. At 300 K,  $\chi T$  is  $3.26 \text{ emu}\cdot\text{K}\cdot\text{mol}^{-1}$ , which is much higher than the expected spin-only value of  $2.25 \text{ emu}\cdot\text{K}\cdot\text{mol}^{-1}$  for two uncoupled spin systems of  $S = 3/2$  and  $S = 1/2$ . This value gradually increases as temperature is lowered from 300 to 84 K. Between 84 and 72 K,  $\chi T$  stays at a maximum value of  $3.49 \text{ emu}\cdot\text{K}\cdot\text{mol}^{-1}$  before decreasing at temperatures below 72 K.

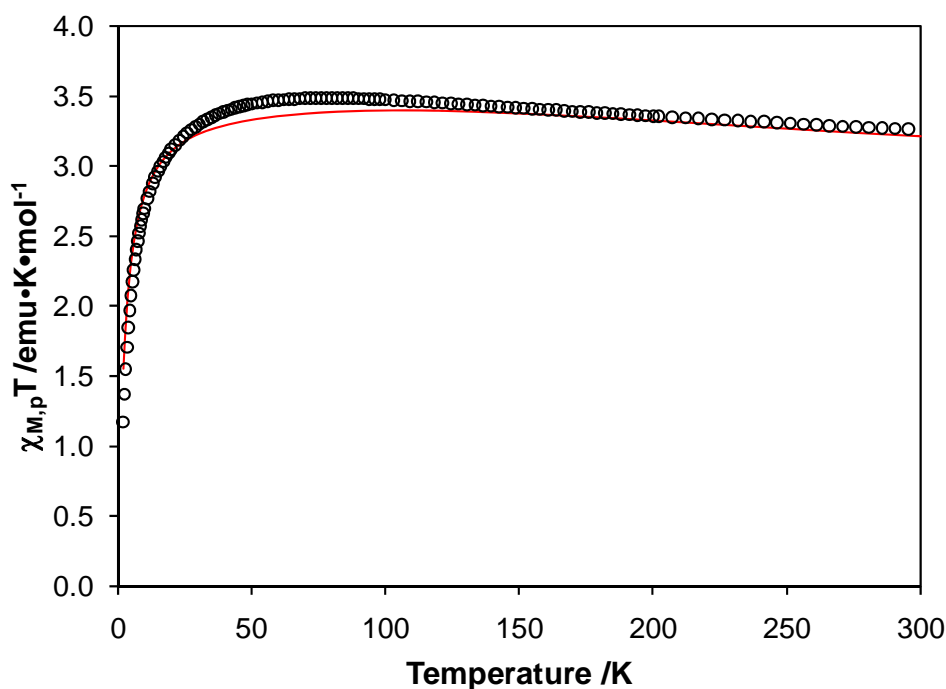


**Figure 2.8:**  $\chi T$  vs.  $T$  for **2.15** between 300 and 2 K. Experimental data (○) and calculated model fit (—).

Magnetic data for **2.15** was modelled (solid red line in Figure 2.8) with Equation 2.2 using the following parameters:  $g_{\text{vd}} = 2.00$ ,  $g_{\text{Co}} = 2.24$ ,  $J = +155 \text{ cm}^{-1}$  and  $\theta = -2.5 \text{ K}$ . The model gave a goodness of fit factor of  $R = 0.034$ . These parameters are consistent

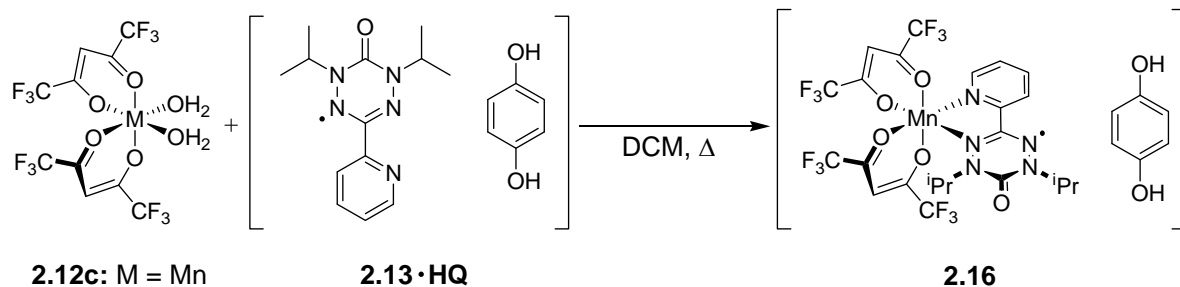
with an  $S = 3/2$   $\text{Co}^{2+}$  ion that is strongly ferromagnetically coupled to an  $S = 1/2$  verdazyl. This assignment is further validated by the fact that the room temperature moment for **2.15** is higher than the expected moment for an  $S = 2$  spin system ( $\chi T = 3.00 \text{ emu}\cdot\text{K}\cdot\text{mol}^{-1}$ ), implying that the ferromagnetically coupled ground state is fully populated at this temperature. Previously reported cobalt-verdazyl coordination compounds have been shown to exhibit ferromagnetic exchange between  $\text{Co}^{2+}$  and coordinated verdazyl radicals.<sup>97, 147</sup> Cobalt complexes incorporating a different radical but the same ancillary ligands and similar coordination geometry have also been reported to exhibit ferromagnetic cobalt-radical coupling.<sup>74</sup> Octahedral cobalt complexes are known to have large spin-orbit coupling parameters, which can exacerbate the difficulties in modelling the magnetic data.<sup>160, 161</sup> The model described by Equation 2.2 and the above parameters does not account for any spin-orbit coupling interactions associated with the cobalt ion and, as such, can only be considered as an estimate of the true metal-verdazyl exchange interactions in **2.15**.

$$\chi = \frac{2N\beta^2}{k(T-\theta)} \frac{5g_1^2 \exp\left(\frac{3J}{kT}\right) + g_2^2 \exp\left(\frac{J}{kT}\right)}{5 \exp\left(\frac{3J}{kT}\right) + 3 \exp\left(\frac{J}{kT}\right)} \quad (2.2)$$

$$g_1 = \frac{g_{\text{vd}} + 3g_{\text{Co}}}{4} \quad g_2 = \frac{-g_{\text{vd}} + 5g_{\text{Co}}}{4}$$

#### 2.4.6 Structural characterisation of manganese-verdazyl complex **2.16**

Attempts to coordinate radical **2.13** to manganese resulted in the product complex **2.16**, which crystallised as a 1:1 adduct with *p*-hydroquinone (Scheme 2.4). The source of the hydroquinone is apparently from insufficient purification of verdazyl **2.13** prior to conducting the coordination reaction.



**Scheme 2.4:** Synthesis of compound **2.16**, crystallised with hydroquinone.

The molecular structure of compound **2.16** is shown in Figure 2.9. Selected bond lengths and angles for **2.16** are given in Table 2.3. The complex crystallised with molecules of both hydroquinone and *n*-pentane in the unit cell.

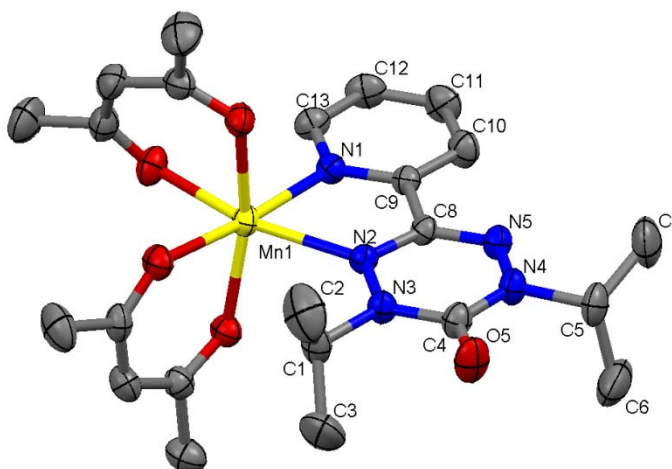


**Figure 2.9:** Molecular structure of manganese complex **2.16**. Thermal ellipsoids displayed at the 50% probability level. Fluorine and hydrogen atoms removed for clarity. Atoms associated with *n*-pentane and *p*-hydroquinone have also been removed.



**Table 2.3:** Selected bond lengths (Å) and angles (degrees) for **2.16**.

Atoms	Length (Å)	Atoms	Angle (°)
C4-O5	1.211(2)	N3-C4-N4	114.83(17)
C4-N3	1.380(3)	N2-C8-N5	127.08(17)
C4-N4	1.373(3)	Mn1-N1-C9	118.19(12)
C8-C9	1.487(3)	Mn1-N2-C8	116.21(12)
C8-N2	1.334(2)	N3-N2-C8	115.08(15)
C8-N5	1.318(2)	N2-N3-C4	123.14(16)
N2-N3	1.366(2)	N5-N4-C4	124.16(16)
N4-N5	1.351(2)	N4-N5-C8	115.42(16)
Mn1-N1	2.2140(16)	N1-Mn1-N2	73.14(16)
Mn1-N2	2.2623(15)		

The verdazyl heterocycle and its substituent pyridine ring are mutually coplanar. The geometry around the central manganese(II) ion is *pseudo*-octahedral, which is consistent with the previously reported 1,5-dimethyl-substituted analogue of this complex.<sup>94</sup> The manganese(II) centre sits just above the plane of the verdazyl radical and forms a 5-membered chelate ring with N1-C9-C8-N2. The two N-substituted isopropyl groups are again positioned with the C5-proton aligned *syn* to the carbonyl group in the verdazyl ring, and the C1-proton *anti* to this same group. This positional alternation is common to all of the **2.13M**(hfac)<sub>2</sub> complexes discussed in this section.

An examination of the bond lengths around the verdazyl ring reveals that the two N-N bonds differ by only 0.015 Å [N2-N3 = 1.366(2) Å; N4-N5 = 1.351(2) Å]. The C-N bonds at the carbonyl carbon (C4) in the verdazyl ring are also almost identical in length [C4-N3 = 1.380(3) Å; C4-N4 = 1.373(3) Å]. There is a small difference in the C-N bond lengths at the point of pyridine-substitution [C8-N2 = 1.334(2) Å; C8-N5 = 1.318(2) Å]. These results, in addition to the various bond angles in the verdazyl moiety, are consistent with those previously reported for analogous verdazyl coordination compounds.<sup>94</sup> A

disparity in the coordinative N-M bond lengths is seen in **2.16**, similar to what was noted in the analogous nickel and cobalt complexes (**2.14** and **2.15**, respectively). The pyridine nitrogen is slightly closer to the metal centre [Mn1-N1 = 2.2140(16) Å] than is the verdazyl nitrogen [Mn1-N2 = 2.2623(15) Å].

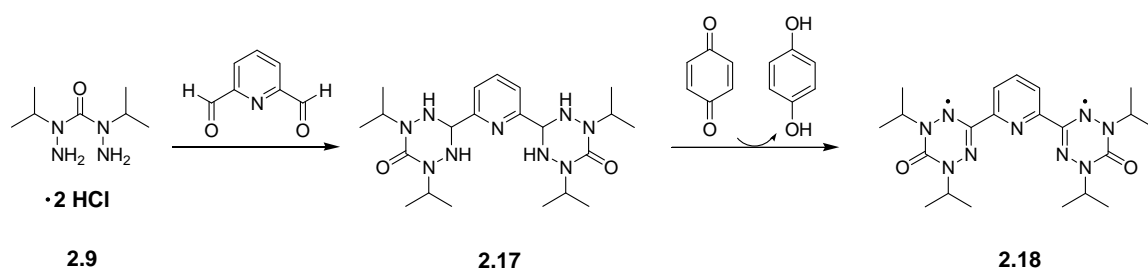
## 2.5 Synthesis and magnetic characterisation of a verdazyl-based diradical and associated coordination compounds

In an effort to further expand the breadth of metal-verdazyl model systems and move beyond discrete 1:1 metal:radical complexes, a new verdazyl-based diradical ligand was prepared. This ligand was subsequently coordinated to a series of first-row transition metals. The verdazyl diradical and the product complexes were analysed with respect to their structural and magnetic properties. The majority of complexes in this series exhibit *pseudo*-trigonal bipyramidal geometry, which represents a novel coordination environment for metal-verdazyl complexes.

### 2.5.1 Synthesis of verdazyl diradical **2.18**

A pyridine-bridged diradical derived from the 1,5-dimethyl-substituted verdazyl moiety (compound **1.54**) was reported in 2004.<sup>155</sup> However, this compound proved to be one of the least stable verdazyl species investigated by previous members of our research group. As such, full characterisation of this compound (including elemental and X-ray diffraction analysis) has not been reported. An investigation of the coordination chemistry of **1.54** was also precluded by its inherent instability. An N-isopropyl-substituted analogue of this diradical was prepared, as shown in Scheme 2.5, which shows greatly enhanced stability over **1.54**. Two equivalents of **2.9** were condensed with

2,6-pyridine dicarboxaldehyde to give the tetrazane precursor **2.17**. Tetrazane **2.17** was then oxidised with three equivalents of *p*-benzoquinone to give diradical **2.18**. Diradical **2.18** was purified on neutral alumina to remove the hydroquinone by-product and recrystallised by slow-cooling of a saturated ethyl acetate solution.



**Scheme 2.5:** Synthesis of diradical **2.18**.

### 2.5.2 Structural characterisation of diradical **2.18**

In the absence of using conventional nuclear magnetic resonance techniques to follow reactions involving verdazyl radicals, infrared spectroscopy provides a convenient means of assessing reaction progress. The C=O bond stretching frequency shows a distinct shift to higher energy upon oxidation; from  $1615\text{ cm}^{-1}$  in tetrazane **2.17** to  $1683\text{ cm}^{-1}$  in diradical **2.18** (Figure 2.10). Additionally, the broad N-H stretching band around  $3240\text{ cm}^{-1}$  in the spectrum of tetrazane **2.17** is not present in the spectrum of **2.18**, indicating the absence of N-H bonds in the diradical.

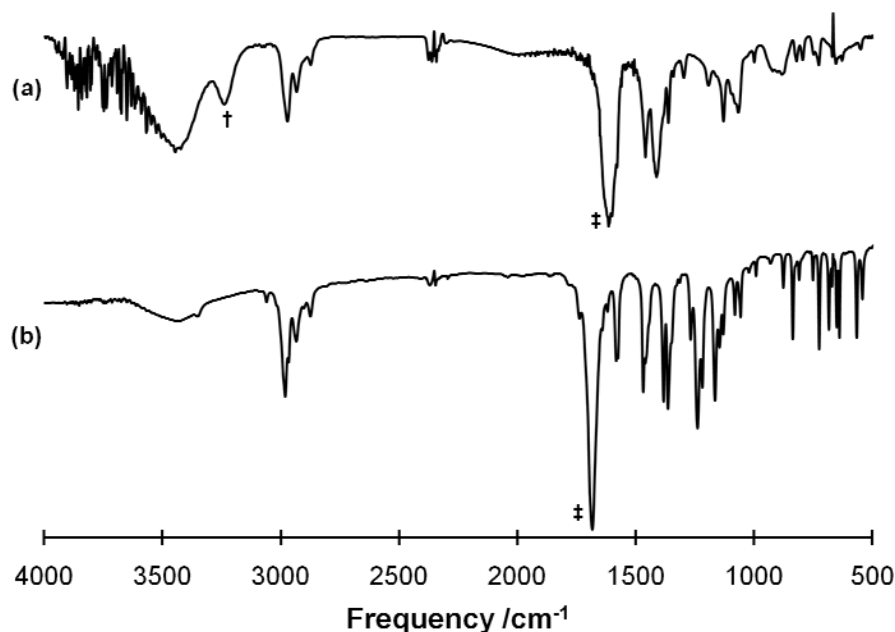


**Figure 2.10:** Infrared spectra of (a) tetrazane **2.17** and (b) diradical **2.18** recorded as pressed KBr disks with air background. Carbonyl band in both (a) and (b) indicated by ‡; N-H band in (a) indicated by †.

The molecular structure of diradical **2.18** is presented in Figure 2.11, with selected bond lengths and angles given in Table 2.4. The two verdazyl rings are coplanar and together are twisted  $14.10^\circ$  with respect to the plane of the central pyridine ring. Bond lengths around the verdazyl rings are consistent with those reported for the 1,5-diisopropyl-3-pyridyl-substituted verdazyl monoradical **2.13**. The two N-N bond lengths in **2.18** are virtually identical [ $N2-N4 = 1.365 \text{ \AA}(2)$ ;  $N3-N5 = 1.3646(19) \text{ \AA}$ ], as are the C-N bonds involving the carbonyl carbon [ $C5-N4 = 1.373(3) \text{ \AA}$ ;  $C5-N5 = 1.374(3) \text{ \AA}$ ]. The C-N bonds at the pyridine-substituted carbon are similarly close in length [ $C4-N2 = 1.331(2) \text{ \AA}$ ;  $C4-N3 = 1.325(2) \text{ \AA}$ ]. Bond angles within the verdazyl ring likewise reflect those reported for the monoradical analogue.

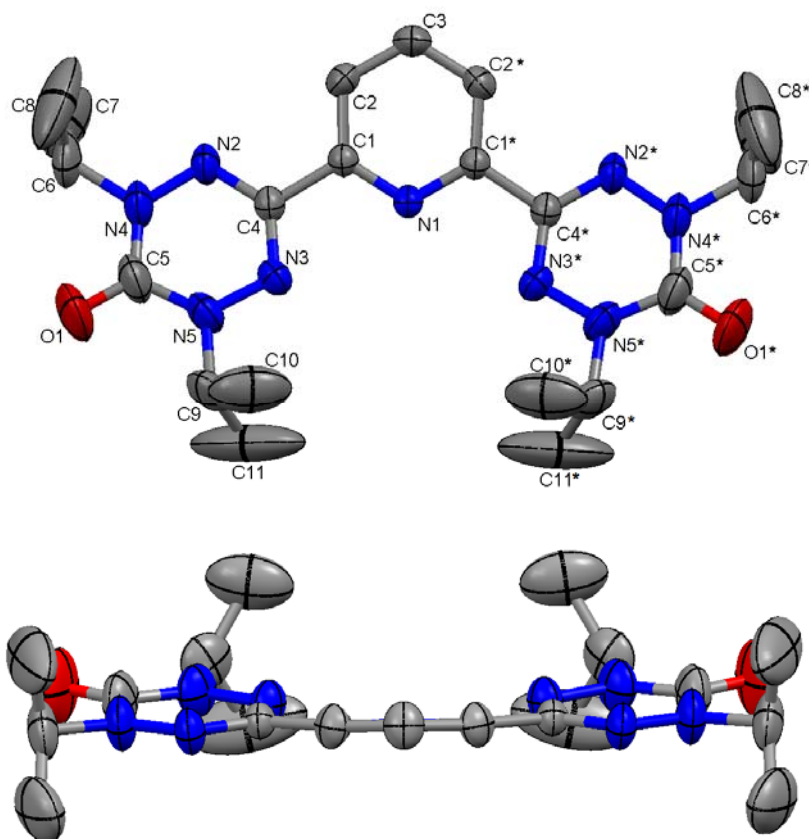


**Figure 2.11:** Face-on (top) and edge-on (bottom) view of the molecular structure of **2.18**. Thermal ellipsoids displayed at 50% probability level. Hydrogen atoms removed for clarity.

**Table 2.4:** Selected bond lengths (Å) and angles (degrees) for **2.18**.

Atoms	Length (Å)	Atoms	Angle (°)
C1-C4	1.490(2)	N2-C4-N3	127.13(14)
C4-N2	1.331(2)	N4-C5-N5	114.03(16)
C4-N3	1.325(2)	C4-N2-N4	115.06(15)
C5-O1	1.214(2)	C4-N3-N5	114.57(14)
C5-N4	1.373(3)	N2-N4-C5	124.10(15)
C5-N5	1.374(3)	N3-N5-C5	124.81(17)
N2-N4	1.365(2)		
N3-N5	1.3646(19)		

A partial view of the packing among individual diradical **2.18** molecules is presented in Figure 2.12. Although there are no close contacts between nitrogen atoms (which bear the majority of the spin density associated with the verdazyl moiety), Figure 2.12 shows selected close contact points between atoms that have been shown to have non-zero spin density in 1,5-diisopropyl-substituted-6-oxoverdazyl radicals.<sup>107</sup> These contact points can have implications for the low temperature magnetic properties of this diradical as they provide a possible pathway for intermolecular exchange interactions. The magnetic properties of **2.18** are discussed in detail in Section 2.5.4.

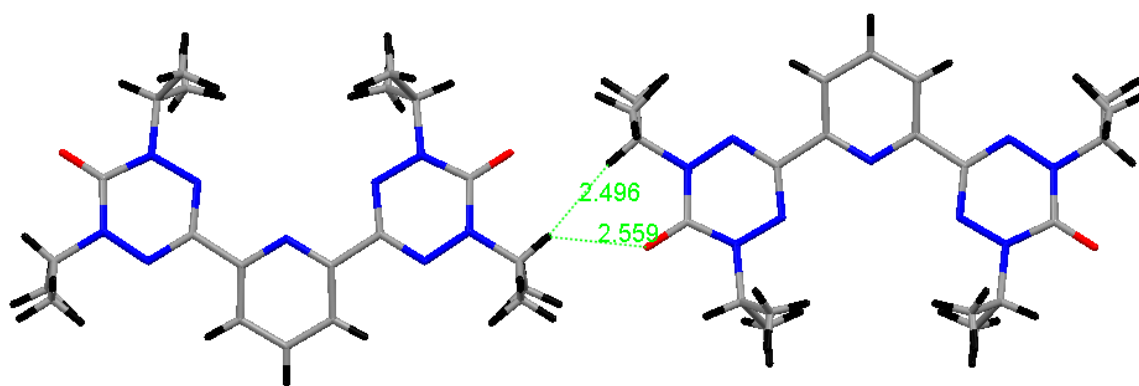


**Figure 2.12:** Partial view of the crystal packing of **2.18** showing close contact points between selected atoms with non-zero spin density.

### 2.5.3 Solution-phase electronic properties of diradical **2.18**

The electron paramagnetic resonance (EPR) spectrum for compound **2.18** is shown in Figure 2.13. The spectrum was recorded on a frozen toluene solution of **2.18** at 77 K. The experimental EPR spectrum consists of a broad multiplet, characteristic of diradicals. Although the simulated spectrum is not an exact match of the experiment, the position of the maxima and minima in the two spectra correspond well (save for the signal due to monoradical impurity, highlighted in the centre of the experimental

spectrum). The simulated spectrum gives the following parameters for **2.18**:  $g = 2.00942$ ,  $|D/hc| = 0.00756 \text{ cm}^{-1}$ ,  $|E/hc| = 0.000218 \text{ cm}^{-1}$ . The parameters  $D$  and  $E$  are zero-field splitting parameters that are commonly reported with EPR spectra of organic diradicals.<sup>162-167</sup> Furthermore,  $D$  is a measure of the dipolar interaction between the two unpaired electrons in a diradical and is related to the distance between these two electrons according to Equation 2.3, where  $\rho$  represents the spin density associated with each radical site and  $d_{a,b}$  is the distance between the unpaired electrons.<sup>168, 169</sup> With respect to the benzene-bridged verdazyl diradicals **1.55** and **1.56**,  $|D/hc| = 0.00210 \text{ cm}^{-1}$  for the *para*-substituted diradical **1.55** and  $0.00348 \text{ cm}^{-1}$  for the *meta*-substituted diradical **1.56**.<sup>107</sup> The larger values of  $|D/hc|$  for diradicals **1.56** and **2.18**, compared with that for **1.55**, correspond to a smaller distance between unpaired electrons in the *meta*-bridged diradicals versus that in the *para*-substituted analogue.

$$D = \frac{3\mu_0 g^2 \beta^2}{16\pi} \frac{\rho_a \rho_b}{d_{a,b}^3} \quad (2.3)$$

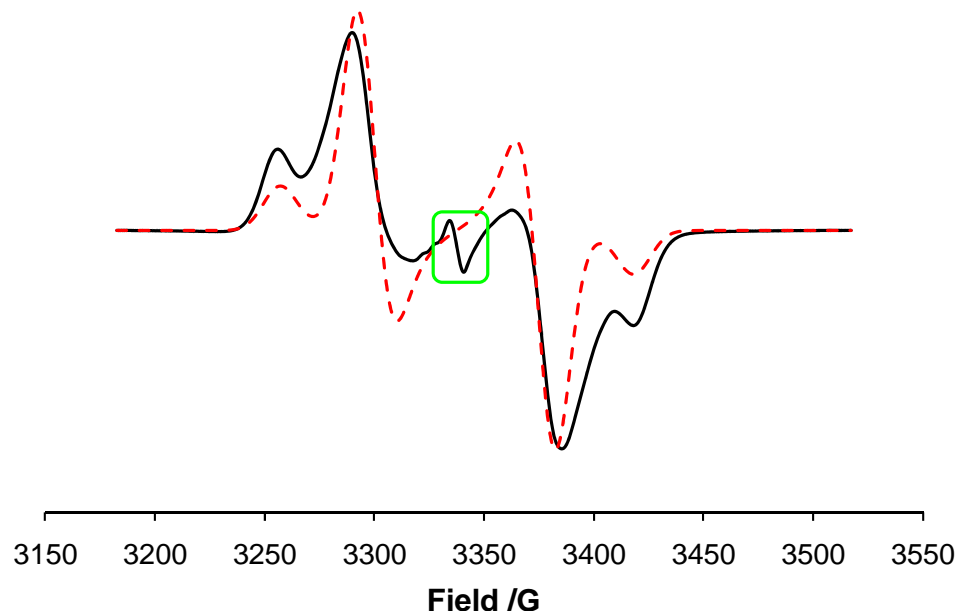


**Figure 2.13:** Experimental (solid line) and simulated (dashed red line) X-band EPR spectra of diradical **2.18** in frozen toluene (77 K). Highlighted (green box) signal in experimental spectrum is due to  $S = \frac{1}{2}$  impurity in the sample.

The intensity of the (formally forbidden) triplet signal ( $\Delta m_s = 2$ ) for **2.18** at half-field was plotted against inverse temperature between 90 and 5 K (Figure 2.14). The linear relationship in this Curie plot can be interpreted two ways: The unpaired electrons of the verdazyl moieties are ferromagnetically coupled, or the respective energies of the singlet and triplet state are degenerate. This distinction is further probed through the study of the solid state magnetic properties of **2.18**, which are discussed in Section 2.5.4.



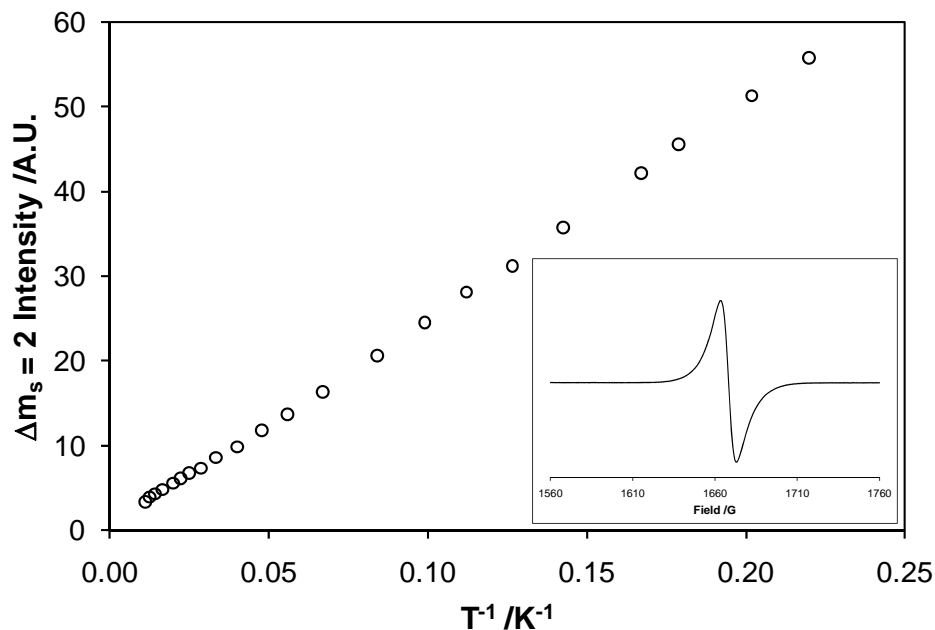


**Figure 2.14:** Curie plot of the intensity of  $\Delta m_s = 2$  signal for **2.18** between 4.5 and 90 K. Inset:  $\Delta m_s$  signal centred at 1667 G.

The electronic spectrum of **2.18** in dichloromethane solution is presented in Figure 2.15, along with the spectrum of monoradical **2.13** for comparison. The absorption maxima at 410 and 460 nm in the spectrum of **2.18** coincide with those reported for other 6-oxoverdazyl diradicals.<sup>107, 153</sup> Previous reports have asserted that the distinct SOMOs in aryl-bridged verdazyl diradicals experience little mutual conjugation, owing to the fact that the aryl substituent is located at a nodal point of the verdazyl SOMO.<sup>107</sup> This claim is further substantiated when comparing  $\lambda_{\text{max}}$  values for the pyridine-substituted verdazyl monoradical **2.13** (409 and 450 nm)<sup>106</sup> and diradical **2.18** (410 and 460 nm). The minor differences between these absorptions in the monoradical versus the diradical imply that there is effectively no electronic communication between the verdazyl SOMOs.

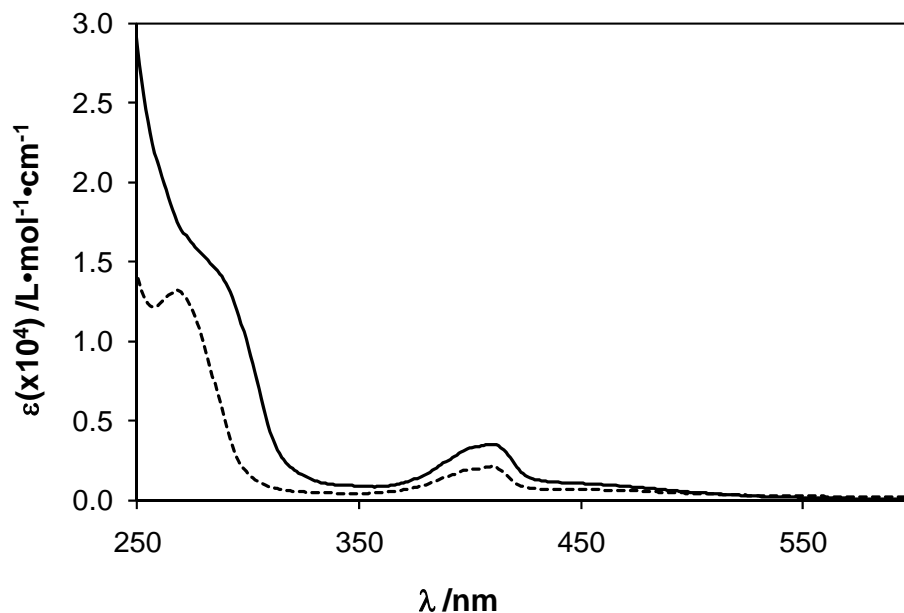


**Figure 2.15:** UV-Vis spectra of monoradical **2.13** (dashed line) and diradical **2.18** (solid line) in dichloromethane.

#### 2.5.4 Magnetic properties of diradical **2.18**

The magnetic properties of **2.18** were recorded between 300 and 2 K and the results are displayed in Figure 2.16. The data was corrected for diamagnetism by subtracting the slope of the line in the paramagnetic regime of the uncorrected  $\chi T$  versus  $T$  plot from the entire data set. The  $\chi T$  value at 300 K is  $0.84 \text{ emu}\cdot\text{K}\cdot\text{mol}^{-1}$ , which is higher than the expected spin-only value of  $0.75 \text{ emu}\cdot\text{K}\cdot\text{mol}^{-1}$  for two non-interacting  $S = \frac{1}{2}$  spin systems. This value remains relatively constant between 300 and 100 K. Below 100 K,  $\chi T$  increases to a maximum value of  $0.92 \text{ emu}\cdot\text{K}\cdot\text{mol}^{-1}$  at 20 K. The  $\chi T$  value drops off rapidly between 20 K and the low temperature limit of the experiment.

The magnetic data was fit to a modified Bleaney-Bowers dimer model<sup>170, 171</sup> using the Hamiltonian operator  $H = -J(S_{Vd}\cdot S_{Vd})$ . The equation defining the interaction of a two-spin system where  $S_A = S_B = \frac{1}{2}$  is given in Equation 2.4. To model the observed low

temperature magnetic behaviour in **2.18**, a molecular field approximation was applied to Equation 2.4.<sup>171-173</sup> An arbitrary parameter  $2zJ'$  was added to account for any intermolecular interactions that might contribute to the overall magnetic moment in the bulk sample, where  $J'$  represents an intermolecular exchange interaction and  $z$  is the number of molecules involved in the interaction (Equation 2.5). Additionally, a purity factor ( $\rho$ ) was incorporated into the model to account for any  $S = \frac{1}{2}$  impurities in the sample, whose magnetic behaviour would deviate from the dimer model. The best fit of the magnetic data for diradical **2.18** with Equation 2.5 (where  $\chi T$  is given by Equation 2.4) gave the following parameters:  $g_{Vd} = 2.00$  (fixed),  $J = +40 \pm 5 \text{ cm}^{-1}$ ,  $2zJ' = -1.46 \pm 0.09 \text{ cm}^{-1}$  and  $\rho = 0.99 \pm 0.01$ .

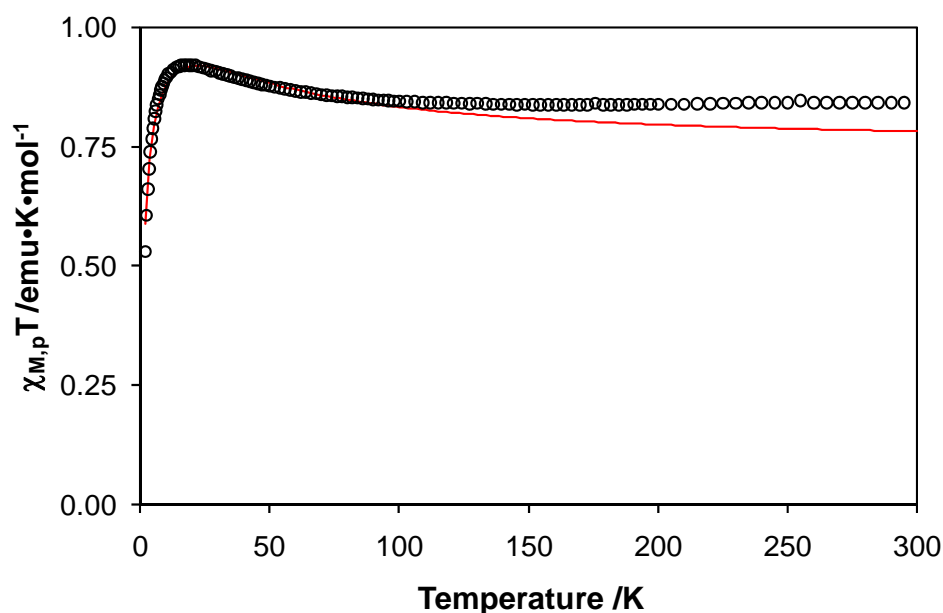


**Figure 2.16:**  $\chi T$  vs.  $T$  data (○) and model fit (—) of diradical **2.18** from 300 – 2 K. Diamagnetic corrections made using the slope method.

$$\chi T = \frac{2Ng^2\beta^2}{k\left[3 + \exp\left(\frac{-J}{kT}\right)\right]} \quad (2.4)$$

$$\chi'T = \rho \frac{\chi T}{1 - \left( \frac{2zJ'}{Ng^2\beta^2} \right) \chi} + (1-\rho) \frac{Ng^2\beta^2}{3k} S(S+1) \quad (2.5)$$

A qualitative examination of Figure 2.16 reveals that the model used here closely replicates the low temperature magnetic exchange. However, there is some discrepancy between the model and experimental data in the high temperature regime. In an attempt to address this situation, Pascal's constants were used to make the diamagnetic correction to the raw data, instead of using the previously described slope method. The resulting corrected data were modelled with Equation 2.5 and the best fit gave the following parameters:  $g_{vd} = 2.00$  (fixed),  $J = +40 \pm 5 \text{ cm}^{-1}$ ,  $2zJ' = -1.05 \pm 0.07 \text{ cm}^{-1}$  and  $\rho = 0.94 \pm 0.01$ . The experimental data and model fit are presented in Figure 2.17. The parameters gained by fitting the data corrected with Pascal's constants do not differ significantly from those found using the slope method correction. In this case Pascal's constants do not appear to sufficiently correct for the diamagnetism in the molecule since the  $\chi T$  plot does not appear to reach the paramagnetic regime even at high temperatures. Furthermore, correcting the data in this manner does not lead to a substantially better fit of the high temperature data.

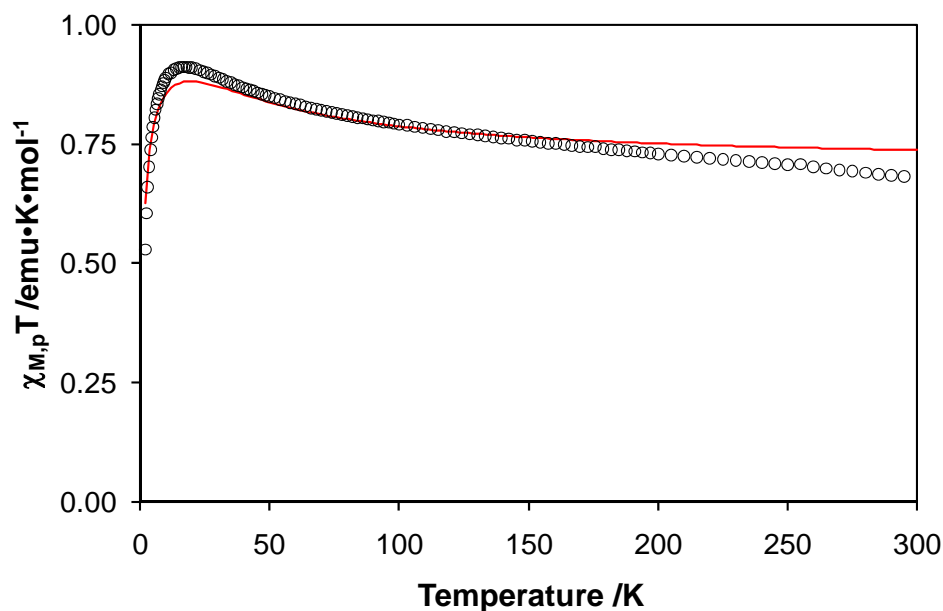


**Figure 2.17:**  $\chi T$  vs.  $T$  data ( $\circ$ ) and model fit ( $-$ ) of diradical **2.18** from 300 – 2 K. Diamagnetic corrections made using Pascal's constants.

Notwithstanding the shortcomings of the model used to describe the magnetic behaviour of diradical **2.18**, there are some important conclusions that can be gleaned from this data. Most importantly, the shape of the  $\chi T$  vs.  $T$  plot is characteristic of two weakly ferromagnetically coupled  $S = \frac{1}{2}$  spins. The  $\chi T$  value does not change significantly in the paramagnetic regime between 300 and 100 K (Figure 2.16). On cooling below 100 K, uncoupled excited states become thermally depopulated, leaving the ferromagnetically coupled ground state as the predominant contributor to the overall spin state of the molecule. This is manifested by the maximum in  $\chi T$  of  $0.92 \text{ emu}\cdot\text{K}\cdot\text{mol}^{-1}$  at 20 K, which is close to the spin-only value of  $1.00 \text{ emu}\cdot\text{K}\cdot\text{mol}^{-1}$  for an  $S = 1$  spin system. Below 20 K, intermolecular antiferromagnetic interactions represent the main source of the observed magnetic behaviour in **2.18**. The value of  $J = +40 \text{ cm}^{-1}$  for **2.18** agrees very well with coupling constants calculated for the

pyridine-bridged, N,N-dimethyl-substituted verdazyl diradical **1.54** ( $J = +37$  or  $+41 \text{ cm}^{-1}$ , depending on the basis set used in the calculation<sup>151</sup>). The experimental  $J$  value for **2.18** is largely unaffected by the diamagnetic correction method employed, which implies that any magnetic interactions affecting the room temperature moment do not influence the singlet-triplet energy gap.

Ferromagnetic exchange interactions are well-established in *meta*-substituted aryl-bridged diradicals.<sup>174, 175</sup> This exchange is rationalised through a spin-polarisation mechanism.<sup>176, 177</sup> Consider first the case of an aryl-substituted monoradical, where the presence of the unpaired electron causes a polarisation of the electrons in the  $\pi$ -system in the aromatic ring (Figure 2.18a). For a *meta*-substituted diradical to satisfy the polarisation pattern in the aromatic bridging unit, the two radical moieties must necessarily be mutually ferromagnetically coupled (Figure 2.18b). The same argument explains the antiferromagnetic coupling that is common to *para*-substituted aryl-bridged diradicals (Figure 2.18c).<sup>178</sup> The experimental coupling constant for **2.18** is slightly higher than that reported for an analogous benzene-bridged bis-verdazyl **1.56** ( $J = 19.3 \pm 1.7 \text{ cm}^{-1}$ ).<sup>107</sup> Inclusion of a heteroatom in the aryl bridge linking the verdazyl moieties does not significantly alter the magnetic exchange pathway in the diradical.

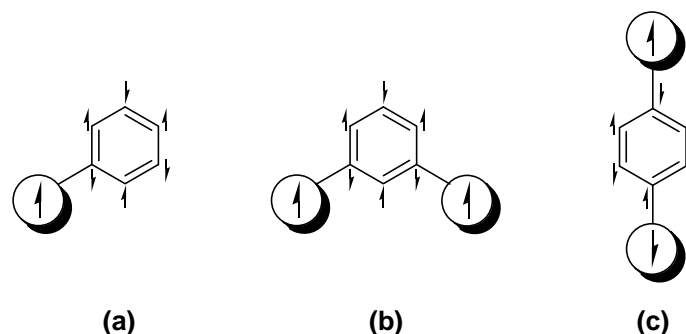
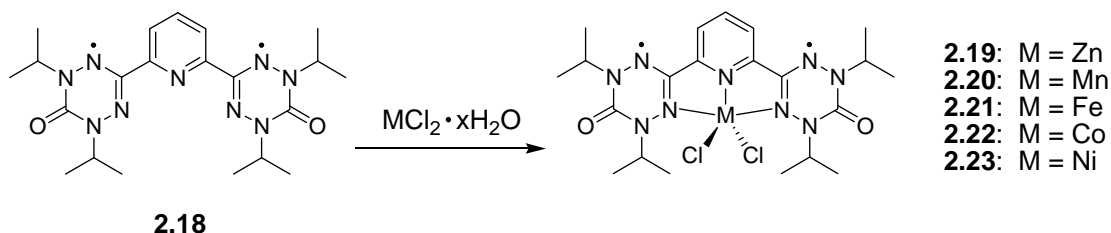


**Figure 2.18:** The presence of a radical polarises the  $\pi$ -electrons in an aromatic ring (a). This spin polarisation mechanism favours ferromagnetic coupling in *meta*-substituted diradicals (b) and antiferromagnetic exchange in a *para*-substituted diradicals (c).

## 2.6 Coordination complexes of diradical 2.18

Diradical **2.18** was used to prepare a series of coordination compounds involving first row transition metals from chromium to zinc, inclusive. Complexes of the general form **2.18**MCl<sub>2</sub>, (M = Mn, Fe, Co, Ni and Zn) were prepared according to Scheme 2.6. A solution of **2.18** was added slowly to an equimolar solution of the appropriate metal dichloride salt and the reaction was allowed to stand without stirring for a period of approximately 16 hours. Crystals were typically separated from the mother liquor by vacuum filtration followed by washing with minimal amounts of ice-cold acetonitrile. Diradical complexes of chromium and copper proved to be structurally dissimilar to those shown in Scheme 2.6 and will be discussed separately.



**Scheme 2.6:** Synthesis of complexes with the general structure **2.18**MCl<sub>2</sub>.

Infrared spectroscopy provided evidence of successful coordination of **2.18** to the various metals; the carbonyl band shifts from  $1683\text{ cm}^{-1}$  in diradical **2.18** to between  $1699$  and  $1704\text{ cm}^{-1}$  in complexes **2.19** – **2.23**. UV-Vis spectra were collected to investigate the electronic nature of this series of coordination compounds. These spectra are presented and compared to that of diradical **2.18** in Figure 2.19. The most notable distinction among the spectra is the modest bathochromic shift of the absorption maximum at  $410\text{ nm}$  in the **2.18** spectrum to about  $430\text{ nm}$  in the spectra of the corresponding coordination complexes **2.19** – **2.23**, analogous to what was observed with the monoradical coordination compounds discussed in Section 2.4.1. The spectra presented in Figure 2.19 for complexes **2.19** – **2.23** are qualitatively nearly identical, despite the range of metals involved.

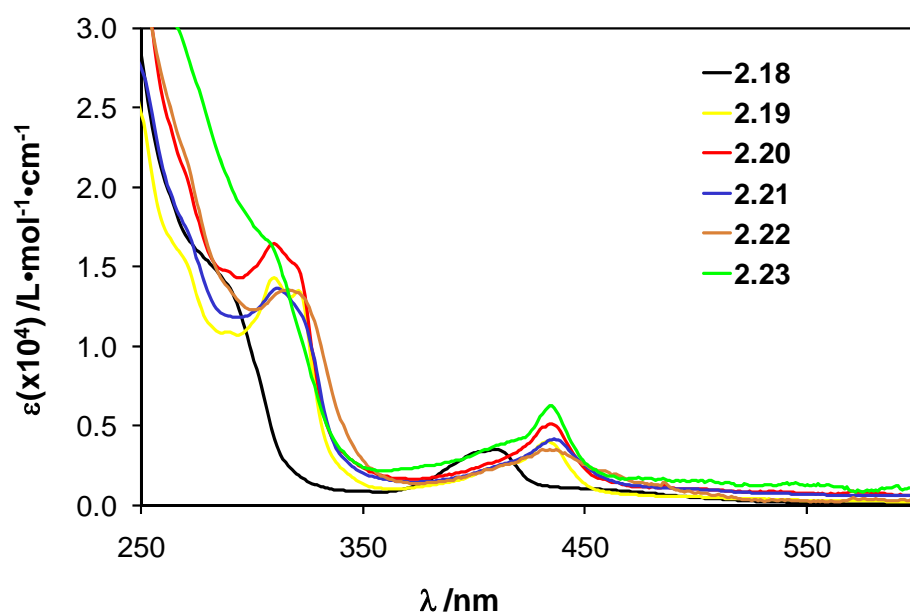


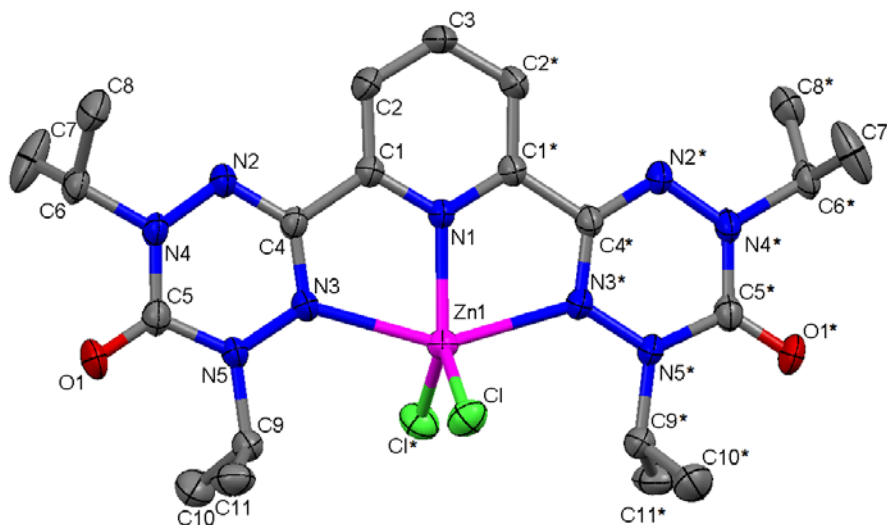
**Figure 2.19:** UV-Vis spectra of diradical **2.18** and related coordination compounds **2.19** – **2.23** in dichloromethane.



### 2.6.1 Structural characterisation of zinc-diradical complex **2.19**

The molecular structure of zinc-diradical complex **2.19** is presented in Figure 2.20 with selected bond lengths and angles summarised in Table 2.5. The geometry around the zinc centre can be described as *pseudo*-trigonal bipyramidal, with the pyridine nitrogen atom and the two chloride ligands forming the trigonal plane. In general, the bond lengths and angles associated with the verdazyl rings are comparable to those reported in Section 2.5.2 for diradical **2.18**. The difference between the two N-N bond lengths in the verdazyl ring is more pronounced in complex **2.19** than in diradical **2.18**. The N-N bond involving the coordinated nitrogen atom is slightly longer [N3-N5 = 1.364(3) Å] than on the non-coordinated side of the radical [N2-N4 = 1.355(3) Å]. The pyridine ring and the two verdazyl rings are mutually coplanar in complex **2.19**. There is a significant difference in the lengths of the coordinative bonds to zinc between the pyridine nitrogen [Zn1-N1 = 2.065(3) Å] and the verdazyl nitrogens [Zn1-N3 = 2.3095(19) Å]. In zinc-terpyridine complexes the central pyridine nitrogen atom is necessarily closer to zinc than are the terminal pyridine nitrogen atoms. This is a result of the bonding geometry and bite angle of the terpyridine ligand, since the three nitrogen atoms are close to equivalent in terms of  $\sigma$ -donor strength. It follows that the verdazyl nitrogen atoms in **2.19** should also be further from the zinc ion than is the central pyridine nitrogen. However, this coordinative bond-length difference is much more pronounced in **2.19** than in comparable terpyridine coordination compounds, such as complexes **2.24** – **2.27**. Among these examples, typical nitrogen-zinc bond length differences with respect to the central pyridine nitrogen versus the terminal pyridine nitrogen atoms range from 0.0778 to 0.125 Å (specifically, the largest

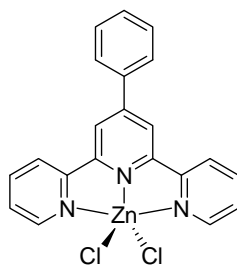
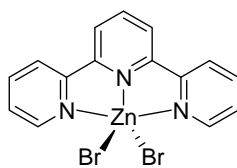
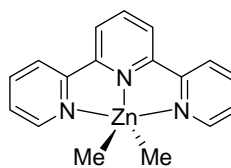
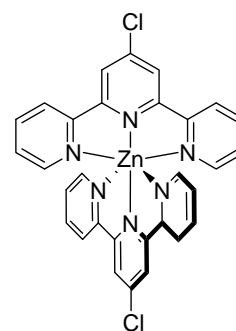
differences are 0.1061 Å in **2.24**, 0.0801 Å in **2.25**, 0.0778 Å in **2.26** and 0.125 Å in **2.27**).<sup>179-182</sup> The large disparity between the corresponding nitrogen-zinc bond lengths in **2.19** ( $\text{Zn-N}_{\text{verdazyl}} - \text{Zn-N}_{\text{pyridine}} = 0.2445$  Å, which is almost double the largest difference in the **2.24** – **2.27** series) suggests that this variation in bond length is influenced by more than just topological factors. Moreover, the difference in  $\sigma$ -donor ability between the different ligating nitrogen atoms is even more evident in **2.19** than in the monoradical complexes **2.14** and **2.15** discussed in Section 2.4.



**Figure 2.20:** Molecular structure of zinc-diradical complex **2.19**. Thermal ellipsoids displayed at 50% probability level. Hydrogen atoms removed for clarity.

**Table 2.5:** Selected bond lengths (Å) and angles (degrees) for **2.19**.

Atoms	Length (Å)	Atoms	Angle (°)
C1-C4	1.480(3)	N2-C4-N3	128.1(2)
C4-N2	1.327(3)	N4-C5-N5	115.0(2)
C4-N3	1.324(3)	C4-N2-N4	114.4(2)
C5-O1	1.209(3)	C4-N3-N5	115.59(19)
C5-N4	1.382(3)	N2-N4-C5	124.35(19)
C5-N5	1.392(3)	N3-N5-C5	122.51(19)
N2-N4	1.355(3)	N1-Zn1-N3	74.21(5)
N3-N5	1.364(3)	N3-Zn1-N3*	148.42(10)
Zn1-N1	2.065(3)	Cl-Zn1-Cl*	114.71(4)
Zn1-N3	2.3095(19)		

**2.24****2.25****2.26****2.27**

### 2.6.2 Magnetic properties of **2.19**

Magnetic properties of zinc complex **2.19** were recorded between 300 – 2 K and the results are displayed in Figure 2.21 as the product of magnetic susceptibility and temperature versus temperature ( $\chi T$  vs. T). The shape of the curve in Figure 2.21 is qualitatively very similar to the analogous data for diradical **2.18**. At room temperature the value of  $\chi T$  for **2.19** is  $0.88 \text{ emu}\cdot\text{K}\cdot\text{mol}^{-1}$ , which is higher than the expected spin-only value of  $0.75 \text{ emu}\cdot\text{K}\cdot\text{mol}^{-1}$  for two non-interacting  $S = \frac{1}{2}$  spin systems. As temperature is decreased,  $\chi T$  increases to a maximum of  $0.97 \text{ emu}\cdot\text{K}\cdot\text{mol}^{-1}$  at 17 K. Below 17 K,  $\chi T$

decreases rapidly. The decrease at cryogenic temperature is most likely caused by intermolecular antiferromagnetic interactions.

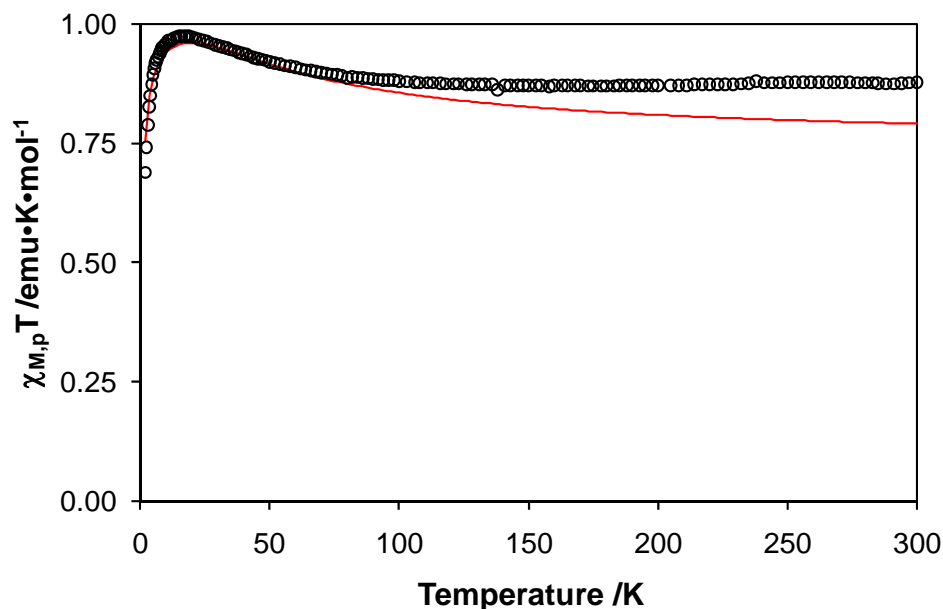


**Figure 2.21:**  $\chi T$  vs.  $T$  data ( $\circ$ ) and model fit ( $-$ ) of complex **2.19** from 300 – 2 K.

Fitting the magnetic data for zinc complex **2.19** to the same two-spin model used to analyse the magnetic properties of diradical **2.18** (Equation 2.5) gives the following parameters:  $g = 2.00$  (fixed),  $J = +50 \pm 9 \text{ cm}^{-1}$ ,  $2zJ' = -0.7 \pm 0.1 \text{ cm}^{-1}$  and  $\rho = 1.00 \pm 0.02$ . As was the case with the model used to reproduce the magnetic behaviour of diradical **2.18**, Figure 2.21 shows that this model is much better at replicating the low temperature magnetic interactions in **2.19** than it is the high temperature behaviour. Similar steps were taken to better fit the data for **2.19** as were described for diradical **2.18**, but the resulting parameters were largely unchanged.

Zinc(II) is a  $d^{10}$  ion and thus has no unpaired electrons. The synthesis and magnetic analysis of **2.19** were designed as a control experiment to examine the magnetic

behaviour of diradical **2.18** when coordinated to a diamagnetic metal. The qualitative aspects of the  $\chi T$  vs.  $T$  plots for diradical **2.18** and zinc complex **2.19** are similar, which indicates that the presence of the zinc(II) ion is not providing any new pathways to mediate magnetic exchange in the diradical ligand. The modest differences in the coupling constants seen for **2.18** and **2.19** further corroborate that the inclusion of zinc into the binding pocket of **2.18** does not dramatically alter the magnetic properties of this verdazyl diradical.

### 2.6.3 Structural characterisation of manganese-diradical complex **2.20**

Figure 2.22 shows the molecular structure of manganese-diradical complex **2.20**. Selected bond lengths and angles are presented in Table 2.6. The manganese coordination compound **2.20** is *pseudo*-trigonal bipyramidal and is structurally similar to zinc complex **2.19**. The bond lengths and angles associated with the verdazyl rings in **2.20** are comparable to those seen in **2.19** and they do not differ significantly from those in diradical **2.18** itself. The three rings of the ligand are also completely co-planar in manganese complex **2.20**. As with other metal-verdazyl complexes, the pyridine nitrogen in **2.20** coordinates to the manganese centre more strongly than do the verdazyl nitrogen atoms [ $\text{Mn1-N1} = 2.1824(15) \text{ \AA}$ ;  $\text{Mn1-N3} = 2.3247(11) \text{ \AA}$ ].

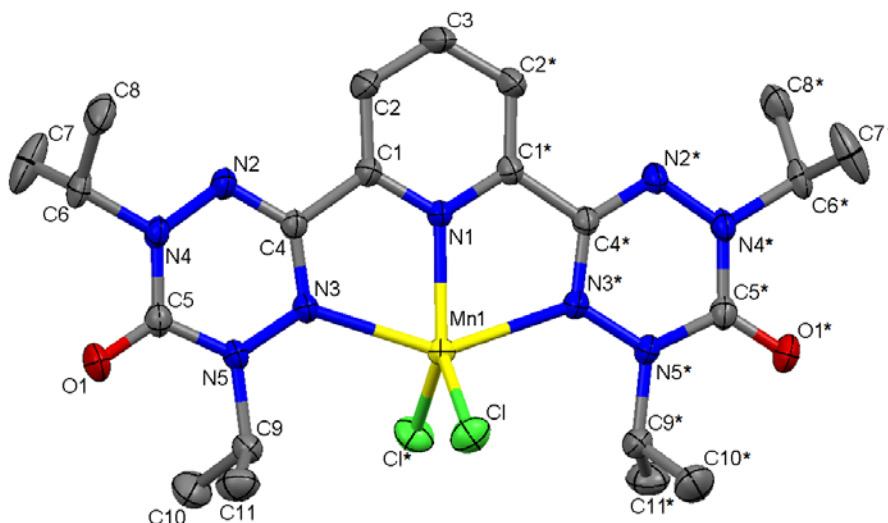


**Figure 2.22:** Molecular structure of manganese-diradical complex **2.20**. Thermal ellipsoids displayed at 50% probability level. Hydrogen atoms removed for clarity.

**Table 2.6:** Selected bond lengths (Å) and angles (degrees) for **2.20**.

Atoms	Length (Å)	Atoms	Angle (°)
C1-C4	1.4793(17)	N2-C4-N3	127.68(12)
C4-N2	1.3215(16)	N4-C5-N5	114.99(11)
C4-N3	1.3344(17)	C4-N2-N4	115.24(11)
C5-O1	1.2118(17)	C4-N3-N5	115.06(11)
C5-N4	1.3824(19)	N2-N4-C5	123.97(10)
C5-N5	1.3892(17)	N3-N5-C5	122.95(11)
N2-N4	1.3512(15)	N1-Mn1-N3	71.98(3)
N3-N5	1.3663(15)	N3-Mn1-N3*	143.96(6)
Mn1-N1	2.1824(15)	Cl-Mn1-Cl*	110.68(2)
Mn1-N3	2.3247(11)		

#### 2.6.4 Magnetic properties of **2.20**

Magnetic properties of manganese complex **2.20** were recorded from 300 – 2 K and the results are displayed in Figure 2.23. At 300 K,  $\chi T$  is  $3.54 \text{ emu} \cdot \text{K} \cdot \text{mol}^{-1}$ , which is considerably lower than the expected spin-only value of  $5.13 \text{ emu} \cdot \text{K} \cdot \text{mol}^{-1}$  for three non-interacting spin systems  $S_{\text{Vd}} - S_{\text{Mn}} - S_{\text{Vd}}$ , where  $S_{\text{Vd}} = 1/2$  and  $S_{\text{Mn}} = 5/2$ . The value of  $\chi T$

decreases with temperature down to a plateau value of  $2.00 \text{ emu}\cdot\text{K}\cdot\text{mol}^{-1}$  between 50 and 25 K, below which point  $\chi T$  increases.

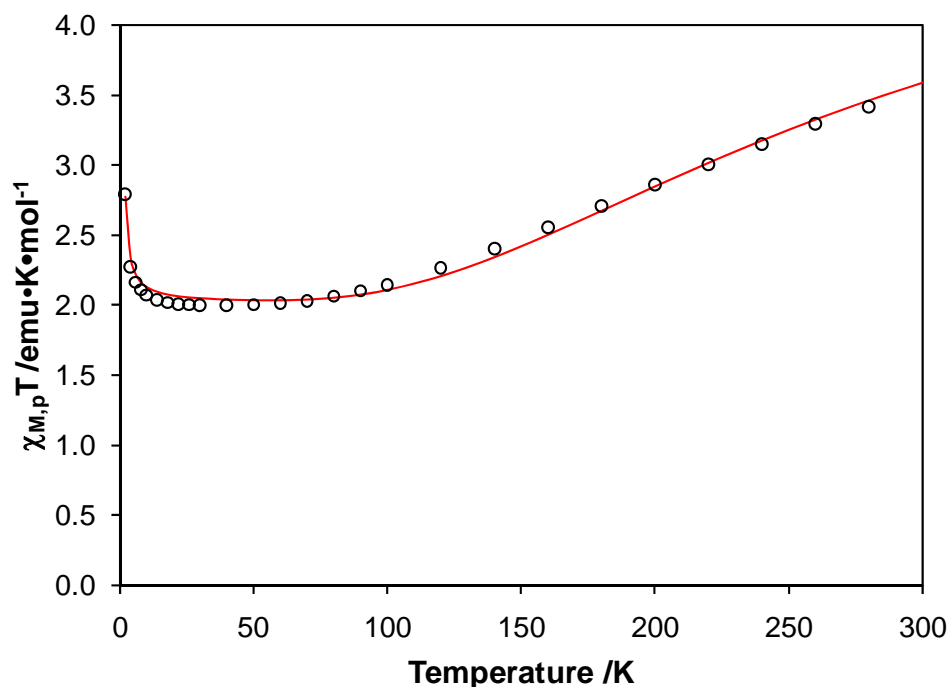


**Figure 2.23:**  $\chi T$  vs.  $T$  data (○) and model fit (—) of complex **2.20** from 300 – 2 K.

The overall shape of the  $\chi T$  vs.  $T$  plot for **2.20** is consistent with an antiferromagnetically coupled system. The solid red line in Figure 2.23 represents the magnetic model calculated from Equation 2.6 with the following parameters:  $g_{Vd} = 2.00$  (fixed),  $g_{Mn} = 2.05$ ,  $J_{Mn-Vd} = -71.0 \text{ cm}^{-1}$ ,  $J_{Vd-Vd} = +40 \text{ cm}^{-1}$  (fixed) and  $\theta = +0.55 \text{ K}$ . The model gave a goodness of fit factor of  $R = 0.017$ . The plateau value of  $2.00 \text{ emu}\cdot\text{K}\cdot\text{mol}^{-1}$  between 50 and 25 K is slightly higher than the spin-only value of  $1.88 \text{ emu}\cdot\text{K}\cdot\text{mol}^{-1}$  for an  $S = 3/2$  system. The  $S = 3/2$  value is important because this represents the spin system for the case where the two unpaired verdazyl electrons are antiferromagnetically coupled to the Mn(II) ion (Figure 2.24). At 300 K the magnetic moment of **2.20** does not reach the expected spin-only value for two  $S = 1/2$  radicals and an  $S = 5/2$  metal centre, implying

that antiferromagnetic coupling interactions persist at room temperature. Antiferromagnetic interactions have been reported in other manganese-verdazyl complexes.<sup>98, 99</sup>

$$\chi = \frac{N\beta^2}{12k(T-\theta)} \frac{30 g_1^2 + 252 g_2^2 \exp\left(\frac{6J_{\text{Mn-Vd}}}{kT}\right) + 105 g_3^2 \exp\left(\frac{7J_{\text{Mn-Vd}} - 2J_{\text{Vd-Vd}}}{2kT}\right)}{2 + 4 \exp\left(\frac{6J_{\text{Mn-Vd}}}{kT}\right) + 3 \exp\left(\frac{7J_{\text{Mn-Vd}} - 2J_{\text{Vd-Vd}}}{2kT}\right)} \quad (2.6)$$

$$g_1 = \frac{-2g_{\text{Vd}} + 7g_{\text{Mn}}}{5} \quad g_2 = \frac{2g_{\text{Vd}} + 5g_{\text{Mn}}}{7} \quad g_3 = g_{\text{Mn}}$$

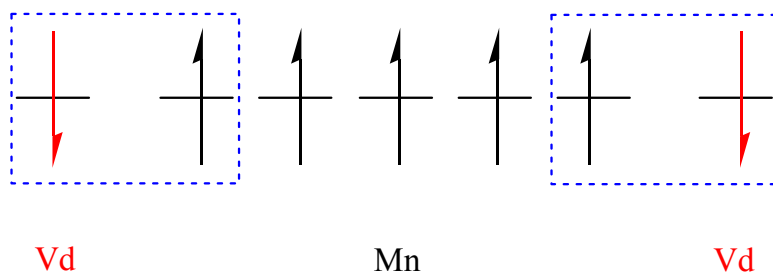


**Figure 2.24:** Simplified antiferromagnetic coupling relationship between  $S = 5/2$   $\text{Mn}^{2+}$  ion and two  $S = 1/2$  verdazyl (Vd) radicals.

Figure 2.24 is an over-simplification of the actual coupling interactions present in **2.20**. In a *pseudo*-trigonal bipyramidal coordination geometry,  $\text{Mn}^{2+}$  has one unpaired electron in each of the five metal-centred  $d$ -orbitals. Each of these orbitals has a different spatial relationship with the  $\pi$ -symmetry orbitals housing the verdazyl unpaired electrons. Figure 2.25 shows the relationship between each of the manganese  $d$ -orbitals and the  $\pi$ -SOMOs of the verdazyl diradical ligand. Rather than a discrete interaction between the verdazyl SOMOs and five energetically degenerate unpaired electrons (as is depicted in Figure 2.24), there are potentially five different coupling interactions taking place at the same time. Magnetic orbitals that have non-zero overlap with respect to each other will



lead to antiferromagnetic exchange, while mutually orthogonal orbitals produce ferromagnetic coupling.<sup>171, 183</sup> The observed magnetic exchange is then determined by the magnitude of the combined antiferromagnetic versus ferromagnetic interactions. For **2.20**, the combined orbital interactions leading to antiferromagnetic coupling dominate the ferromagnetic interactions. In the frame of reference shown in Figure 2.25, the only interaction leading to orbital overlap is between the verdazyl SOMOs and the manganese  $d_{xz}$ -orbital. Therefore this interaction must be the prevalent factor contributing to the intramolecular magnetic exchange in **2.20**. The overall magnetic behaviour of **2.20** is also influenced by weak *intermolecular* ferromagnetic interactions, as evidenced by the increase in  $\chi T$  below 20 K. These low-temperature intermolecular interactions were addressed by incorporating a Weiss constant,  $\theta$ , into the magnetic model for this system (Equation 2.6).

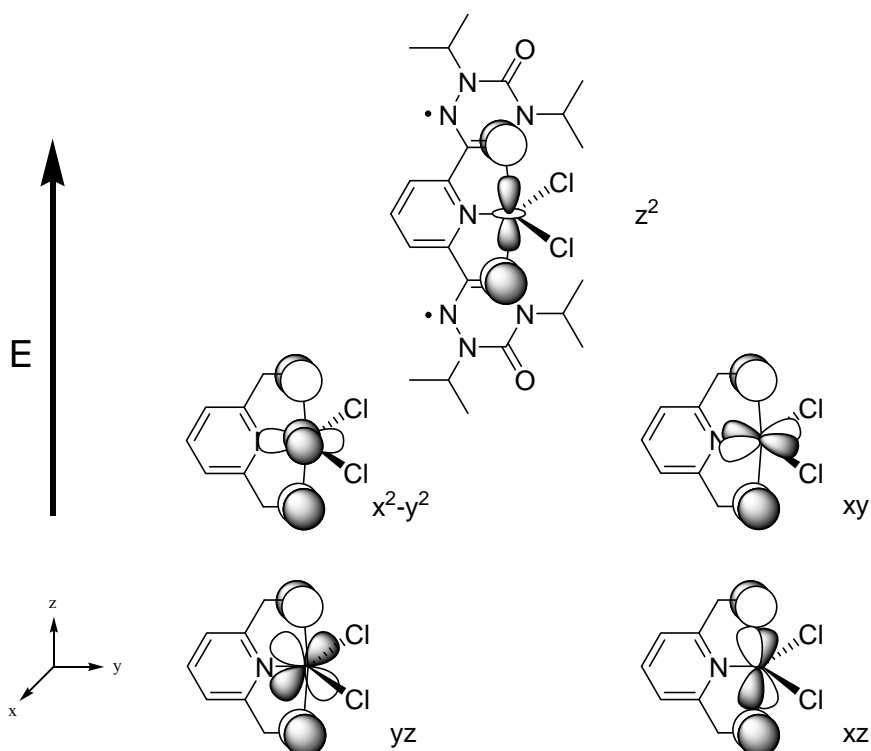


**Figure 2.25:** Metal-based  $d$ -orbitals in order of relative energies in trigonal bipyramidal coordination geometry.  $p$ -Orbitals represent  $\pi$ -SOMO of verdazyl radicals to show relationship with metal  $d$ -orbitals (6-oxoverdazyl rings omitted in some cases for clarity).

### 2.6.5 Structural characterisation of iron-diradical complex **2.21**

The molecular structure of **2.21** is displayed in Figure 2.26 with selected bond lengths and angles highlighted in Table 2.7. The iron coordination compound **2.21** is structurally similar to the other diradical coordination compounds presented in this section. The bond lengths and angles associated with the verdazyl rings in **2.21** are comparable to those seen in complexes **2.19** and **2.20** and they do not differ significantly from those in diradical **2.18**. The three rings in the ligand framework are co-planar in iron complex **2.21**. The three coordinating nitrogen atoms have different bond lengths to iron, with the pyridine nitrogen located closer to the metal than are the two verdazyl nitrogen atoms [ $\text{Fe1-N1} = 2.088(2) \text{ \AA}$ ;  $\text{Fe1-N3} = 2.2772(14) \text{ \AA}$ ].

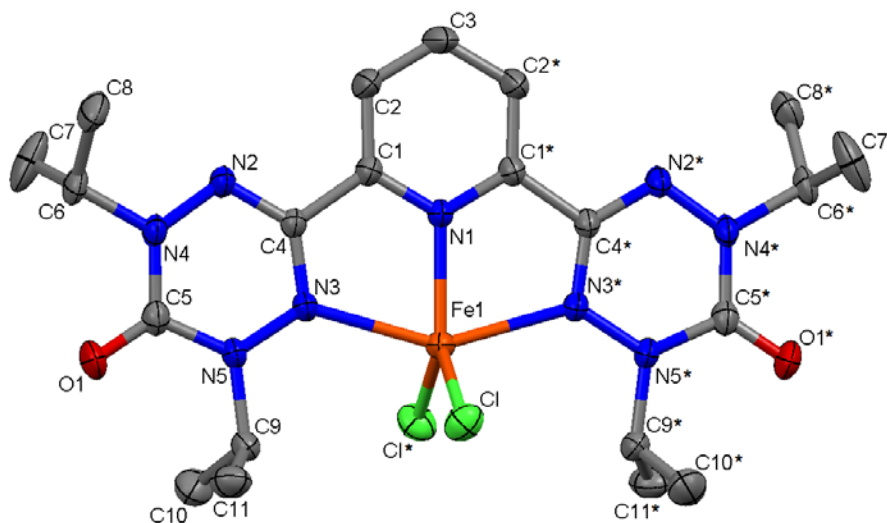


**Figure 2.26:** Molecular structure of iron-diradical complex **2.21**. Thermal ellipsoids displayed at 50% probability level. Hydrogen atoms removed for clarity.

**Table 2.7:** Selected bond lengths (Å) and angles (degrees) for **2.21**.

Atoms	Length (Å)	Atoms	Angle (°)
C1-C4	1.478(2)	N2-C4-N3	127.74(16)
C4-N2	1.325(2)	N4-C5-N5	114.95(15)
C4-N3	1.337(2)	C4-N2-N4	115.02(15)
C5-O1	1.211(2)	C4-N3-N5	115.03(14)
C5-N4	1.384(3)	N2-N4-C5	124.13(14)
C5-N5	1.389(2)	N3-N5-C5	123.03(15)
N2-N4	1.351(2)	N1-Fe1-N3	74.41(4)
N3-N5	1.365(2)	N3-Fe1-N3*	148.81(8)
Fe1-N1	2.088(2)	Cl-Fe1-Cl*	114.48(3)
Fe1-N3	2.2772(14)		

### 2.6.6 Magnetic properties of **2.21**

Figure 2.27 shows the  $\chi T$  versus  $T$  plot for **2.21** from 300 – 2 K. At 300 K,  $\chi T$  is 2.95  $\text{emu}\cdot\text{K}\cdot\text{mol}^{-1}$ . In this case,  $S_{\text{Fe}} = 2$ ,  $S_{\text{Vd}} = \frac{1}{2}$  and the expected spin-only  $\chi T$  value for these three non-interacting spin systems is 3.75  $\text{emu}\cdot\text{K}\cdot\text{mol}^{-1}$ . On lowering the temperature,  $\chi T$  gradually decreases down to a plateau value of 1.21  $\text{emu}\cdot\text{K}\cdot\text{mol}^{-1}$  between about 50 and 15 K. Below 15 K,  $\chi T$  drops off significantly.

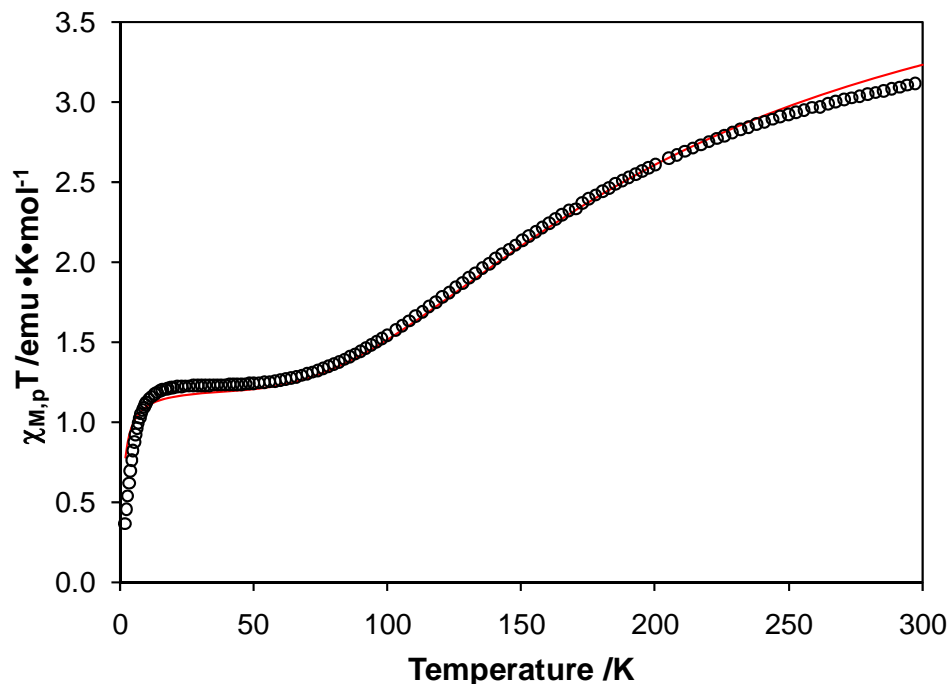


**Figure 2.27:**  $\chi T$  vs.  $T$  data ( $\circ$ ) and model fit ( $-$ ) of complex **2.21** from 300 – 2 K.

The shape of the  $\chi T$  vs.  $T$  plot for **2.21** is consistent with an antiferromagnetically coupled system. The model fit (red line) in Figure 2.27 was calculated from Equation 2.7 with the following parameters:  $g_{Vd} = 2.00$  (fixed),  $g_{Fe} = 2.14$ ,  $J_{Fe-Vd} = -59.0 \text{ cm}^{-1}$ ,  $J_{Vd-Vd} = +40 \text{ cm}^{-1}$  (fixed) and  $\theta = -1.15 \text{ K}$ . The model gave a goodness of fit factor of  $R = 0.041$ . The magnitude of the coupling constants for **2.20** and **2.21** indicates that the antiferromagnetic exchange interaction between manganese(II) and diradical **2.18** is stronger than that between iron(II) and the same ligand. The plateau value of about  $1.2 \text{ emu}\cdot\text{K}\cdot\text{mol}^{-1}$  between 50 and 15 K is slightly higher than the spin-only value of  $1.00 \text{ emu}\cdot\text{K}\cdot\text{mol}^{-1}$  for an  $S = 1$  system.

$$\chi = \frac{2N\beta^2}{k(T-\theta)} \frac{g_1^2 + 14 g_2^2 \exp\left(\frac{5J_{\text{Fe-Vd}}}{kT}\right) + 5 g_3^2 \exp\left(\frac{3J_{\text{Fe-Vd}} - J_{\text{Vd-Vd}}}{kT}\right)}{3 + 7 \exp\left(\frac{5J_{\text{Fe-Vd}}}{kT}\right) + 5 \exp\left(\frac{3J_{\text{Fe-Vd}} - J_{\text{Vd-Vd}}}{kT}\right)} \quad (2.7)$$

$$g_1 = \frac{-g_{\text{Vd}} + 3g_{\text{Fe}}}{2} \quad g_2 = \frac{g_{\text{Vd}} + 2g_{\text{Fe}}}{3} \quad g_3 = g_{\text{Fe}}$$

Orbital symmetry arguments, analogous to those described in Section 2.6.4 for manganese complex **2.20**, also apply to the iron complex **2.21** in this situation. However, in this case, the iron(II) centre in **2.21** has four unpaired electrons in metal-centred *d*-orbitals. Antiferromagnetic coupling between the unpaired ligand electrons and two of the *d*-electrons on iron would result in an *S* = 1 spin system, in an over-simplified view of the magnetic coupling. A more rigorous treatment of the magnetic orbital interactions would again show the verdazyl SOMOs experiencing simultaneous distinct relationships to the various iron *d*-orbitals. Similarly to what was observed in manganese complex **2.20**, the antiferromagnetic orbital interactions must account for the major contribution to the intramolecular exchange in iron compound **2.21**. Evidence of weak *intermolecular* interactions is also present in the magnetic profile of **2.21**. These intermolecular interactions were again modelled by incorporating a Weiss constant into Equation 2.7. In this case, the intermolecular contribution to the overall magnetic behaviour is antiferromagnetic in nature.

### 2.6.7 Structural characterisation of cobalt-diradical complex **2.22**

The molecular structure of **2.22** is displayed in Figure 2.28 with selected bond lengths and angles highlighted in Table 2.8. Cobalt complex **2.22** is structurally similar to the other diradical coordination compounds presented in this section and the bond lengths and angles associated with the verdazyl rings do not differ significantly among

the complexes described so far. The pyridine nitrogen coordinates more strongly to the cobalt ion [ $\text{Co1-N1} = 2.031(2) \text{ \AA}$ ] in **2.22** than do the verdazyl nitrogens [ $\text{Co1-N3} = 2.2564(14) \text{ \AA}$ ].

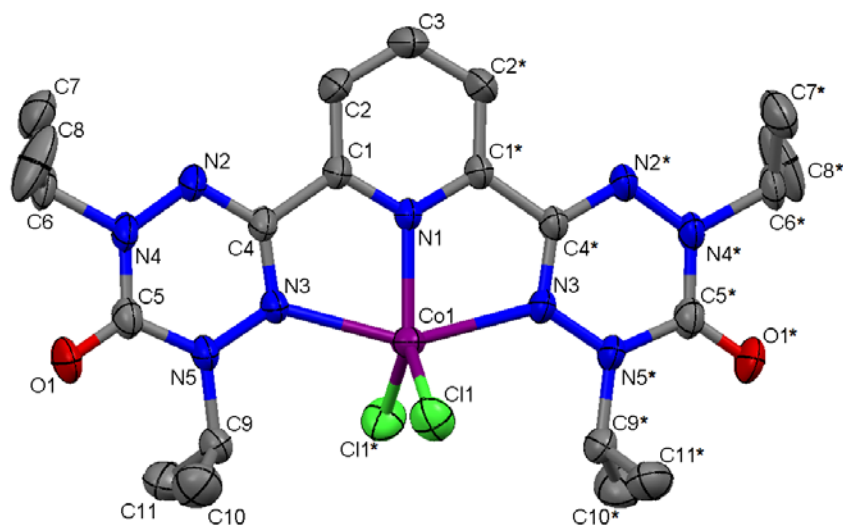


**Figure 2.28:** Molecular structure of cobalt-diradical complex **2.22**. Thermal ellipsoids displayed at 50% probability level.

**Table 2.8:** Selected bond lengths ( $\text{\AA}$ ) and angles (degrees) for **2.22**.

Atoms	Length ( $\text{\AA}$ )	Atoms	Angle ( $^\circ$ )
C1-C4	1.472(2)	N2-C4-N3	127.90(16)
C4-N2	1.323(2)	N4-C5-N5	115.03(15)
C4-N3	1.327(2)	C4-N2-N4	114.96(15)
C5-O1	1.207(2)	C4-N3-N5	115.03(14)
C5-N4	1.376(3)	N2-N4-C5	124.09(14)
C5-N5	1.389(2)	N3-N5-C5	122.92(15)
N2-N4	1.349(2)	N1-Co1-N3	75.40(4)
N3-N5	1.363(2)	N3-Co1-N3*	150.80(8)
Co1-N1	2.031(2)	Cl-Co1-Cl*	113.38(3)
Co1-N3	2.2564(14)		

### 2.6.8 Magnetic properties of **2.22**

Magnetic properties of cobalt complex **2.22** were recorded from 300 – 2 K and the  $\chi T$  vs. T plot is displayed in Figure 2.29. The expected spin-only magnetic moment

for an  $S = 3/2$  cobalt(II) ion and two  $S = 1/2$  radicals is  $2.63 \text{ emu}\cdot\text{K}\cdot\text{mol}^{-1}$ . At 300 K,  $\chi T$  is  $3.06 \text{ emu}\cdot\text{K}\cdot\text{mol}^{-1}$ , which is higher than the expected value if the three spin systems considered here are not coupled.

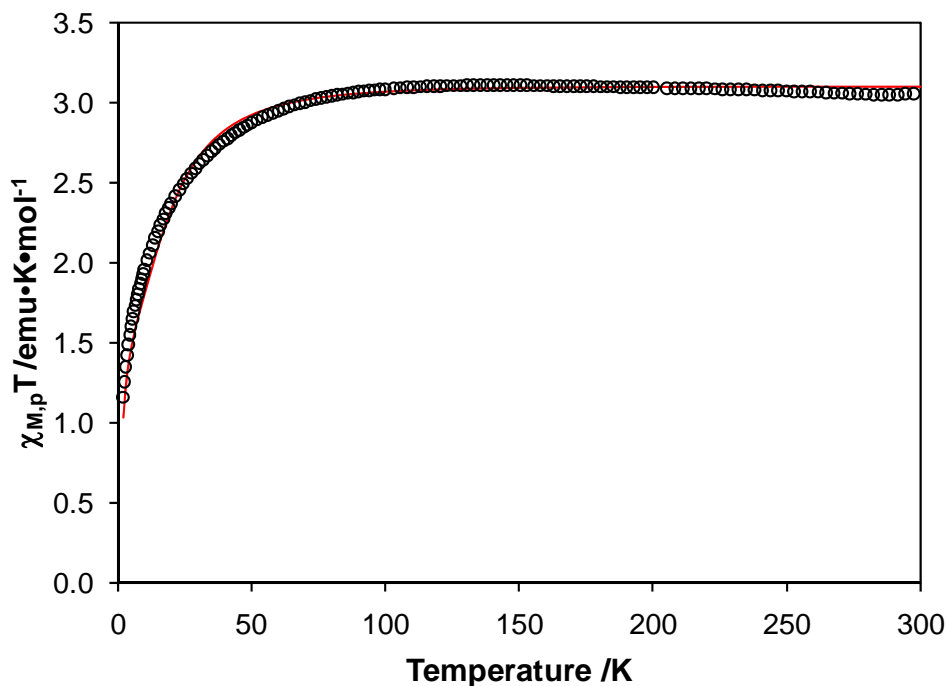


**Figure 2.29:**  $\chi T$  vs.  $T$  data ( $\circ$ ) and model fit ( $-$ ) of complex **2.22** from 2 – 300 K.

The high-temperature  $\chi T$  value for **2.22** is consistent with ferromagnetic coupling, which has been observed in other cobalt-verdazyl complexes.<sup>97, 147</sup> The model fit (red line) in Figure 2.29 was calculated from Equation 2.8 with the following parameters:  $g_{Vd} = 2.00$  (fixed),  $g_{Co} = 2.10$ ,  $J_{Co-Vd} = +10.0 \text{ cm}^{-1}$ ,  $J_{Vd-Vd} = +40 \text{ cm}^{-1}$  (fixed) and  $\theta = -2.00 \text{ K}$ . This model appears to be a good qualitative fit of the data ( $R = 0.021$ ). However, a closer inspection of the resulting parameters reveals an important inconsistency with the observed magnetic behaviour. The metal-radical coupling constant of  $+10 \text{ cm}^{-1}$  is representative of very weak ferromagnetic coupling. This contradicts the high-temperature  $\chi T$  data, which is consistent with a  $\text{Co}^{2+}$  ion that is

strongly ferromagnetically coupled to two  $S = \frac{1}{2}$  verdazyl radicals. The most probable explanation for this discrepancy arises from strong spin-orbit coupling associated with the  $\text{Co}^{2+}$  ion. Cobalt complexes can exhibit a large contribution to the magnetic moment from the first-order orbital contribution to the magnetic moment associated with the cobalt  $d$ -orbitals alone, making it difficult to model the magnetic behaviour based on simple isotropic interactions.<sup>183</sup> Zero-field splitting effects, including spin-orbit coupling, are common to other cobalt-radical complexes.<sup>184, 185</sup> It is clear, in this case, that the model described by Equation 2.8 underestimates the strength of the magnetic exchange in **2.22**. For this reason, the  $J_{\text{Co-Vd}}$  value presented here should be considered an approximation of the lower limit of the true ferromagnetic coupling constant.

$$\chi = \frac{N\beta^2}{4k(T-\theta)} \frac{35 g_1^2 + g_2^2 \exp\left(\frac{-4J_{\text{Co-Vd}}}{kT}\right) + 10 g_3^2 \exp\left(\frac{-3J_{\text{Co-Vd}} + 2J_{\text{Vd-Vd}}}{2kT}\right)}{3 + \exp\left(\frac{-4J_{\text{Co-Vd}}}{kT}\right) + 2 \exp\left(\frac{-3J_{\text{Co-Vd}} + 2J_{\text{Vd-Vd}}}{2kT}\right)} \quad (2.8)$$

$$g_1 = \frac{2g_{\text{Vd}} + 3g_{\text{Co}}}{5} \quad g_2 = \frac{-2g_{\text{Vd}} + 5g_{\text{Co}}}{3} \quad g_3 = g_{\text{Co}}$$

### 2.6.9 Structural characterisation of nickel-diradical complex **2.23**

The molecular structure of **2.23** is presented in Figure 2.30. Selected bond lengths and angles are presented in Table 2.9. Nickel complex **2.23** is crystallographically distinct from the other diradical coordination compounds presented in this chapter in that **2.23** does not lie on a crystallographic mirror plane. Furthermore, the three rings in the diradical ligand of complex **2.23** are not perfectly coplanar; one of the verdazyl rings is slightly twisted out of the plane. Nonetheless, **2.23** is analogous to



compounds **2.19** – **2.22** in that the bond lengths and angles of the two verdazyl rings in **2.23** are not appreciably altered from those reported for diradical **2.18**. The pyridine nitrogen is again closer to the nickel ion [Ni1-N1 = 1.9728(18) Å] in **2.23** than are the verdazyl nitrogens [Ni1-N2 = 2.1478(19) Å, Ni1-N6 = 2.1213(19) Å]. The Cl-M-Cl bond angle is noticeably larger in **2.23** [140.44(3)°] than in any of the previously described metal-diradical complexes **2.19** – **2.22** (in which the analogous bond angle ranges from 110.68° – 114.71°).

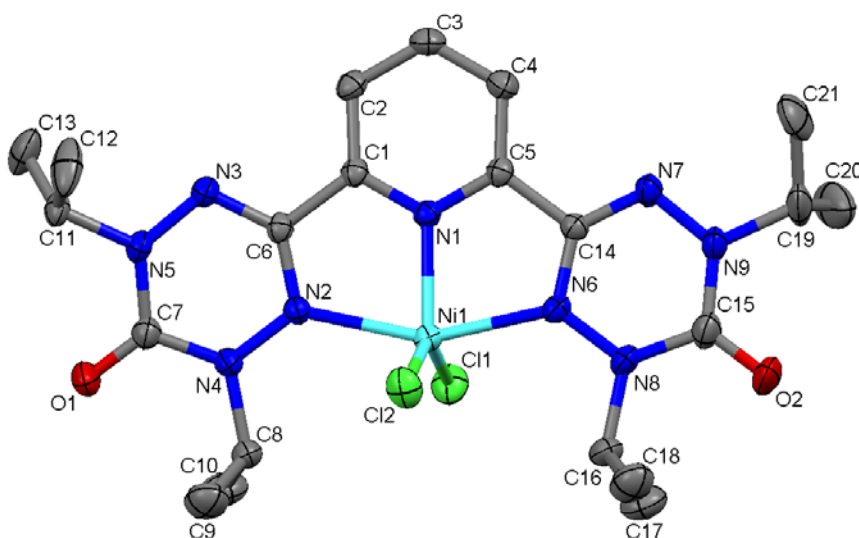


**Figure 2.30:** Molecular structure of nickel-diradical complex **2.23**. Thermal ellipsoids displayed at 50% probability level. Hydrogen atoms removed for clarity.

**Table 2.9:** Selected bond lengths (Å) and angles (degrees) for **2.23**.

Atoms	Length (Å)	Atoms	Angle (°)
C1-C6	1.478(3)	N2-C6-N3	127.3(2)
C5-C14	1.478(3)	N4-C7-N5	114.6(2)
C6-N2	1.336(3)	N6-C14-N7	127.9(2)
C6-N3	1.322(3)	N8-C15-N9	114.9(2)
C7-O1	1.213(3)	N4-N2-C6	115.73(18)
C7-N4	1.382(3)	N5-N3-C6	114.81(19)
C7-N5	1.393(3)	N2-N4-C7	122.84(19)
C14-N6	1.334(3)	N3-N5-C7	124.13(18)
C14-N7	1.318(3)	N8-N6-C14	115.46(19)
C15-O2	1.210(3)	N9-N7-C14	114.57(19)
C15-N8	1.383(3)	N6-N8-C15	122.7(2)
C15-N9	1.387(3)	N7-N9-C15	124.41(19)
N2-N4	1.368(2)	N1-Ni1-N2	77.49(7)
N3-N5	1.359(3)	N1-Ni1-N6	78.11(7)
N6-N8	1.369(3)	N2-Ni1-N6	155.58(8)
N7-N9	1.357(3)	Cl1-Ni1-Cl2	140.44(3)
Ni1-N1	1.9728(18)		
Ni1-N2	2.1478(19)		
Ni1-N6	2.1213(19)		

### 2.6.10 Magnetic properties of **2.23**

Magnetic properties of nickel complex **2.23** were recorded from 300 – 2 K and the results are displayed in Figure 2.31. At 300 K,  $\chi T$  is  $3.51 \text{ emu}\cdot\text{K}\cdot\text{mol}^{-1}$ , which is much higher than the expected spin-only value of  $1.75 \text{ emu}\cdot\text{K}\cdot\text{mol}^{-1}$  for three non-coupled spin systems of  $S = 1$ ,  $S = \frac{1}{2}$  and  $S = \frac{1}{2}$ . The value of  $\chi T$  does not change drastically as temperature is decreased from 300 to 80 K. Below approximately 80 K, however, the magnetic moment begins to decrease. This behaviour is consistent with strong ferromagnetic coupling between the nickel(II) and the verdazyl moieties of the diradical ligand. Ferromagnetic exchange has been reported for other nickel coordination compounds involving verdazyl monoradicals<sup>94</sup> and pyridine-bridged imino nitroxide diradicals.<sup>186</sup>

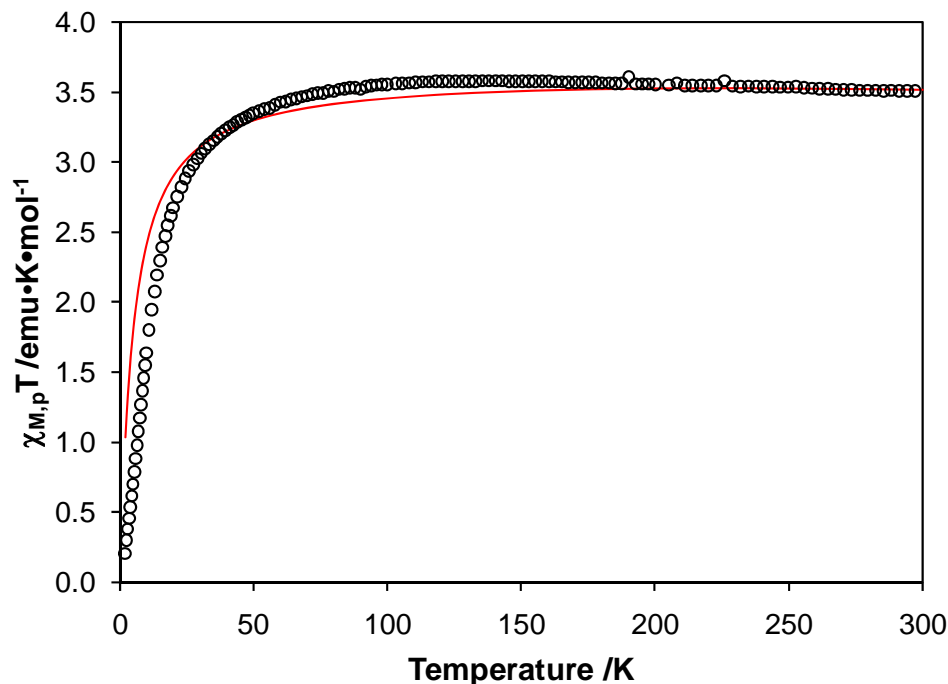


**Figure 2.31:**  $\chi T$  vs.  $T$  data (○) and model fit (—) for complex **2.23** from 2 – 300 K.

The red line in Figure 2.31 was calculated from Equation 2.9 with the following parameters:  $g_{Vd} = 2.00$  (fixed),  $g_{Ni} = 2.40$ ,  $J_{Ni-Vd} = +180.0 \text{ cm}^{-1}$ ,  $J_{Vd-Vd} = +40 \text{ cm}^{-1}$  (fixed) and  $\theta = -5.00 \text{ K}$ . The model gave a goodness of fit factor of  $R = 0.114$ . The metal-radical coupling constant of  $+180 \text{ cm}^{-1}$  infers strong ferromagnetic coupling between the nickel ion and the two verdazyl moieties, which is consistent with the high-temperature  $\chi T$  data shown in Figure 2.31. The low temperature drop in  $\chi T$  was again modelled using a Weiss constant in Equation 2.9. However, the low-temperature magnetic behaviour in nickel-diradical complex **2.23** (Figure 2.31) is qualitatively dissimilar to that observed for the nickel-monoradical complex **2.14** (Figure 2.6). This indicates that there is more contributing to the low-temperature magnetic moment in **2.23** than just weak intermolecular interactions. The Weiss constant used in this case appears insufficient to completely model this behaviour. Zero-field splitting in the nickel ion is likely also

contributing to the magnetic behaviour in **2.23**. Additionally, the nickel g-value in **2.23** is higher than those described in other five-coordinate nickel complexes,<sup>187</sup> which can be a sign of strong spin-orbit coupling.<sup>188</sup>

$$\chi = \frac{2N\beta^2}{k(T-\theta)} \frac{5g_1^2 + g_2^2 \exp\left(\frac{-J_{Ni-Vd}J_{Vd-Vd}}{kT}\right)}{5 + \exp\left(\frac{-3J_{Ni-Vd}}{kT}\right) + 3\exp\left(\frac{-J_{Ni-Vd}J_{Vd-Vd}}{kT}\right)} \quad (2.9)$$

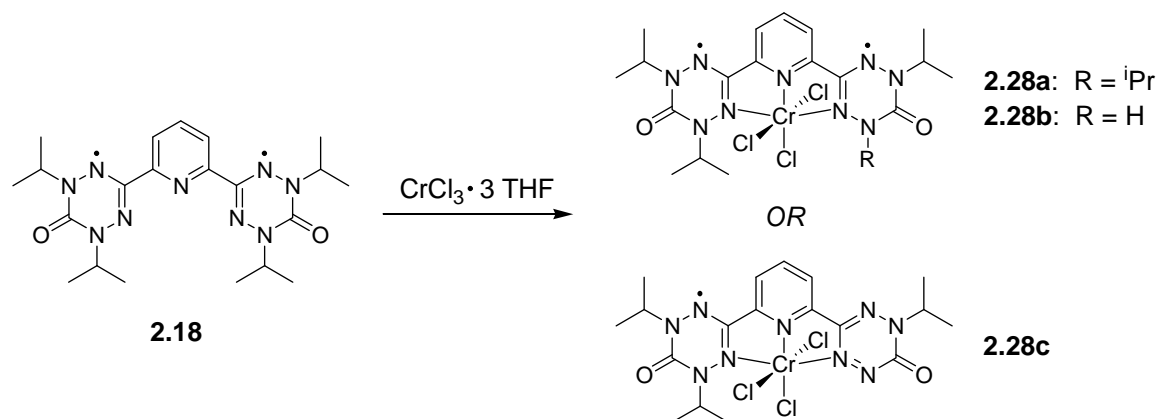
$$g_1 = \frac{g_{Ni} + g_{Vd}}{2} \quad g_2 = g_{Ni}$$

## 2.7 Synthesis and characterisation of other coordination compounds involving diradical **2.18**

### 2.7.1 Synthesis and characterisation of chromium complex **2.28**

At the outset of this research, there had been no verdazyl-chromium complexes reported. In an effort to use diradical **2.18** to investigate an as yet unexplored aspect of verdazyl coordination chemistry, the general synthesis presented in Scheme 2.6 (used to prepare compounds **2.19** – **2.23**) was modified to incorporate a Cr(III) starting material. This procedure is shown in Scheme 2.7. Chromium trichloride tris(tetrahydrofuran) and diradical **2.18** were combined in dichloromethane and stirred at room temperature for a period of 16 hours. However, analysis of the product revealed that the ligand did not simply coordinate to the chromium(III) centre to give the expected complex **2.28a**. In fact, structural analysis of the product revealed that one of the N-isopropyl substituents is absent in the resulting metal complex. Intuitively, this leaves two likely possibilities with respect to the structure of the product: One of the verdazyl rings may have a hydrogen-

substituted amide-type nitrogen atom, and the radical nature of the heterocycle remains intact (**2.28b**); or that particular ring is no longer a radical and there should be alternating double and single bonds (**2.28c**).



**Scheme 2.7:** Synthesis of the chromium(III) coordination compound **2.28**.

The molecular structure of the chromium-diradical complex is presented in Figure 2.32. Selected bond lengths and angles are highlighted in Table 2.10. The most conspicuous aspect of this structure is the replacement of one N-substituted isopropyl group with a hydrogen atom (H4N), which was located in difference maps and refined isotropically during the X-ray diffraction experiment. The presence of this hydrogen atom points toward **2.28b** as the accurate representation of this chromium-verdazyl complex. However, locating hydrogen atoms in an X-ray diffraction experiment is not always reliable. Additional structural evidence to support the assignment of this coordination compound as **2.28b**, rather than **2.28c**, can be gleaned from an inspection of the bond lengths and angles around the two verdazyl moieties. The ring bearing only one N-isopropyl substituent is structurally similar to its disubstituted counterpart and the bond lengths around the respective rings are consistent with delocalisation of the unpaired electron in each radical unit. The N-N bonds [N2-N4 = 1.351(4) Å; N3-N5 = 1.354(4) Å]

in the N-H substituted ring are comparable to those in the diisopropyl-substituted heterocycle [N6-N8 = 1.361(4) Å; N7-N9 = 1.360(4) Å]. These values also correlate well with the corresponding N-N bond lengths in diradical **2.18** [1.365(2) Å and 1.3646(19) Å]. There is no evidence of single and double bond alternation around the ring, as would be expected in the case where the disparate ring is not a radical (structure **2.28c**). The structural similarities between the two verdazyl rings imply that both of the  $\pi$ -SOMOs are still electronically intact.

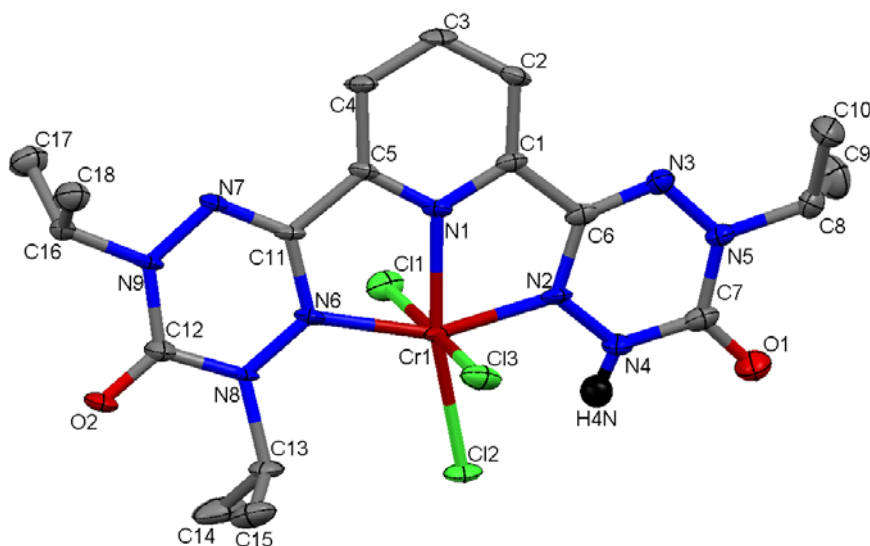


**Figure 2.32:** Molecular structure of **2.28b**. Thermal ellipsoids displayed at 50% probability level. Calculated hydrogen atoms removed for clarity.

**Table 2.10:** Selected bond lengths (Å) and angles (degrees) for **2.28b**.

Atoms	Length (Å)	Atoms	Angle (°)
C1-C6	1.471(5)	N2-C6-N3	126.0(4)
C5-C11	1.479(5)	N4-C7-N5	114.5(4)
C6-N2	1.348(5)	N6-C11-N7	127.2(4)
C6-N3	1.313(5)	N8-C12-N9	115.2(4)
C7-O1	1.207(5)	N4-N2-C6	114.6(3)
C7-N4	1.360(6)	N5-N3-C6	116.6(3)
C7-N5	1.385(5)	N2-N4-C7	125.1(4)
C11-N6	1.356(5)	N3-N5-C7	123.0(3)
C11-N7	1.300(5)	N8-N6-C11	114.5(3)
C12-O2	1.207(5)	N9-N7-C11	115.7(3)
C12-N8	1.374(5)	N6-N8-C12	123.4(3)
C12-N9	1.378(5)	N7-N9-C12	123.6(3)
N2-N4	1.351(4)	N1-Cr1-N2	77.28(13)
N3-N5	1.354(4)	N1-Cr1-N6	77.41(13)
N6-N8	1.361(4)	N2-Cr1-N6	154.68(13)
N7-N9	1.360(4)	Cl1-Cr1-Cl2	91.21(5)
Cr1-N1	2.001(3)	Cl2-Cr1-Cl3	91.16(4)
Cr1-N2	1.980(3)	Cl1-Cr1-Cl3	176.91(5)
Cr1-N6	2.093(3)		
Cr1-Cl1	2.2986(13)		
Cr1-Cl2	2.3274(12)		
Cr1-Cl3	2.3071(13)		

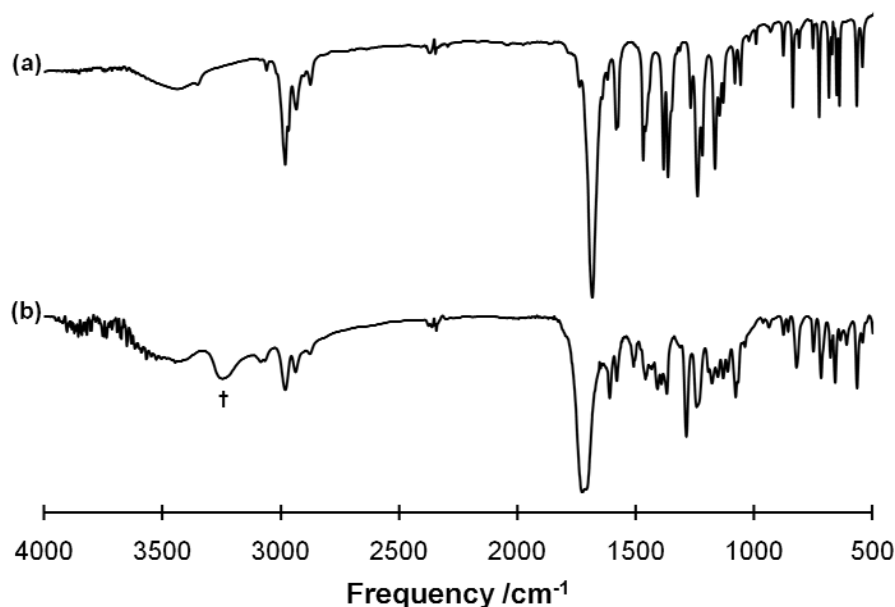


**Figure 2.33:** Infrared spectra of (a) diradical **2.18** and (b) chromium complex **2.28b** recorded as pressed KBr disks with air background. N-H band in **2.28b** indicated by †.

The infrared spectrum of this complex (Figure 2.33) further substantiates the presence of a hydrogen atom at the N4 position. The broad signal around 3250 cm<sup>-1</sup> corresponds to an N-H stretch. An analogous band is seen at 3240 cm<sup>-1</sup> in the IR spectrum of tetrazane **2.17**, but not in the corresponding spectrum of diradical **2.18** (see Figure 2.10). Furthermore, the characteristic carbonyl band appears as a small fork, indicating two discrete C=O stretching frequencies are represented. This is consistent with two distinct verdazyl radical rings comprising the ligand in this chromium coordination compound.

The electronic spectrum of the chromium complex is compared to that of diradical **2.18** in Figure 2.34. The typical bathochromic shift of the absorption maximum associated with the verdazyl SOMO is also evident in this spectrum. The magnitude of



the shift is consistent with that seen in the **2.18**MCl<sub>2</sub> series (**2.19** – **2.23**). The energy and intensity of these electronic transitions indicate that a verdazyl radical is present in this species. However, examination of the UV-Vis spectrum alone does not relieve the ambiguity as to whether the ligand is a mono- or diradical, as the reported transitions would still be present in the case where only one of the verdazyl rings contains an unpaired electron.

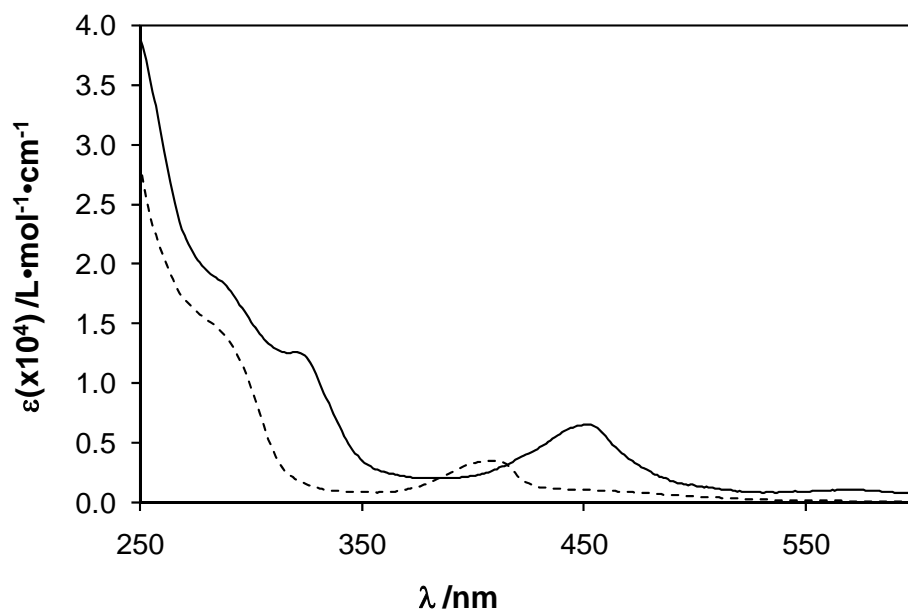


**Figure 2.34:** UV-Vis spectra of diradical **2.18** (dashed line) and chromium complex **2.28b** (solid line) in dichloromethane.

### 2.7.2 Magnetic properties of chromium complex **2.28b**

Figure 2.35 plots the magnetic behaviour of **2.28b** as  $\chi T$  vs.  $T$  from 300 – 2 K. At 300 K,  $\chi T$  for this complex is 0.63 emu•K•mol<sup>-1</sup>. On lowering the temperature from 300 to 150 K,  $\chi T$  shows a steady decrease. Between 150 and 10 K,  $\chi T$  remains relatively constant at about 0.46 emu•K•mol<sup>-1</sup>. Below 10 K there is a rapid drop-off in the magnetic moment.

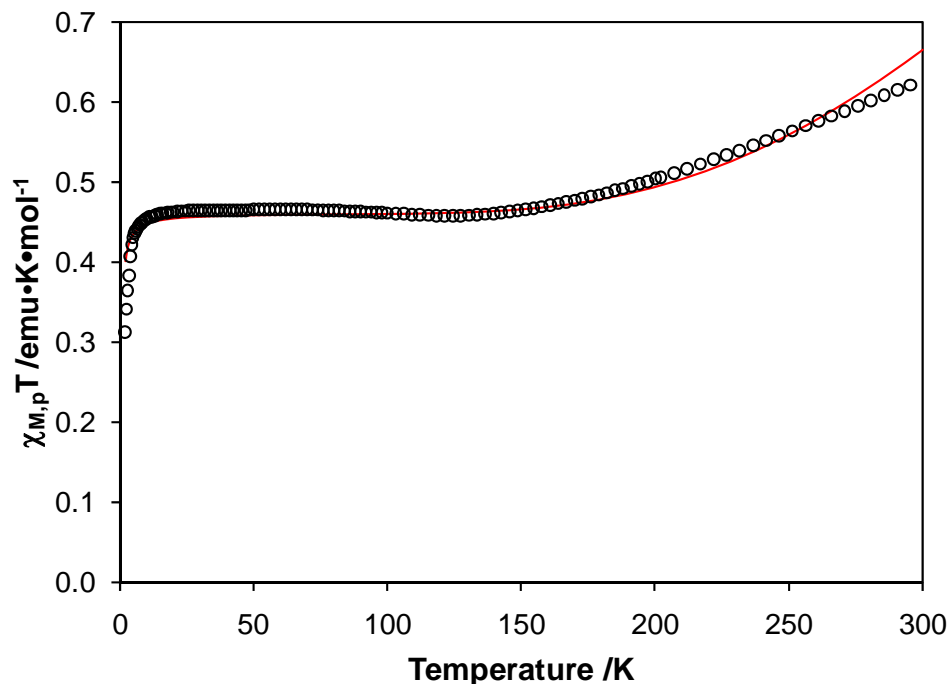


**Figure 2.35:**  $\chi T$  vs.  $T$  data (○) and model fit (—) of complex **2.28b** from 2 – 300 K.

A close examination of the magnetic behaviour presented in Figure 2.35 provides the best evidence for the assertion that the verdazyl ligand remains a diradical despite the acute physical change that occurs upon coordination to chromium. The high temperature  $\chi T$  value of  $0.63 \text{ emu}\cdot\text{K}\cdot\text{mol}^{-1}$  is considerably lower than the spin-only value of  $2.63 \text{ emu}\cdot\text{K}\cdot\text{mol}^{-1}$  for an  $S = 3/2$  chromium(III) ion and two  $S = 1/2$  radicals. However, it is also much lower than the spin-only value of  $2.25 \text{ emu}\cdot\text{K}\cdot\text{mol}^{-1}$  that would result from an  $S = 3/2$  chromium(III) ion and only one  $S = 1/2$  radical. Whether the ligand is a mono- or diradical is uncertain, based on this value alone. For the case of a diradical ligand coordinated to an  $S = 3/2$  chromium(III) ion, an antiferromagnetically coupled system would result in an  $S = 1/2$  complex and a spin-only  $\chi T$  value of  $0.375 \text{ emu}\cdot\text{K}\cdot\text{mol}^{-1}$ , with each of the two diradical spins compensating one of the three unpaired electrons on chromium. Conversely, antiferromagnetic coupling between the same chromium ion and

only one  $S = \frac{1}{2}$  radical would leave two unpaired electrons on the metal, resulting in an  $S = 1$  system and a spin-only  $\chi T$  value of  $1.00 \text{ emu}\cdot\text{K}\cdot\text{mol}^{-1}$ . The observed plateau value of  $0.46 \text{ emu}\cdot\text{K}\cdot\text{mol}^{-1}$  (between 150 and 10 K in Figure 2.35) represents the ground state for this molecule. Since this value is less than  $1.00 \text{ emu}\cdot\text{K}\cdot\text{mol}^{-1}$ , it could only arise from antiferromagnetic coupling of a  $\text{Cr}^{3+}$  ion with *two*  $S = \frac{1}{2}$  radicals. Modelling the magnetic data with Equation 2.10, based on a three-spin system, gave the following parameters:  $g_{\text{Vd}} = 2.00$  (fixed),  $g_{\text{Cr}} = 2.13$ ,  $J_{\text{Vd-Cr}} = -255 \text{ cm}^{-1}$ ,  $J_{\text{Vd-Vd}} = +40.0 \text{ cm}^{-1}$  (fixed) and  $\theta = -0.3 \text{ K}$ . The model gave a goodness of fit factor of  $R = 0.031$ . The combined structural and magnetic analyses provide compelling evidence that the chromium complex here is, in fact, the diradical coordination compound **2.28b**. This is the first example of a 6-oxoverdazyl radical that does not bear an N-alkyl or N-aryl substituent alpha to the carbonyl group.

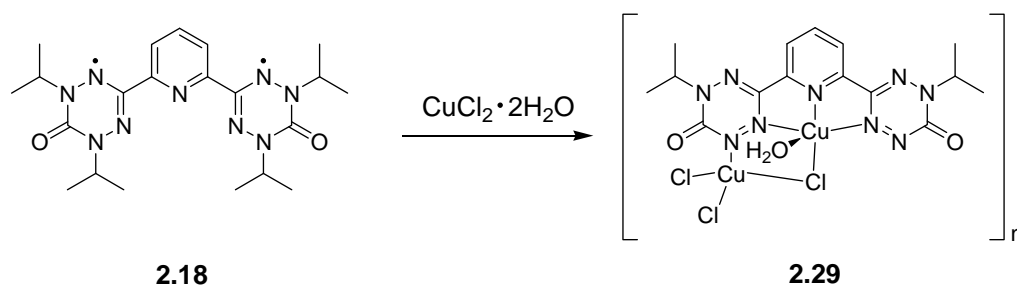
$$\chi = \frac{N\beta^2}{4k(T-\theta)} \frac{g_1^2 + 35 g_2^2 \exp\left(\frac{4J_{\text{Cr-Vd}}}{kT}\right) + 10 g_3^2 \exp\left(\frac{5J_{\text{Cr-Vd}} - 2J_{\text{Vd-Vd}}}{2kT}\right)}{1 + 3 \exp\left(\frac{4J_{\text{Cr-Vd}}}{kT}\right) + 2 \exp\left(\frac{5J_{\text{Cr-Vd}} - 2J_{\text{Vd-Vd}}}{2kT}\right)} \quad (2.10)$$

$$g_1 = \frac{-2g_{\text{Vd}} + 5g_{\text{Cr}}}{3} \quad g_2 = \frac{2g_{\text{Vd}} + 3g_{\text{Cr}}}{5} \quad g_3 = g_{\text{Cr}}$$

### 2.7.3 Synthesis and characterisation of copper complex 2.29

Copper complexes are well-represented in the realm of metal-radical coordination chemistry.<sup>146, 189-192</sup> The general procedure from Scheme 2.6 that was used to prepare the **2.18MCl<sub>2</sub>** series of coordination compounds **2.19** – **2.23** was employed in an attempt to realise an analogous copper(II) complex. However, the result of this reaction was

dramatically different from all of the other coordination compounds involving diradical **2.18**. Rather than a discrete verdazyl-copper complex, the product crystallised as an extended structure with two distinct copper ions in the asymmetric unit. Furthermore, the ligand in complex **2.29** was significantly altered from its original diradical structure. This reaction is shown in Scheme 2.8.



**Scheme 2.8:** Synthesis of the copper(II) coordination compound **2.29**.

Figure 2.36 shows the molecular structure of the asymmetric unit as well as a view of the extended structure of **2.29**. A number of structural differences discriminate **2.29** from the other coordination compounds presented here; the most obvious feature is the polymeric nature of the structure. Another distinguishing feature of this compound is the presence of two distinct copper ions in the asymmetric unit. The typical tridentate binding pocket of the ligand contains one copper ion with octahedral geometry while a second copper centre is tetrahedrally coordinated to three chlorides and the N5 nitrogen atom; a coordination mode that is not seen in any other complexes involving this ligand. Furthermore, the ligand in **2.29** has two fewer N-isopropyl substituents than does the parent diradical **2.18**.

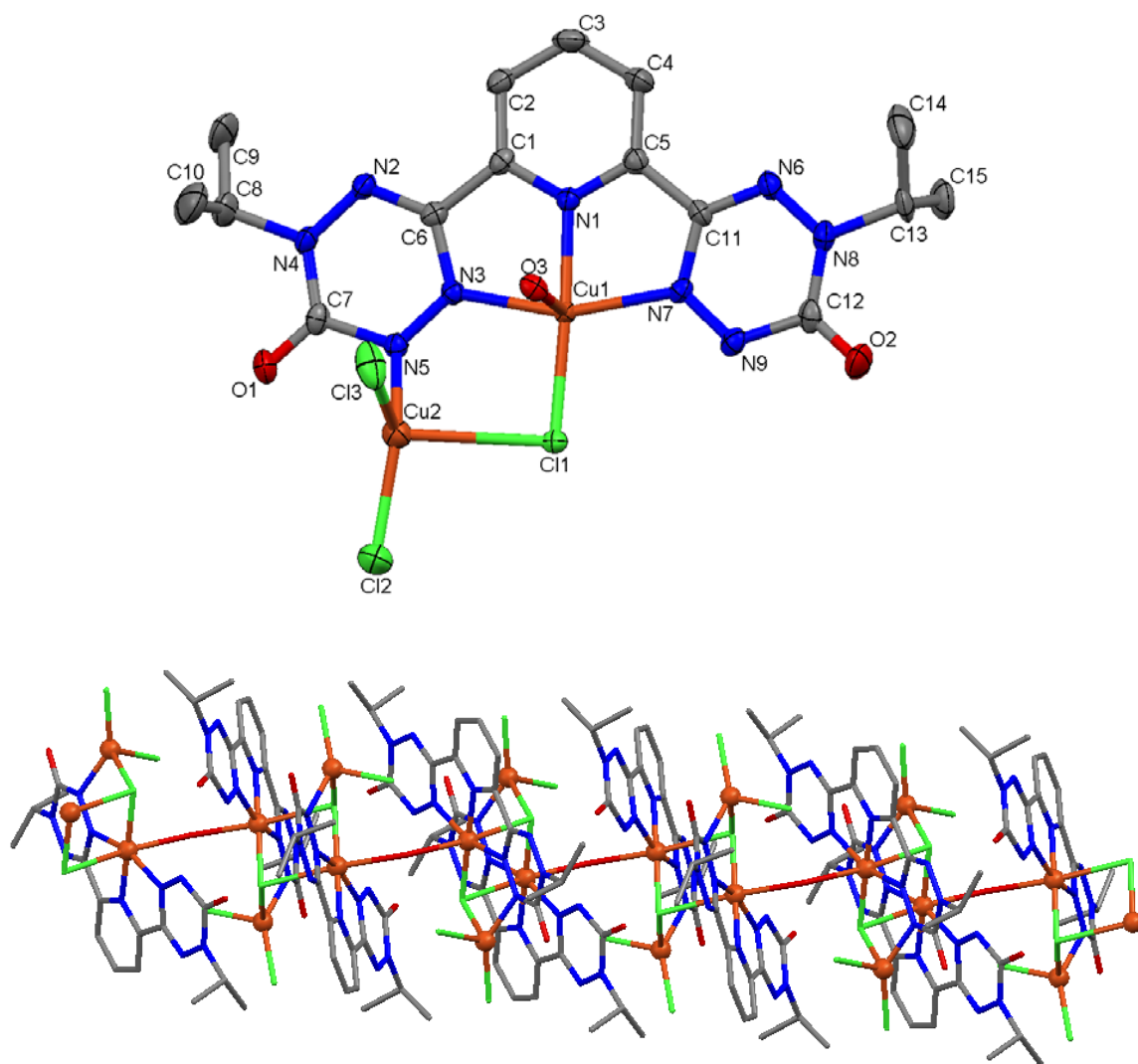


**Figure 2.36:** Molecular structure of **2.29** showing structure of repeat unit (top) and extended structure (bottom). Thermal ellipsoids displayed at 50% probability level. Hydrogen atoms removed for clarity.

**Table 2.11:** Selected bond lengths (Å) and angles (degrees) for **2.29**.

Atoms	Length (Å)	Atoms	Angle (°)
C1-C6	1.470(6)	N2-C6-N3	125.6(4)
C5-C11	1.460(6)	N4-C7-N5	117.4(4)
C6-N2	1.300(5)	N6-C11-N7	123.9(4)
C6-N3	1.370(5)	N8-C12-N9	115.8(4)
C7-O1	1.209(5)	N4-N2-C6	115.2(3)
C7-N4	1.370(5)	N5-N3-C6	119.5(3)
C7-N5	1.418(5)	N2-N4-C7	124.0(3)
C11-N6	1.299(5)	N3-N5-C7	118.2(3)
C11-N7	1.364(5)	N8-N6-C11	116.7(4)
C12-O2	1.197(5)	N9-N7-C11	120.4(4)
C12-N8	1.387(6)	N6-N8-C12	123.7(4)
C12-N9	1.414(6)	N7-N9-C12	119.4(4)
N2-N4	1.346(5)	N1-Cu1-N3	79.71(14)
N3-N5	1.323(5)	N1-Cu1-N7	79.70(14)
N6-N8	1.322(5)	N3-Cu1-N7	159.41(14)
N7-N9	1.292(5)		
Cu1-N1	1.941(3)		
Cu1-N3	2.018(3)		
Cu1-N7	2.046(3)		

A close examination of the bond lengths and angles of the ligand reveals further dissimilarities between **2.29** and other complexes involving this ligand, particularly with respect to the verdazyl rings. The differences in N-N bond lengths within the verdazyl rings are not insignificant in **2.29** [N2-N4 = 1.346(5) Å; N3-N5 = 1.323(5) Å; N6-N8 = 1.322(5) Å; N7-N9 = 1.292(5) Å]. This is indicative of alternating single and double bonds in at least one of the verdazyl heterocycles. Furthermore, no N-H hydrogen atoms were located in the crystal structure determination for **2.29**. This arrangement of alternating bonds contrasts what is seen in other verdazyl radicals and coordination compounds. The bonding motif observed in **2.29** suggests that the electronic nature of these rings is something other than an unpaired electron delocalised over four nitrogen

atoms, as is typical of other verdazyl radicals. In fact, it is likely that the ligand in **2.29** is no longer a diradical upon coordination to copper.

It should be noted that elemental analysis of this product does not match the molecular structure as determined by X-ray diffraction analysis. This suggests that the bulk material isolated is different from the single crystal that was analysed. The UV-Vis spectrum of **2.29** (Figure 2.37) shows a broad band between 350 and 450 nm, rather than any discrete absorptions in this region. Owing to the apparent structural and electronic complexity associated with **2.29**, no magnetic studies were pursued with this compound.

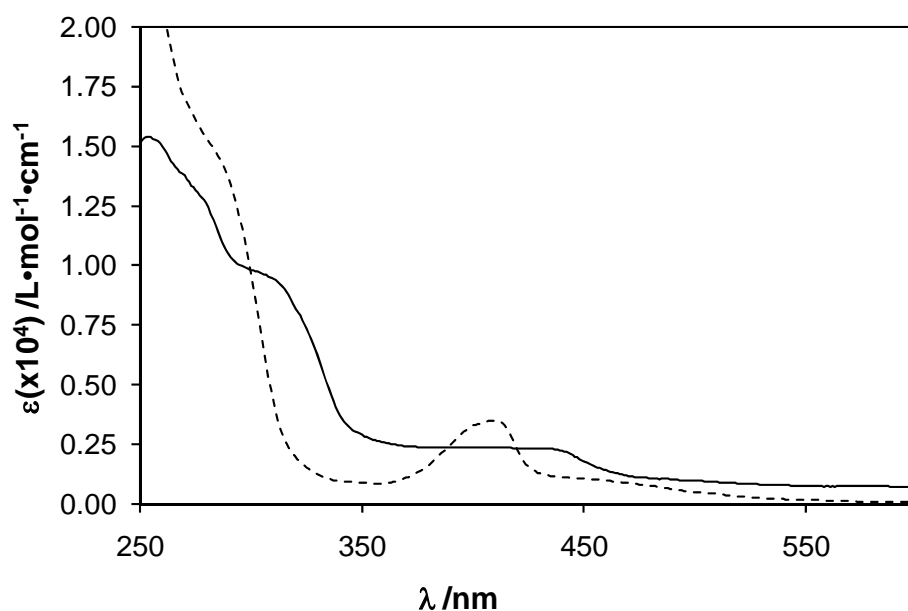


**Figure 2.37:** UV-Vis spectra of diradical **2.18** (dashed line) and copper complex **2.29** (solid line) in dichloromethane.

## 2.8 Summary

The work presented in this chapter represents a fundamental study of the coordination chemistry of highly stable 6-oxoverdazyl radicals and diradicals. The

compounds presented here can be envisioned as model systems to further the understanding of discrete metal-radical electronic interactions that give rise to magnetic coupling. The series of complexes studied here encompasses new coordination compounds using a known verdazyl radical as the ligand, as well as the design and coordination chemistry of a novel verdazyl diradical ligand.

Incorporation of isopropyl substituents onto the framework of a chelating verdazyl monoradical ligand allowed a comparison of the structural and magnetic properties between the new complexes prepared and presented here and previously reported methyl-substituted analogues. While switching from the methyl to the isopropyl derivatives increases the stability of the resulting verdazyl radicals, it has no significant impact on the coordination mode of the ligand. In turn, the magnetic properties of the resulting complexes show little significant variation with this change.

The enhanced stability of the isopropyl verdazyl framework allowed for the synthesis and complete characterisation of a novel diradical, as well as a rigorous study of the associated coordination chemistry of this ligand. This *meta*-substituted pyridine diradical exhibits weak ferromagnetic coupling between the two verdazyl moieties, which is consistent with other nitroxide and verdazyl diradicals featuring similar aryl linkers. The lack of any noteworthy intermolecular exchange pathways in the crystal packing motif of this diradical allowed for an unambiguous examination of the intramolecular electronic communication parameters.

A series of metal complexes was prepared using this ligand, which represents the first systematic study of the coordination chemistry of a verdazyl diradical. The *pseudo*-trigonal bipyramidal geometry observed in the majority of complexes presented herein is



a unique coordination framework for verdazyl complexes, further adding to their value as model systems in the metal-radical paradigm. The nature of the magnetic interactions among these compounds is highly dependent on the metal involved, owing to the spatial relationship between the magnetic orbitals of the respective metals and the diradical ligand. Incorporation of a diamagnetic zinc centre was shown to have minimal impact on the magnetic exchange in the diradical ligand. Manganese(II) and iron(II) complexes experience strong antiferromagnetic exchange between the metal ion and the two verdazyl moieties. Conversely, nickel(II) couples ferromagnetically (and rather strongly) to the diradical ligand. Cobalt(II) also exhibits ferromagnetic metal-radical coupling. However, spin-orbit coupling clearly plays a significant role in the magnetic behaviour of the cobalt complex, making it difficult to obtain the exact metal-radical coupling parameters. A more rigid analysis of the magnetic data for the cobalt and nickel diradical complexes could endeavour to fully account for the low-temperature zero-field splitting effects that were discussed for these compounds. The compounds presented in this chapter are intended to be considered as a series of magnetic model systems. In this light, it is the trend in magnetic exchange within this series of coordination compounds (that is to say the sign and relative magnitude of the metal-radical coupling) that represents the real value in this study.

Two of the diradical coordination compounds studied proved to be noticeably structurally distinct from the rest of the series. Complex **2.28b** is the first example of a chromium-verdazyl complex. Perhaps even more intriguingly, this compound represents a unique example of a verdazyl radical where one nitrogen atom in the heterocyclic framework is bonded to a hydrogen atom, rather than an alkyl or aryl substituent.

Although the origin of the ligand transformation upon coordination to chromium is not known, the magnetic and structural data for **2.28b** provide confirmation that the ligand is indeed a diradical. This study is an interesting example of magnetic data being used to confirm the electronic structure of what might otherwise be an ambiguous characterisation. Conversely, structural characterisation of the coordination polymer **2.29** shows that this same ligand not only loses its radical nature upon coordination to copper, but also undergoes pronounced structural changes to the ligand framework.

## **2.9 Experimental**

### **2.9.1 General considerations**

Solvents were typically dried over an appropriate drying agent<sup>193</sup> and distilled under argon prior to use. Reagents were purchased from various commercial supply companies and used without further purification (1,4-benzoquinone was recrystallised prior to its use as oxidant in the preparation of 6-oxoverdazyl radicals and diradicals). NMR spectra were recorded using a Bruker Avance III 300 MHz spectrometer with IconNMR 4.2 acquisition software. Infrared spectra were recorded as pressed KBr disks using a Perkin Elmer Spectrum One FT-IR spectrometer with Spectrum 5.0 acquisition software. Electronic spectra were recorded using an Agilent 8453 UV-Vis spectrometer with Chemstation acquisition software. EPR spectra were recorded using a Bruker EMX EPR spectrometer with an X-band microwave bridge and using WinEPR acquisition software. Variable-temperature EPR data were collected by Drs. Joe Gilroy (University of Victoria) and Pierre Kennepohl (University of British Columbia) using a Bruker AMX360 EPR spectrometer with a helium cryostat. Samples for VT-EPR studies were prepared in deoxygenated toluene, using three freeze-pump-thaw cycles. All EPR spectra were simulated using WinEPR SimFonia. Magnetic measurements were made using a

Quantum Design MPMS SQUID magnetometer operating at a field strength of 1 T. (measurements of **2.20** were made by Dr. Laurence Thompson at the Memorial University of Newfoundland). Diamagnetic corrections were made by subtracting either Pascal's constants (**2.18**, **2.20**, **2.21**, **2.28b**) or the slope of the uncorrected  $\chi T$  vs.  $T$  plot in the paramagnetic regime (**2.14**, **2.15**, **2.18**, **2.19**, **2.22**, **2.23**) from the  $\chi T$  data. Elemental analyses were carried out at Canadian Microanalytical Services, Ltd. in Delta, British Columbia. Melting points were determined using a Gallenkamp melting point apparatus. Mass spectra were obtained using a Kratos Concept H spectrometer using electron impact (EI-MS) or liquid secondary ionisation (LSI-MS) or a Micromass Q-TOF II spectrometer using electrospray ionisation (ESI-MS) in the positive mode.

## **2.9.2 Synthesis and characterisation of 2.13M(hfac)<sub>2</sub> coordination compounds**

### **1,5-diisopropyl-3-(pyridine-2'-yl)-6-oxoverdazylbis-(1,1,1,5,5,5-**

**hexafluoroacetylacetonato)nickel(II) (2.14).** Equimolar amounts of **2.13**<sup>106</sup> (259.9 mg, 0.9984 mmol) and Ni(hfac)<sub>2</sub>•2H<sub>2</sub>O (507.6 mg, 0.9976 mmol) were dissolved in CH<sub>2</sub>Cl<sub>2</sub> (100 mL) and heated at reflux for 1.25 hours. After 1.25 hours, heat was removed and solvent was removed under reduced pressure to yield red solid residue. The residue was further dried under vacuum for 30 minutes. Hexanes (50 mL) were added to residue and the mixture was heated at reflux for 15 minutes then filtered while still hot to remove any unreacted Ni(hfac)<sub>2</sub>•2H<sub>2</sub>O. Filtrate was allowed to cool to room temperature, then set in a freezer for 36 hours. X-ray quality crystals of **2.14** were isolated by filtration and washed with 3 × 5 mL cold hexanes. Yield 479.3 mg (65.4 %). Mp. 110 – 112 °C (uncorrected). FT-IR (KBr): 3284 (m), 3137 (w), 2987 (w), 2943 (w), 1711 (vs), 1643 (vs), 1608 (m), 1554 (s), 1527 (s), 1484 (vs), 1395 (m), 1370 (m), 1348 (m), 1258 (s),

1200 (s), 1146 (s), 1097 (m), 1051 (w), 796 (s), 671 (s), 589 (s), 529  $\text{cm}^{-1}$  (w). UV-Vis ( $\text{CH}_2\text{Cl}_2$ ):  $\lambda_{\text{max}}$  318 ( $\epsilon = 15500$ ), 403 ( $\epsilon = 1650$ ), 418 ( $\epsilon = 2020$ ), 431 ( $\epsilon = 1880$ ), 494 nm ( $\epsilon = 462 \text{ L}\cdot\text{mol}^{-1}\cdot\text{cm}^{-1}$ ). Anal. Calcd. for  $\text{C}_{23}\text{H}_{20}\text{F}_{12}\text{N}_5\text{NiO}_5$ : C, 37.68; H, 2.75; N, 9.55. Found: C, 37.94; H, 2.70; N, 9.44.

**1,5-diisopropyl-3-(pyridine-2'-yl)-6-oxoverdazylbis-(1,1,1,5,5,5-**

**hexafluoroacetylacetonato)cobalt(II) (2.15).** Equimolar amounts of **2.13**<sup>106</sup> (311.6 mg, 1.197 mmol) and  $\text{Co}(\text{hfac})_2\cdot 2\text{H}_2\text{O}$  (611.3 mg, 1.201 mmol) were dissolved in  $\text{CH}_2\text{Cl}_2$  (50 mL) and heated at reflux for one hour. After one hour, heat was removed and solvent was removed under reduced pressure to yield red solid residue. The residue was further dried under vacuum for 30 minutes. Hexanes (50 mL) were added to residue and the mixture was heated at reflux for 15 minutes then filtered while still hot to remove any unreacted  $\text{Co}(\text{hfac})_2\cdot 2\text{H}_2\text{O}$ . Filtrate was allowed to cool to room temperature, then set in a freezer for 20 hours. Crystals were observed in the cold flask, but attempts to isolate the crystals at room temperature resulted in the crystals apparently melting to yield a red, tarry mixture. X-ray quality crystals of **2.15** were attained by vapour diffusion with ethyl acetate as solvent and n-pentane as counter solvent. Yield 663.8 mg (75.8 %). Mp. 106 – 108 °C (uncorrected). FT-IR (KBr): 3262 (m), 3142 (w), 2987 (w), 2943 (w), 1709 (vs), 1640 (vs), 1606 (m), 1554 (s), 1529 (s), 1486 (vs), 1460 (sh), 1395 (m), 1370 (m), 1346 (m), 1256 (s), 1202 (s), 1146 (s), 1097 (m), 1049 (w), 796 (s), 669 (s), 585 (s), 527  $\text{cm}^{-1}$  (w). UV-Vis ( $\text{CH}_2\text{Cl}_2$ ):  $\lambda_{\text{max}}$  289 ( $\epsilon = 23900$ ), 404 ( $\epsilon = 2320$ ), 417 ( $\epsilon = 2330$ ), 430 ( $\epsilon = 2380$ ), 474 nm ( $\epsilon = 990 \text{ L}\cdot\text{mol}^{-1}\cdot\text{cm}^{-1}$ ). Anal. Calcd. for  $\text{C}_{23}\text{H}_{20}\text{CoF}_{12}\text{N}_5\text{O}_5$ : C, 37.67; H, 2.75; N, 9.55. Found: C, 38.09; H, 2.71; N, 9.30.

**1,5-diisopropyl-3-(pyridine-2'-yl)-6-oxoverdazylbis-(1,1,1,5,5,5-hexafluoroacetylacetonato)manganese(II) (2.16).** Equimolar amounts of **2.13**<sup>106</sup> (205.3 mg, 0.7887 mmol) and Mn(hfac)<sub>2</sub>•2H<sub>2</sub>O (398.8 mg, 0.7896 mmol) were dissolved in CH<sub>2</sub>Cl<sub>2</sub> (100 mL) and heated at reflux for 1.25 hours. After 1.25 hours, heat was removed and solvent was removed under reduced pressure to yield red solid residue. The residue was further dried under vacuum for one hour. X-ray quality crystals of **2.16** were attained from vapour diffusion by dissolving the bulk reaction product in dichloromethane and using n-pentane as counter solvent. Yield 109.9 mg (19.1 %).

### 2.9.3 Synthesis and characterisation of diradical 2.18

**2,6-pyridinebis(1,5-diisopropyl-1,2,4,5-tetrazane-6-oxide-3-yl) (2.17).** A solution of 2,6-pyridinedicarboxaldehyde<sup>194</sup> (0.77 g, 5.7 mmol) in methanol (200 mL) was added drop-wise to a refluxing mixture of carbonic acid bis(1-isopropylhydrazide)•2HCl (2.84 g, 11.5 mmol) and sodium acetate (1.89 g, 23.0 mmol) in methanol (30 mL) over a period of 3 h. After complete addition of the dialdehyde solution, the reaction was refluxed in air overnight. After 16 h at reflux, heat was removed from the reaction and methanol was removed under reduced pressure. The residue was dissolved in dichloromethane and washed with distilled water (3 × 50 mL). The organic fraction was dried with MgSO<sub>4</sub>, gravity filtered, and then dichloromethane was removed under reduced pressure. The residue was taken up in boiling ethyl acetate (50 mL) and set in the freezer overnight, which gave **2.17** (1.39 g, 54 %) as a white powder. This product was further purified by dissolving in dichloromethane and evaporating the solvent under reduced pressure. The cycle of dissolving in dichloromethane followed by evaporating the solvent under reduced pressure was then carried out two additional times to remove

any traces of ethyl acetate. The white powder was then heated under vacuum at 70 °C for 48 h. Mp. 189 – 191 °C (uncorrected).  $^1\text{H}$  NMR (DMSO- $d_6$ ):  $\delta$  1.01 (d, 24 H,  $^3J = 7$  Hz), 4.38 (t, 2 H,  $^3J = 12$  Hz), 4.49 (m, 4 H,  $^3J = 7$  Hz), 5.18 (d, 4 H,  $^3J = 12$  Hz), 7.61 (d, 2 H,  $^3J = 8$  Hz), 7.90 ppm (t, 1 H,  $^3J = 8$  Hz).  $^{13}\text{C}$  NMR (DMSO- $d_6$ ): 18.4, 19.5, 47.0, 71.1, 104.7, 123.2, 138.4, 153.6, 154.3 ppm. FT-IR (KBr): 3445 (br), 3236 (m), 2967 (s), 2928 (m), 2868 (w), 1613 (vs), 1602 (sh), 1456 (s), 1410 (s), 1360 (m), 1294 (w), 1193 (w), 1127 (m), 1064 (m), 880 (w), 820 (w), 792 (w), 727  $\text{cm}^{-1}$  (w). MS (ESI-MS):  $m/z$  448.3  $\{[\text{M}+1]^+, 100 \%\}$ . Anal. Calcd. for  $\text{C}_{21}\text{H}_{37}\text{N}_9\text{O}_2$ : C, 56.35; H, 8.33; N, 28.17. Found: C, 55.74; H, 8.38; N, 27.71.

**2,6-pyridinebis(1,5-diisopropyl-6-oxoverdazyl-3-yl) (2.18).** **2.17** (1.44 g, 3.21 mmol) and *p*-benzoquinone (1.04 g, 9.64 mmol) were dissolved in toluene (100 mL). The solution was refluxed in air for 45 minutes, by which point the solution had turned a deep red colour. Toluene was removed under reduced pressure and the residue was then purified by column chromatography on neutral alumina with dichloromethane as eluent. Like fractions were combined and the solvent was removed under reduced pressure to yield **2.18** (1.12 g, 78.8 %) as a bright red microcrystalline solid. X-ray quality crystals were attained by cooling a saturated ethyl acetate solution of the microcrystalline solid in the freezer overnight. Mp. 154 – 156 °C (uncorrected). FT-IR (KBr): 2978 (s), 2928 (m), 2868 (w), 1681 (vs), 1574 (m), 1467 (m), 1382 (s), 1363 (s), 1237 (s), 1163 (s), 1080 (m), 1056 (m), 724 (m), 683 (m), 650 (m), 565  $\text{cm}^{-1}$  (m). UV-Vis ( $\text{CH}_2\text{Cl}_2$ ):  $\lambda_{\text{max}}$  238 ( $\epsilon = 42160$ ), 285 ( $\epsilon = 14600$ ), 410 ( $\epsilon = 3510$ ), 460 nm ( $\epsilon = 980 \text{ L}\cdot\text{mol}^{-1}\cdot\text{cm}^{-1}$ ). MS (ESI-MS):  $m/z$  464.25  $\{[\text{M}+\text{Na}]^+, 100 \%\}$ . Anal. Calcd. for  $\text{C}_{21}\text{H}_{31}\text{N}_9\text{O}_2$ : C, 57.13; H, 7.08; N, 28.55. Found: C, 57.12; H, 7.04; N, 28.89.

#### 2.9.4 Synthesis and characterisation of 2.18MCl<sub>2</sub> coordination compounds

**2,6-pyridinebis(1,5-diisopropyl-6-oxoverdazyl-3-yl)zinc(II) chloride (2.19).** To a solution of **2.18** (197.5 mg, 0.447 mmol) in acetonitrile (3 mL) was added drop-wise via Pasteur pipet a solution of ZnCl<sub>2</sub> (63.6 mg, 0.467 mmol) in acetonitrile (5 mL) in a 25 mL Erlenmyer flask. The reaction was left to stand without stirring for approximately 18 hours. Deep red plate-like crystals were isolated by vacuum filtration, followed by washing with 3 × 5 mL ice-cold acetonitrile, to yield 182.6 mg of **2.19** (70.7 %) X-ray quality crystals were attained by slow cooling of a saturated acetonitrile solution of the crude crystalline product, followed by sitting in a freezer for 24 hours. Crystals were isolated by vacuum filtration and then dried under vacuum for 24 hours. Mp. 258 – 260 °C (uncorrected). FT-IR (KBr): 2972 (m), 2934 (m), 2879 (w), 1700 (vs), 1604 (s), 1577 (s), 1484 (s), 1451 (w), 1380 (w), 1363 (s), 1283 (s), 1242 (s), 1160 (s), 1127 (m), 1075 (s), 817 (m), 716 (m), 661 (m), 642 (m), 562 (m), 524 cm<sup>-1</sup> (m). UV-Vis (CH<sub>2</sub>Cl<sub>2</sub>): λ<sub>max</sub> 244 (ε = 27270), 310 (ε = 14320), 321 (ε = 13510), 412 (ε = 2510), 433 nm (ε = 4030 L•mol<sup>-1</sup>•cm<sup>-1</sup>). Anal. Calcd. for C<sub>21</sub>H<sub>31</sub>N<sub>9</sub>O<sub>2</sub>ZnCl<sub>2</sub>: C, 43.65; H, 5.41; N, 21.82. Found: C, 43.67; H, 5.32; N, 21.85.

**2,6-pyridinebis(1,5-diisopropyl-6-oxoverdazyl-3-yl)manganese(II) chloride (2.20).**

To a solution of **2.18** (101.3 mg, 0.2294 mmol) in acetonitrile (3 mL) was added drop-wise via Pasteur pipet a solution of MnCl<sub>2</sub>•4H<sub>2</sub>O (45.8 mg, 0.231 mmol) in acetonitrile and methanol (10 mL CH<sub>3</sub>CN, 5 mL CH<sub>3</sub>OH) in a 25 mL Erlenmyer flask. The reaction was left to stand without stirring for approximately 18 hours. Red plate-like crystals were isolated by vacuum filtration, followed by washing with 3 × 5 mL ice-cold acetonitrile, then dried under vacuum for 24 hours to yield 79.2 mg of **2.20** (60.7 %). No

further recrystallisations were necessary. Mp. 244 – 246 °C (uncorrected). FT-IR (KBr): 2972 (s), 2934 (m), 2879 (w), 1700 (vs), 1602 (s), 1577 (s), 1484 (s), 1451 (m), 1382(m), 1363 (s), 1283 (s), 1242 (s), 1157 (s), 1127 (m), 1075 (s), 817 (m), 716 (m), 658 (m), 642 (m), 562 (m), 524  $\text{cm}^{-1}$  (m). UV-Vis ( $\text{CH}_2\text{Cl}_2$ ):  $\lambda_{\text{max}}$  245 ( $\epsilon = 36110$ ), 310 ( $\epsilon = 16460$ ), 434 ( $\epsilon = 5153$ ), 501 ( $\epsilon = 1045$ ), 529 (908), 575 nm ( $\epsilon = 848 \text{ L}\cdot\text{mol}^{-1}\cdot\text{cm}^{-1}$ ). Anal. Calcd. for  $\text{C}_{21}\text{H}_{31}\text{N}_9\text{O}_2\text{MnCl}_2$ : C, 44.45; H, 5.51; N, 22.22. Found: C, 44.06; H, 5.47; N, 22.11.

**2,6-pyridinebis(1,5-diisopropyl-6-oxoverdazyl-3-yl)iron(II) chloride (2.21).** To a solution of **2.18** (488.7 mg, 1.106 mmol) in dichloromethane (30 mL) was added drop-wise via Pasteur pipet a solution of  $\text{FeCl}_2\cdot 4\text{H}_2\text{O}$  (224.0 mg, 1.127 mmol) in dichloromethane (100 mL) in a 500 mL Erlenmyer flask. The reaction was left to stand without stirring for approximately 18 hours. Red plate-like crystals were isolated by vacuum filtration, followed by washing with  $3 \times 5$  mL ice-cold acetonitrile, then dried under vacuum for 24 hours to yield 232.8 mg of **2.21** (37.04 %). No further recrystallisations were necessary. Mp. 236 – 238 °C (uncorrected). FT-IR (KBr): 2972 (s), 2934 (m), 2873 (w), 1700 (vs), 1604 (s), 1577 (s), 1484 (s), 1451 (m), 1382 (m), 1363 (s), 1283 (s), 1242 (s), 1157 (s), 1127 (m), 1072 (s), 817 (m), 716 (m), 661 (m), 642 (m), 559 (m), 526  $\text{cm}^{-1}$  (m). UV-Vis ( $\text{CH}_2\text{Cl}_2$ ):  $\lambda_{\text{max}}$  246 ( $\epsilon = 28790$ ), 312 ( $\epsilon = 13640$ ), 436 nm ( $\epsilon = 4164 \text{ L}\cdot\text{mol}^{-1}\cdot\text{cm}^{-1}$ ). Anal. Calcd. for  $\text{C}_{21}\text{H}_{31}\text{N}_9\text{O}_2\text{FeCl}_2$ : C, 44.38; H, 5.50; N, 22.18. Found: C, 44.58; H, 5.59; N, 22.15.

**2,6-pyridinebis(1,5-diisopropyl-6-oxoverdazyl-3-yl)cobalt(II) chloride (2.22).** To a solution of **2.18** (176.4 mg, 0.3995 mmol) in acetonitrile (5 mL) was added drop-wise via Pasteur pipet a solution of  $\text{CoCl}_2\cdot 6\text{H}_2\text{O}$  (96.8 mg, 0.4068 mmol) in acetonitrile (5 mL) in a 25 mL Erlenmyer flask. The reaction was left to stand without stirring for



approximately 48 hours. Purple plate-like crystals were isolated by vacuum filtration, followed by washing with  $3 \times 5$  mL ice-cold acetonitrile, then dried under vacuum for 24 hours to yield 184.4 mg of **2.22** (80.78 %). No further recrystallisations were necessary. Mp. 279 – 281 °C (uncorrected). FT-IR (KBr): 2972 (s), 2934 (m), 2873 (w), 1703 (vs), 1607 (s), 1577 (s), 1486 (s), 1451 (w), 1382 (w), 1363 (s), 1286 (s), 1240 (s), 1157 (s), 1127 (m), 1072 (s), 817 (m), 716 (s), 666 (w), 642 (m), 562 (m), 526  $\text{cm}^{-1}$  (m). UV-Vis ( $\text{CH}_2\text{Cl}_2$ ):  $\lambda_{\text{max}}$  245 ( $\epsilon = 34500$ ), 316 ( $\epsilon = 13560$ ), 434 ( $\epsilon = 3545$ ), 571 nm ( $\epsilon = 474 \text{ L}\cdot\text{mol}^{-1}\cdot\text{cm}^{-1}$ ). Anal. Calcd. for  $\text{C}_{21}\text{H}_{31}\text{N}_9\text{O}_2\text{CoCl}_2$ : C, 44.14; H, 5.47; N, 22.06. Found: C, 44.52; H, 5.35; N, 22.27.

**2,6-pyridinebis(1,5-diisopropyl-6-oxoverdazyl-3-yl)nickel(II) chloride (2.23).** To a solution of **2.18** (218.0 mg, 0.4937 mmol) in acetonitrile (3 mL) was added drop-wise via Pasteur pipet a solution of  $\text{NiCl}_2\cdot 6\text{H}_2\text{O}$  (117.6 mg, 0.4947 mmol) in acetonitrile and methanol (5 mL  $\text{CH}_3\text{CN}$ , 5 mL  $\text{CH}_3\text{OH}$ ) in a 50 mL Erlenmyer flask. The reaction was left to stand without stirring for approximately 72 hours. Red plate-like crystals were isolated by vacuum filtration, followed by washing with  $3 \times 5$  mL ice-cold acetonitrile and  $3 \times 5$  mL cold hexanes, then dried under vacuum for 24 hours to yield 117.6 mg of **2.23** (41.71 %). No further recrystallisations were carried out. Mp. 252 – 254 °C (uncorrected). FT-IR (KBr): 2972 (s), 2934 (m), 2879 (w), 1698 (vs), 1604 (s), 1577 (s), 1489 (s), 1456 (s), 1390 (w), 1366 (s), 1286 (s), 1237 (s), 1157 (m), 1130 (w), 1075 (s), 823 (s), 718 (m), 672 (m), 644 (m), 565 (m), 526  $\text{cm}^{-1}$  (m). UV-Vis ( $\text{CH}_2\text{Cl}_2$ ):  $\lambda_{\text{max}}$  250 ( $\epsilon = 35350$ ), 305 ( $\epsilon = 16890$ ), 434 nm ( $\epsilon = 6276 \text{ L}\cdot\text{mol}^{-1}\cdot\text{cm}^{-1}$ ). MS (EI-MS):  $m/z$  571.1  $\{[\text{M}]^+, 7 \%\}$ . Anal. Calcd. for  $\text{C}_{21}\text{H}_{31}\text{N}_9\text{O}_2\text{NiCl}_2$ : C, 44.16; H, 5.47; N, 22.07. Found: C, 43.49; H, 5.42; N, 21.81.

**2-(1,5-diisopropyl-6-oxoverdazyl-3-yl)-6-(1-isopropyl-6-oxoverdazyl-3-yl)pyridine chromium(III) chloride (2.28b).** Inside an inert-atmosphere glove box, a dry 50 mL Erlenmyer (filter) flask, equipped with a dry dropping funnel was charged with  $\text{CrCl}_3 \cdot 3\text{THF}$  (174 mg, 0.464 mmol). The flask was removed from the glove box and attached to a Schlenk line. Dry acetonitrile (10 mL) was added to the flask, via syringe, to dissolve  $\text{CrCl}_3 \cdot 3\text{THF}$ . In a separate, dry flask, **2.18** (204.5 mg, 0.4632 mmol) was dissolved in dry dichloromethane (5 mL) and this solution was transferred via syringe to the dropping funnel. **2.18** was then added slowly, drop-wise to the solution of  $\text{CrCl}_3 \cdot 3\text{THF}$  and the reaction was left to stand under argon for 8 days. Argon was removed and the solvent was allowed to evaporate slowly in air to yield deep green crystalline material with a yield of 121.1 mg (46.89 %). X-ray quality crystals were attained by dissolving the crude crystalline product in a minimal amount of refluxing ethyl acetate, then cooling the solution in a freezer for 2 days. Mp. > 385 °C. FT-IR (KBr): 3241 (br), 3081 (w), 3068 (w), 2982 (s), 2935 (m), 2875 (w), 1724 (vs), 1709 (sh), 1610 (s), 1580 (m), 1509 (m), 1458 (m), 1408 (m), 1391 (m), 1367 (m), 1286 (s), 1241 (s), 1178 (m), 1152 (m), 1131 (m), 1112 (w), 1077 (m), 935 (w), 875 (w), 856 (w), 821 (m), 750 (m), 716 (m), 656 (m), 563 (m), 497  $\text{cm}^{-1}$  (m). UV-Vis ( $\text{CH}_2\text{Cl}_2$ ):  $\lambda_{\text{max}}$  245 ( $\epsilon = 40200$ ), 320 ( $\epsilon = 12600$ ), 451 ( $\epsilon = 6530$ ), 570 nm ( $\epsilon = 1080 \text{ L} \cdot \text{mol}^{-1} \cdot \text{cm}^{-1}$ ). Anal. Calcd. for  $\text{C}_{18}\text{H}_{25}\text{N}_9\text{O}_2\text{CrCl}_3$ : C, 38.76; H, 4.52; N, 22.60. Found: C, 38.64; H, 4.29; N, 22.89.

**Reaction of 2,6-pyridinebis(1,5-diisopropyl-6-oxoverdazyl-3-yl) with copper(II) chloride dihydrate (2.29).** To a solution of **2.18** (45.3 mg, 0.103 mmol) in acetonitrile (5 mL) was added drop-wise via Pasteur pipet a solution of  $\text{CuCl}_2 \cdot 2\text{H}_2\text{O}$  (18.2 mg, 0.107

mmol) in acetonitrile (10 mL) in a 25 mL Erlenmyer flask. The reaction was left to stand without stirring for approximately 16 hours. Purple needle crystals were isolated by vacuum filtration, followed by washing with  $3 \times 5$  mL ice-cold acetonitrile, then dried under vacuum for 24 hours to yield 53.8 mg of **2.29** (93.4 %). No further recrystallisations were carried out. Mp. 156 – 160 °C (dec.). FT-IR (KBr): 3081 (w), 2982 (m), 2935 (w), 2879 (vw), 2349 (s), 1703 (vs), 1458 (w), 1367 (m), 1292 (m), 1245 (m), 1159 (w), 1131 (w), 1107 (w), 1079 (m), 1032 (w), 824 (m), 746 (w), 720 (w), 649 (m),  $566\text{ cm}^{-1}$  (m). UV-Vis ( $\text{CH}_2\text{Cl}_2$ ):  $\lambda_{\text{max}}$  253 ( $\epsilon = 15390$ ), 308 ( $\epsilon = 9550$ ), 405 nm ( $\epsilon = 2390\text{ L}\cdot\text{mol}^{-1}\cdot\text{cm}^{-1}$ ). Anal. Calcd. for  $\text{C}_{15}\text{H}_{17}\text{N}_9\text{O}_2\text{Cu}_2\text{Cl}_3\cdot 2\text{H}_2\text{O}$ : C, 28.83; H, 2.74; N, 20.17. Found: C, 40.71; H, 5.01; N, 23.51.

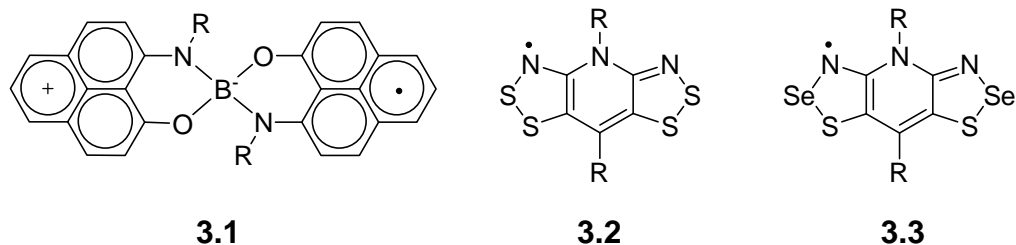
## Chapter 3: Redox properties of verdazyl radicals, diradicals and derived coordination compounds

### 3.1 Redox properties of stable radicals and their coordination compounds

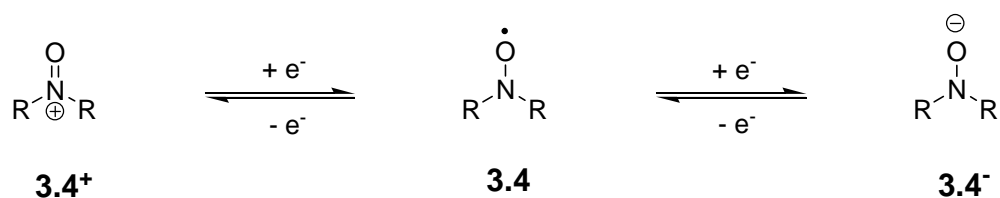
Much of the interest in stable radical chemistry stems from using the unpaired electron as a building block for magnetic materials, as described in the preceding chapter. The ability to do chemistry on a stable organic radical, while preserving its paramagnetic nature, has driven a new line of materials-based research. Intuitively, a stable open-shell molecule should have two other stable states arising from either the addition or removal of one electron to give the corresponding closed-shell anion or cation, respectively. This has led to intense study of the fundamental redox properties of stable radicals.

#### 3.1.1 Redox-based applications of stable radicals

A great deal of research into the redox properties of stable radicals has focused on their potential application as molecular conductors. Stable radicals have a half-filled molecular orbital. If such radicals were made into polymers, the SOMO then becomes akin to a conducting band. The idea is that stable-radical based polymers would then show the combined advantages of being intrinsically conducting materials that are easy to process. In this respect, the phenalenyl radical has been extensively derivatised and the associated redox properties studied.<sup>195</sup> Haddon et al. have thoroughly delineated the conductance observed in phenalenyl-derived radicals **3.1**.<sup>196-201</sup> Sulfur-nitrogen based radicals **3.2** (and others, as introduced in Chapter 1) have also been investigated in terms of their electrical conductivity.<sup>202-204</sup> Recently, heavy-element congeners of the sulfur-nitrogen radicals **3.3** have also been synthesised and their conductivity reported.<sup>205, 206</sup>

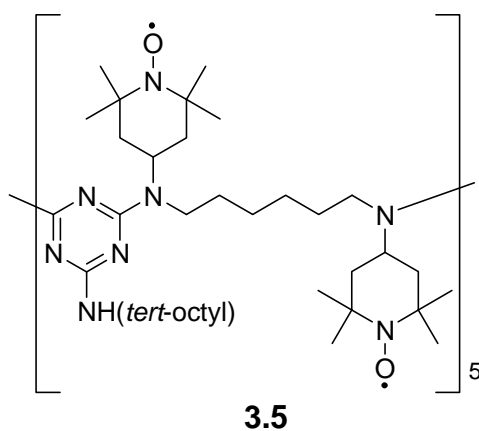


Redox properties of nitroxide radicals have been extensively studied by Nishide *et al.* with a focus on the design of flexible organic batteries.<sup>207-211</sup> This class of radicals is thought to be a promising avenue towards the design of commercial flexible batteries for a number of reasons. Nitroxide radicals **3.4** can be reversibly reduced or oxidised to give an aminoxy anion **3.4<sup>-</sup>** or an oxoammonium cation **3.4<sup>+</sup>**, respectively, as shown in Scheme 3.1.<sup>212</sup> Perhaps even more importantly, stable oxoammonium salts of TEMPO have been isolated, which translates to the possibility of using nitroxide radicals as both cathode and anode in an organic battery set-up.<sup>207</sup> Furthermore, the redox potentials of nitroxide radicals can be tuned by synthetically altering the organic framework around the NO<sup>•</sup> moiety.<sup>213</sup> Nitroxide radicals can be appended to a polymeric backbone to give a fully organic battery whose electrochemical functionality and processability are combined in one package, eliminating the need for excess support materials.



**Scheme 3.1:** Redox properties of nitroxide radicals.

Another increasingly important application of stable radicals is the use of TEMPO and other nitroxides in the catalytic oxidation of alcohols.<sup>11, 214, 215</sup> The catalytic activity of the nitroxide radical again stems from its reversible redox couples to generate both cationic and anionic species. In fact, the oxoammonium cation, rather than the nitroxide radical itself, has been proposed as the active oxidant in TEMPO-catalysed alcohol oxidations.<sup>216</sup> The cation is generated *in situ* from the stable TEMPO radical. Oxidation of the substrate alcohol is accompanied by reduction of the oxoammonium salt to its hydroxylamine form. Bleach is used in this system to regenerate the oxoammonium catalyst. TEMPO-based catalytic systems have been intensely studied in terms of their potential as eco-friendly alternatives to metal-based catalysts. As such, there is a lot of interest in reducing the need for co-catalysts as well as facilitating the process of recycling the radical catalyst itself. In this respect, various heterogeneous catalysts have been investigated using TEMPO radicals anchored to solid supports.<sup>217</sup> Polymeric versions of TEMPO – coined polymer-immobilised piperidinyloxyl, or PIPO, **3.5** – have also been investigated where the nitroxide radical is synthetically grafted onto a polymer backbone,<sup>218, 219</sup> eliminating the need for silica or other support material.



### 3.1.2 Stable radicals as redox-active ligands

Many transition metal complexes of radical-anion quinoid-type compounds have been reported.<sup>110, 220</sup> These compounds have been studied extensively in terms of valence tautomerism<sup>221</sup> and potential applications as molecular switches.<sup>222</sup> Furthermore, many studies have been dedicated to unambiguously assigning oxidation states to both the metal and ligand,<sup>223</sup> a non-trivial task when dealing with open-shell ligands. Radical-anion ligands based on bis(imino)pyridine have experienced a recent surge in popularity based on their use as catalysts in conjunction with base metals such as iron and cobalt.<sup>224-232</sup> While these compounds are nonetheless important in terms of redox-active radical ligands, they do not involve *neutral* radicals, and will not be discussed in any further detail here.

With respect to redox properties of coordination compounds involving neutral radicals, studies have been driven, in large part, by the interest in galactose oxidase<sup>64, 233, 234</sup> (see Chapter 1). Interest in GO-type phenoxyl-metal complexes has focused on the ability of these compounds to catalyse the oxidation of alcohols to carbonyls. Especially fascinating is how the interplay of the electronic states of the metal centre and radical ligand gives rise to the catalytic activity of this enzyme. To this end, model complexes that mimic the catalytic activity of GO have been extensively studied with copper<sup>235, 236</sup> and other transition metals.<sup>59, 237</sup>

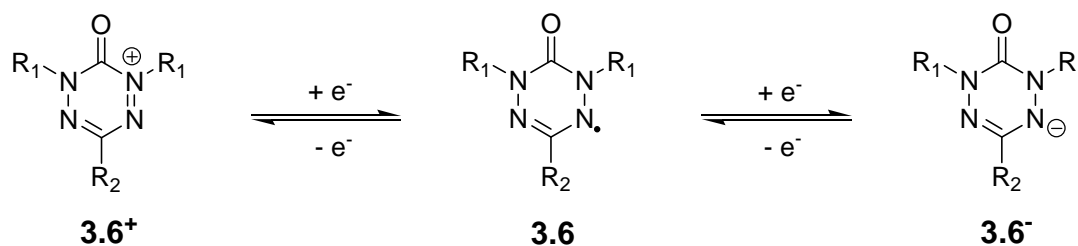
Nitroxide radicals have also figured prominently in metal-based catalysis.<sup>32</sup> Metal-TEMPO systems have been shown to catalyse the oxidation of alcohols to aldehydes or ketones in air.<sup>238-242</sup> However, these nitroxide systems are distinct from the

galactose oxidase mimics in that they do not consist of well characterised, pre-made metal-TEMPO complexes. Rather, mixtures of free TEMPO radical and metal pre-catalysts are typically combined and the active species is formed *in situ*.<sup>243</sup> Conversely, certain coordination compounds involving aminyl radicals have been synthesised and characterised.<sup>244</sup> Selected examples of this class of compounds were presented in Chapter 1. In light of the interest in replicating the catalytic activity of galactose oxidase, aminyl coordination compounds have also been investigated in terms of their potential use in catalysis.<sup>85, 86</sup>

### 3.2 Redox properties of verdazyl radicals and coordination compounds

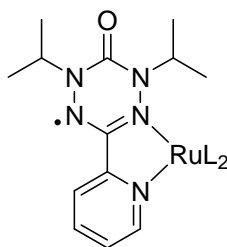
Redox properties of verdazyl radicals<sup>245-248</sup> and diradicals<sup>249</sup> have been reported, although to a lesser extent than with nitroxides. In general, 6-oxoverdazyl radicals **3.6** show similar redox behaviour to nitroxides in that they can be both reversibly oxidised and reduced electrochemically, as shown in Scheme 3.2. Previous group members have thoroughly studied the substituent-effects on the oxidation and reduction potentials of verdazyl radicals.<sup>108</sup> In general, for the 6-oxoverdazyl radicals examined, electron-withdrawing N-substituents lead to more facile reduction of the radical while making oxidation more difficult. However, this same work found that the overall cell potential ( $E_{\text{cell}} = |E^{\circ}_{\text{ox}} - E^{\circ}_{\text{red}}|$ ) was relatively unaffected by the electronic nature of the N-substituent; the reduction and oxidation potentials changed by approximately the same amount throughout a given series of substituents.





**Scheme 3.2:** Redox properties of verdazyl radicals.

Despite the variety of investigations into the redox properties of verdazyl radicals themselves, there had been no reports on the redox activity of verdazyl coordination compounds until a 2010 paper detailed the electrochemical behaviour of various ruthenium-verdazyl complexes **3.7a,b**.<sup>111</sup> The primary aim of this chapter is to further elucidate the redox properties of verdazyl radicals and diradicals both as stand-alone compounds and as non-innocent ligands in transition metal complexes. A new, tridentate verdazyl radical was prepared and its electrochemical behaviour was studied. The redox properties of diradical **2.18**, whose coordination chemistry and magnetic properties were the focus of Chapter 2, are also described in this chapter. In order to probe the electrochemical behaviour of these two verdazyl species as ligands, zinc complexes were prepared and studied. The use of a redox-inert metal centre facilitated the examination of the ligand-based redox properties.



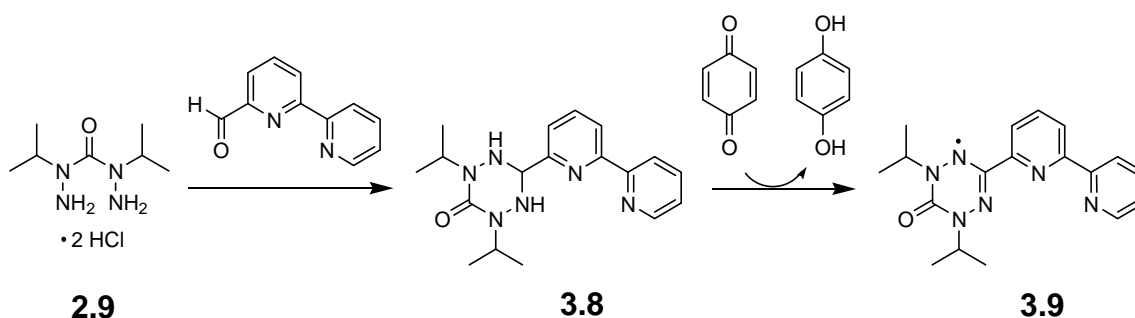
**3.7a:** L = acac

**3.7b:** L = hfac

## Results and Discussion

### 3.3 Synthesis of verdazyl radical 3.9

A new verdazyl radical ligand **3.9** was designed to have similar coordination properties to diradical **2.18**. Both compounds feature a tridentate binding pocket and can coordinate to a metal centre through at least one verdazyl nitrogen atom bearing significant spin density. Carbonic acid bis(1-isopropylhydrazide) **2.9** was condensed with 2,2'-bipyridinecarboxaldehyde to give the bipyridine-substituted tetrazane **3.8**, which was identified in the  $^1\text{H}$  NMR spectrum of the product mixture but could not be sufficiently purified to allow its full characterisation. Nonetheless, this *in situ* generated tetrazane **3.8** could be oxidised with *p*-benzoquinone to generate the corresponding radical in a similar fashion to other verdazyl radicals and diradicals (Scheme 3.3). Verdazyl radical **3.9** was isolated as an orange microcrystalline product and purified on a column of neutral alumina. Elemental analysis of the recrystallised product indicated that none of the impurities associated with the tetrazane precursor **3.8** were carried through to the final radical product.



**Scheme 3.3:** Synthesis of radical **3.9**.

### 3.4 Structural characterisation of verdazyl radical 3.9

The molecular structure of **3.9** is presented in Figure 3.1, with selected bond lengths, bond angles and torsion angles given in Table 3.1. The verdazyl ring is twisted almost  $40^\circ$  with respect to the plane of the central pyridine ring [N3-C2-C9-N5 torsion angle is  $38.80(15)^\circ$ ]. Additionally, the angle between the planes formed by the two pyridine rings is about  $10^\circ$  [N5-C13-C14-C15 =  $10.58(17)^\circ$ ]. Bond lengths around the verdazyl ring are consistent with those reported for other 1,5-diisopropyl-3-pyridyl-substituted verdazyl radicals.

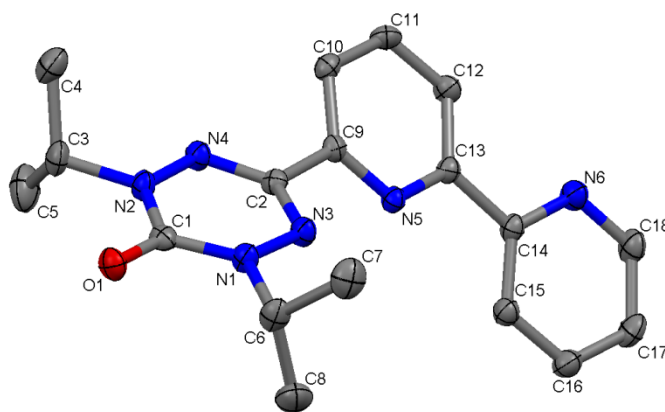


**Figure 3.1:** Molecular structure of **3.9**. Thermal ellipsoids displayed at 50% probability level. Hydrogen atoms removed for clarity.



### 3.6 Structural characterisation of zinc complex **3.10**

The molecular structure of zinc complex **3.10** is presented in Figure 3.2, with selected bond lengths, bond angles and torsion angles given in Table 3.2. The bond lengths and angles associated with the verdazyl moiety do not differ significantly from those reported for verdazyl radical **3.9**. The three rings of the verdazyl ligand become nearly mutually coplanar upon coordination to the zinc ion. In complex **3.10** the verdazyl moiety is twisted  $7.5(2)^\circ$  with respect to the plane of the central pyridine ring, compared to the  $38.80(15)^\circ$  twist in the free ligand **3.9**. The two pyridine rings are also closer to coplanarity in complex **3.10** [N5-C13-C14-N6 dihedral angle =  $-1.99(19)^\circ$ ] than in radical **3.9** [N5-C13-C14-N6 =  $-170.06(11)^\circ$ ]. As with the series of diradical **2.18** coordination compounds, the geometry around the metal centre is *pseudo*-trigonal bipyramidal. The two chloride ligands, along with the nitrogen atom on the central pyridine ring constitute the equatorial ligands while two other nitrogen atoms (one from the coordinating verdazyl and the terminal pyridine nitrogen) are in axial positions. In this case there are three distinct coordinating nitrogens. The two bipyridine nitrogen atoms are much closer to the metal [Zn1-N5 =  $2.0910(13)$  Å; Zn1-N6 =  $2.1461(12)$  Å] than is the verdazyl nitrogen [Zn1-N3 =  $2.3658(12)$  Å]. This is further evidence that the coordinating verdazyl nitrogen atom is a much weaker  $\sigma$ -donor than are the bipyridine nitrogen atoms.

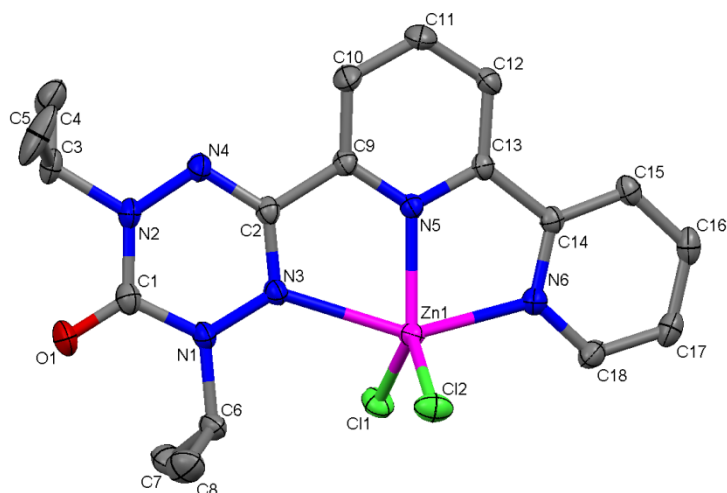


**Figure 3.2:** Molecular structure of **3.10**. Thermal ellipsoids displayed at 50% probability level. Hydrogen atoms removed for clarity.

**Table 3.2:** Selected bond lengths (Å) and angles (degrees) for **3.10**.

Atoms	Length (Å)	Atoms	Angle (°)
C1-O1	1.2141(19)	N1-C1-N2	114.89(13)
C1-N1	1.387(2)	N3-C2-N4	127.82(14)
C1-N2	1.382(2)	C1-N1-N3	123.00(13)
C2-C9	1.481(2)	C1-N2-N4	124.31(13)
C2-N3	1.330(2)	N1-N3-C2	115.43(12)
C2-N4	1.3291(19)	N2-N4-C2	114.41(13)
N1-N3	1.3637(17)	N3-Zn1-N6	148.38(5)
N2-N4	1.3604(18)	N3-Zn1-N5	72.29(4)
Zn1-N3	2.3658(12)	N5-Zn1-N6	76.43(5)
Zn1-N5	2.0910(13)	Cl1-Zn1-Cl2	118.290(18)
Zn1-N6	2.1461(12)	N3-C2-C9-N5	7.5(2)
		N5-C13-C14-N6	-1.99(19)

### 3.7 Solution-phase electronic properties of **3.9** and **3.10**

The electronic spectra of **3.9** and **3.10** are presented in Figure 3.3. The spectrum of **3.9** shows the typical absorption maximum associated with the verdazyl SOMO at 408 nm. This absorption is shifted to lower energy in the spectrum of complex **3.10**,

where  $\lambda_{\text{max}}$  is at 432 nm. These values are consistent with the radicals and associated coordination compounds presented in Chapter 2.

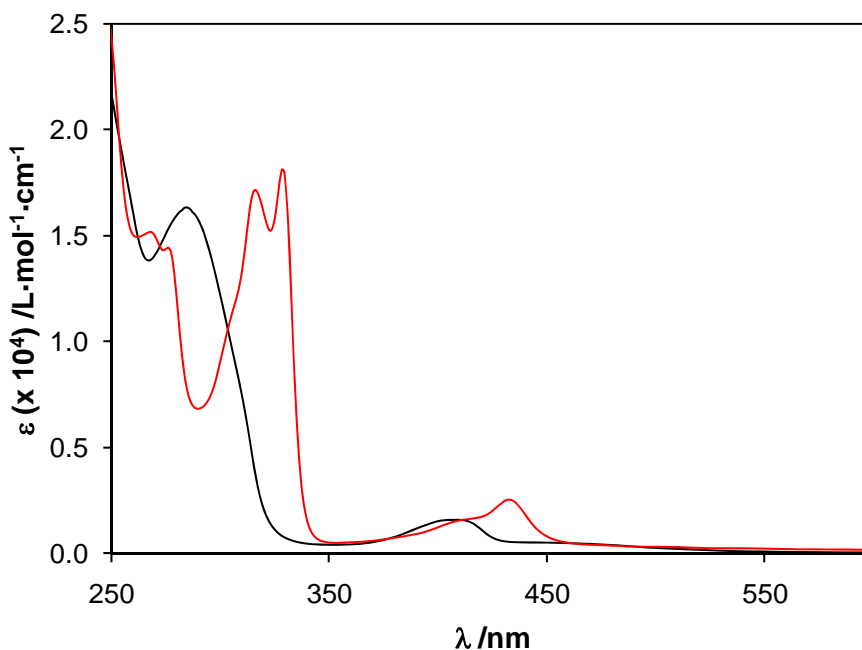


**Figure 3.3:** UV-Vis spectra of radical **3.9** (black) and zinc complex **3.10** (red) in dichloromethane.

The solution electron paramagnetic resonance spectra for compounds **3.9** and **3.10** are shown in Figures 3.4 and 3.5, respectively. Hyperfine coupling parameters calculated from the simulated spectra are presented in Table 3.3. Coupling to two sets of two equivalent nitrogen nuclei ( $I = 1$ ), and also to one pair of equivalent protons ( $I = \frac{1}{2}$ ) can be seen in the spectrum of **3.9**. The typical nine-line pattern from coupling to four nitrogen nuclei is also seen in the experimental spectrum of **3.10**. However, coupling to the hydrogen nuclei on C3 and C6 of the isopropyl groups is not observed in the spectrum of zinc complex **3.10** because of the line-broadening that is seen in this spectrum. Coordination of the verdazyl radical in **3.10** breaks the equivalency of N3 and N4

(compared with **3.9**) and this was taken into account when simulating the spectrum (see Table 3.3).

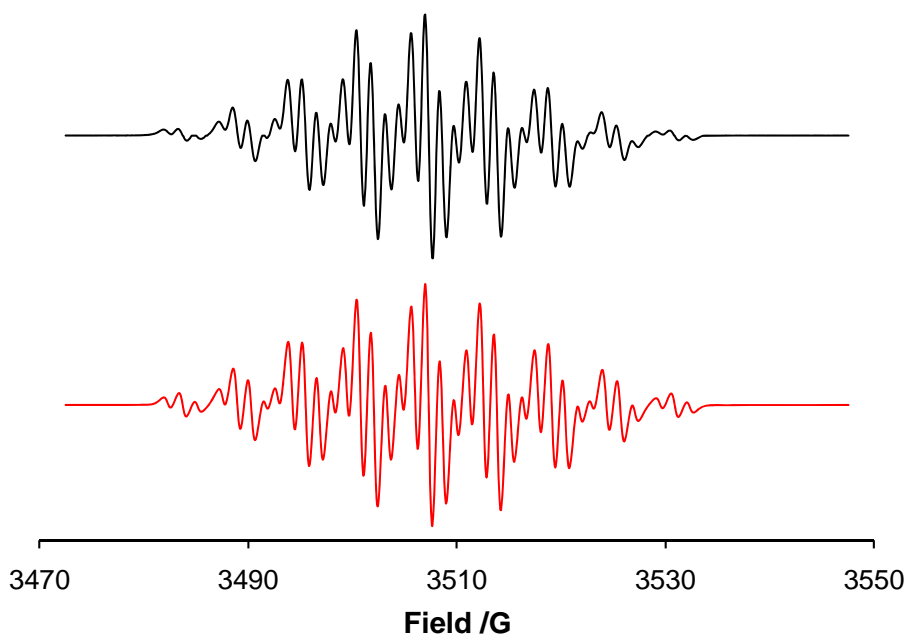


**Figure 3.4:** Experimental (black) and simulated (red) X-band EPR spectra of **3.9** ( $5.0 \times 10^{-4}$  M in toluene).



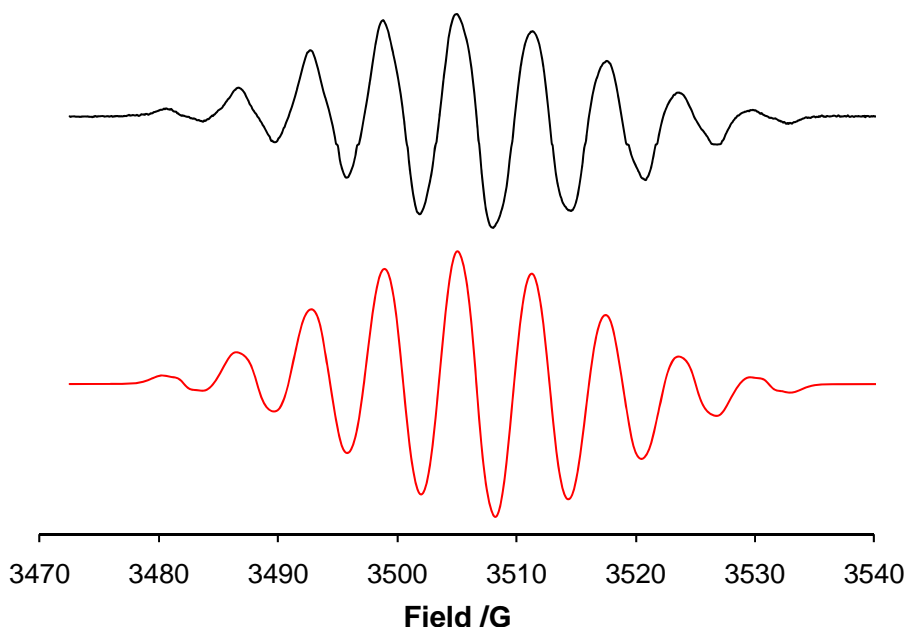


**Figure 3.5:** Experimental (black) and simulated (red) X-band EPR spectra of **3.10** ( $9.5 \times 10^{-6}$  M in  $\text{CH}_2\text{Cl}_2$ ).

**Table 3.3:** Calculated hyperfine coupling parameters for **3.9** and **3.10**.

Compound	$g$	$a_{\text{N}3}$ /mT	$a_{\text{N}4}$ /mT	$a_{\text{N}1,2}$ /mT	$a_{\text{H}3,6}$ /mT
<b>3.9</b>	2.0036	0.651*	0.651*	0.527	0.142
<b>3.10</b>	2.0034	0.651	0.637	0.583	0.143

\* Simulation for **3.9** was performed with  $N_3 = N_4$ , **3.10** was simulated with  $N_3 \neq N_4$

### 3.8 Redox properties of verdazyl radical **3.9** and zinc complex **3.10**

Cyclic voltammograms (CVs) for compounds **3.9** and **3.10** are presented in Figure 3.6 and the accompanying data is summarised in Table 3.4. Verdazyl radical **3.9** undergoes a reversible, one-electron reduction at -1.36 V versus  $\text{Fc}/\text{Fc}^+$  and a corresponding quasi-reversible one-electron oxidation at +0.20 V. The differences in peak-to-peak potentials between anodic and cathodic waves for the oxidation and reduction processes are 60 mV and 80 mV, respectively. A redox process is deemed to be reversible if it meets the following electrochemical conditions: The cathodic and

anodic waves are equal in size (i.e. they integrate to approximately a 1:1 ratio), the cathodic and anodic peak separation is within the acceptable limit (0.059 V for a one-electron process) and the peak potential does not change with scan rate.<sup>250-252</sup> In zinc complex **3.10**, both the oxidation and reduction processes are quasi-reversible and are shifted to more positive potentials. The complex is reduced at -0.87 V ( $\Delta E_p = 100$  mV) and oxidised at +0.43 V ( $\Delta E_p = 70$  mV). The cell potential of zinc complex **3.10** (1.30 V) is noticeably smaller than that of the uncoordinated verdazyl **3.9** (1.56 V).

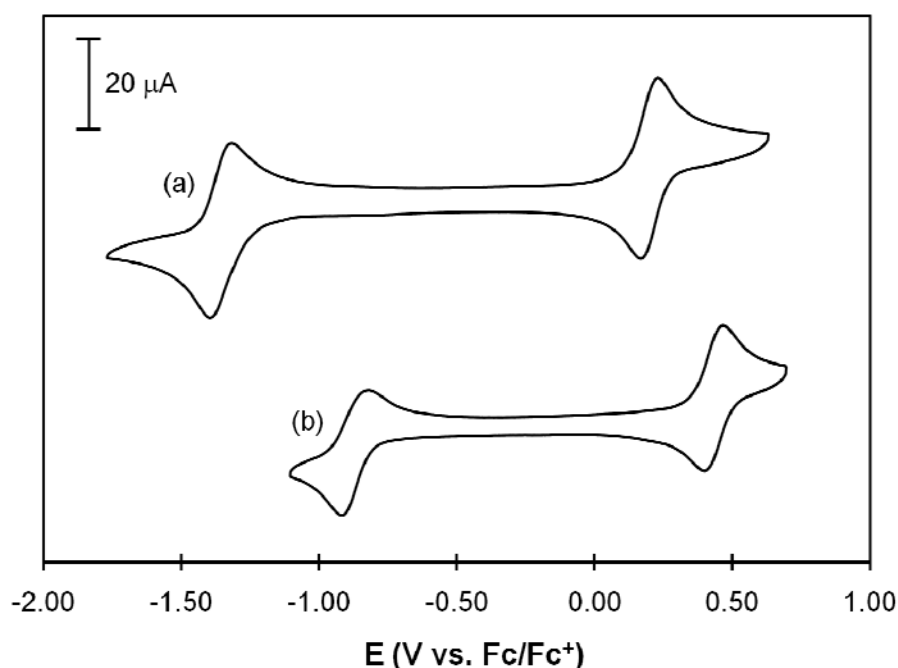


**Figure 3.6:** Cyclic voltammograms of **3.9** (a, 1.1 mM) and **3.10** (b, 1.0 mM). Both CVs recorded in CH<sub>3</sub>CN with 0.1 M Bu<sub>4</sub>NBF<sub>4</sub> as supporting electrolyte.

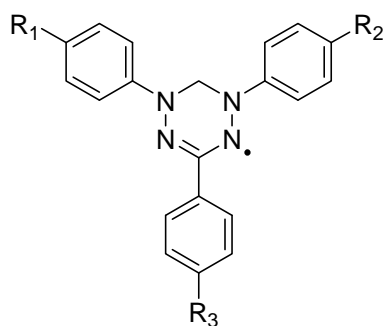
**Table 3.4:** Electrochemical parameters for **3.9** and **3.10**.

Compound	$E^\circ_{\text{ox}}$	$E^\circ_{\text{red}}$	$E^\circ_{\text{cell}}$
<b>3.9</b>	+0.20	-1.36	1.56
<b>3.10</b>	+0.43	-0.87	1.30

Potentials reported in volts versus ferrocene/ferrocenium couple.

Coordination of radical **3.9** through one of the verdazyl nitrogen atoms directly affects the energetics of the  $\pi$ -SOMO in complex **3.10**. Ultimately, the verdazyl-based  $\pi$ -SOMO is more stabilised in complex **3.10**, relative to radical **3.9**. Because this is the orbital that factors in the verdazyl redox chemistry, the addition of one electron to complex **3.10** is more facile, with respect to **3.9**, while the removal of one electron is more difficult.

Electron-withdrawing substituents have been shown to affect the energy of the verdazyl SOMO and thus, the electrochemical potentials of a variety of verdazyl radicals **3.6**, **3.11**.<sup>108</sup> Electron-withdrawing substituents lower the energy of the verdazyl SOMO, making the radical at the same time easier to reduce and more difficult to oxidise. However, for a given type of verdazyl radical (methylene-bridged, **3.11**, versus 6-oxoverdazyl, **3.6**), the substituent effects on the reduction and oxidation potentials are approximately equal (the reduction and oxidation potentials shift by about the same amount) and the overall cell potential remains essentially constant.



**3.11**

The origin of the observed difference in redox properties between verdazyl radical **3.9** and its corresponding zinc complex **3.10** must be different from the substituent effects described above. A shift to more positive potential of both the reduction and oxidation waves of complex **3.10** (compared to radical **3.9**) is consistent with the presence of an

electron-withdrawing substituent. However, the magnitude of the respective shifts is different and, as a result, the cell potential of zinc complex **3.10** is 260 mV smaller than that of radical **3.9**. Coordination to zinc, therefore, should not be considered as a simple substituent effect when considering the differences between the CVs of **3.9** and **3.10**. Furthermore, the substituent effects described above have been linked to the amount of delocalisation of spin density onto a given substituent.<sup>108</sup> In the case of complex **3.10**, there is no evidence of any spin delocalisation onto the zinc ion.

### **3.9 Redox properties of diradical 2.18 and zinc complex 2.19**

Cyclic voltammograms (CVs) for verdazyl diradical **2.18** and its related zinc complex **2.19** are presented in Figure 3.7 and the important potentials are highlighted in Table 3.5. The electrochemical behaviour of diradical **2.18** is qualitatively similar to that of verdazyl radical **3.9** (Figure 3.7, Table 3.5). An important distinction between the CV of radical **3.9** and that of diradical **2.18** is that both the oxidation and reduction waves in the CV of **2.18** represent two-electron transfer processes. Diradical **2.18** is quasi-reversibly reduced to a dianion at -1.30 V versus Fc/Fc<sup>+</sup>. A quasi-reversible two-electron oxidation process occurs at +0.26 V. The reduction and oxidation potentials for diradical **2.18** are both shifted by +60 mV with respect to radical **3.9**.

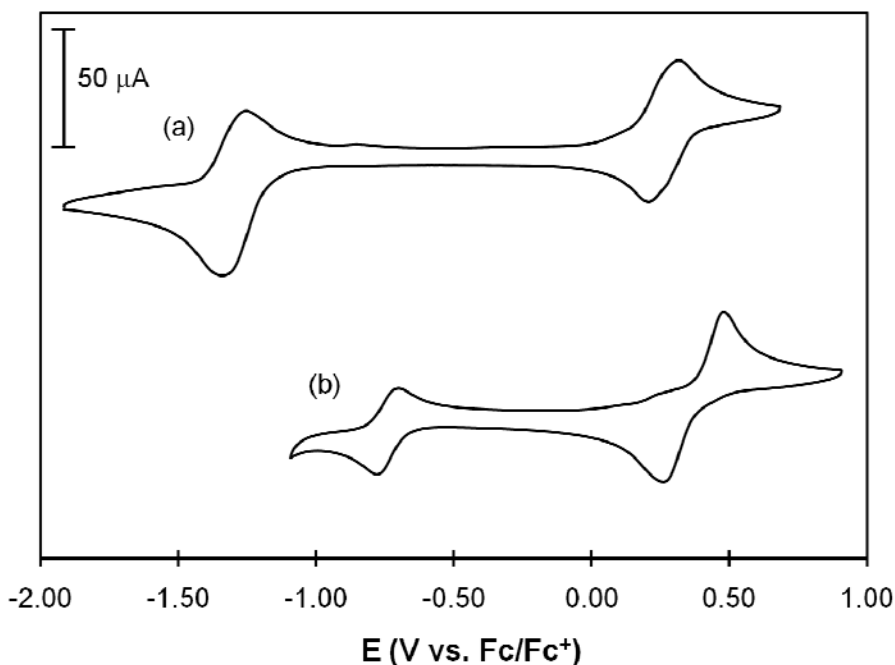


**Figure 3.7:** Cyclic voltammograms of (a) **2.18** and (b) **2.19**. Both CVs recorded on 1.0 mM solutions in CH<sub>3</sub>CN with 0.1 M Bu<sub>4</sub>NBF<sub>4</sub> as supporting electrolyte. Potentials reported in volts versus ferrocene/ferrocenium couple.

**Table 3.5:** Electrochemical parameters for **2.18** and **2.19**.

Compound	$E_{\text{ox}}^{\circ}$	$E_{\text{red}}^{\circ}$	$E_{\text{cell}}^{\circ}$
<b>2.18</b>	+0.26	-1.30	1.56
<b>2.19</b>	+0.48*	-0.74	1.22*

Potentials reported in volts versus ferrocene/ferrocenium couple.  $E_{\text{ox}}^{\circ}$  and  $E_{\text{cell}}^{\circ}$  for **2.19** based on the cathodic wave of oxidation process.

Previous studies have highlighted reversible or quasi-reversible two-electron redox processes in other verdazyl diradicals.<sup>107, 249</sup> Furthermore, electrochemical studies of benzene-bridged verdazyl diradicals **1.55** and **1.56** relieved the ambiguity as to whether the respective diradical oxidation and reduction processes are best considered as a two-electron transfer process or two subsequent one-electron transfer processes.<sup>107</sup> In the case of diradical **2.18**, as was the case for both diradicals **1.55** and **1.56**, each of the respective redox processes (i.e. oxidation and reduction) should be considered as two

distinct one-electron transfers that occur at virtually the same potential. The differences in peak-to-peak potentials between anodic and cathodic waves for the oxidation and reduction processes are 110 mV and 100 mV, respectively. A condition for electrochemical reversibility is that the peak-to-peak potential difference should follow the equation  $\Delta E_p = 59/n$  mV at 25 °C; where  $n$  = number of electrons transferred.<sup>250</sup> According to this relationship, the oxidation and reduction waves in the CV of **2.18** would be much smaller than the observed  $\Delta E_p$  values of 110 and 100 mV if these redox processes, respectively, involved concomitant two-electron transfer.

To further elucidate the nature of the electron-transfer processes in **2.18**, Osteryoung square wave voltammetry (OSWV) experiments were performed. Oxidation and reduction processes for equimolar amounts of **2.18** and octamethylferrocene are presented in Figure 3.8. OSWV experiments reported for benzene-bridged diradicals **1.55** and **1.56** were able to resolve the signals associated with the respective reduction processes into two discernable peaks (showing that in both cases the reduction proceeds by two separate one-electron processes).<sup>107, 158</sup> Unfortunately, the experiment presented in Figure 3.8 was not able to resolve the individual electron transfer processes for diradical **2.18** in this case. However, a comparison of the peak areas of the diradical oxidation and reduction processes with that of the octamethylferrocene redox couple indicates that the redox processes in diradical **2.18** involve two electrons. On the basis of the CV and OSWV data, and by comparison with the benzene-bridged analogues, the respective redox processes observed in diradical **2.18** can each be assigned as two separate, but overlapping, one-electron transfers. In essence, oxidation or reduction of one of the verdazyl rings does not affect the corresponding potential of the second radical

moiety. This electrochemical behaviour is consistent with a lack of conjugation between the two verdazyl SOMOs, which was established in Chapter 2 by comparing the electronic spectrum of **2.18** with that of an analogous verdazyl monoradical.

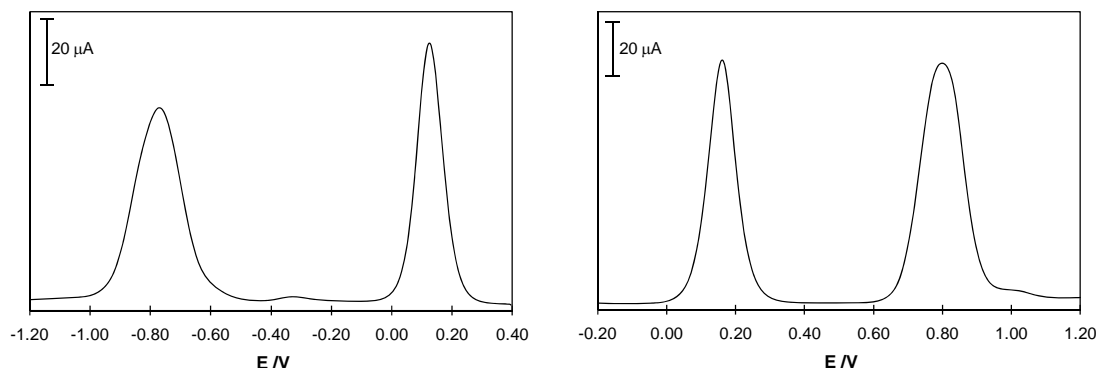


**Figure 3.8:** Osteryoung square wave voltammograms showing reduction (left) and oxidation (right) of **2.18** (0.997 mM solution in CH<sub>3</sub>CN with 0.1 M Bu<sub>4</sub>NBF<sub>4</sub> as supporting electrolyte). Peak centred at 160 mV is due to octamethylferrocene (added as internal standard, 0.972 mM).

There are obvious qualitative differences in the CV of zinc complex **2.19** (Figure 3.7b) when compared with either diradical **2.18** or zinc-monoverdazyl complex **3.10**. The cell potential of **2.19** is smaller than the cell potential of the diradical alone, which mirrors the change in cell potential between monoradical **3.9** and its corresponding zinc complex **3.10** (see Figure 3.6 and Table 3.4). The reduction process at -0.74 V vs. Fc/Fc<sup>+</sup> is quasi-reversible (peak-to-peak potential difference is 75 mV), but the peak size is about half that of the oxidation process, inferring that the reduction is actually a one-electron process. The oxidation process, on the other hand, is electrochemically irreversible; the peak-to-peak separation between the cathodic and anodic waves of this process is more than 220 mV. Both redox processes associated with **2.19** were afforded further study, and will be discussed in greater detail, individually.

### 3.10 Reduction of zinc diradical complex **2.19**

The cyclic voltammogram of **2.19** (Figure 3.7) indicates that the quasi-reversible reduction centred at -0.74 V is a one-electron process. The size of this wave is half the size of the corresponding two-electron reduction wave for diradical **2.18**. The reversibility of this redox event was probed by comparing the CVs recorded as a function of scan rate (Figure 3.9). The difference in peak-to-peak potentials between the cathodic and anodic waves does not change significantly with scan rate in the range 10 mV/s to 500 mV/s, which is consistent with a reversible or quasi-reversible electron-transfer process. Furthermore, scanning this region multiple times at a given scan rate does not alter the shape or position of the peak potentials (Figure 3.9).

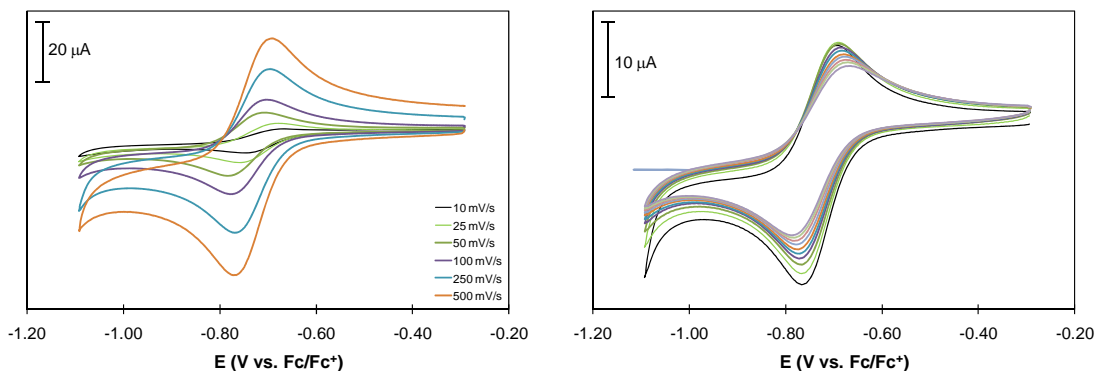


**Figure 3.9:** Cyclic voltammograms of reduction process for **2.19** (1.0 mM solution in  $\text{CH}_3\text{CN}$  with 0.1 M  $\text{Bu}_4\text{NBF}_4$  as supporting electrolyte) showing scan-rate dependence (left) and multiple scan reproducibility at 100 mV/s (right).

Upon scanning to more negative potentials, another electron-transfer process is evident in the cyclic voltammogram for **2.19** (dashed line in Figure 3.10). A second, irreversible reduction is centred at -1.30 V vs.  $\text{Fc}/\text{Fc}^+$ . Additionally, the cathodic wave associated with this scan to more negative potentials shows that the original one-electron



reduction no longer appears to be reversible, as the anodic and cathodic peaks are not symmetric. While diradical **2.18** can be reversibly reduced to a dianion, the corresponding zinc complex **2.19** can be reversibly reduced by only one electron. Further reduction generates a reactive species.

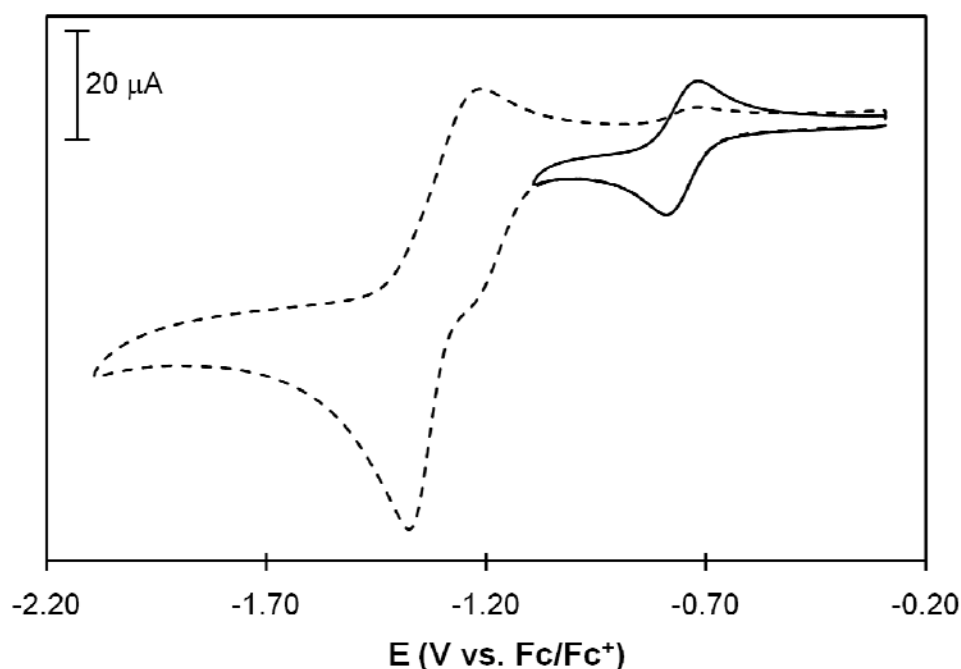


**Figure 3.10:** Cyclic voltammogram of **2.19** (1.0 mM in  $\text{CH}_3\text{CN}$  with 0.1 M  $\text{Bu}_4\text{NBF}_4$  as supporting electrolyte) showing a reversible one-electron reduction at -0.74 V (solid line) and a second irreversible reduction at more negative potential (dashed line).

### 3.11 Oxidation of zinc diradical complex **2.19**

The oxidation process for **2.19** is electrochemically irreversible. The peak potential of the cathodic wave is +0.48 V while that of the corresponding anodic wave is +0.26 V; a difference of 0.22 V. However, the size and shape of these two CV waves are very similar, which is not typical of a simple irreversible electron-transfer process.

To further probe this electrochemical process, scan-rate dependence experiments were carried out. Figure 3.11 shows that neither the shape nor the position of the cathodic or anodic waves of this oxidation process change significantly with scan rate.

Additional data was collected by cycling through the potential range of the oxidation with multiple scans at the same scan rate (Figure 3.11, right). Again, the overall shape and position of the CV waves for this process remain unchanged throughout multiple scans.

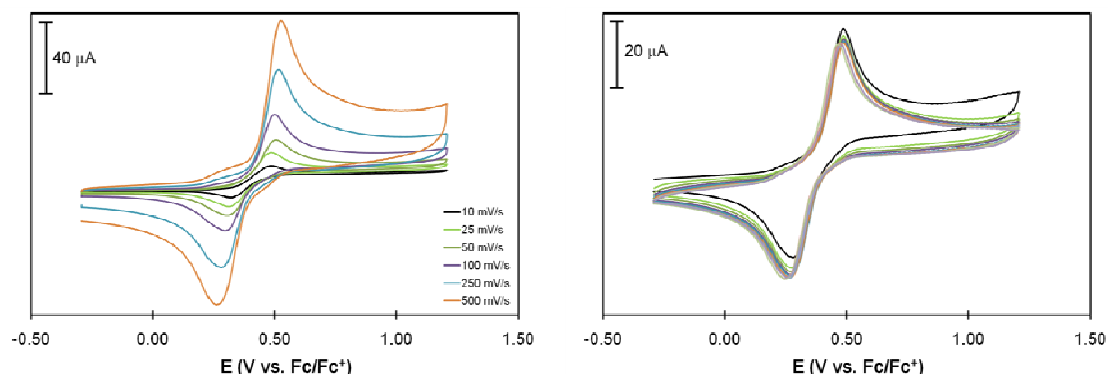
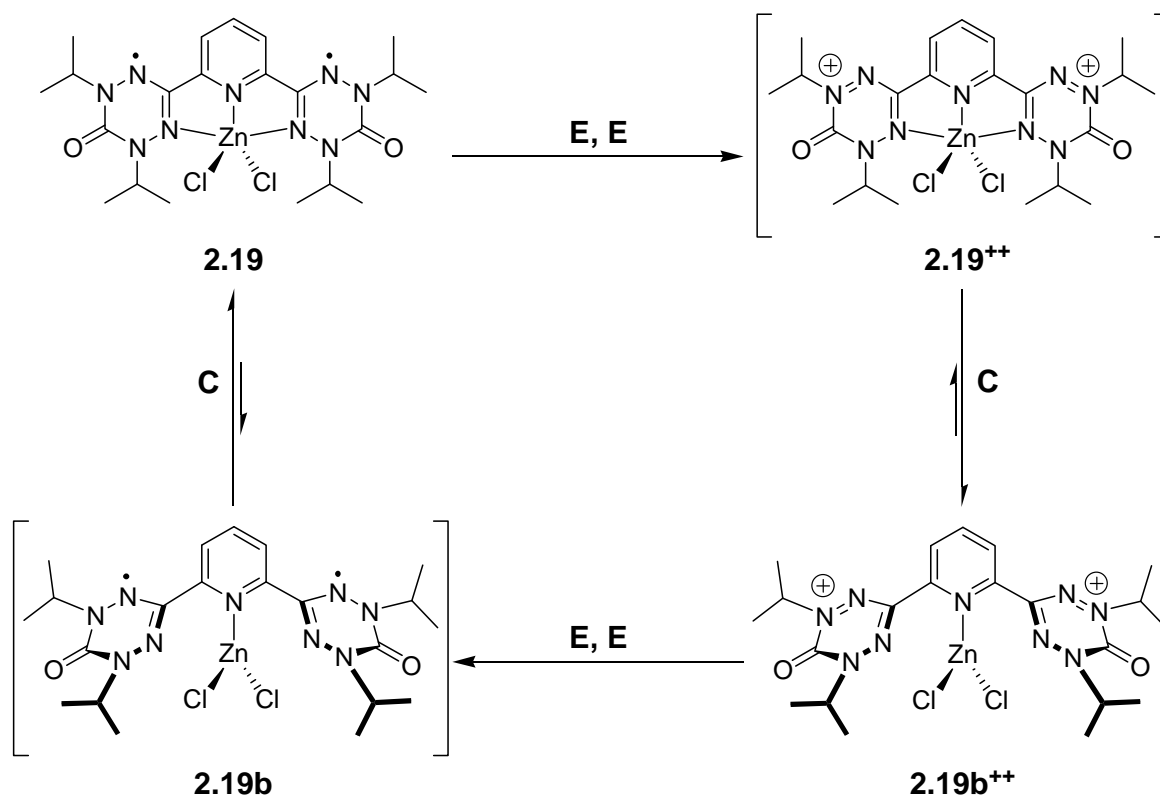


**Figure 3.11:** Cyclic voltammograms of oxidation process for **2.19** (1.0 mM solution in CH<sub>3</sub>CN with 0.1 M Bu<sub>4</sub>NBF<sub>4</sub> as supporting electrolyte) showing scan-rate dependence (left) and multiple scan reproducibility at 100 mV/s (right).

The observed  $\Delta E_p$  value of 220 mV for the oxidation of **2.19** indicates an electrochemically irreversible process. One plausible explanation is that diradical **2.19** experiences a structural change upon oxidation, and this new species is subsequently reduced at a potential that is 220 mV more negative than the original oxidation. However, the reproducibility of the data in Figure 3.11 indicates that the overall sequence of oxidation and reduction events must be reversible. Scheme 3.5 proposes an ECEEC (where E is an electron-transfer step and C represents a chemical change) mechanism, which results in an overall reversible cycle. Oxidation of **2.19** to a dicationic species **2.19<sup>++</sup>** is followed quickly by a chemical change that yields a structurally distinct species **2.19b<sup>++</sup>**. This species is subsequently reduced at a different potential from the original oxidation to give **2.19b**. This electron-transfer is followed by a second chemical change that regenerates the original zinc-diradical complex **2.19**. Analysis of the crystal structure of **2.19** (see Section 2.6.1) reveals that the verdazyl nitrogen atoms do not

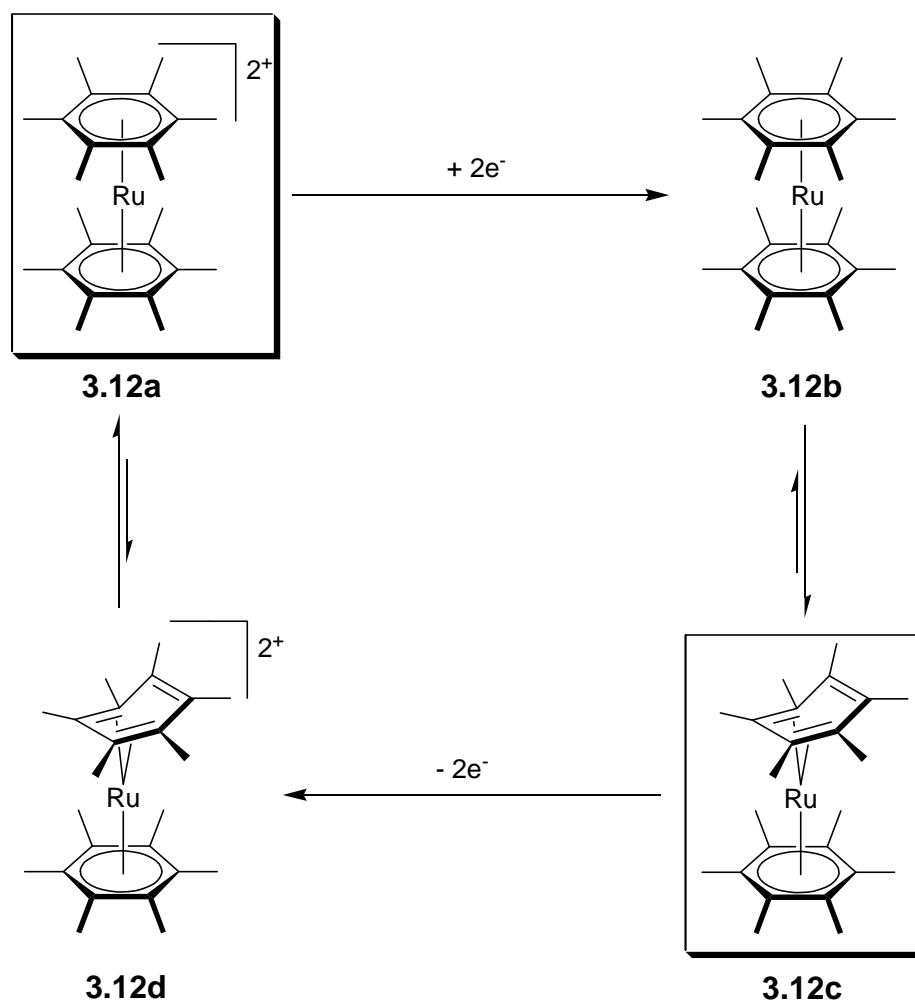
coordinate to the zinc centre as strongly as the central pyridine nitrogen of the diradical ligand. Upon oxidation of the verdazyl rings, these nitrogen atoms should be even weaker  $\sigma$ -donors than in the diradical form of the ligand. Therefore a plausible structural change would be for the verdazyl rings of the diradical ligand to dissociate from the zinc centre, as shown in **2.19b<sup>++</sup>**. Because the ligand remains coordinated through the pyridine nitrogen atom, this new species is sufficiently stable on the time-scale of the CV experiment that it can be re-reduced to the uncoordinated diradical form **2.19b**. The verdazyl rings of this regenerated diradical then re-coordinate to the zinc centre to give the original species **2.19**.



**Scheme 3.5:** **2.19** undergoes two electron-transfer processes (E, E) to give the dicationic species **2.19<sup>++</sup>**. This species undergoes a chemical change (C) to yield the uncoordinated dication **2.19b<sup>++</sup>**. Two-electron reduction of this species (E, E) gives an uncoordinated diradical **2.19b**, which undergoes a chemical change whereby the verdazyl rings re-coordinate to zinc to regenerate the original species **2.19**.

### 3.12 Redox-induced structural changes in organometallic compounds

Reversible redox-induced structural changes have been described for a number of organometallic compounds.<sup>253</sup> Scheme 3.6 shows an example of a sandwich complex **3.12a** in which one of the arene ligands undergoes a shift in hapticity, from  $\eta^6$  to  $\eta^4$ , upon reduction.<sup>254, 255</sup> This system was the first example where the reduced form, exhibiting  $\eta^4$ -arene hapticity, was characterised by X-ray crystallography.<sup>253</sup> Other systems have subsequently been shown to undergo electrochemically instigated structural changes including hapticity shifts,<sup>256-260</sup> geometric isomerisation<sup>261</sup> and bond rearrangements.<sup>262,</sup>

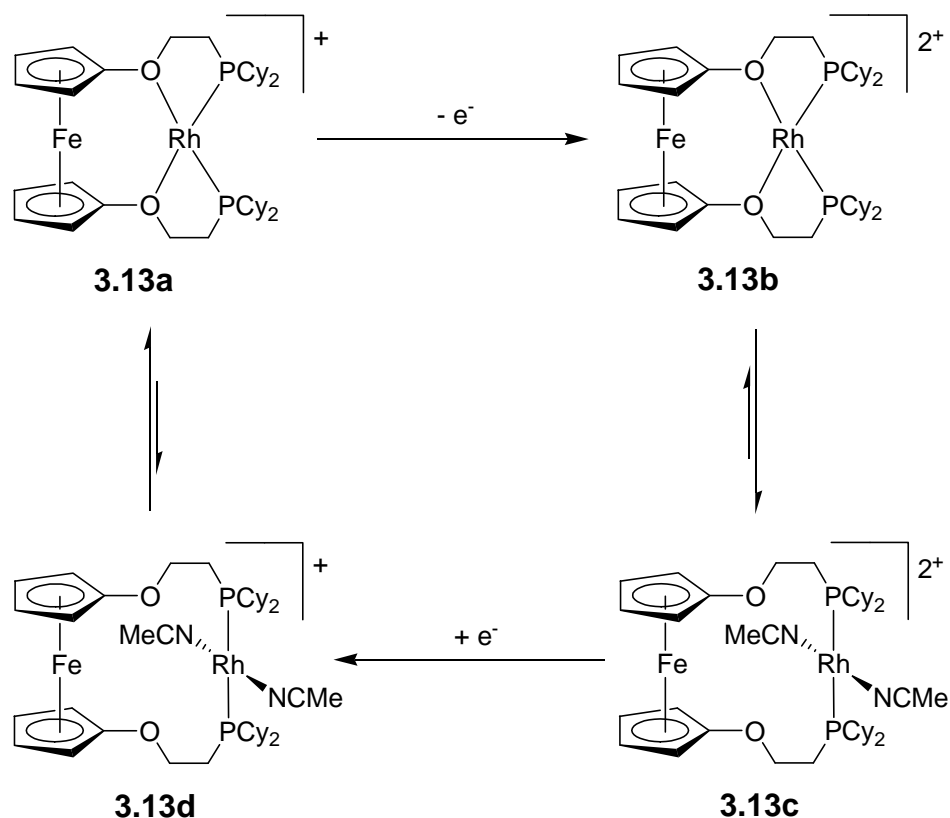


**Scheme 3.6:** Redox-induced structural changes in the ruthenium sandwich complex **3.12a** whereby ligand hapticity changes upon reduction. Boxed structures represent isolated and characterised species.

The redox process presented in Scheme 3.6 is proposed to proceed by an EEC<sub>2</sub>EC mechanism, analogous to the one presented in Scheme 3.5. Two-electron reduction of complex **3.12a** gives **3.12b**. This electron-transfer event is quickly followed by a structural change in which the coordinating ligand experiences a hapticity shift to generate **3.12c**. This new species (**3.12c**) is then re-oxidised to give a dicationic,  $\eta^4$ -sandwich complex **3.12d**. Complex **3.12d** experiences a fast chemical structural change and the original  $\eta^6$ -structure (**3.12a**) is regenerated. The structure of **3.12c** was

later solved by X-ray diffraction analysis, confirming the presence of both  $\eta^4$  and  $\eta^6$  ligands.<sup>264</sup>

The redox-induced structural changes described above involve metal-centred electron-transfer. Ligand-based redox-induced structural changes have also been described.<sup>265</sup> However, many of these so-called ligand-derived redox processes actually occur at appended ferrocene groups, distal to the inner coordination sphere of the metal centre.<sup>266, 267</sup> An example of this type of “ligand-based” redox-induced structural change is presented in Scheme 3.7.<sup>268</sup> The mechanism in this case is similar to those presented in Schemes 3.5 and 3.6; the main difference is that the mechanism shown in Scheme 3.7 involves the transfer of only one electron (and is therefore described as ECEC). Oxidation of the ferrocene moiety in **3.13a** effects a change in the organic framework of the ligand, resulting in the oxygen atoms becoming more labile. This oxidation is followed by a chemical change whereby the coordinating oxygen atoms in **3.13b** are replaced by coordinating solvent molecules to give **3.13c**. Reduction of the ferrocenium moiety in **3.13c** gives **3.13d** and restores the ligand to its original electronic structure. The oxygen atoms recoordinate to rhodium, replacing the coordinated acetonitrile molecules and the original structure of the complex (**3.13a**) is restored.



**Scheme 3.7:** Ligand-based redox-induced structural changes in **3.13a** rely on redox-activity of appended ferrocene groups.

Elaborate ligand designs have utilised the redox-activity of distal ferrocene groups to indirectly control the inner coordination sphere of the metal, giving these systems possible catalytic applications.<sup>269</sup> Conversely, genuine ligand-based redox activity leading to structural changes in coordination compounds is rare. Metal complexes involving quinonyl-substituted phosphine ligands have been reported wherein the metal coordination sphere can be influenced by the intrinsic redox-activity of the quinonyl moiety.<sup>270</sup> However, the redox reactions involved in these systems are also accompanied by corresponding proton-transfer chemistry. The electrochemical process described for zinc-diradical **2.19** offers the prospect of exercising a measure of control over the zinc

coordination sphere based solely on the redox-activity of the organic diradical ligand and without the need to account for any extraneous proton-transfer chemistry.

### **3.13 Potential-dependent spectroscopy of verdazyl ligands and metal complexes**

Although the voltammetric experiments presented in the preceding section point towards some interesting electrochemical behaviour with respect to **2.19**, no structural information can be gleaned from this data alone. Potential-dependent spectroscopy was employed in an effort to identify the possible species present in solution at the varying potentials throughout the electron-transfer processes described for **2.19**. Unfortunately, there are thus far no systematic reports on the spectroscopic features of verdazyl dications. To this end, the bipyridine monoradical **3.9** and its corresponding zinc complex **3.10** were first investigated using potential-dependent UV-Vis spectroscopy. The rationale behind these experiments was to first try to identify a spectroscopic “signature” of the redox products of a structurally analogous compound in which there is only one radical moiety to consider. These experiments are described in the ensuing section.

#### **3.13.1 Potential-dependent spectroscopy of radical **3.9** and zinc complex **3.10****

Potential-dependent UV-Vis spectra were recorded for verdazyl radical **3.9** and its corresponding zinc complex **3.10**. The spectra were recorded using a quartz glass cell with a 1 mm path length, coupled to a standard potentiostat (see Section 3.16.1 for a detailed description of electrochemistry and potential-dependent spectroscopy experiments). The cell was held at a given potential while the spectrum was collected.



The data in Figure 3.12 indicate that there is little change in the respective electronic spectra with changing potential.

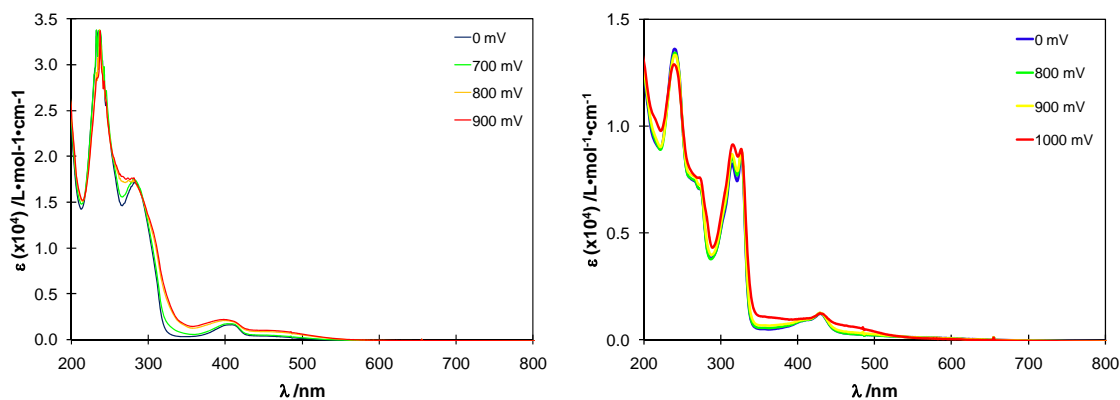


**Figure 3.12:** Potential-dependent UV-Vis spectra for **3.9** (left) and **3.10** (right). Successive coloured lines correspond to spectra recorded at different potentials. Potentials listed represent actual applied potential and are not corrected to the  $\text{Fc}/\text{Fc}^+$  redox couple.

### 3.13.2 Chemical titration of monoradical **3.9**

Inspection of the spectra in Figure 3.12 indicates that there is very little change to the electronic spectra of **3.9** or **3.10** with varying potential in the range of the respective oxidation processes. This is inconsistent with the CV data presented for both of these compounds, which indicates that cationic species should be electrochemically attainable (it follows intuitively that the cationic species generated should have distinct electronic spectra). In a further effort to determine the spectroscopic signature of a cationic derivative of a verdazyl monoradical, **3.9** was titrated with  $\text{NOPF}_6$  to chemically oxidise the radical. Figure 3.13 shows the UV-Vis spectra collected after successive additions of  $\text{NOPF}_6$ . Substantial changes in the UV region of the spectrum are evident, stemming from a modification of the conjugated  $\pi$ -system of the bipyridine portion of radical **3.9**.

The presence of isosbestic points in Figure 3.13 is consistent with radical **3.9** being converted to a single new species as the oxidation proceeds. However, the band at 400 nm remains largely qualitatively unchanged, which implies that the cation generated has an electronic transition that is very close in energy to the 400 nm transition involving the SOMO of **3.9**. The lack of a significant observable change in this region of the spectrum makes it difficult to unequivocally identify the oxidised species using this spectroscopic technique.

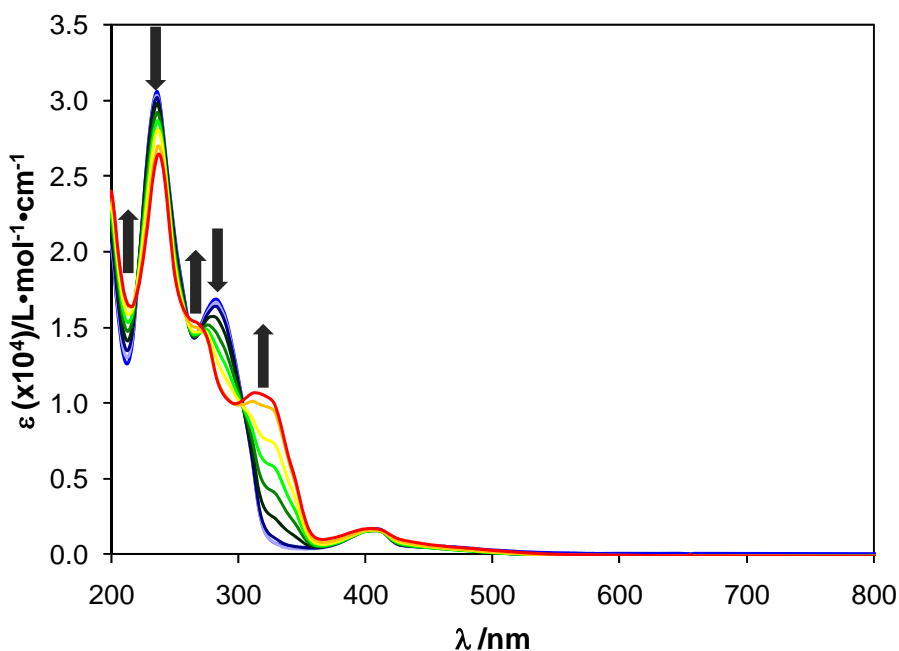


**Figure 3.13:** UV-Vis spectra for the chemical titration of **3.9** with  $\text{NOPF}_6$  as the oxidant.

### 3.13.3 Spectroelectrochemical studies of diradical **2.18** and zinc complex **2.19**

Similar potential dependent experiments were carried out with diradical **2.18** and the corresponding zinc complex **2.19** and these results are displayed in Figure 3.14. The response in both spectra (**2.18** and **2.19**) is qualitatively better than what was observed for

the parallel monoradical compounds **3.9** and **3.10**. As the applied potential is increased, the shoulder around 300 nm in the spectrum of **2.18** becomes more pronounced and also slightly red-shifted. An entirely new absorption grows in at 337 nm and the absorption centred at 400 nm becomes significantly broadened. The spectra for zinc complex **2.19** also show distinct changes with varying applied potential. The absorption at 308 nm with a shoulder at 319 nm is blue shifted to 296 nm and the shoulder is almost indiscernible. There is also a noticeable broadening of the absorption maximum near 430 nm.

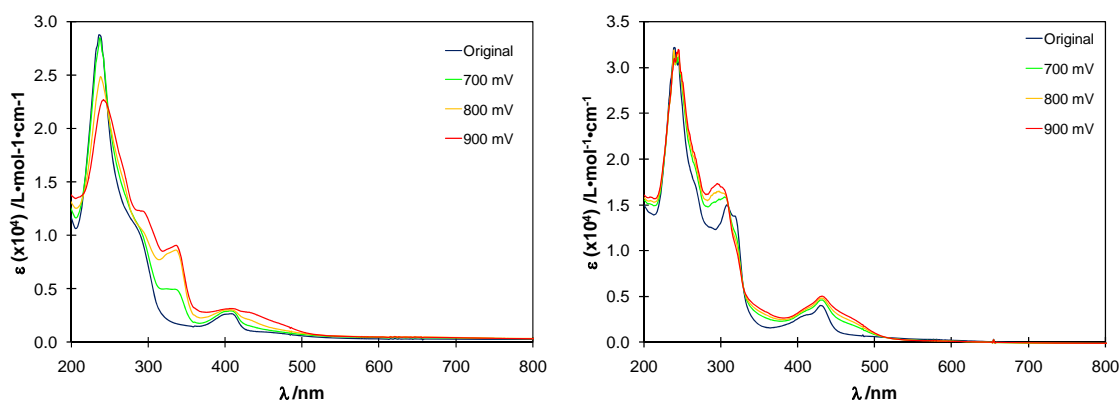


**Figure 3.14:** Potential-dependent UV-Vis spectra for **2.18** (left) and **2.19** (right). Successive coloured lines correspond to spectra recorded at different potentials. Potentials listed represent actual applied potential and are not corrected to the  $\text{Fc}/\text{Fc}^+$  redox couple.

### 3.14 Chemical oxidations of verdazyl radical and diradical compounds

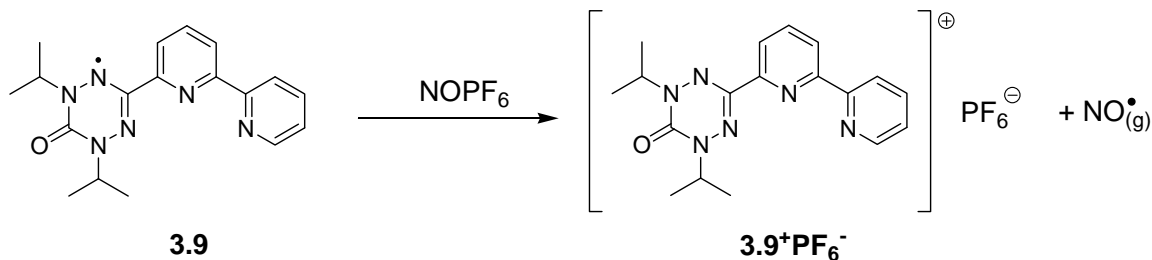
In light of the fact that few systematic studies of ionic verdazyl species have been reported, it was difficult to correlate the spectroelectrochemical studies presented in the preceding sections to any meaningful structural characteristics of the associated compounds. For this reason, much effort was dedicated to carrying out chemical oxidations of **3.9**, **3.10**, **2.18** and **2.19** in an attempt to isolate, crystallise and structurally

characterise a verdazyl cation or dication. This would then allow for the determination of spectroscopic signatures of known cationic verdazyl species.

#### 3.14.1 Synthetic efforts towards verdazyl-derived cationic and dicationic species

After experimenting with a variety of oxidising agents,<sup>271</sup> NOPF<sub>6</sub> was chosen as a suitable chemical oxidant and reactions were carried out as shown in Scheme 3.8. Equimolar amounts of **3.9** and NOPF<sub>6</sub> were dissolved in dichloromethane and stirred overnight, under argon. The colour of the reaction mixture changed from the deep orange of the verdazyl radical to a green solution after stirring overnight. A green powder was recovered by removing the solvent under reduced pressure. Oxidations of diradical **2.18** and zinc complexes **3.10** (Zn-monoradical) and **2.19** (Zn-diradical) were conducted in a comparable manner (two molar equivalents of NOPF<sub>6</sub> were used in reactions with **2.18** and **2.19**). Attempts to recrystallise the powder residues were carried out using a variety of different techniques; slow evaporation of solvent, layering of counter-solvent on a saturated solution of the respective cationic species and vapour diffusion methods. Unfortunately, none of these approaches resulted in the recovery of any crystalline material. Additionally, attempts to characterise the putative closed-shell cationic species using <sup>1</sup>H NMR spectroscopy resulted in spectra that showed substantial line broadening, making it difficult to identify any reaction species using this technique. Any unreacted radical species remaining in the analytical sample (i.e. in the NMR tube) would cause significant line broadening because of spin-spin coupling between the protons and the unpaired electrons associated with the unreacted radical species. Nonetheless, samples of the hexafluorophosphate salts of **2.18**, **2.19**, **3.9** and **3.10** that were stored under argon for weeks showed no appreciable signs of deterioration (the green colour of the salts

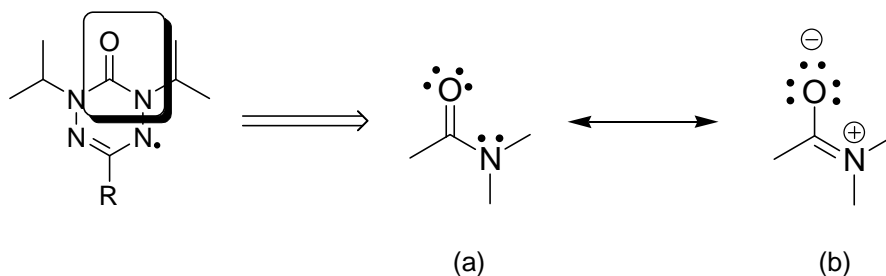
persisted and infrared spectra of the stored salt samples showed no change from the original spectra).



**Scheme 3.8:** Chemical oxidation of **3.9** using NOPF<sub>6</sub> as oxidant.

### 3.14.2 Electronic nature of amide moiety in 6-oxoverdazyl radical species

In light of the difficulty in obtaining any structural data on verdazyl cations and dications, another approach to identifying these putative species was necessary. As described in Chapter 2, the use of infrared spectroscopy to monitor the carbonyl stretching frequency in 6-oxoverdazyl species is invaluable to identifying coordinated versus uncoordinated verdazyl radicals. This analytical tool should also prove useful in identifying ionic verdazyl species. The sensitivity of the carbonyl stretch to the electronic nature of the verdazyl ring stems from the amide moiety; this relationship is shown in Scheme 3.9.



**Scheme 3.9:** Resonance contributions to the amide moiety in the verdazyl ring that dictate the sensitivity of the carbonyl stretch in the infrared spectrum.

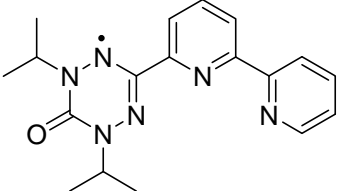
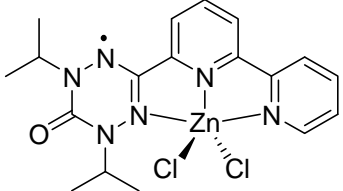
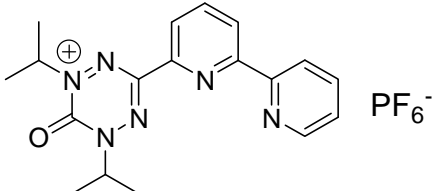
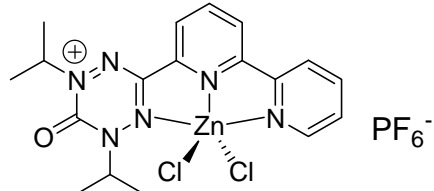
Any perturbation to the verdazyl system that increases the contribution of the neutral resonance structure (Scheme 3.9a) should lead to more double-bond character between carbon and oxygen, resulting in a higher infrared frequency for the carbonyl stretch. In cases where the Zwitterionic resonance structure (Scheme 3.9b) is the major contributor, the carbonyl group has more single-bond character and a lower infrared frequency is expected.

### 3.14.3 Infrared spectra of verdazyl monoradical and monocationic species

Infrared spectra were collected for samples of the chemical oxidation products of **3.9** and **3.10**. Table 3.6 shows the trend in the carbonyl stretching frequency that accompanies coordination and oxidation of the neutral verdazyl radical **3.9**. Upon coordination to zinc, the infrared signal for the carbonyl group increases from 1677 to 1701  $\text{cm}^{-1}$ . This coincides with a decrease in electron density at the coordinating nitrogen, which requires a stronger contribution from the neutral resonance structure (Scheme 3.9a) to avoid having positive charge on adjacent nitrogen atoms. The same trend is evident with oxidation of the radical; oxidation of **3.9** to **3.9<sup>+</sup>PF<sub>6</sub><sup>-</sup>** is accompanied by an increase in  $\nu_{\text{CO}}$  from 1677 to 1688  $\text{cm}^{-1}$ . Oxidation also decreases electron density at the sites hosting the largest spin density (i.e. the non-substituted nitrogen atoms in the verdazyl ring). Intuitively, it follows that the cationic zinc complex **3.10<sup>+</sup>PF<sub>6</sub><sup>-</sup>** should have a carbonyl stretching band at a higher frequency than that of the neutral zinc complex **3.10** and the uncoordinated cation **3.9<sup>+</sup>PF<sub>6</sub><sup>-</sup>**, since both oxidation and coordination are working to reduce electron density at the imine-like nitrogen atoms. In fact this is the case, and the cationic zinc complex **3.10<sup>+</sup>PF<sub>6</sub><sup>-</sup>** has a carbonyl stretch at

1706  $\text{cm}^{-1}$ , the result of the cationic nitrogen also being the coordinating nitrogen, which requires a very strong contribution of the neutral resonance structure (Scheme 3.9a).

**Table 3.6:** Infrared frequency of the carbonyl group in radicals **3.9** and **3.10** and salts **3.9<sup>+</sup>PF<sub>6</sub><sup>-</sup>** and **3.10<sup>+</sup>PF<sub>6</sub><sup>-</sup>**.

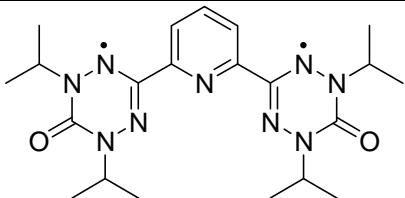
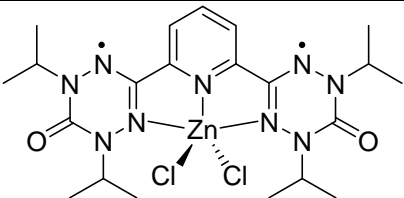
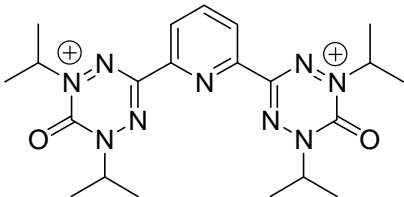
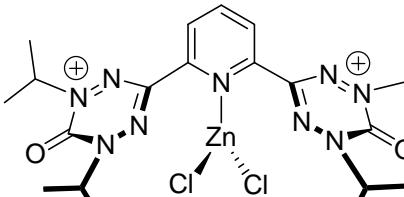
 <p style="text-align: center;"><b>3.9</b></p> <p style="text-align: center;"><math>\nu_{\text{CO}} = 1677 \text{ cm}^{-1}</math></p>	 <p style="text-align: center;"><b>3.10</b></p> <p style="text-align: center;"><math>\nu_{\text{CO}} = 1701 \text{ cm}^{-1}</math></p>
 <p style="text-align: center;"><b>3.9<sup>+</sup>PF<sub>6</sub><sup>-</sup></b></p> <p style="text-align: center;"><math>\nu_{\text{CO}} = 1688 \text{ cm}^{-1}</math></p>	 <p style="text-align: center;"><b>3.10<sup>+</sup>PF<sub>6</sub><sup>-</sup></b></p> <p style="text-align: center;"><math>\nu_{\text{CO}} = 1706 \text{ cm}^{-1}</math></p>

#### 3.14.4 Infrared spectra of verdazyl diradical and dicationic species

Infrared spectra were collected for samples of the chemical oxidation products of diradical **2.18** and zinc complex **2.19** and the relevant data is summarised in Table 3.7. The carbonyl stretching frequency increases from 1683  $\text{cm}^{-1}$  in diradical **2.18** to 1704  $\text{cm}^{-1}$  in the coordination compound **2.19**. Oxidation of diradical **2.18** is also accompanied by an increase in the carbonyl stretching frequency from 1683 to 1698  $\text{cm}^{-1}$  in the dicationic species **2.18<sup>2+</sup>(PF<sub>6</sub><sup>-</sup>)<sub>2</sub>**. By the same reasoning that was presented for the monoradical/monocationic species in the preceeding section, the carbonyl groups in the

zinc dication complex  $\mathbf{2.19}^{2+}(\text{PF}_6^-)_2$  should exhibit a stretching frequency at higher energy than both the neutral zinc complex  $\mathbf{2.19}$  and the uncoordinated dication  $\mathbf{2.18}^{2+}(\text{PF}_6^-)_2$ . However, the data presented in Table 3.7 indicate that this is not the case. The carbonyl signal in zinc dication  $\mathbf{2.19}^{2+}(\text{PF}_6^-)_2$  is found at  $1696\text{ cm}^{-1}$ , a value that is almost identical to that for the uncoordinated dication  $\mathbf{2.18}^{2+}(\text{PF}_6^-)_2$  ( $\nu_{\text{CO}} = 1698\text{ cm}^{-1}$ ). This indicates that the electronic structures of dication  $\mathbf{2.18}^{2+}(\text{PF}_6^-)_2$  and zinc dication  $\mathbf{2.19}^{2+}(\text{PF}_6^-)_2$  have similar contributions from the two limiting resonance structures, which is consistent with the verdazyl rings not being coordinated to zinc in the dicationic structure  $\mathbf{2.19}^{2+}(\text{PF}_6^-)_2$ .

**Table 3.7:** Infrared frequency of the carbonyl group in diradicals  $\mathbf{2.18}$  and  $\mathbf{2.19}$  and dications  $\mathbf{2.18}^{2+}(\text{PF}_6^-)_2$  and  $\mathbf{2.19}^{2+}(\text{PF}_6^-)_2$ .

 <p style="text-align: center;"><b>2.18</b></p> <p style="text-align: center;"><math>\nu_{\text{CO}} = 1683\text{ cm}^{-1}</math></p>	 <p style="text-align: center;"><b>2.19</b></p> <p style="text-align: center;"><math>\nu_{\text{CO}} = 1704\text{ cm}^{-1}</math></p>
 <p style="text-align: center;"><b><math>\mathbf{2.18}^{2+}(\text{PF}_6^-)_2</math></b></p> <p style="text-align: center;"><math>\nu_{\text{CO}} = 1698\text{ cm}^{-1}</math></p>	 <p style="text-align: center;"><b><math>\mathbf{2.19}^{2+}(\text{PF}_6^-)_2</math></b></p> <p style="text-align: center;"><math>\nu_{\text{CO}} = 1696\text{ cm}^{-1}</math></p>



### 3.15 Summary

This chapter presents a detailed analysis of the electrochemical behaviour of four discrete compounds based on the 6-oxoverdazyl framework; a monoradical, a diradical and the respective zinc coordination complexes. Prior to the work described in this chapter, only one electrochemical study of metal-verdazyl complexes had been published,<sup>111</sup> which involved a 6-oxoverdazyl radical coordinated to a redox-active metal centre. For the study at hand, zinc was chosen as the metal of interest in an effort to better understand the redox properties of the coordinated verdazyl radicals and diradicals in the absence of metal-centred electron-transfer processes.

A bipyridine-substituted verdazyl radical **3.9** was prepared and fully characterised. The oxidation and reduction potentials of this compound fall well within the expected range, based on other similar verdazyl monoradicals.<sup>108</sup> The observed electrochemical behaviour of the corresponding zinc complex **3.10** was slightly unexpected. The oxidation potential of the zinc complex (+0.42 V) is slightly more positive than that of the radical itself (+0.20 V). However, the zinc complex is much more easily reduced (at -0.87 V) than is the radical (at -1.36 V). This corresponds to a difference in cell potential of 260 mV between the verdazyl radical and its zinc coordination compound. Reports of substituent effects on oxidation and reduction potentials of verdazyl radicals indicate that oxidation and reduction potentials are typically shifted by approximately equal amounts, resulting in no significant change to the overall cell potential. Based on these data and the electrochemical behaviour observed herein, the addition of a metal – even a redox-inert one – to the binding pocket

of this verdazyl ligand cannot be considered in the same way as simple organic substituent effects.

Pyridine-bridged diradical **2.18** was also subjected to a number of electrochemical experiments. In Chapter 2, the magnetic properties of diradical **2.18** and zinc-diradical complex **2.19** were compared. The addition of a diamagnetic metal had a negligible impact on the magnetic coupling between the two verdazyl moieties of the diradical. However, the electrochemical properties of this same diradical were greatly affected by the introduction of the redox-inert metal. The oxidation and reduction potentials of the diradical (+0.20 V and -1.36 V, respectively) do not differ significantly from those of the bipyridine monoradical **3.9** described in this chapter. These redox potentials also compare well with those reported for other aryl-bridged verdazyl diradicals **1.55** and **1.56**.<sup>107</sup> Coordination of this diradical to zinc brought about significant changes in the redox properties of the resulting complex **2.19**. A shift in the reduction potential was observed, qualitatively similar to that seen in the zinc monoradical complex **3.10**. However, further examination showed that this reduction represented only a one-electron process. The oxidation process for diradical **2.19** was also affected by coordination to zinc. The process appears to be irreversible, with the cathodic and anodic waves associated with the process separated by more than 200 mV. Oxidation of zinc complex **2.19** was subsequently shown to be reversible, overall, although not in the strict electrochemical sense. A square, EEC<sub>2</sub>EC mechanism is proposed for this oxidation whereby removal of two electrons from the zinc-diradical complex (EE) is quickly followed by a chemical structural change (C) in which the verdazyl nitrogens dissociate from the zinc centre. Re-reduction of this compound regenerates the original zinc-

diradical, again via a two-step process in which electron-transfer (EE) is followed by a structural change (C).

A number of spectroscopic experiments were carried out in an attempt to identify a spectroscopic signature of the putative cationic species. These efforts were, in large part, unsuccessful at unambiguously identifying the target species. Ultimately, infrared spectroscopy was employed in conjunction with chemical oxidation to observe the difference in stretching frequency of the carbonyl group between the radical and cationic species. A comparison of the carbonyl stretch among the various species (diradical, zinc-diradical, dication, zinc-dication) indicates that the zinc-dication has an electronic structure very similar to that of the uncoordinated dication. In the absence of direct structural characterisation of the cationic verdazyl analogues, this interpretation of the infrared spectra offers convincing, albeit indirect, evidence that the zinc-diradical complex does in fact undergo a significant redox-induced structural change. On the other hand, CV and IR data imply that oxidation of the zinc-monoradical complex **3.10** does not induce the same structural change (dissociation of the verdazy moiety from the metal). Complex **3.10** represents a rare example of a coordinated cationic ligand.

## **3.16 Experimental**

### **3.16.1 General Electrochemical Considerations**

Cyclic voltammetry and Osteryoung square wave voltammetry experiments were performed using Bioanalytical Systems CV-50W voltammetric analyser with a cell consisting of a glassy carbon working electrode, platinum wire counter electrode and silver wire reference electrode. Potential-dependent electronic spectra were recorded in a

quartz glass cell with 1 mm path length, using a platinum gauze working electrode, platinum wire counter electrode and silver wire reference electrode. Voltammetric experiments were conducted using analyte concentrations of ~1 mM in distilled and degassed acetonitrile with  $\text{nBu}_4\text{N}^+\text{BF}_4^-$  (~0.1 M) as supporting electrolyte and were referenced against the ferrocene/ferrocenium redox couple.

### 3.16.2 Synthesis of verdazyl 3.9 and zinc complex 3.10

**1,5-diisopropyl-3-(2',2''-bipyridin-6'-yl)-6-oxoverdazyl (3.9)** To a solution of **2.9**<sup>106</sup> (1.417 g, 5.733 mmol) and sodium acetate (0.941 g, 11.5 mmol) in refluxing methanol (50 mL) was added drop-wise a solution of 2,2'-bipyridine-6-carboxaldehyde<sup>272, 273</sup> (1.053 g, 5.717 mmol) in methanol (200 mL). After complete addition (2-3 hours) the reaction was heated at reflux for a further 20 hours. Heat was then removed and solvent was removed under reduced pressure to yield a yellow slurry. *n*-Heptane was added and the mixture was heated at reflux for 10 minutes, and then hot-filtered to remove insoluble material. Solvent was removed from filtrate under reduced pressure to yield an off-white solid (1.628 g). 1,5-diisopropyl-3-(2',2''-bipyridin-6'-yl)-1,2,4,5-tetrazane-6-oxide **3.8** was identified in the <sup>1</sup>H NMR spectrum of this off-white solid (Appendix A, Figure A-1), which also contained significant impurities. The tetrazane product could not be sufficiently purified to allow complete characterisation. Nonetheless, the off-white solid product of the above reaction and *p*-benzoquinone (0.7876 g, 7.286 mmol) were dissolved in toluene (200 mL) to give a faint yellow-coloured solution. The solution was refluxed in air for 60 minutes, by which point the solution had turned dark orange. Toluene was removed under reduced pressure and the residue was then purified by column chromatography on neutral alumina with dichloromethane as eluent. Like

fractions were combined and the solvent was removed under reduced pressure to yield **3.9** (0.681 g, 35.30%, based on 5.717 mmol of 2,2'-bipyridine-6-carboxaldehyde) as an orange microcrystalline solid. A saturated dichloromethane solution of the microcrystalline solid was layered with hexanes and X-ray quality crystals were attained by slow evaporation of this solvent mixture. Mp. 122-124 °C (uncorrected). FT-IR (KBr): 2972 (s), 2928 (m), 2868 (m), 1677 (vs), 1577 (s), 1563 (s), 1426 (s), 1385 (s), 1240 (s), 1163 (s), 1127 (m), 1083 (m), 1039 (m), 990 (m), 790 (s), 751 (m), 721 (m), 694 (m), 620  $\text{cm}^{-1}$  (m). UV-Vis ( $\text{CH}_2\text{Cl}_2$ ):  $\lambda_{\text{max}}$  237 ( $\epsilon = 28840$ ), 284 ( $\epsilon = 16110$ ), 407 nm ( $\epsilon = 1690 \text{ L}\cdot\text{mol}^{-1}\cdot\text{cm}^{-1}$ ). MS (ESI-MS):  $m/z$  337.7  $\{[\text{M}]^+, 90 \%\}$ . Anal. Calcd. for  $\text{C}_{18}\text{H}_{21}\text{N}_6\text{O}$ : C, 64.08; H, 6.27; N, 24.91. Found: C, 64.13; H, 6.32; N, 24.55.

**1,5-diisopropyl-3-(2',2''-bipyridin-6'-yl)-6-oxoverdazylzinc(II) chloride (3.10)** To a solution of  $\text{ZnCl}_2$  (43.8 mg, 0.32 mmol) in  $\text{CH}_3\text{CN}$  (10 mL) was added drop-wise a solution of **3.9** (111 mg, 0.33 mmol) in  $\text{CH}_3\text{CN}$  (5 mL). Upon standing in air for 3 days dark purple microcrystalline material was isolated from the mother liquor by vacuum filtration to yield **3.10** (94.2 mg, 60%). A saturated dichloromethane solution of the microcrystalline solid was layered with diethyl ether and X-ray quality crystals were attained by slow evaporation of this solvent mixture. Mp. 256 - 258 °C (uncorrected). FT-IR (KBr): 3445 (br), 2967 (m), 2928 (m), 1700 (vs), 1596 (s), 1577 (s), 1492 (m), 1465 (s), 1363 (m), 1248 (s), 1160 (s), 1078 (s), 1026 (m), 790 (s), 685 (m), 663  $\text{cm}^{-1}$  (m). UV-Vis ( $\text{CH}_3\text{CN}$ ):  $\lambda_{\text{max}}$  243 ( $\epsilon = 25760$ ), 268 ( $\epsilon = 14910$ ), 276 ( $\epsilon = 14240$ ), 315 ( $\epsilon = 16150$ ), 328 ( $\epsilon = 16930$ ), 432 nm ( $\epsilon = 1524 \text{ L}\cdot\text{mol}^{-1}\cdot\text{cm}^{-1}$ ). Anal. Calcd. for  $\text{C}_{18}\text{H}_{21}\text{N}_6\text{OZnCl}_2$ : C, 45.64; H, 4.47; N, 17.74. Found: C, 45.98; H, 4.51; N, 17.60.

### 3.16.3 Chemical oxidations of **2.18**, **2.19**, **3.9** and **3.10**

The following experiments were carried out using dry glassware, dry, distilled solvents and standard dry-box and Schlenk techniques.

**Reaction of 2,6-pyridinebis(1,5-diisopropyl-6-oxoverdazyl-3-yl) with nitrosonium hexafluorophosphate [**2.18**<sup>2+</sup>(PF<sub>6</sub><sup>-</sup>)<sub>2</sub>]** A side-arm round bottom flask was charged with **2.18** (74 mg, 0.17 mmol) and NOPF<sub>6</sub> (98 mg, 0.56 mmol). The flask was put under argon and acetonitrile (50 mL) was added via gas-tight syringe. The reaction was stirred for 17 hours at room temperature, under argon. After stirring for 17 hours, the reaction mixture had changed colour from orange to dark green. Solvent was removed under reduced pressure and **2.18**<sup>2+</sup>(PF<sub>6</sub><sup>-</sup>)<sub>2</sub> was isolated as a green powder (58 mg, 47%). FT-IR (KBr): 3262 (w), 3228 (w), 3116 (w), 2987 (m), 2939 (m), 2983 (m), 1698 (vs), 1623 (s), 1524 (m), 1460 (m), 1391 (m), 1370 (m), 1294 (m), 1254 (m), 1219 (w), 1170 (w), 1140 (w), 1049 (w), 843 (vs), 723 (m), 637 (w), 557 (s), 492 cm<sup>-1</sup> (m).

**Reaction of 2,6-pyridinebis(1,5-diisopropyl-6-oxoverdazyl-3-yl)zinc(II)chloride with nitrosonium hexafluorophosphate [**2.19**<sup>2+</sup>(PF<sub>6</sub><sup>-</sup>)<sub>2</sub>]** A side-arm round bottom flask was charged with **2.19** (46 mg, 0.080 mmol) and NOPF<sub>6</sub> (30 mg, 0.17 mmol). The flask was put under argon and acetonitrile (50 mL) was added via gas-tight syringe. The reaction was stirred for 3 days at room temperature, under argon. After stirring for 3 days, the reaction mixture had changed colour from orange to dark green. Solvent was removed under reduced pressure and **2.19**<sup>2+</sup>(PF<sub>6</sub><sup>-</sup>)<sub>2</sub> was isolated as a green powder (68 mg, 99%). FT-IR (KBr): 3431 (w), 3262 (w), 3224 (w), 3116 (w), 2987 (m), 2939 (m), 1696 (vs),

1623 (s), 1524 (m), 1460 (m), 1389 (m), 1370 (m), 1297 (s), 1249 (m), 1219 (w), 1165 (m), 1140 (m), 1131 (m), 1082 (w), 845 (s), 723 (m), 634 (w), 557 (m), 492  $\text{cm}^{-1}$  (m).

**Reaction of 1,5-diisopropyl-3-(2',2''-bipyridin-6'-yl)-6-oxoverdazyl with nitrosonium hexafluorophosphate ( $3.9^+\text{PF}_6^-$ )** A side-arm round bottom flask was charged with **3.9** (36 mg, 0.11 mmol) and  $\text{NOPF}_6$  (33 mg, 0.19 mmol). The flask was put under argon and acetonitrile (50 mL) was added via gas-tight syringe. The reaction was stirred for 17 hours at room temperature, under argon. After stirring for 17 hours, the reaction mixture had changed colour from orange to dark green. Solvent was removed under reduced pressure and  $3.9^+\text{PF}_6^-$  was isolated as a green powder (30 mg, 58%). FT-IR (KBr): 3422 (br, m), 3258 (m), 3116 (m), 2982 (m), 2935 (m), 2879 (m), 1688 (s), 1623 (s), 1589 (m), 1535 (m), 1458 (m), 1391 (w), 1370 (w), 1297 (s), 1262 (w), 1223 (w), 1174 (w), 1135 (w), 1112 (w), 1041 (w), 996 (w), 843 (vs), 778 (s), 740 (m), 619 (w), 557 (s), 497  $\text{cm}^{-1}$  (m).

**Reaction of 1,5-diisopropyl-3-(2',2''-bipyridin-6'-yl)-6-oxoverdazylzincdichloride with nitrosonium hexafluorophosphate ( $3.10^+\text{PF}_6^-$ )** A side-arm round bottom flask was charged with **3.10** (64 mg, 0.14 mmol) and  $\text{NOPF}_6$  (24 mg, 0.14 mmol). The flask was put under argon and acetonitrile (50 mL) was added via gas-tight syringe. The reaction was stirred for 4 days at room temperature, under argon. After stirring for 4 days, the reaction mixture was a deep red-brown colour. Solvent was removed under reduced pressure to give a dark green powder,  $3.10\text{PF}_6$  (55 mg, 66%). FT-IR (KBr): 3439 (br, m), 3094 (w), 2918 (s), 2849 (s), 1706 (s), 1608 (m), 1597 (m), 1580 (w), 1492 (w), 1464 (s), 1389 (w), 1367 (m), 1299 (w), 1260 (m), 1232 (w), 1159 (w), 1133 (w),

1107 (w), 1051 (w), 1026 (m), 1015 (m), 907 (w), 845 (s), 781 (m), 720 (w), 688 (w),  
669 (w), 637 (w), 557 (s), 495  $\text{cm}^{-1}$  (m).



## Chapter 4: Conclusions and future work

The design of new stable radicals continues to be a driving force behind the development of modern materials. Biological and chemical spin labels, molecular conductors, organic batteries, catalysis and, of course, molecule-based magnets are all tied to stable organic radicals. The work described herein offers new insights into stable radical chemistry by presenting a detailed study of the magnetic and redox properties of novel 6-oxoverdazyl radicals and diradicals, and their corresponding coordination compounds.

A known 1,5-diisopropyl-3-pyridine-substituted chelating verdazyl monoradical was employed to prepare coordination compounds using nickel, cobalt and manganese. Methyl disubstituted analogues of the Ni and Mn complexes have been previously reported.<sup>94</sup> The isopropyl version of the nickel complex that was presented in this work exhibits magnetic behaviour that qualitatively matches that of the methyl analogue. Both complexes show relatively strong ferromagnetic coupling between the  $S = 1$  nickel ion and the  $S = \frac{1}{2}$  verdazyl radical, although the magnitude of the coupling constant in the isopropyl version is smaller than that in the methyl variety. The sign of the coupling constant for the isopropyl-verdazyl cobalt complex agrees with other cobalt-radical complexes reported;<sup>74, 97, 274</sup> this is another example of ferromagnetic metal-radical coupling in an octahedral (or in this case, *pseudo*-octahedral) cobalt coordination compound. Unfortunately, the manganese complex presented in this work could not be crystallised in a high enough yield to allow for its magnetic characterisation. Nonetheless, some important conclusions can be drawn based on the nickel and cobalt

complexes of the isopropyl verdazyl monoradical ligand. The superior stability of the isopropyl verdazyl derivative over the methyl version has been discussed both in this thesis and elsewhere.<sup>106</sup> The advantages of increased radical stability as it relates to materials design have also been established.<sup>27</sup> However, with respect to magnetism, the benefits of the enhanced radical stability from the isopropyl groups would be lost if it were also accompanied by a decrease in metal-radical magnetic exchange. A comparison of the magnetic properties of the nickel and cobalt complexes here with those of similar coordination compounds shows that there is no significant change in the magnetic properties of the complexes in changing from methyl substituents to isopropyl groups. This finding is important to the rest of the thesis, as all subsequent compounds studied here are based on the isopropyl verdazyl paradigm.

A new stable organic diradical **2.18** was prepared and its electronic and magnetic properties were described. The magnetic properties of this diradical are consistent with previously reported *meta*-bridged aryl diradicals.<sup>107</sup> Diradical **2.18** exhibits weak ferromagnetic exchange between the radical moieties, according to an established spin polarisation mechanism (see Chapter 2). This verdazyl diradical was then employed as a ligand in the preparation of a comprehensive series of first row transition metal complexes. A  $\text{Zn}^{2+}$  complex **2.19** was prepared and used as a control to examine the effect of adding a diamagnetic metal to the binding pocket of the diradical. The magnetic properties of zinc complex **2.19** showed no significant change from those of diradical **2.18**. This indicates that the presence of a diamagnetic metal centre does not provide any new pathways for magnetic exchange.

Coordination compounds incorporating manganese, iron, cobalt and nickel were also prepared. Each of these complexes was structurally similar to the zinc-diradical complex. However, each showed unique magnetic behaviour. Both iron and manganese displayed antiferromagnetic coupling to the diradical ligand, although the magnitude of the coupling constants differed. Analysis of the magnetic behaviour of the cobalt-diradical complex indicates that ferromagnetic metal-radical coupling is the predominant intramolecular exchange mechanism. This complex also shows signs of zero-field splitting effects, which are common in cobalt coordination compounds, and which make it difficult to precisely evaluate the magnitude of the metal-radical coupling constant. Ferromagnetic interactions were also observed for the nickel-diradical complex. Although zero-field splitting effects are also manifested in the magnetic behaviour of this complex, the quantitative values gained from the magnetic analysis are on the same order of magnitude as those seen in other nickel-diradical complexes.<sup>186</sup> In general, this sequence of diradical coordination compounds represents a detailed, systematic study of the magnetic interactions of a stable diradical ligand with a series of first row transition metals. These compounds can be envisioned as discrete model systems in the study of metal-radical interactions that expand beyond 1:1 metal:radical complexes. Furthermore, these *pseudo*-trigonal bipyramidal complexes represent a novel coordination environment for verdazyl radicals and diradicals.

In addition to the isostructural series of complexes discussed above, two other diradical coordination compounds were synthesised whose composition was distinct from the rest of the series. Chromium complex **2.28b** is notable not only because of its structural irregularity with respect to the other compounds in the series (one verdazyl

nitrogen is substituted by a hydrogen rather than the typical isopropyl group), but also because it is the first example of a chromium-verdazyl complex. This compound is also a distinctive example of an open-shell verdazyl species in which there is no organic substituent on one of the verdazyl nitrogen atoms. This compound presents an interesting avenue for future study with respect to the origin of this structural change. Although the studies presented in this thesis detail the structural and magnetic properties of this unique complex, they do not attempt to address the mechanism by which diradical **2.18** essentially loses one of its isopropyl substituents upon coordination to chromium. Whether or not this modification is intrinsic to the synthesis of the complex itself or perhaps an aspect of the crystallisation of this particular compound are interesting questions that could be addressed in the future.

Finally, the same diradical ligand was combined with copper(II) chloride leading to an unpredictable result. The product of this synthesis was a coordination polymer **2.29**, in which the diradical ligand undergoes a structural change that is even more pronounced than the one seen in the chromium complex **2.28b**. In the case of copper complex **2.29**, the verdazyl ligand appears to lose the radical nature of at least one of the verdazyl rings upon coordination to copper. This complex represents a severe departure from the structure shared by most of the other diradical coordination compounds presented in this work. Elemental analysis of this compound indicates that the composition of the bulk material is different from the individual crystal that was studied by X-ray diffraction. This presents a few interesting questions with respect to this compound: Are there possibly other discrete complexes present in the bulk sample? Does the coordination polymer observed by X-ray diffraction break down to give other

by-products? And if there are multiple products present, can these somehow be controlled by varying the synthetic procedure to favour one product over the others?

In addition to a detailed magnetic study of metal-verdazyl complexes, this thesis also encompasses an in-depth analysis of the redox properties of verdazyl radicals, diradicals and coordination compounds. A bipyridine-substituted verdazyl radical **3.9** was prepared and fully characterised. This compound, having a tridentate binding pocket, was designed as a monoradical analogue of diradical **2.18**. Both compounds show reversible or quasi-reversible redox processes, with the oxidation and reduction potentials of the verdazyl mono- and diradicals being almost identical. However, one distinct difference is that both the oxidation and reduction processes associated with diradical **2.18** represent two-electron processes. Nitroxide radicals have been extensively studied as potential building blocks for the manufacture of flexible organic batteries (see Chapter 3). Verdazyl diradicals could also be promising candidates in this field. Verdazyl radicals are known to exhibit stability that is on par with nitroxides and the prospect of increasing the number of electrons transferred adds to their potential utility in this respect.

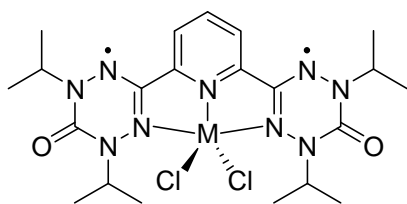
The addition of zinc, a diamagnetic and redox-inert metal, to diradical **2.18** proved to have no significant affect on the magnetic properties of the diradical. However, the same cannot be said for the redox properties of the radical and diradical studied here. Addition of zinc to the binding pocket of the bipyridine-substituted verdazyl monoradical **3.9** produced a significant decrease in the observed cell potential. The origin of this modification is not clear and high-level calculations of the molecular orbitals involved with these electron-transfer processes may help elucidate the source of

this change. Coordination of diradical **2.18** to zinc produced a complex that showed drastically different redox properties, compared to the original diradical. Not only did the cell potential decrease, but the character of both the oxidation and reduction processes showed remarkable changes. While the diradical displays a quasi-reversible two-electron reduction, the zinc complex can only be reversibly reduced by one electron. Addition of a second electron to the system results in an unstable species. Oxidation of the zinc complex **2.19** is electrochemically irreversible, with the cathodic and anodic waves separated by 220 mV. However, the reproducibility of the CV of this complex indicates that the overall combination of oxidation and reduction processes results in a reversible process. A possible mechanism to explain the observed redox behaviour involves a redox-induced structural change in the zinc-diradical complex (see Chapter 3). Although no cationic species could be isolated, infrared spectroscopy of the chemically oxidised verdazyl species supports the proposed structural change in the zinc-dication.

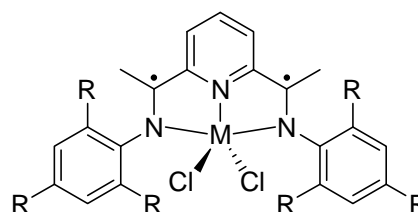
There is a lot of room for future work with respect to the electrochemical properties of verdazyl diradical coordination compounds. The most obvious is to continue the efforts to realise an isolable verdazyl cation or dication. A full spectroscopic analysis of such a species would then facilitate the explicit identification of the dicationic species described in this thesis. However, in the absence of such a study, the combination of electrochemical and spectroscopic data presented herein indicates that the zinc-diradical complex **2.19** undergoes an interesting redox-induced structural change.

Another valuable and intriguing area for future study would be to examine the redox properties of other metal-diradical complexes whose structural and magnetic properties were described in this thesis. Coordination compounds involving radical-

anionic ligands **4.1**, **4.2** have been employed to expand the realm of base-metal catalysis using iron and cobalt.<sup>224, 225, 275, 276</sup> These complexes share structural similarities with the iron **2.21** and cobalt **2.22** diradical complexes presented in Chapter 2. The potential to influence the coordination sphere in **2.21** and **2.22** via the redox properties of the diradical ligand could make verdazyl diradical complexes interesting targets to study any potential catalytic activity.



**2.21:** M = Fe  
**2.22:** M = Co



**4.1:** M = Fe  
**4.2:** M = Co

## References

1. Gomberg, M. *J. Am. Chem. Soc.*, **1900**, 22, 757-771.
2. McBride, J. M. *Tetrahedron*, **1974**, 30, 2009-2022.
3. Hicks, R. G. *Org. Biomol. Chem.*, **2007**, 5, 1321-1338.
4. Power, P. P. *Chem. Rev.*, **2003**, 103, 789-810.
5. Ingold, K. U.; Griller, D. *Acc. Chem. Res.*, **1976**, 9, 13-19.
6. Janzen, E. G. *Acc. Chem. Res.*, **1971**, 4, 31-40.
7. Zoia, L.; Argyropoulos, D. S.; *J. Phys. Org. Chem.*, **2010**, 23, 505-512.
8. Berliner, L. *Appl. Magn. Reson.*, **2009**, 36, 157-170.
9. Spulber, M.; Schlick, S. *J. Phys. Chem. A*, **2010**, 114, 6217-6225.
10. Pou, S.; Halpern, H. J.; Tsai, P.; Rosen, G. M. *Acc. Chem. Res.*, **1999**, 32, 155-161.
11. Sheldon, R. A.; Arends, I. W. C. E.; ten Brink, G-J; Dijkstra, A. *Acc. Chem. Res.*, **2002**, 35, 774-781.
12. Tamura, M.; Nakazawa, Y.; Shiomi, D.; Nozawa, K.; Hosokoshi, Y.; Ishikawa, M.; Takahashi, M.; Kinoshita, M. *Chem. Phys. Lett.*, **1991**, 186, 401-404.
13. Turek, P.; Nozawa, K.; Shiomi, D.; Awaga, K.; Inabe, T.; Maruyama, Y.; Kinoshita, M. *Chem. Phys. Lett.*, **1991**, 180, 327-331.
14. Nakatsuji, S.; Anzai, H. *J. Mater. Chem.*, **1997**, 7, 2161-2174.
15. Feig, A. L.; Lippard, S. J. *Chem. Rev.*, **1994**, 94, 759-805.
16. Hañller, L. J. L.; Mas-Marzá, E.; Moreno, A.; Lowe, J. P.; Macgregor, S. A.; Mahon, M. F.; Pregosin, P. S.; Whittlesey, M. K. *J. Am. Chem. Soc.*, **2009**, 131, 9618-9619.
17. Hayton, T. W.; Legzdins, P.; Sharp, W. B. *Chem. Rev.*, **2002**, 102, 935-992.
18. Klotz, I. M.; Kurtz, D. M. *Chem. Rev.*, **1994**, 94, 567-568.



19. Momenteau, M.; Reed, C. A. *Chem. Rev.*, **1994**, *94*, 659-698.
20. Punniyamurthy, T.; Velusamy, S.; Iqbal, J. *Chem. Rev.*, **2005**, *105*, 2329-2364.
21. Eaton, S. S.; Eaton, G. R. *Coord. Chem. Rev.*, **1988**, *83*, 29-72.
22. Forrester, A. R.; Hay, J. M.; Thomson, R. H. *Organic Chemistry of Stable Free Radicals*, Academic Press, New York, N.Y., 1968.
23. Franchi, P.; Lucarini, M.; Pedulli, G. F. *Curr. Org. Chem.*, **2004**, *8*, 1831-1849.
24. Hideg, K.; Kálai, T.; Sár, C. P. *J. Heterocycl. Chem.*, **2005**, *42*, 437-450.
25. Kokorin, A. I.; Grigor'ev, I. A. *Mendeleev Commun.*, **2006**, *16*, 195-200.
26. Karoui, H.; Le Moigne, F.; Ouari, O.; Tordo, P. in *Stable Radicals: Fundamentals and Applied Aspects of Odd-Electron Compounds*, ed. R. G. Hicks, John Wiley & Sons, Ltd., West Sussex, UK, 2010, pp. 173-229.
27. Caneschi, A.; Gatteschi, D.; Rey, P. in *Prog. Inorg. Chem.*, Vol. 39, ed. S. J. Lippard, John Wiley & Sons Inc., New York, 1991, pp. 331-429.
28. Beck, W.; Schmidtner, K.; Keller, H. J. *Chem. Ber.*, **1967**, *100*, 503-511.
29. Zelonka, R. A.; Baird, M. C. *J. Am. Chem. Soc.*, **1971**, *93*, 6066-6070.
30. Dickman, M. H.; Doedens, R. J. *Inorg. Chem.*, **1981**, *20*, 2677-2681.
31. Caneschi, A.; Grand, A.; Laugier, J.; Rey, P.; Subra, R. *J. Am. Chem. Soc.*, **1988**, *110*, 2307-2309.
32. Sheldon, R. A.; Arends, I. W. C. E. *J. Mol. Catal. A: Chem.*, **2006**, *251*, 200-214.
33. Kaizaki, S. *Coord. Chem. Rev.*, **2006**, *250*, 1804-1818.
34. Benelli, C.; Caneschi, A.; Gatteschi, D.; Pardi, L.; Rey, P. *Inorg. Chem.*, **1990**, *29*, 4223-4228.
35. Benelli, C.; Caneschi, A.; Gatteschi, D.; Sessoli, R. *Inorg. Chem.*, **1993**, *32*, 4797-4801.
36. Inoue, K.; Iwamura, H. *J. Am. Chem. Soc.*, **1994**, *116*, 3173-3174.
37. Oshio, H. *Inorg. Chim. Acta*, **2001**, *324*, 188-193.

38. Caneschi, A.; Gatteschi, D.; Laugier, J.; Rey, P.; Sessoli, R.; Zanchini, C. *J. Am. Chem. Soc.*, **1988**, *110*, 2795-2799.
39. Caneschi, A.; Gatteschi, D.; Renard, J. P.; Rey, P.; Sessoli, R. *Inorg. Chem.*, **1989**, *28*, 3314-3319.
40. Wang, H.; Liu, Z.; Liu, C.; Zhang, D.; Lu, Z.; Geng, H.; Shuai, Z.; Zhu, D. *Inorg. Chem.*, **2004**, *43*, 4091-4098.
41. Luneau, D.; Rey, P.; Laugier, J.; Fries, P.; Caneschi, A.; Gatteschi, D.; Sessoli, R. *J. Am. Chem. Soc.*, **1991**, *113*, 1245-1251.
42. Oshio, H.; Watanabe, T.; Ohto, A.; Ito, T.; Ikoma, T.; Tero-Kubota, S. *Inorg. Chem.*, **1997**, *36*, 3014-3021.
43. Oshio, H.; Watanabe, T.; Ohto, A.; Ito, T.; Nagashima, U. *Angew. Chem. Int. Ed. Engl.*, **1994**, *33*, 670-671.
44. Luneau, D.; Risoan, G.; Rey, P.; Grand, A.; Caneschi, A.; Gatteschi, D.; Laugier, J. *Inorg. Chem.*, **1993**, *32*, 5616-5622.
45. Kaizaki, S.; Shirotani, D.; Tsukahara, Y.; Nakata, H. *Eur. J. Inorg. Chem.*, **2005**, *2005*, 3503-3505.
46. Lescop, C.; Luneau, D.; Rey, P.; Bussiere, G.; Reber, C. *Inorg. Chem.*, **2002**, *41*, 5566-5574.
47. Tsukuda, T.; Suzuki, T.; Kaizaki, S. *J. Chem. Soc., Dalton Trans.*, **2002**, 1721-1726.
48. Ishida, T.; Adachi, K.; Kawata, S.; Suzuki, T.; Fuyuhiko, A.; Kaizaki, S. *Polyhedron*, **2007**, *26*, 2013-2020.
49. Stubbe, J.; van der Donk, W. A. *Chem. Rev.*, **1998**, *98*, 705-762.
50. Chaudhuri, P.; Wieghardt, K. in *Prog. Inorg. Chem.*, Vol. 50, ed. K. D. Karlin, John Wiley & Sons Inc, New York, 2001, pp. 151-216.
51. Nordlund, P.; Eklund, H. *J. Mol. Biol.*, **1993**, *232*, 123-164.
52. Whittaker, J. W. *Chem. Rev.*, **2003**, *103*, 2347-2364.
53. Ito, N.; Phillips, S. E. V.; Stevens, C.; Ogel, Z. B.; McPherson, M. J.; Keen, J.N.; Yadav, D. S.; Knowles, P. F. *Nature*, **1991**, *350*, 87-90.

54. Whittaker, M. M.; Ekberg, C. A.; Peterson, J.; Sendova, M. S.; Day, E. P.; Whittaker, J. W. *J. Mol. Catal. B: Enzym.*, **2000**, *8*, 3-15.
55. Landrum, G. A.; Ekberg, C. A.; Whittaker, J. W. *Biophys. J.*, **1995**, *69*, 674-689.
56. Klibanov, A. M.; Alberti, B. N.; Marletta, M. A. *Biochem. Biophys. Res. Commun.*, **1982**, *108*, 804-808.
57. Que, L. Jr.; Tolman, W. B. *Nature*, **2008**, *455*, 333-340.
58. Adam, B.; Bill, E.; Bothe, E.; Goerdts, B.; Haselhorst, G.; Hildenbrand, K.; Sokolowski, A.; Steenken, S.; Weyhermüller, T.; Wieghardt, K. *Chem. Eur. J.*, **1997**, *3*, 308-319.
59. Sokolowski, A.; Müller, J.; Weyhermüller, T.; Schnepf, R.; Hildebrandt, P.; Hildenbrand, K.; Bothe, E.; Wieghardt, K. *J. Am. Chem. Soc.*, **1997**, *119*, 8889-8900.
60. Thomas, F. *Eur. J. Inorg. Chem.*, **2007**, 2379-2404.
61. Auerbach, U.; Eckert, U.; Wieghardt, K.; Nuber, B.; Weiss, J. *Inorg. Chem.*, **1990**, *29*, 938-944.
62. Itoh, S.; Takayama, S.; Arakawa, R.; Furuta, A.; Komatsu, M.; Ishida, A.; Takamuku, S.; Fukuzumi, S. *Inorg. Chem.*, **1997**, *36*, 1407-1416.
63. Zurita, D.; Gautier-Luneau, I.; Ménage, S.; Pierre, J. L.; Saint-Aman, E. *J. Biol. Inorg. Chem.*, **1997**, *2*, 46-55.
64. Chaudhuri, P.; Hess, M.; Flörke, U.; Wieghardt, K. *Angew. Chem. Int. Ed.*, **1998**, *37*, 2217-2220.
65. Hicks, R. G. in *Stable Radicals: Fundamentals and Applied Aspects of Odd-Electron Compounds*, ed. R. G. Hicks, John Wiley & Sons, Ltd., West Sussex, UK, 2010, pp. 317-380.
66. Oakley, R. T. in *Prog. Inorg. Chem.*, Vol. 36, ed. S. J. Lippard, John Wiley & Sons Inc. New York, 1988, pp. 299-391.
67. Rawson, J. M.; Luzon, J.; Palacio, F. *Coord. Chem. Rev.*, **2005**, *249*, 2631-2641.
68. Banister, A. J.; Gorrell, I. B.; Clegg, W.; Jorgensen, K. A. *J. Chem. Soc., Dalton Trans.*, **1989**, 2229-2233.
69. Banister, A. J.; May, I.; Rawson, J. M.; Smith, J. N. B. *J. Organomet. Chem.*, **1998**, *550*, 241-253.

70. Boere, R. T.; Moock, K. H.; Klassen, V.; Weaver, J.; Lentz, D.; Michaelsschulz, H. *Can. J. Chem.* **1995**, *73*, 1444-1453.
71. Banister, A. J.; Gorrell, I. B.; Clegg, W.; Jorgensen, K. A. *J. Chem. Soc., Dalton Trans.*, **1991**, 1105-1109.
72. Banister, A. J.; Gorrell, I. B.; Lawrence, S. E.; Lehmann, C. W.; May, I.; Tate, G.; Blake, A. J.; Rawson, J. M. *J. Chem. Soc., Chem. Commun.*, **1994**, 1779-1780.
73. Britten, J.; Hearn, N. G. R.; Preuss, K. E.; Richardson, J. F.; Bin-Salamon, S. *Inorg. Chem.*, **2007**, *46*, 3934-3945.
74. Hearn, N. G. R.; Preuss, K. E.; Richardson, J. F.; Bin-Salamon, S. *J. Am. Chem. Soc.*, **2004**, *126*, 9942-9943.
75. Jennings, M.; Preuss, K. E.; Wu, J. *Chem. Commun.*, **2006**, 341-343.
76. Hearn, N. G. R.; Hesp, K. D.; Jennings, M.; Korcok, J. L.; Preuss, K. E.; Smithson, C. S. *Polyhedron*, **2007**, *26*, 2047-2053.
77. Fujita, W.; Awaga, K. *J. Am. Chem. Soc.*, **2001**, *123*, 3601-3602.
78. Danen, W. C.; Neugebauer, F. A. *Angew. Chem. Int. Ed. Engl.*, **1975**, *14*, 783-789.
79. Ballester, M.; Castañer, J.; Olivella, S. *Tetrahedron Lett.*, **1974**, *15*, 615-616.
80. Sellmann, D.; Müller, J.; Hofmann, P. *Angew. Chem. Int. Ed. Engl.*, **1982**, *21*, 691-692.
81. Buttner, T.; Geier, J.; Frison, G.; Harmer, J.; Calle, C.; Schweiger, A.; Schonberg, H.; Grützmacher, H. *Science*, **2005**, *307*, 235-238.
82. Maire, P.; Königsmann, M.; Sreekanth, A.; Harmer, J.; Schweiger, A.; Grützmacher, H. *J. Am. Chem. Soc.*, **2006**, *128*, 6578-6580.
83. Adhikari, D.; Mossin, S.; Basuli, F.; Huffman, J. C.; Szilagy, R. K.; Meyer, K.; Mindiola, D. J. *J. Am. Chem. Soc.*, **2008**, *130*, 3676-3682.
84. Miyazato, Y.; Wada, T.; Muckerman, J.; Fujita, T. E.; Tanaka, K. *Angew. Chem. Int. Ed.*, **2007**, *46*, 5728-5730.
85. Donati, N.; Königsmann, M.; Stein, D.; Udino, L.; Grützmacher, H. *C. R. Chim.*, **2007**, *10*, 721-730.

86. Königsman, M.; Donati, N.; Stein, D.; Schönberg, H.; Harmer, J.; Sreekanth, A.; Grützmacher, H. *Angew. Chem. Int. Ed.*, **2007**, *46*, 3567-3570.
87. Hicks, R. G. in *Stable Radicals: Fundamentals and Applied Aspects of Odd-Electron Compounds*, ed. R. G. Hicks, John Wiley & Sons, Ltd., West Sussex, UK, 2010, pp. 245-279.
88. Kuhn, R.; Trischmann, H. *Angew. Chem. Int. Ed. Engl.*, **1963**, *2*, 155.
89. Neugebauer, F. A.; Fischer, H. *Angew. Chem. Int. Ed. Engl.*, **1980**, *19*, 724-725.
90. Neugebauer, F. A.; Fischer, H.; Siegel, R. *Chem. Ber.*, **1988**, *121*, 815-822.
91. Ozaki, Y.; Kawano, M.; Fujita, M. *Chem. Commun.*, **2009**, 4245-4247.
92. Nakabayashi, K.; Ozaki, Y.; Kawano, M.; Fujita, M. *Angew. Chem. Int. Ed.*, **2008**, *47*, 2046-2048.
93. Gilroy, J. B.; Koivisto, B. D.; McDonald, R.; Ferguson, M. J.; Hicks, R. G. *J. Mater. Chem.*, **2006**, *16*, 2618-2624.
94. Hicks, R. G.; Lemaire, M. T.; Thompson, L. K.; Barclay, T. M. *J. Am. Chem. Soc.*, **2000**, *122*, 8077-8078.
95. Train, C.; Norel, L.; Baumgarten, M. *Coord. Chem. Rev.*, **2009**, *253*, 2342-2351.
96. Brook, D. J. R.; Fornell, S.; Noll, B.; Yee, G. T.; Koch, T. H. *J. Chem. Soc., Dalton Trans.*, **2000**, 2019-2022.
97. Lemaire, M. T.; Barclay, T. M.; Thompson, L. K.; Hicks, R. G. *Inorg. Chim. Acta*, **2006**, *359*, 2616-2621.
98. Barclay, T. M.; Hicks, R. G.; Lemaire, M. T.; Thompson, L. K. *Inorg. Chem.*, **2003**, *42*, 2261-2267.
99. Barclay, T. M.; Hicks, R. G.; Lemaire, M. T.; Thompson, L. K. *Inorg. Chem.*, **2001**, *40*, 5581-5584.
100. Pointillart, F.; Train, C.; Herson, P.; Marrot, J.; Verdaguer, M. *New J. Chem.*, **2007**, *31*, 1001-1006.
101. Brook, D. J. R.; Lynch, V.; Conklin, B.; Fox, M. A. *J. Am. Chem. Soc.*, **1997**, *119*, 5155-5162.
102. Norel, L.; Chamoreau, L.-M.; Journaux, Y.; Oms, O.; Chastanet, G.; Train, C. *Chem. Commun.*, **2009**, 2381-2383.

103. Yang, A.; Kasahara, T.; Chen, E. K. Y.; Hamer, G. K.; Georges, M. K. *Eur. J. Org. Chem.*, **2008**, 2008, 4571-4574.
104. Szkurhan, A. R.; Lukkarila, J.; Georges, M. K. in *Stable Radicals: Fundamentals and Applied Aspects of Odd-Electron Compounds*, ed. R. G. Hicks, John Wiley & Sons, Ltd., West Sussex, UK, 2010, pp. 407-431.
105. Chen, E. K. Y.; Teertstra, S. J.; Chan-Seng, D.; Otieno, P. O.; Hicks, R. G.; Georges, M. K. *Macromolecules*, **2007**, 40, 8609-8616.
106. Brook, D. J. R.; Pare, E. C.; Brieger, A.; Badik, M.; Schinke, M. *Org. Biomol. Chem.*, **2005**, 3, 4258-4261.
107. Gilroy, J. B.; McKinnon, S. D. J.; Kennepohl, P.; Zsombor, M. S.; Ferguson, M. J.; Thompson, L. K.; Hicks, R. G. *J. Org. Chem.*, **2007**, 72, 8062-8069.
108. Hicks, R. G.; Gilroy, J. B.; McKinnon, S. D. J.; Koivisto, B. D. *Org. Lett.*, **2007**, 9, 4837-4840.
109. Boyer, J. L.; Rochford, J.; Tsai, M.-K.; Muckerman, J. T.; Fujita, E. *Coord. Chem. Rev.*, **2010**, 254, 309-330.
110. Zanello, P.; Corsini, M. *Coord. Chem. Rev.*, **2006**, 250, 2000-2022.
111. McKinnon, S. D. J.; Patrick, B. O.; Lever, A. B. P.; Hicks, R. G. *Chem. Commun.*, **2010**, 46, 773-775.
112. Blundell, S. J. *Contemp. Phys.*, **2007**, 48, 275-290.
113. Gatteschi, D.; Sessoli, R. *J. Magn. Magn. Mater.*, **2004**, 272-276, 1030-1036.
114. Murray, K. S. *Aust. J. Chem.*, **2009**, 62, 1081-1101.
115. Brooker, S.; Kitchen, J. A. *Dalton Trans.*, **2009**, 7331-7340.
116. Chaudhuri, P.; Kataev, V.; Büchner, B.; Klauss, H.-H.; Kersting, B.; Meyer, F. *Coord. Chem. Rev.*, **2009**, 253, 2261-2285.
117. Gatteschi, D.; Bogani, L.; Cornia, A.; Mannini, M.; Sorace, L.; Sessoli, R. *Solid State Sci.*, **2008**, 10, 1701-1709.
118. Pali, A.; Tsukerblat, B.; Clemente-Juan, J. M.; Coronado, E. *Int. Rev. Phys. Chem.*, **2010**, 29, 135 - 230.

119. Shen, B. G.; Sun, J. R.; Hu, F. X.; Zhang, H. W.; Cheng, Z. H. *Adv. Mater.*, **2009**, *21*, 4545-4564.
120. Fujita, I.; Teki, Y.; Takui, T.; Kinoshita, T.; Itoh, K.; Miko, F.; Sawaki, Y.; Iwamura, H.; Izuoka, A.; Sugawara, T. *J. Am. Chem. Soc.*, **1990**, *112*, 4074-4075.
121. Alberola, A.; Pilkington, M. *Curr. Org. Synth.*, **2009**, *6*, 66-78.
122. García-Couceiro, U.; Castillo, O.; Cepeda, J.; Luque, A.; Pérez-Yáñez, S.; Román, P. *Inorg. Chim. Acta*, **2009**, *362*, 4212-4218.
123. Lescouëzec, R.; Toma, L. M.; Vaissermann, J.; Verdaguer, M.; Delgado, F. S.; Ruiz-Pérez, C.; Lloret, F.; Julve, M. *Coord. Chem. Rev.*, **2005**, *249*, 2691-2729.
124. Nastase, S.; Maxim, C.; Tuna, F.; Duhayon, C.; Sutter, J.-P.; Andruh, M. *Polyhedron*, **2009**, *28*, 1688-1693.
125. Patrick, B. O.; Reiff, W. M.; Sánchez, V.; Storr, A.; Thompson, R. C. *Polyhedron*, **2001**, *20*, 1577-1585.
126. Caneschi, A.; Gatteschi, D.; Sessoli, R.; Rey, P. *Acc. Chem. Res.*, **1989**, *22*, 392-398.
127. Shatruk, M.; Avendano, C.; Dunbar, K. R. in *Prog. Inorg. Chem.*, Vol. 56, ed. K. D. Karlin, John Wiley & Sons Inc., New York, 2009, pp. 155-334.
128. Ferlay, S.; Mallah, T.; Ouahes, R.; Veillet, P.; Verdaguer, M. *Nature*, **1995**, *378*, 701-703.
129. Hatlevik, Ø.; Buschmann, W. E.; Zhang, J.; Manson, J. L.; Miller, J. S. *Adv. Mater.*, **1999**, *11*, 914-918.
130. Holmes, S. M.; Girolami, G. S. *J. Am. Chem. Soc.*, **1999**, *121*, 5593-5594.
131. Miller, J. S. *Inorg. Chem.*, **2000**, *39*, 4392-4408.
132. Miller, J. S.; Epstein, A. J. *Coord. Chem. Rev.*, **2000**, *206-207*, 651-660.
133. Miller, J. S.; Epstein, A. J.; Reiff, W. M. *Chem. Rev.*, **1988**, *88*, 201-220.
134. Miller, J. S. *J. Mater. Chem.*, **2010**, *20*, 1846-1857.
135. Bernot, K.; Bogani, L.; Caneschi, A.; Gatteschi, D.; Sessoli, R. *J. Am. Chem. Soc.*, **2006**, *128*, 7947-7956.

136. Bogani, L.; Sangregorio, C.; Sessoli R.; Gatteschi, D. *Angew. Chem. Int. Ed.*, **2005**, *44*, 5817-5821.
137. Caneschi, A.; Gatteschi, D.; Lalioti, N.; Sangregorio, C.; Sessoli, R.; Venturi, G.; Vindigni, A.; Rettori, A.; Pini, M. G.; Novak, M. A. *Angew. Chem. Int. Ed.*, **2001**, *40*, 1760-1763.
138. Ishii, N.; Ishida, T.; Nogami, T. *Inorg. Chem.*, **2006**, *45*, 3837-3839.
139. Ishii, N.; Okamura, Y.; Chiba, S.; Nogami, T.; Ishida, T. *J. Am. Chem. Soc.*, **2008**, *130*, 24-25.
140. Roques, N.; Domingo, N.; MasPOCH, D.; Wurst, K.; Rovira, C.; Tejada, J.; Ruiz-Molina, D.; Veciana, J. *Inorg. Chem.*, **2010**, *49*, 3482-3488.
141. AlDamen, M. A.; Cardona-Serra, S.; Clemente-Juan, J. M.; Coronado, E.; Gaita-Arínfo, A.; Martí-Gastaldo, C.; Luis, F.; Montero, O. *Inorg. Chem.*, **2009**, *48*, 3467-3479.
142. Hoshino, N.; Ako, A. M.; Powell, A. K.; Oshio, H. *Inorg. Chem.*, **2009**, *48*, 3396-3407.
143. Rogez, G.; Donnio, B.; Terazzi, E.; Gallani, J.-L.; Kappler, J.-P.; Bucher, J.-P.; Drillon, M. *Adv. Mater.*, **2009**, *21*, 4323-4333.
144. Sessoli, R.; Powell, A. K. *Coord. Chem. Rev.*, **2009**, *253*, 2328-2341.
145. Gatteschi, D.; Cornia, A.; Mannini, M.; Sessoli, R. *Inorg. Chem.*, **2009**, *48*, 3408-3419.
146. Barclay, T. M.; Hicks, R. G.; Lemaire, M. T.; Thompson, L. K. *Inorg. Chem.*, **2001**, *40*, 6521-6524.
147. Barclay, T. M.; Hicks, R. G.; Lemaire, M. T.; Thompson, L. K.; Xu, Z. *Chem. Commun.*, **2002**, 1688-1689.
148. Rota, J.-B.; Calzado, C.; Train, C.; Robert, V. *J. Chem. Phys.*, **2010**, *132*, 154702.
149. Rota, J.-B.; Norel, L.; Train, C.; Amor, N. B.; Maynau, D.; Robert, V. *J. Am. Chem. Soc.*, **2008**, *130*, 10380-10385.
150. Yakovenko, A. V.; Kolotilov, S. V.; Cador, O.; Golhen, S.; Ouahab, L.; Pavlishchuk, V. V. *Eur. J. Inorg. Chem.*, **2009**, *2009*, 2354-2361.
151. Bhattacharya, D.; Misra, A. *J. Phys. Chem. A*, **2009**, *113*, 5470-5475.



- 152. Polo, V.; Alberola, A.; Andres, J.; Anthony, J.; Pilkington, M. *Phys. Chem. Chem. Phys.*, **2008**, *10*, 857-864.
- 153. Brook, D. J. R.; Yee, G. T. *J. Org. Chem.*, **2006**, *71*, 4889-4895.
- 154. Chahma, M.; Wang, X.; van der Est, A.; Pilkington, M. *J. Org. Chem.*, **2006**, *71*, 2750-2755.
- 155. Hicks, R. G.; Koivisto, B. D.; Lemaire, M. T. *Org. Lett.*, **2004**, *6*, 1887-1890.
- 156. Poddutoori, P. K.; Pilkington, M.; Alberola, A.; Polo, V.; Warren, J. E.; van der Est, A. *Inorg. Chem.*, **2010**, *49*, 3516-3524.
- 157. Lemaire, M. T. in *Department of Chemistry Ph. D. Thesis*, University of Victoria, Victoria, 2002, p. 293.
- 158. Gilroy, J. B. in *Department of Chemistry Ph. D. Thesis*, University of Victoria, Victoria, 2008, p. 282.
- 159. Brook, D. J. R.; Fornell, S.; Stevens, J. E.; Noll, B.; Koch, T. H.; Eisfeld, W. *Inorg. Chem.*, **2000**, *39*, 562-567.
- 160. Lloret, F.; Julve, M.; Cano, J.; Ruiz-García, R.; Pardo, E. *Inorg. Chim. Acta*, **2008**, *361*, 3432-3445.
- 161. Murrie, M. *Chem. Soc. Rev.*, **2010**, *39*, 1986-1995.
- 162. Abe, M.; Adam, W. *J. Chem. Soc., Perkin Trans. 2*, **1998**, 1063-1068.
- 163. Adam, W.; Harrer, H. M.; Kita, F.; Korth, H.-G.; Nau, W. M. *J. Org. Chem.*, **1997**, *62*, 1419-1426.
- 164. Adam, W.; van Barneveld, C. *J. Am. Chem. Soc.*, **1999**, *121*, 10820-10827.
- 165. Adam, W.; van Barneveld, C.; Emmert, O. *J. Chem. Soc., Perkin Trans. 2*, **2000**, *4*, 637-641.
- 166. Adam, W.; van Barneveld, C.; Gerke, J. S.; Klarner, F. G. *J. Chem. Soc., Perkin Trans. 2*, **1999**, 2723-2728.
- 167. Veciana, J.; Ratera, I. in *Stable Radicals: Fundamentals and Applied Aspects of Odd-Electron Compounds*, ed. R. G. Hicks, John Wiley & Sons, Ltd., West Sussex, UK, 2010, pp. 33-80.
- 168. Adam, W.; Emmert, O.; Heidenfelder, T. *J. Org. Chem.*, **1999**, *64*, 3417-3421.

169. Adam, W.; Kita, F.; Harrer, H. M.; Nau, W. M.; Zipf, R. *J. Org. Chem.*, **1996**, *61*, 7056-7065.
170. Bleaney, B.; Bowers, K. D. *Proc. R. Soc. London, Ser. A*, **1952**, *214*, 451-465.
171. Kahn, O. *Molecular magnetism*, VCH, New York ; London, 1993.
172. Bowles, S. E.; Dooley, B. M.; Benedict, J. B.; Kaminsky, W.; Frank, N. L. *Polyhedron*, **2009**, *28*, 1704-1709.
173. Zakrassov, A.; Shteiman, V.; Sheynin, Y.; Tumanskii, B.; Botoshansky, M.; Kapon, M.; Keren, A.; Kaftory, M.; Vos, T. E.; Miller, J. S. *J. Mater. Chem.*, **2004**, *14*, 1827-1837.
174. Caneschi, A.; Chiesi, P.; David, L.; Ferraro, F.; Gatteschi, D.; Sessoli, R. *Inorg. Chem.*, **1993**, *32*, 1445-1453.
175. Tukada, H.; Mutai, K. *Tetrahedron Lett.*, **1992**, *33*, 6665-6668.
176. Trindle, C.; Datta, S. N. *Int. J. Quantum Chem.*, **1996**, *57*, 781-799.
177. Trindle, C.; Datta, S. N.; Mallik, B. *J. Am. Chem. Soc.*, **1997**, *119*, 12947-12951.
178. Tukada, H. *J. Am. Chem. Soc.*, **1991**, *113*, 8991-8992.
179. Ma, Z.; Cao, Y.; Li, Q.; Guedes da Silva, M. F. C.; Fraústo da Silva J. J. R.; Pombeiro, A. J. L. *J. Inorg. Biochem.*, **2010**, *104*, 704-711.
180. Shalumova, T.; Tanski, J. M. *Acta Crystallogr., Sect. E: Struct. Rep. Online*, **2009**, *65*, M1325-U1786.
181. You, W.; Huang, W.; Fan, T.; Yao, C. *J. Coord. Chem.*, **2009**, *62*, 2125 - 2137.
182. Zhao, Q. L.; Li, G. P. *Acta Crystallogr., Sect. E: Struct. Rep. Online*, **2009**, *65*, M693-U871.
183. Carlin, R. L. *Magnetochemistry*, Springer, Berlin, 1986.
184. Caneschi, A.; Gatteschi, D.; Laugier, J.; Rey, P.; Sessoli, R. *Inorg. Chem.*, **1988**, *27*, 1553-1557.
185. Luneau, D.; Romero, F. M.; Ziessel, R. *Inorg. Chem.*, **1998**, *37*, 5078-5087.
186. Oshio, H.; Yamamoto, M.; Ito, T.; Kawauchi, H.; Koga, N.; Ikoma, T.; Tero-Kubota, S. *Inorg. Chem.*, **2001**, *40*, 5518-5525.

187. Kou, H.-Z.; Hishiya, S.; Sato, O. *Inorg. Chim. Acta*, **2008**, *361*, 2396-2406.
188. Wu, C.-D.; Lu, C.-Z.; Lu, S.-F.; Zhuang, H.-H.; Huang, J.-S. *Inorg. Chem. Commun.*, **2002**, *5*, 171-174.
189. Brook, D. J. R.; Abeyta, V. *J. Chem. Soc., Dalton Trans.*, **2002**, 4219-4223.
190. Burdukov, A. B.; Gladkikh, E. A.; Nefedova, E. V.; Tronin, A. V.; Roshchupkina, G. I.; Pervukhina, N. V.; Shvedenkov, Y. G.; Reznikov, V. A. *Cryst. Growth Des.*, **2004**, *4*, 595-598.
191. Fedin, M.; Ovcharenko, V.; Sagdeev, R.; Reijerse, E.; Lubitz, W.; Bagryanskaya, E. *Angew. Chem. Int. Ed.*, **2008**, *47*, 6897-6899.
192. Lu, W.; Zhang, Y.; Dai, J.; Zhu, Q.-Y.; Bian, G.-Q.; Zhang, D.-Q. *Eur. J. Inorg. Chem.*, **2006**, *2006*, 1629-1634.
193. Gordon, A. J.; Ford, R. A. *The chemist's companion : a handbook of practical data, techniques, and references*, Wiley, New York, 1972.
194. Froidevaux, P.; Harrowfield, J. M.; Sobolev, A. N. *Inorg. Chem.*, **2000**, *39*, 4678-4687.
195. Morita, Y.; Nishida, S. in *Stable Radicals: Fundamentals and Applied Aspects of Odd-Electron Compounds*, ed. R. G. Hicks, John Wiley & Sons, Ltd., West Sussex, UK, 2010, pp. 81-145.
196. Chi, X.; Itkis, M. E.; Patrick, B. O.; Barclay, T. M.; Reed, R. W.; Oakley, R. T.; Cordes, A. W.; Haddon, R. C. *J. Am. Chem. Soc.*, **1999**, *121*, 10395-10402.
197. Chi, X.; Itkis, M. E.; Tham, F. S.; Oakley, R. T.; Cordes, A. W.; Haddon, R. C. *Int. J. Quantum Chem.*, **2003**, *95*, 853-865.
198. Haddon, R. C.; Chichester, S. V.; Stein, S. M.; Marshall, J. H.; Muijsce, A. M. *J. Org. Chem.*, **1987**, *52*, 711-712.
199. Haddon, R. C.; Wudl, F.; Kaplan, M. L.; Marshall, J. H.; Cais, R. E.; Bramwell, F. B. *J. Am. Chem. Soc.*, **1978**, *100*, 7629-7633.
200. Pal, S. K.; Itkis, M. E.; Reed, R. W.; Oakley, R. T.; Cordes, A. W.; Tham, F. S.; Siegrist, T.; Haddon, R. C. *J. Am. Chem. Soc.*, **2004**, *126*, 1478-1484.
201. Pal, S. K.; Itkis, M. E.; Tham, F. S.; Reed, R. W.; Oakley, R. T.; Haddon, R. C. *Science*, **2005**, *309*, 281-284.

202. Beer, L.; Brusso, J. L.; Cordes, A. W.; Haddon, R. C.; Itkis, M. E.; Kirschbaum, K.; MacGregor, D. S.; Oakley, R. T.; Pinkerton, A. A.; Reed, R. W. *J. Am. Chem. Soc.*, **2002**, *124*, 9498-9509.
203. Davis, W. M.; Hicks, R. G.; Oakley, R. T.; Zhao, B. Y.; Taylor, N. J. *Can. J. Chem.*, **1993**, *71*, 180-185.
204. Oakley, R. T. *Can. J. Chem.*, **1993**, *71*, 1775-1784.
205. Leitch, A. A.; Yu, X.; Winter, S. M.; Secco, R. A.; Dube, P. A.; Oakley, R. T. *J. Am. Chem. Soc.*, **2009**, *131*, 7112-7125.
206. Robertson, C. M.; Leitch, A. A.; Cvrkalj, K.; Reed, R. W.; Myles, D. J. T.; Dube, P. A.; Oakley, R. T. *J. Am. Chem. Soc.*, **2008**, *130*, 8414-8425.
207. Nishide, H.; Koshika, K.; Oyaizu, K. *Pure Appl. Chem.*, **2009**, *81*, 1961-1970.
208. Suga, T.; Konishi H.; Nishide, H. *Chem. Commun.*, **2007**, 1730-1732.
209. Yoshihara, S.; Isozumi, H.; Kasai, M.; Yonehara, H.; Ando, Y.; Oyaizu, K.; Nishide, H. *J. Phys. Chem. B*, **2010**, *114*, 8335-8340.
210. Nishide, H.; Oyaizu, K. *Science*, **2008**, *319*, 737-738.
211. Suga, T.; Nishide, H. in *Stable Radicals: Fundamentals and Applied Aspects of Odd-Electron Compounds*, ed. R. G. Hicks, John Wiley & Sons, Ltd., West Sussex, UK, 2010, pp. 507-519.
212. Nishide, H.; Suga, T. *Electrochem. Soc. Interface*, **2005**, *14*, 32-36.
213. Kato, F.; Hayashi, N.; Murakami, T.; Okumura, C.; Oyaizu, K.; Nishide, H. *Chem. Lett.*, **2010**, *39*, 464-465.
214. Sheldon, R. A.; Arends, I. W. C. E. *Adv. Synth. Catal.*, **2004**, *346*, 1051-1071.
215. Bruckner, C. in *Stable Radicals: Fundamentals and Applied Aspects of Odd-Electron Compounds*, ed. R. G. Hicks, John Wiley & Sons, Ltd., West Sussex, UK, 2010, pp. 433-460.
216. Anelli, P. L.; Biffi, C.; Montanari, F.; Quici, S. *J. Org. Chem.*, **1987**, *52*, 2559-2562.
217. Bolm, C.; Fey, T. *Chem. Commun.*, **1999**, 1795-1796.
218. Dijkman, A. E.; Arends, I.; Sheldon, R. A. *Synlett*, **2001**, 102-104.

219. Dijkman, A. E.; Arends, I.; Sheldon, R. A. *Chem. Commun.*, **2000**, 271-272.
220. Kharisov, B. I.; Mendez-Rojas, M. A.; Garnovskii, A. D.; Ivakhnenko, E. P.; Ortiz-Mendez, U. *J. Coord. Chem.*, **2002**, 55, 745-770.
221. Hendrickson, D. N.; Pierpont, C. G. in *Topics in Current Chemistry, Vol. 234: Spin Crossover in Transition Metal Compounds II*, Springer, Berlin, 2004, pp. 63-95.
222. Dei, A.; Gatteschi, D.; Sangregorio, C.; Sorace, L. *Acc. Chem. Res.*, **2004**, 37, 827-835.
223. Chaudhuri, P.; Verani, C. N.; Bill, E.; Bothe, E.; Weyhermüller, T.; Wieghardt, K. *J. Am. Chem. Soc.*, **2001**, 123, 2213-2223.
224. Chirik, P. J.; Wieghardt, K. *Science*, **2010**, 327, 794-795.
225. Enthaler, S.; Junge, K.; Beller, M. *Angew. Chem. Int. Ed.*, **2008**, 47, 3317-3321.
226. Small, B. L.; Brookhart, M.; Bennett, A. M. A. *J. Am. Chem. Soc.*, **1998**, 120, 4049-4050.
227. Britovsek, G. J. P.; Bruce, M.; Gibson, V. C.; Kimberley, B. S.; Maddox, P. J.; Mastroianni, S.; McTavish, S. J.; Redshaw, C.; Solan, G. A.; Strömberg, S.; White, A. J. P.; Williams, D. J. *J. Am. Chem. Soc.*, **1999**, 121, 8728-8740.
228. Small, B. L.; Brookhart, M. *J. Am. Chem. Soc.*, **1998**, 120, 7143-7144.
229. Bart, S. C.; Lobkovsky, E.; Chirik, P. J. *J. Am. Chem. Soc.*, **2004**, 126, 13794-13807.
230. Bart, S. C.; Chłopek, K.; Bill, E.; Bouwkamp, M. W.; Lobkovsky, E.; Neese, F.; Wieghardt, K.; Chirik, P. J. *J. Am. Chem. Soc.*, **2006**, 128, 13901-13912.
231. Bart, S. C.; Lobkovsky, E.; Bill, E.; Wieghardt, K.; Chirik, P. J. *Inorg. Chem.*, **2007**, 46, 7055-7063.
232. Bowman, A. C.; Milsman, C.; Atienza, C. C. H.; Lobkovsky, E.; Wieghardt, K.; Chirik, P. J. *J. Am. Chem. Soc.*, **2010**, 132, 1676-1684.
233. Jazdzewski, B. A.; Tolman, W. B. *Coord. Chem. Rev.*, **2000**, 200-202, 633-685.
234. Thomas, F. in *Stable Radicals: Fundamentals and Applied Aspects of Odd-Electron Compounds*, ed. R. G. Hicks, John Wiley & Sons, Ltd., West Sussex, UK, 2010, pp. 281-316.

235. Wang, Y. D.; Stack, T. D. P. *J. Am. Chem. Soc.*, **1996**, *118*, 13097-13098.
236. Wang, Y. D.; DuBois, J. L.; Hedman, B.; Hodgson, K. O.; Stack, T. D. P. *Science*, **1998**, *279*, 537-540.
237. Sokolowski, A.; Bothe, E.; Bill, E.; Weyhermuller, T.; Wieghardt, K. *Chem. Commun.*, **1996**, 1671-1672.
238. Betzemeier, B.; Cavazzini, M.; Quici, S.; Knochel, P. *Tetrahedron Lett.*, **2000**, *41*, 4343-4346.
239. Cecchetto, A.; Fontana, F.; Minisci, F.; Recupero, F. *Tetrahedron Lett.*, **2001**, *42*, 6651-6653.
240. Dijksman, A. E.; Arends, I.; Sheldon, R. A. *Chem. Commun.*, **1999**, 1591-1592.
241. Dijksman, A. E.; Marino-González, A.; Mairata i Payeras, A.; Arends, I. W. C. E.; Sheldon, R. A. *J. Am. Chem. Soc.*, **2001**, *123*, 6826-6833.
242. Semmelhack, M. F.; Schmid, C. R.; Cortes, D. A.; Chou, C. S. *J. Am. Chem. Soc.*, **1984**, *106*, 3374-3376.
243. Gamez, P.; Arends, I. W. C. E.; Sheldon, R. A.; Reedijk, J. *Adv. Synth. Catal.*, **2004**, *346*, 805-811.
244. Donati, N.; Stein, D.; Büttner, T.; Schönberg, H.; Harmer, J.; Anadaram, S.; Grützmacher, H. *Eur. J. Inorg. Chem.*, **2008**, *2008*, 4691-4703.
245. Chemistruck, V.; Chambers, D.; Brook, D. J. R. *J. Org. Chem.*, **2009**, *74*, 1850-1857.
246. Jaworski, J. S.; Krawczyk, I. *Monatsh. Chem.*, **1992**, *123*, 43-50.
247. Mihara, N.; Y. Teki, Y. *Inorg. Chim. Acta*, **2008**, *361*, 3891-3894.
248. Chahma, M.; Macnamara, K.; van der Est, A.; Alberola, A.; Polo, V.; Pilkington, M. *New J. Chem.*, **2007**, *31*, 1973-1978.
249. Fico, R. M.; Hay, M. F.; Reese, S.; Hammond, S.; Lambert, E.; Fox, M. A. *J. Org. Chem.*, **1999**, *64*, 9386-9392.
250. Bard, A. J.; Faulkner, L. R. *Electrochemical methods: fundamentals and applications*, Wiley, New York, 1980.
251. Heineman, W. R.; Kissinger, P. T. *Laboratory techniques in electroanalytical chemistry*, Marcel Dekker, Inc., New York, 1996.

- 252. Wang, J. *Analytical electrochemistry*, Wiley-VCH, Hoboken, N.J., 2006.
- 253. Geiger, W. E. *Organometallics*, **2007**, 26, 5738-5765.
- 254. Darensbourg, M. Y.; Muetterties, E. L. *J. Am. Chem. Soc.*, **1978**, 100, 7425-7428.
- 255. Fischer, E. O.; Elschenbroich, C. *Chem. Ber. Recl.*, **1970**, 103, 162-172.
- 256. Albright, T. A.; Geiger, W. E.; Moraczewski, J.; Tulyathan, B. *J. Am. Chem. Soc.*, **1981**, 103, 4787-4794.
- 257. Geiger, W. E.; Rieger, P. H.; Corbato, C.; Edwin, J.; Fonseca, E.; Lane, G. A.; Mevs, J. M. *J. Am. Chem. Soc.*, **1993**, 115, 2314-2323.
- 258. Moraczewski J.; Geiger, W. E. *J. Am. Chem. Soc.*, **1979**, 101, 3407-3408.
- 259. Moraczewski, J.; Geiger, W. E. *J. Am. Chem. Soc.*, **1981**, 103, 4779-4787.
- 260. Rieke, R. D.; Arney, J. S.; Rich, W. E.; Willeford, B. R.; Poliner, B. S. *J. Am. Chem. Soc.*, **1975**, 97, 5951-5953.
- 261. Edwin, J.; Geiger, W. E. *J. Am. Chem. Soc.*, **1990**, 112, 7104-7112.
- 262. Geiger, W. E.; Salzer, A.; Edwin, J.; Von Philipsborn, W.; Piantini, U.; Rheingold, A. L. *J. Am. Chem. Soc.*, **1990**, 112, 7113-7121.
- 263. Takao, T.; Moriya M.; Suzuki, H. *Organometallics*, **2007**, 26, 1349-1360.
- 264. Huttner, G.; Lange, S. *Acta Crystallogr., Sect. B: Struct. Sci*, **1972**, 28, 2049-2060.
- 265. Allgeier, A. M.; Mirkin, C. A. *Angew. Chem. Int. Ed.*, **1998**, 37, 894-908.
- 266. Sassano, C. A.; Mirkin, C. A. *J. Am. Chem. Soc.*, **1995**, 117, 11379-11380.
- 267. Singewald, E. T.; Mirkin, C. A.; Stern, C. L. *Angew. Chem. Int. Ed. Engl.*, **1995**, 34, 1624-1627.
- 268. Allgeier, A. M.; Slone, C. S.; Mirkin, C. A.; Liable-Sands, L. M.; Yap, G. P. A.; Rheingold, A. L. *J. Am. Chem. Soc.*, **1997**, 119, 550-559.
- 269. Gregson, C. K. A.; Gibson, V. C.; Long, N. J.; Marshall, E. L.; Oxford, P. J.; White, A. J. P. *J. Am. Chem. Soc.*, **2006**, 128, 7410-7411.
- 270. Sembiring, S. B.; Colbran S. B.; Craig, D. C. *Inorg. Chem.*, **1995**, 34, 761-762.

- 271. Connelly, N. G.; Geiger, W. E. *Chem. Rev.*, **1996**, 96, 877-910.
- 272. Heirtzler, F. R.; Neuburger, M.; Zehnder, M.; Constable, E. C. *Liebigs Ann. Recl.*, **1997**, 1997, 297-301.
- 273. Kauffmann, T.; König, J.; Woltermann, A. *Chem. Ber.*, **1976**, 109, 3864-3868.
- 274. Yamamoto, Y.; Suzuki T.; Kaizaki, S. *J. Chem. Soc., Dalton Trans.*, **2001**, 1566-1572.
- 275. Britovsek, G. J. P.; Gibson, V. C.; Kimberley, B. S.; Maddox, P. J.; McTavish, S. J.; Solan, G. A.; White, A. J. P.; Williams, D. J. *Chem. Commun.*, **1998**, 849-850.
- 276. Sylvester, K. T.; Chirik, P. J. *J. Am. Chem. Soc.*, **2009**, 131, 8772-8774.
- 277. Kahn, O. *Molecular magnetism*, VCH, New York ; London, 1993. p. 213.
- 278. Kahn, O. *Molecular magnetism*, VCH, New York ; London, 1993. p. 211.



# Appendix A: $^1\text{H}$ NMR Spectrum of tetrazane precursor of 3.9

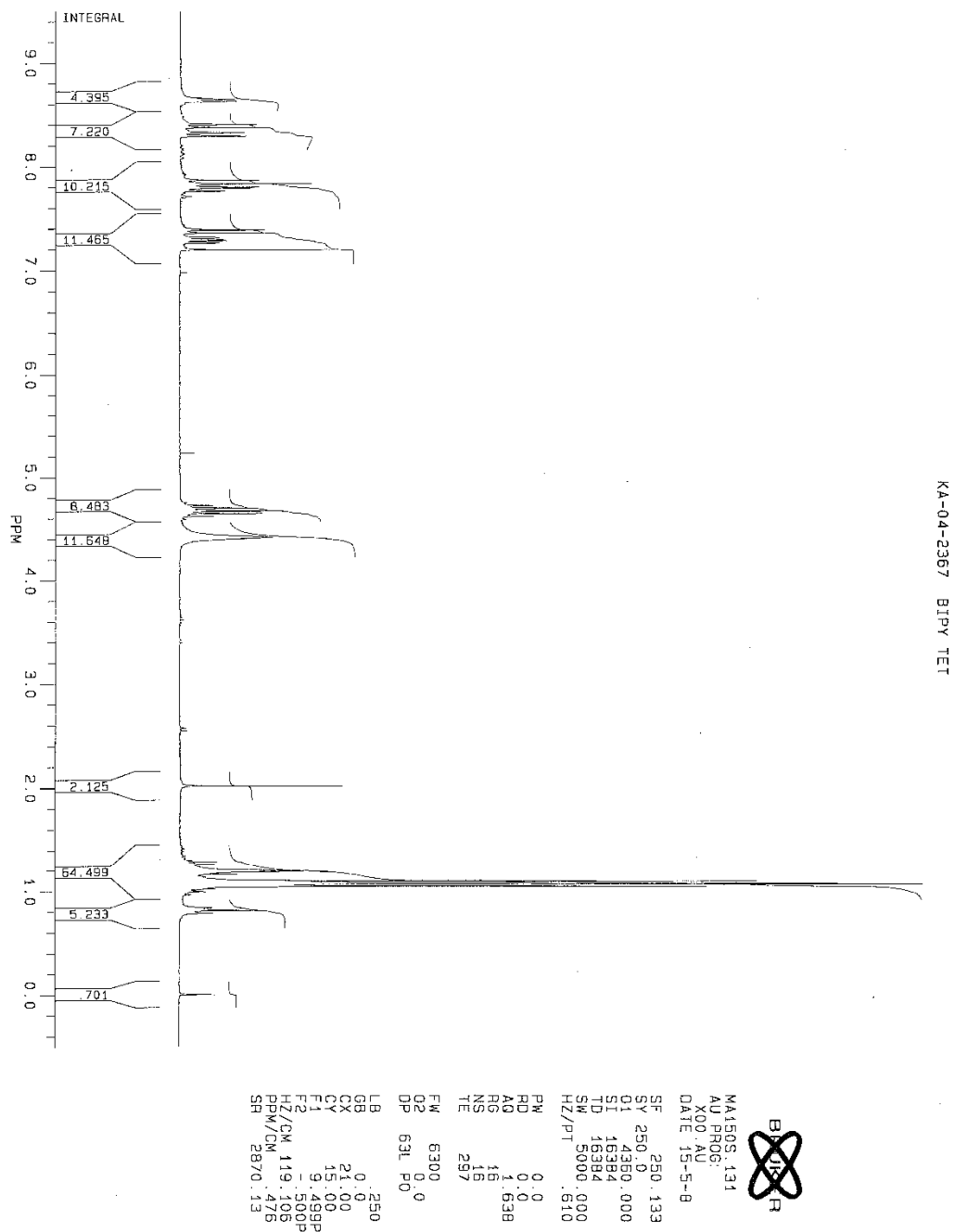


Figure A-1: Raw  $^1\text{H}$  NMR Spectrum of tetrazane precursor of 3.9.

## Appendix B: Crystallographic parameters

**Table B-1:** Crystallographic parameters.

Parameters	2.14	2.15	2.16
Formula	C <sub>23</sub> H <sub>20</sub> N <sub>5</sub> O <sub>5</sub> F <sub>12</sub> Ni	C <sub>23</sub> H <sub>20</sub> N <sub>5</sub> O <sub>5</sub> CoF <sub>12</sub>	C <sub>23</sub> H <sub>20</sub> N <sub>5</sub> O <sub>5</sub> F <sub>12</sub> Mn <sub>4</sub> /5[C <sub>6</sub> H <sub>4</sub> O <sub>2</sub> ].1/5[C <sub>5</sub> H <sub>12</sub> ]
FW	733.15	733.37	783.43
Dimensions (mm)	0.02 × 0.04 × 0.12	0.10 × 0.25 × 0.40	0.20 × 0.50 × 0.50
a (Å)	10.0255(17)	10.0154(13)	9.3133(6)
b (Å)	10.7689(18)	10.8054(14)	12.6040(8)
c (Å)	15.015(2)	15.012(2)	14.9205(11)
α (°)	108.466(7)	108.201(5)	101.182(3)
β (°)	94.629(7)	95.264(5)	96.267(3)
γ (°)	105.188(7)	104.628(5)	104.943(3)
Volume (Å <sup>3</sup> )	1460.0(4)	1467.3(3)	1636.5(2)
ρ <sub>calc</sub> (g/cm <sup>3</sup> )	1.668	1.660	1.590
System	Triclinic	Triclinic	Triclinic
Space Group	<i>P</i> -1 (#2)	<i>P</i> -1 (#2)	<i>P</i> -1 (#2)
Z	2	2	2
μ (cm <sup>-1</sup> )	7.84	7.04	5.19
T (K)	173.15	173.15	173.15
2θ <sub>max</sub> (°)	46.4	50.1	56.0
Unique	4077	9770	7599
Reflections	(R <sub>int</sub> = 0.075)	(R <sub>int</sub> = 0.041)	(R <sub>int</sub> = 0.028)
R1 <sup>a</sup>	0.114	0.088	0.064
wR2 <sup>b</sup>	0.075	0.204	0.107

$$^a R1 = \sum ||F_0| - |F_c|| / \sum |F_0|; \quad ^b wR2 = [\sum (w(F_0^2 - F_c^2)^2) / \sum w(F_0^2)^2]^{1/2}$$

**Table B-1, continued:** Crystallographic parameters.

Parameters	<b>2.18</b>	<b>2.19</b>	<b>2.20</b>	<b>2.21</b>
Formula	C <sub>21</sub> H <sub>31</sub> N <sub>9</sub> O <sub>2</sub>	C <sub>21</sub> H <sub>31</sub> Cl <sub>2</sub> N <sub>9</sub> O <sub>2</sub> Zn	C <sub>21</sub> H <sub>31</sub> Cl <sub>2</sub> MnN <sub>9</sub> O <sub>2</sub>	C <sub>21</sub> H <sub>31</sub> Cl <sub>2</sub> FeN <sub>9</sub> O <sub>2</sub>
FW	441.53	577.82	567.39	568.30
Dimensions (mm)	0.50 × 0.40 × 0.25	0.25 × 0.19 × 0.03	0.63 × 0.53 × 0.27	0.42 × 0.17 × 0.07
a (Å)	11.3905(4)	22.8237 (15)	23.1108 (14)	22.8409 (18)
b (Å)	29.861(1)	9.2189 (6)	9.3629 (6)	9.2524 (7)
c (Å)	7.4195(3)	13.2976 (9)	13.1463 (8)	13.3575 (11)
α (°)	90.0	90.0	90.0	90.0
β (°)	90.0	107.5370 (10)	107.5997 (7)	107.9432 (12)
γ (°)	90.0	90.0	90.0	90.0
Volume (Å <sup>3</sup> )	2523.6(2)	2667.9 (3)	2711.5 (3)	2685.6 (4)
ρ <sub>calc</sub> (g/cm <sup>3</sup> )	1.162	1.439	1.390	1.406
System	Orthorhombic	Monoclinic	Monoclinic	Monoclinic
Space Group	<i>Pnma</i> (#62)	<i>C2/c</i> (#15)	<i>C2/c</i> (#15)	<i>C2/c</i> (#15)
Z	4	4	4	4
μ	0.80 cm <sup>-1</sup>	1.157 mm <sup>-1</sup>	0.720 mm <sup>-1</sup>	0.797 mm <sup>-1</sup>
T (K)	296.15	193.15	193.15	193.15
2θ <sub>max</sub> (°)	55.8	52.74	52.78	52.70
Unique	3074	2739	2776	2756
Reflections	(R <sub>int</sub> = 0.027)	(R <sub>int</sub> = 0.0473)	(R <sub>int</sub> = 0.0138)	(R <sub>int</sub> = 0.0334)
R1 <sup>a</sup>	0.088	0.0377	0.0262	0.0326
wR2 <sup>b</sup>	0.189	0.0981	0.0714	0.0846

$$^a R1 = \Sigma ||F_o| - |F_c|| / \Sigma |F_o|; \quad ^b wR2 = [\Sigma (w(F_o^2 - F_c^2)^2) / \Sigma w(F_o^2)^2]^{1/2}$$

**Table B-1, continued:** Crystallographic parameters.

Parameters	<b>2.22</b>	<b>2.23</b>	<b>2.28b</b>
Formula	C <sub>21</sub> H <sub>31</sub> N <sub>9</sub> O <sub>2</sub> CoCl <sub>2</sub>	C <sub>21</sub> H <sub>31</sub> N <sub>9</sub> O <sub>2</sub> NiCl <sub>2</sub>	C <sub>18</sub> H <sub>25</sub> N <sub>9</sub> O <sub>2</sub> CrCl <sub>3</sub>
FW	571.38	571.16	557.82
Dimensions (mm)	0.05 × 0.20 × 0.25	0.05 × 0.15 × 0.45	0.07 × 0.25 × 0.25
a (Å)	22.711(2)	9.1374(5)	10.3177(13)
b (Å)	9.2571(9)	12.4841(9)	13.607(2)
c (Å)	13.5063(12)	13.2342(9)	17.176(2)
α (°)	90.0	108.147(1)	90.0
β (°)	108.394(4)	108.704(2)	98.217(3)
γ (°)	90.0	91.302(2)	90.0
Volume (Å <sup>3</sup> )	2694.5(4)	1346.1(2)	2386.7(5)
ρ <sub>calc</sub> (g/cm <sup>3</sup> )	1.409	1.409	1.552
System	Monoclinic	Triclinic	Monoclinic
Space Group	C2/c (#15)	P-1 (#2)	P2 <sub>1</sub> /c (#14)
Z	4	2	4
μ	8.71 cm <sup>-1</sup>	9.55 cm <sup>-1</sup>	8.51 cm <sup>-1</sup>
T (K)	298.15	173.15	173.15
2θ <sub>max</sub> (°)	55.9	50.0	50.4
Unique	3230	4525	4235
Reflections	(R <sub>int</sub> = 0.030)	(R <sub>int</sub> = 0.038)	(R <sub>int</sub> = 0.051)
R1 <sup>a</sup>	0.051	0.043	0.093
wR2 <sup>b</sup>	0.088	0.083	0.137

$$^a R1 = \Sigma ||F_o| - |F_c|| / \Sigma |F_o|; \quad ^b wR2 = [\Sigma (w(F_o^2 - F_c^2)^2) / \Sigma w(F_o^2)^2]^{1/2}$$

**Table B-1, continued:** Crystallographic parameters.

Parameters	<b>2.29</b>	<b>3.9</b>	<b>3.10</b>
Formula	C <sub>15</sub> H <sub>17</sub> N <sub>9</sub> O <sub>2</sub> Cu <sub>2</sub> Cl <sub>3</sub> •2H <sub>2</sub> O	C <sub>18</sub> H <sub>21</sub> N <sub>6</sub> O	C <sub>18</sub> H <sub>21</sub> N <sub>6</sub> OZnCl <sub>2</sub>
FW	624.84	337.41	473.68
Dimensions (mm)	0.04 × 0.08 × 0.25	0.22 × 0.40 × 0.55	0.20 × 0.31 × 0.36
a (Å)	22.541(2)	9.8826(3)	16.7156(16)
b (Å)	18.535(2)	9.4674(3)	9.2917(9)
c (Å)	13.379(2)	9.9540(3)	13.3007(13)
α (°)	90.0	90.0	90.0
β (°)	121.664(6)	109.959(1)	98.978(4)
γ (°)	90.0	90.0	90.0
Volume (Å <sup>3</sup> )	4757(1)	875.38(5)	2040.5(3)
ρ <sub>calc</sub> (g/cm <sup>3</sup> )	1.745	1.280	1.542
System	Monoclinic	Monoclinic	Monoclinic
Space Group	C2/c (#15)	P2 <sub>1</sub> (#4)	P2 <sub>1</sub> /c (#14)
Z	8	2	4
μ	21.67 cm <sup>-1</sup>	0.85 cm <sup>-1</sup>	14.87 cm <sup>-1</sup>
T (K)	173.15	103.15	173.15
2θ <sub>max</sub> (°)	50.4	56.1	56.0
Unique	4211	4223	4914
Reflections	(R <sub>int</sub> = 0.055)	(R <sub>int</sub> = 0.026)	(R <sub>int</sub> = 0.023)
R1 <sup>a</sup>	0.066	0.035	0.034
wR2 <sup>b</sup>	0.100	0.083	0.064

$$^a R1 = \Sigma ||F_o| - |F_c|| / \Sigma |F_o|; \quad ^b wR2 = [\Sigma (w(F_o^2 - F_c^2)^2) / \Sigma w(F_o^2)^2]^{1/2}$$

## Appendix C: Complete list of bond lengths and angles

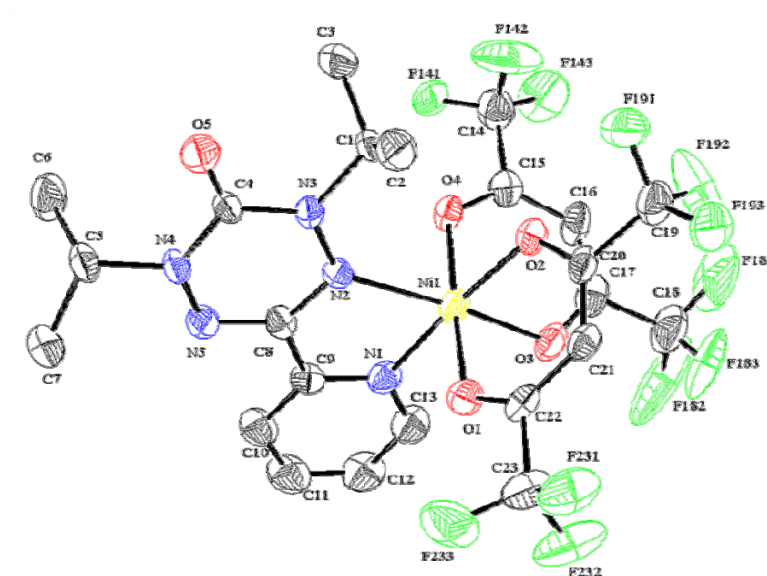


**Figure C-1:** ORTEP view of **2.14**. Thermal ellipsoids displayed at 50% probability level. Hydrogen atoms removed for clarity.

**Table C-1:** Bond lengths (Å) and angles (°) for **2.14**.

C(1)	N(3)	1.484(5)
C(1)	C(2)	1.508(5)
C(1)	C(3)	1.517(5)
C(1)	H(1)	1.0000
C(2)	H(2A)	0.9800
C(2)	H(2B)	0.9800
C(2)	H(2C)	0.9800
C(3)	H(3A)	0.9800
C(3)	H(3B)	0.9800
C(3)	H(3C)	0.9800
C(4)	O(5)	1.219(5)
C(4)	N(3)	1.378(5)
C(4)	N(4)	1.382(5)
C(5)	N(4)	1.479(5)
C(5)	C(7)	1.494(5)
C(5)	C(6)	1.522(5)
C(5)	H(5)	1.0000
C(6)	H(6A)	0.9800

C(6)	H(6B)	0.9800
C(6)	H(6C)	0.9800
C(7)	H(7A)	0.9800
C(7)	H(7B)	0.9800
C(7)	H(7C)	0.9800
C(8)	N(5)	1.316(5)
C(8)	N(2)	1.341(5)
C(8)	C(9)	1.480(5)
C(9)	N(1)	1.345(5)
C(9)	C(10)	1.373(5)
C(10)	C(11)	1.374(6)
C(10)	H(10)	0.9500
C(11)	C(12)	1.364(6)
C(11)	H(11)	0.9500
C(12)	C(13)	1.372(6)
C(12)	H(12)	0.9500
C(13)	N(1)	1.334(5)
C(13)	H(13)	0.9500
C(14)	F(143)	1.307(6)
C(14)	F(145)	1.308(8)
C(14)	F(141)	1.308(6)
C(14)	F(144)	1.311(9)
C(14)	F(146)	1.312(8)
C(14)	F(142)	1.316(6)
C(14)	C(15)	1.523(6)
C(15)	O(4)	1.248(5)
C(15)	C(16)	1.390(5)
C(16)	C(17)	1.376(6)
C(16)	H(16)	0.9500
C(17)	O(3)	1.257(5)
C(17)	C(18)	1.527(7)
C(18)	F(183)	1.284(7)
C(18)	F(184)	1.286(8)
C(18)	F(186)	1.291(8)
C(18)	F(182)	1.291(7)
C(18)	F(185)	1.298(8)
C(18)	F(181)	1.302(6)
C(19)	F(192)	1.296(6)
C(19)	F(193)	1.325(5)
C(19)	F(191)	1.330(5)
C(19)	C(20)	1.526(6)
C(20)	O(2)	1.251(4)
C(20)	C(21)	1.377(5)
C(21)	C(22)	1.386(6)
C(21)	H(21)	0.9500
C(22)	O(1)	1.249(5)

C(22)	C(23)	1.528(6)
C(23)	F(233)	1.314(6)
C(23)	F(231)	1.318(5)
C(23)	F(232)	1.343(5)
N(1)	Ni(1)	2.040(3)
N(2)	N(3)	1.370(4)
N(2)	Ni(1)	2.120(3)
N(4)	N(5)	1.367(4)
O(1)	Ni(1)	2.049(3)
O(2)	Ni(1)	2.032(3)
O(3)	Ni(1)	2.028(3)
O(4)	Ni(1)	2.032(3)

N(3)	C(1)	C(2)	110.1(3)
N(3)	C(1)	C(3)	111.1(3)
C(2)	C(1)	C(3)	113.8(3)
N(3)	C(1)	H(1)	107.2
C(2)	C(1)	H(1)	107.2
C(3)	C(1)	H(1)	107.2
C(1)	C(2)	H(2A)	109.5
C(1)	C(2)	H(2B)	109.5
H(2A)	C(2)	H(2B)	109.5
C(1)	C(2)	H(2C)	109.5
H(2A)	C(2)	H(2C)	109.5
H(2B)	C(2)	H(2C)	109.5
C(1)	C(3)	H(3A)	109.5
C(1)	C(3)	H(3B)	109.5
H(3A)	C(3)	H(3B)	109.5
C(1)	C(3)	H(3C)	109.5
H(3A)	C(3)	H(3C)	109.5
H(3B)	C(3)	H(3C)	109.5
O(5)	C(4)	N(3)	123.2(4)
O(5)	C(4)	N(4)	122.1(4)
N(3)	C(4)	N(4)	114.7(4)
N(4)	C(5)	C(7)	110.6(3)
N(4)	C(5)	C(6)	109.6(3)
C(7)	C(5)	C(6)	112.6(4)
N(4)	C(5)	H(5)	108.0
C(7)	C(5)	H(5)	108.0
C(6)	C(5)	H(5)	108.0
C(5)	C(6)	H(6A)	109.5
C(5)	C(6)	H(6B)	109.5
H(6A)	C(6)	H(6B)	109.5
C(5)	C(6)	H(6C)	109.5
H(6A)	C(6)	H(6C)	109.5
H(6B)	C(6)	H(6C)	109.5



C(5)	C(7)	H(7A)	109.5
C(5)	C(7)	H(7B)	109.5
H(7A)	C(7)	H(7B)	109.5
C(5)	C(7)	H(7C)	109.5
H(7A)	C(7)	H(7C)	109.5
H(7B)	C(7)	H(7C)	109.5
N(5)	C(8)	N(2)	127.5(4)
N(5)	C(8)	C(9)	116.0(4)
N(2)	C(8)	C(9)	116.5(4)
N(1)	C(9)	C(10)	122.6(4)
N(1)	C(9)	C(8)	114.6(4)
C(10)	C(9)	C(8)	122.7(5)
C(9)	C(10)	C(11)	118.3(5)
C(9)	C(10)	H(10)	120.9
C(11)	C(10)	H(10)	120.9
C(12)	C(11)	C(10)	119.3(5)
C(12)	C(11)	H(11)	120.3
C(10)	C(11)	H(11)	120.3
C(11)	C(12)	C(13)	119.7(4)
C(11)	C(12)	H(12)	120.1
C(13)	C(12)	H(12)	120.1
N(1)	C(13)	C(12)	121.7(5)
N(1)	C(13)	H(13)	119.1
C(12)	C(13)	H(13)	119.1
F(143)	C(14)	F(145)	27(3)
F(143)	C(14)	F(141)	106.1(9)
F(145)	C(14)	F(141)	116(2)
F(143)	C(14)	F(144)	87(4)
F(145)	C(14)	F(144)	105(3)
F(141)	C(14)	F(144)	26(5)
F(143)	C(14)	F(146)	130(2)
F(145)	C(14)	F(146)	107(3)
F(141)	C(14)	F(146)	73(3)
F(144)	C(14)	F(146)	99(3)
F(143)	C(14)	F(142)	107.2(8)
F(145)	C(14)	F(142)	80(3)
F(141)	C(14)	F(142)	108.2(8)
F(144)	C(14)	F(142)	131(4)
F(146)	C(14)	F(142)	37(3)
F(143)	C(14)	C(15)	112.1(7)
F(145)	C(14)	C(15)	122(2)
F(141)	C(14)	C(15)	113.6(6)
F(144)	C(14)	C(15)	107(2)
F(146)	C(14)	C(15)	113.3(16)
F(142)	C(14)	C(15)	109.4(6)
O(4)	C(15)	C(16)	129.0(4)

O(4)	C(15)	C(14)	113.3(4)
C(16)	C(15)	C(14)	117.7(5)
C(17)	C(16)	C(15)	122.3(5)
C(17)	C(16)	H(16)	118.9
C(15)	C(16)	H(16)	118.9
O(3)	C(17)	C(16)	128.9(4)
O(3)	C(17)	C(18)	112.4(5)
C(16)	C(17)	C(18)	118.6(5)
F(183)	C(18)	F(184)	137.3(12)
F(183)	C(18)	F(186)	58(3)
F(184)	C(18)	F(186)	105(3)
F(183)	C(18)	F(182)	105.2(7)
F(184)	C(18)	F(182)	60.8(16)
F(186)	C(18)	F(182)	49(4)
F(183)	C(18)	F(185)	55(3)
F(184)	C(18)	F(185)	108(3)
F(186)	C(18)	F(185)	109(2)
F(182)	C(18)	F(185)	140.3(12)
F(183)	C(18)	F(181)	106.6(8)
F(184)	C(18)	F(181)	52.1(14)
F(186)	C(18)	F(181)	130.5(13)
F(182)	C(18)	F(181)	108.1(10)
F(185)	C(18)	F(181)	57(3)
F(183)	C(18)	C(17)	112.5(6)
F(184)	C(18)	C(17)	110.0(13)
F(186)	C(18)	C(17)	116.0(13)
F(182)	C(18)	C(17)	110.7(6)
F(185)	C(18)	C(17)	108.8(12)
F(181)	C(18)	C(17)	113.2(6)
F(192)	C(19)	F(193)	107.2(4)
F(192)	C(19)	F(191)	107.3(5)
F(193)	C(19)	F(191)	104.4(4)
F(192)	C(19)	C(20)	112.3(4)
F(193)	C(19)	C(20)	114.6(5)
F(191)	C(19)	C(20)	110.5(4)
O(2)	C(20)	C(21)	129.2(4)
O(2)	C(20)	C(19)	112.6(4)
C(21)	C(20)	C(19)	118.2(4)
C(20)	C(21)	C(22)	122.1(4)
C(20)	C(21)	H(21)	119.0
C(22)	C(21)	H(21)	119.0
O(1)	C(22)	C(21)	128.2(4)
O(1)	C(22)	C(23)	114.2(5)
C(21)	C(22)	C(23)	117.6(4)
F(233)	C(23)	F(231)	107.7(5)
F(233)	C(23)	F(232)	106.9(5)

F(231)	C(23)	F(232)	105.9(4)
F(233)	C(23)	C(22)	112.4(4)
F(231)	C(23)	C(22)	114.8(4)
F(232)	C(23)	C(22)	108.8(4)
C(13)	N(1)	C(9)	118.3(4)
C(13)	N(1)	Ni(1)	125.0(3)
C(9)	N(1)	Ni(1)	116.5(3)
C(8)	N(2)	N(3)	115.3(3)
C(8)	N(2)	Ni(1)	112.8(3)
N(3)	N(2)	Ni(1)	131.9(3)
N(2)	N(3)	C(4)	122.9(4)
N(2)	N(3)	C(1)	116.9(3)
C(4)	N(3)	C(1)	120.3(3)
N(5)	N(4)	C(4)	124.5(4)
N(5)	N(4)	C(5)	116.8(4)
C(4)	N(4)	C(5)	118.4(4)
C(8)	N(5)	N(4)	114.5(4)
C(22)	O(1)	Ni(1)	124.8(3)
C(20)	O(2)	Ni(1)	123.7(3)
C(17)	O(3)	Ni(1)	121.9(3)
C(15)	O(4)	Ni(1)	121.8(3)
O(3)	Ni(1)	O(4)	89.64(12)
O(3)	Ni(1)	O(2)	85.16(12)
O(4)	Ni(1)	O(2)	85.58(11)
O(3)	Ni(1)	N(1)	92.42(14)
O(4)	Ni(1)	N(1)	97.33(12)
O(2)	Ni(1)	N(1)	176.21(12)
O(3)	Ni(1)	O(1)	91.61(12)
O(4)	Ni(1)	O(1)	173.68(12)
O(2)	Ni(1)	O(1)	88.35(11)
N(1)	Ni(1)	O(1)	88.81(13)
O(3)	Ni(1)	N(2)	170.56(13)
O(4)	Ni(1)	N(2)	88.15(12)
O(2)	Ni(1)	N(2)	103.80(12)
N(1)	Ni(1)	N(2)	78.78(14)
O(1)	Ni(1)	N(2)	91.59(12)

---

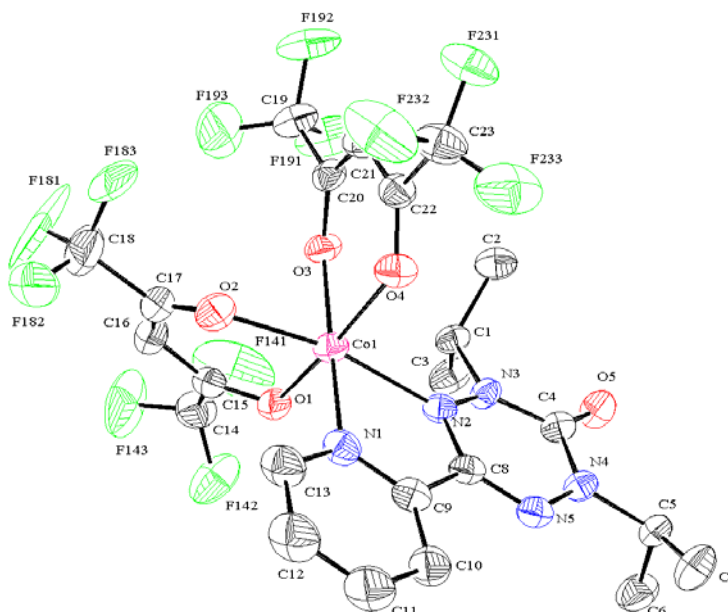


**Figure C-2:** ORTEP view of **2.15**. Thermal ellipsoids displayed at 50% probability level. Hydrogen atoms removed for clarity.

**Table C-2:** Bond lengths (Å) and angles (°) for **2.15**.

---

C(1)	N(3)	1.495(5)
C(1)	C(3)	1.510(6)
C(1)	C(2)	1.521(6)
C(1)	H(1)	1.0000
C(2)	H(2A)	0.9800
C(2)	H(2B)	0.9800
C(2)	H(2C)	0.9800
C(3)	H(3A)	0.9800
C(3)	H(3B)	0.9800
C(3)	H(3C)	0.9800
C(4)	O(5)	1.209(5)
C(4)	N(3)	1.387(5)
C(4)	N(4)	1.389(5)
C(5)	N(4)	1.481(5)
C(5)	C(7)	1.505(6)
C(5)	C(6)	1.528(6)
C(5)	H(5)	1.0000
C(6)	H(6A)	0.9800
C(6)	H(6B)	0.9800
C(6)	H(6C)	0.9800
C(7)	H(7A)	0.9800
C(7)	H(7B)	0.9800
C(7)	H(7C)	0.9800
C(8)	N(5)	1.308(5)
C(8)	N(2)	1.339(5)

C(8)	C(9)	1.485(6)
C(9)	N(1)	1.334(5)
C(9)	C(10)	1.386(6)
C(10)	C(11)	1.388(7)
C(10)	H(10)	0.9500
C(11)	C(12)	1.367(7)
C(11)	H(11)	0.9500
C(12)	C(13)	1.389(7)
C(12)	H(12)	0.9500
C(13)	N(1)	1.343(5)
C(13)	H(13)	0.9500
C(14)	F(141)	1.288(6)
C(14)	F(145)	1.294(7)
C(14)	F(142)	1.296(6)
C(14)	F(146)	1.296(7)
C(14)	F(144)	1.301(7)
C(14)	F(143)	1.305(6)
C(14)	C(15)	1.536(6)
C(15)	O(1)	1.254(5)
C(15)	C(16)	1.397(6)
C(16)	C(17)	1.391(7)
C(16)	H(16)	0.9500
C(17)	O(2)	1.246(6)
C(17)	C(18)	1.550(7)
C(18)	F(182)	1.278(7)
C(18)	F(186)	1.283(8)
C(18)	F(184)	1.285(8)
C(18)	F(183)	1.295(7)
C(18)	F(181)	1.303(7)
C(18)	F(185)	1.309(8)
C(19)	F(193)	1.305(6)
C(19)	F(192)	1.319(5)
C(19)	F(191)	1.331(6)
C(19)	C(20)	1.531(6)
C(20)	O(3)	1.268(5)
C(20)	C(21)	1.369(6)
C(21)	C(22)	1.392(6)
C(21)	H(21)	0.9500
C(22)	O(4)	1.255(5)
C(22)	C(23)	1.545(6)
C(23)	F(233)	1.305(6)
C(23)	F(231)	1.323(5)
C(23)	F(232)	1.333(6)
N(1)	Co(1)	2.092(3)
N(2)	N(3)	1.365(4)
N(2)	Co(1)	2.163(3)

N(4)	N(5)	1.347(5)	
O(1)	Co(1)	2.055(3)	
O(2)	Co(1)	2.061(3)	
O(3)	Co(1)	2.066(3)	
O(4)	Co(1)	2.070(3)	
N(3)	C(1)	C(3)	111.4(3)
N(3)	C(1)	C(2)	110.1(3)
C(3)	C(1)	C(2)	113.6(4)
N(3)	C(1)	H(1)	107.1
C(3)	C(1)	H(1)	107.1
C(2)	C(1)	H(1)	107.1
C(1)	C(2)	H(2A)	109.5
C(1)	C(2)	H(2B)	109.5
H(2A)	C(2)	H(2B)	109.5
C(1)	C(2)	H(2C)	109.5
H(2A)	C(2)	H(2C)	109.5
H(2B)	C(2)	H(2C)	109.5
C(1)	C(3)	H(3A)	109.5
C(1)	C(3)	H(3B)	109.5
H(3A)	C(3)	H(3B)	109.5
C(1)	C(3)	H(3C)	109.5
H(3A)	C(3)	H(3C)	109.5
H(3B)	C(3)	H(3C)	109.5
O(5)	C(4)	N(3)	123.5(4)
O(5)	C(4)	N(4)	122.7(4)
N(3)	C(4)	N(4)	113.8(3)
N(4)	C(5)	C(7)	110.6(3)
N(4)	C(5)	C(6)	109.6(3)
C(7)	C(5)	C(6)	112.4(4)
N(4)	C(5)	H(5)	108.0
C(7)	C(5)	H(5)	108.0
C(6)	C(5)	H(5)	108.0
C(5)	C(6)	H(6A)	109.5
C(5)	C(6)	H(6B)	109.5
H(6A)	C(6)	H(6B)	109.5
C(5)	C(6)	H(6C)	109.5
H(6A)	C(6)	H(6C)	109.5
H(6B)	C(6)	H(6C)	109.5
C(5)	C(7)	H(7A)	109.5
C(5)	C(7)	H(7B)	109.5
H(7A)	C(7)	H(7B)	109.5
C(5)	C(7)	H(7C)	109.5
H(7A)	C(7)	H(7C)	109.5
H(7B)	C(7)	H(7C)	109.5
N(5)	C(8)	N(2)	127.4(4)

N(5)	C(8)	C(9)	116.8(3)
N(2)	C(8)	C(9)	115.8(3)
N(1)	C(9)	C(10)	122.9(4)
N(1)	C(9)	C(8)	115.1(3)
C(10)	C(9)	C(8)	121.9(4)
C(9)	C(10)	C(11)	117.5(4)
C(9)	C(10)	H(10)	121.3
C(11)	C(10)	H(10)	121.3
C(12)	C(11)	C(10)	120.2(4)
C(12)	C(11)	H(11)	119.9
C(10)	C(11)	H(11)	119.9
C(11)	C(12)	C(13)	119.0(4)
C(11)	C(12)	H(12)	120.5
C(13)	C(12)	H(12)	120.5
N(1)	C(13)	C(12)	121.5(5)
N(1)	C(13)	H(13)	119.2
C(12)	C(13)	H(13)	119.2
F(141)	C(14)	F(142)	107.7(6)
F(145)	C(14)	F(146)	107.5(7)
F(145)	C(14)	F(144)	107.2(7)
F(146)	C(14)	F(144)	106.9(7)
F(141)	C(14)	F(143)	107.4(6)
F(142)	C(14)	F(143)	106.8(6)
F(141)	C(14)	C(15)	109.0(7)
F(145)	C(14)	C(15)	117.3(10)
F(142)	C(14)	C(15)	114.6(8)
F(146)	C(14)	C(15)	108.1(11)
F(144)	C(14)	C(15)	109.5(7)
F(143)	C(14)	C(15)	111.0(8)
O(1)	C(15)	C(16)	128.3(4)
O(1)	C(15)	C(14)	114.0(4)
C(16)	C(15)	C(14)	117.7(4)
C(17)	C(16)	C(15)	121.7(4)
C(17)	C(16)	H(16)	119.1
C(15)	C(16)	H(16)	119.1
O(2)	C(17)	C(16)	129.2(4)
O(2)	C(17)	C(18)	113.1(4)
C(16)	C(17)	C(18)	117.7(4)
F(186)	C(18)	F(184)	108.2(7)
F(182)	C(18)	F(183)	108.0(6)
F(182)	C(18)	F(181)	107.4(6)
F(183)	C(18)	F(181)	105.4(6)
F(186)	C(18)	F(185)	106.3(7)
F(184)	C(18)	F(185)	105.8(7)
F(182)	C(18)	C(17)	115.5(6)
F(186)	C(18)	C(17)	113.7(11)

F(184)	C(18)	C(17)	116.3(10)
F(183)	C(18)	C(17)	109.1(6)
F(181)	C(18)	C(17)	111.0(6)
F(185)	C(18)	C(17)	105.7(7)
F(193)	C(19)	F(192)	108.0(4)
F(193)	C(19)	F(191)	108.4(5)
F(192)	C(19)	F(191)	105.2(4)
F(193)	C(19)	C(20)	111.1(4)
F(192)	C(19)	C(20)	113.8(4)
F(191)	C(19)	C(20)	110.2(4)
O(3)	C(20)	C(21)	128.0(4)
O(3)	C(20)	C(19)	112.6(4)
C(21)	C(20)	C(19)	119.3(4)
C(20)	C(21)	C(22)	122.5(4)
C(20)	C(21)	H(21)	118.8
C(22)	C(21)	H(21)	118.8
O(4)	C(22)	C(21)	127.9(4)
O(4)	C(22)	C(23)	114.3(4)
C(21)	C(22)	C(23)	117.6(4)
F(233)	C(23)	F(231)	107.8(4)
F(233)	C(23)	F(232)	109.2(5)
F(231)	C(23)	F(232)	106.2(4)
F(233)	C(23)	C(22)	111.5(4)
F(231)	C(23)	C(22)	113.1(4)
F(232)	C(23)	C(22)	108.9(4)
C(9)	N(1)	C(13)	118.9(4)
C(9)	N(1)	Co(1)	117.5(3)
C(13)	N(1)	Co(1)	123.4(3)
C(8)	N(2)	N(3)	114.9(3)
C(8)	N(2)	Co(1)	114.4(3)
N(3)	N(2)	Co(1)	130.6(2)
N(2)	N(3)	C(4)	123.2(3)
N(2)	N(3)	C(1)	116.8(3)
C(4)	N(3)	C(1)	120.0(3)
N(5)	N(4)	C(4)	124.5(3)
N(5)	N(4)	C(5)	117.6(3)
C(4)	N(4)	C(5)	117.6(3)
C(8)	N(5)	N(4)	115.3(3)
C(15)	O(1)	Co(1)	122.7(3)
C(17)	O(2)	Co(1)	122.3(3)
C(20)	O(3)	Co(1)	125.0(3)
C(22)	O(4)	Co(1)	126.0(3)
O(1)	Co(1)	O(2)	87.70(12)
O(1)	Co(1)	O(3)	84.92(11)
O(2)	Co(1)	O(3)	85.22(12)
O(1)	Co(1)	O(4)	170.97(11)



O(2)	Co(1)	O(4)	93.86(12)
O(3)	Co(1)	O(4)	86.35(11)
O(1)	Co(1)	N(1)	99.99(12)
O(2)	Co(1)	N(1)	93.35(13)
O(3)	Co(1)	N(1)	174.84(12)
O(4)	Co(1)	N(1)	88.80(12)
O(1)	Co(1)	N(2)	87.59(11)
O(2)	Co(1)	N(2)	167.90(12)
O(3)	Co(1)	N(2)	105.45(11)
O(4)	Co(1)	N(2)	92.53(12)
N(1)	Co(1)	N(2)	76.52(12)

---

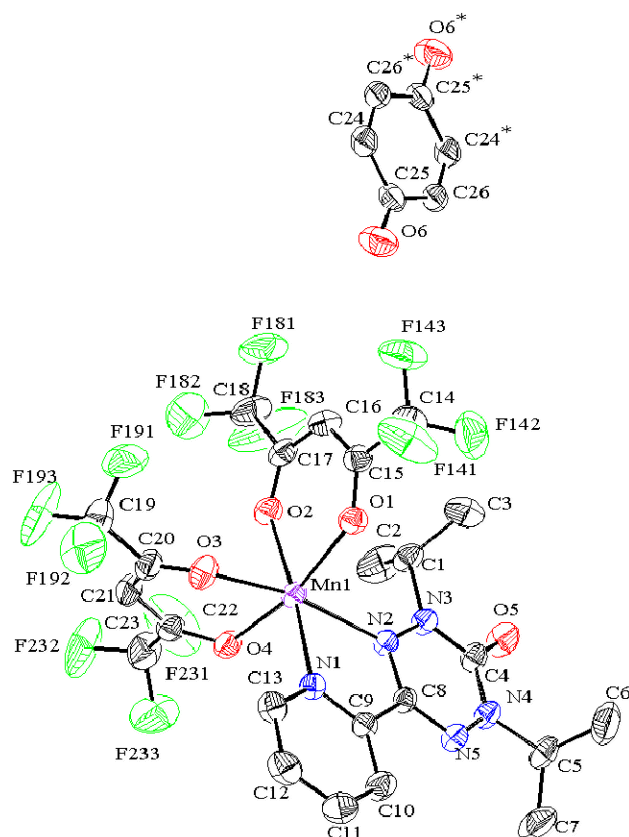


**Figure C-3:** ORTEP view of **2.16**. Thermal ellipsoids displayed at 50% probability level. Hydrogen atoms removed for clarity.

**Table C-3:** Bond lengths (Å) and angles (°) for **2.16**.

---

C(1)	N(3)	1.476(3)
C(1)	C(2)	1.498(4)
C(1)	C(3)	1.506(3)
C(1)	H(1)	1.0000
C(2)	H(2A)	0.9800
C(2)	H(2B)	0.9800
C(2)	H(2C)	0.9800
C(3)	H(3A)	0.9800
C(3)	H(3B)	0.9800
C(3)	H(3C)	0.9800
C(4)	O(5)	1.211(2)
C(4)	N(4)	1.373(3)
C(4)	N(3)	1.380(3)
C(5)	N(4)	1.489(2)
C(5)	C(7)	1.497(3)
C(5)	C(6)	1.512(4)
C(5)	H(5)	1.0000
C(6)	H(6A)	0.9800
C(6)	H(6B)	0.9800
C(6)	H(6C)	0.9800
C(7)	H(7A)	0.9800
C(7)	H(7B)	0.9800
C(7)	H(7C)	0.9800
C(8)	N(5)	1.318(2)
C(8)	N(2)	1.334(2)
C(8)	C(9)	1.487(3)
C(9)	N(1)	1.341(2)
C(9)	C(10)	1.375(3)
C(10)	C(11)	1.384(3)
C(10)	H(10)	0.9500
C(11)	C(12)	1.374(3)
C(11)	H(11)	0.9500
C(12)	C(13)	1.370(3)
C(12)	H(12)	0.9500
C(13)	N(1)	1.341(2)
C(13)	H(13)	0.9500
C(14)	F(141)	1.318(3)
C(14)	F(143)	1.320(3)
C(14)	F(142)	1.326(3)
C(14)	C(15)	1.523(3)
C(15)	O(1)	1.249(2)
C(15)	C(16)	1.390(3)
C(16)	C(17)	1.389(3)

C(16)	H(16)	0.9500
C(17)	O(2)	1.245(2)
C(17)	C(18)	1.526(3)
C(18)	F(183)	1.285(3)
C(18)	F(182)	1.311(4)
C(18)	F(181)	1.317(3)
C(19)	F(194)	1.170(13)
C(19)	F(193)	1.287(6)
C(19)	F(195)	1.297(17)
C(19)	F(191)	1.299(5)
C(19)	F(192)	1.335(6)
C(19)	F(196)	1.401(15)
C(19)	C(20)	1.537(3)
C(20)	O(3)	1.249(3)
C(20)	C(21)	1.379(3)
C(21)	C(22)	1.392(3)
C(21)	H(21)	0.9500
C(22)	O(4)	1.245(2)
C(22)	C(23)	1.528(3)
C(23)	F(235)	1.220(13)
C(23)	F(234)	1.241(9)
C(23)	F(231)	1.280(5)
C(23)	F(232)	1.289(6)
C(23)	F(233)	1.339(5)
C(23)	F(236)	1.363(9)
C(24)	C(26)#1	1.302(5)
C(24)	C(25)	1.480(5)
C(24)	H(24)	0.9500
C(25)	O(6)	1.207(4)
C(25)	C(26)	1.466(5)
C(26)	C(24)#1	1.302(5)
C(26)	H(26)	0.9500
N(1)	Mn(1)	2.2140(16)
N(2)	N(3)	1.366(2)
N(2)	Mn(1)	2.2623(15)
N(4)	N(5)	1.351(2)
O(1)	Mn(1)	2.1395(14)
O(2)	Mn(1)	2.1726(14)
O(3)	Mn(1)	2.1498(14)
O(4)	Mn(1)	2.1411(14)
C(27)	C(28)	1.483(9)
C(27)	H(27A)	0.9800
C(27)	H(27B)	0.9800
C(27)	H(27C)	0.9800
C(28)	C(29)	1.490(13)
C(28)	H(28A)	0.9900

C(28)	H(28B)	0.9900
C(29)	C(30)	1.490(13)
C(29)	H(29A)	0.9900
C(29)	H(29B)	0.9900
C(30)	C(31)	1.42(7)
C(30)	H(30A)	0.9900
C(30)	H(30B)	0.9900
C(31)	H(31A)	0.9800
C(31)	H(31B)	0.9800
C(31)	H(31C)	0.9800

N(3)	C(1)	C(2)	111.5(2)
N(3)	C(1)	C(3)	111.34(19)
C(2)	C(1)	C(3)	114.7(2)
N(3)	C(1)	H(1)	106.2
C(2)	C(1)	H(1)	106.2
C(3)	C(1)	H(1)	106.2
C(1)	C(2)	H(2A)	109.5
C(1)	C(2)	H(2B)	109.5
H(2A)	C(2)	H(2B)	109.5
C(1)	C(2)	H(2C)	109.5
H(2A)	C(2)	H(2C)	109.5
H(2B)	C(2)	H(2C)	109.5
C(1)	C(3)	H(3A)	109.5
C(1)	C(3)	H(3B)	109.5
H(3A)	C(3)	H(3B)	109.5
C(1)	C(3)	H(3C)	109.5
H(3A)	C(3)	H(3C)	109.5
H(3B)	C(3)	H(3C)	109.5
O(5)	C(4)	N(4)	122.96(19)
O(5)	C(4)	N(3)	122.19(19)
N(4)	C(4)	N(3)	114.83(17)
N(4)	C(5)	C(7)	110.91(19)
N(4)	C(5)	C(6)	109.04(19)
C(7)	C(5)	C(6)	112.4(2)
N(4)	C(5)	H(5)	108.1
C(7)	C(5)	H(5)	108.1
C(6)	C(5)	H(5)	108.1
C(5)	C(6)	H(6A)	109.5
C(5)	C(6)	H(6B)	109.5
H(6A)	C(6)	H(6B)	109.5
C(5)	C(6)	H(6C)	109.5
H(6A)	C(6)	H(6C)	109.5
H(6B)	C(6)	H(6C)	109.5
C(5)	C(7)	H(7A)	109.5
C(5)	C(7)	H(7B)	109.5

H(7A)	C(7)	H(7B)	109.5
C(5)	C(7)	H(7C)	109.5
H(7A)	C(7)	H(7C)	109.5
H(7B)	C(7)	H(7C)	109.5
N(5)	C(8)	N(2)	127.08(17)
N(5)	C(8)	C(9)	116.23(16)
N(2)	C(8)	C(9)	116.69(16)
N(1)	C(9)	C(10)	122.75(18)
N(1)	C(9)	C(8)	115.66(16)
C(10)	C(9)	C(8)	121.59(18)
C(9)	C(10)	C(11)	118.5(2)
C(9)	C(10)	H(10)	120.8
C(11)	C(10)	H(10)	120.8
C(12)	C(11)	C(10)	119.4(2)
C(12)	C(11)	H(11)	120.3
C(10)	C(11)	H(11)	120.3
C(13)	C(12)	C(11)	118.5(2)
C(13)	C(12)	H(12)	120.7
C(11)	C(12)	H(12)	120.7
N(1)	C(13)	C(12)	123.1(2)
N(1)	C(13)	H(13)	118.4
C(12)	C(13)	H(13)	118.4
F(141)	C(14)	F(143)	107.0(2)
F(141)	C(14)	F(142)	106.2(2)
F(143)	C(14)	F(142)	106.5(2)
F(141)	C(14)	C(15)	112.11(19)
F(143)	C(14)	C(15)	114.2(2)
F(142)	C(14)	C(15)	110.4(2)
O(1)	C(15)	C(16)	128.4(2)
O(1)	C(15)	C(14)	113.82(18)
C(16)	C(15)	C(14)	117.71(19)
C(17)	C(16)	C(15)	121.82(19)
C(17)	C(16)	H(16)	119.1
C(15)	C(16)	H(16)	119.1
O(2)	C(17)	C(16)	128.29(19)
O(2)	C(17)	C(18)	112.7(2)
C(16)	C(17)	C(18)	118.9(2)
F(183)	C(18)	F(182)	107.2(3)
F(183)	C(18)	F(181)	107.9(3)
F(182)	C(18)	F(181)	105.0(2)
F(183)	C(18)	C(17)	111.3(2)
F(182)	C(18)	C(17)	110.7(2)
F(181)	C(18)	C(17)	114.4(2)
F(194)	C(19)	F(193)	122.8(8)
F(194)	C(19)	F(195)	112.2(15)
F(193)	C(19)	F(191)	112.1(5)

F(193)	C(19)	F(192)	104.9(5)
F(191)	C(19)	F(192)	104.2(5)
F(194)	C(19)	F(196)	109.2(17)
F(195)	C(19)	F(196)	95.4(11)
F(194)	C(19)	C(20)	118.6(8)
F(193)	C(19)	C(20)	114.4(3)
F(195)	C(19)	C(20)	112.8(10)
F(191)	C(19)	C(20)	111.4(3)
F(192)	C(19)	C(20)	109.1(3)
F(196)	C(19)	C(20)	105.7(5)
O(3)	C(20)	C(21)	128.9(2)
O(3)	C(20)	C(19)	112.8(2)
C(21)	C(20)	C(19)	118.3(2)
C(20)	C(21)	C(22)	122.17(19)
C(20)	C(21)	H(21)	118.9
C(22)	C(21)	H(21)	118.9
O(4)	C(22)	C(21)	128.4(2)
O(4)	C(22)	C(23)	114.0(2)
C(21)	C(22)	C(23)	117.6(2)
F(235)	C(23)	F(234)	112.6(10)
F(235)	C(23)	F(231)	128.8(9)
F(231)	C(23)	F(232)	112.1(5)
F(231)	C(23)	F(233)	106.7(5)
F(232)	C(23)	F(233)	102.1(4)
F(235)	C(23)	F(236)	98.2(9)
F(234)	C(23)	F(236)	105.7(9)
F(235)	C(23)	C(22)	114.9(8)
F(234)	C(23)	C(22)	116.4(5)
F(231)	C(23)	C(22)	111.8(3)
F(232)	C(23)	C(22)	114.4(4)
F(233)	C(23)	C(22)	108.9(3)
F(236)	C(23)	C(22)	106.8(4)
C(26)#1	C(24)	C(25)	121.6(3)
C(26)#1	C(24)	H(24)	119.2
C(25)	C(24)	H(24)	119.2
O(6)	C(25)	C(26)	121.8(4)
O(6)	C(25)	C(24)	121.5(4)
C(26)	C(25)	C(24)	116.7(3)
C(24)#1	C(26)	C(25)	121.7(3)
C(24)#1	C(26)	H(26)	119.1
C(25)	C(26)	H(26)	119.1
C(13)	N(1)	C(9)	117.70(17)
C(13)	N(1)	Mn(1)	124.06(13)
C(9)	N(1)	Mn(1)	118.19(12)
C(8)	N(2)	N(3)	115.08(15)
C(8)	N(2)	Mn(1)	116.21(12)

N(3)	N(2)	Mn(1)	128.72(11)
N(2)	N(3)	C(4)	123.14(16)
N(2)	N(3)	C(1)	116.02(15)
C(4)	N(3)	C(1)	120.83(16)
N(5)	N(4)	C(4)	124.16(16)
N(5)	N(4)	C(5)	117.11(16)
C(4)	N(4)	C(5)	118.55(17)
C(8)	N(5)	N(4)	115.42(16)
C(15)	O(1)	Mn(1)	129.97(13)
C(17)	O(2)	Mn(1)	129.15(13)
C(20)	O(3)	Mn(1)	122.87(14)
C(22)	O(4)	Mn(1)	123.97(14)
O(1)	Mn(1)	O(4)	164.76(5)
O(1)	Mn(1)	O(3)	93.86(6)
O(4)	Mn(1)	O(3)	83.20(6)
O(1)	Mn(1)	O(2)	82.06(5)
O(4)	Mn(1)	O(2)	82.80(5)
O(3)	Mn(1)	O(2)	85.60(6)
O(1)	Mn(1)	N(1)	101.79(6)
O(4)	Mn(1)	N(1)	93.25(6)
O(3)	Mn(1)	N(1)	91.26(6)
O(2)	Mn(1)	N(1)	175.21(6)
O(1)	Mn(1)	N(2)	90.98(6)
O(4)	Mn(1)	N(2)	95.82(6)
O(3)	Mn(1)	N(2)	164.32(6)
O(2)	Mn(1)	N(2)	109.86(6)
N(1)	Mn(1)	N(2)	73.14(6)
C(28)	C(27)	H(27A)	108.3
C(28)	C(27)	H(27B)	109.5
H(27A)	C(27)	H(27B)	109.5
C(28)	C(27)	H(27C)	110.5
H(27A)	C(27)	H(27C)	109.5
H(27B)	C(27)	H(27C)	109.5
C(27)	C(28)	C(29)	115.4(14)
C(27)	C(28)	H(28A)	109.6
C(29)	C(28)	H(28A)	110.8
C(27)	C(28)	H(28B)	108.4
C(29)	C(28)	H(28B)	104.7
H(28A)	C(28)	H(28B)	107.5
C(30)	C(29)	C(28)	114.2(17)
C(30)	C(29)	H(29A)	105.2
C(28)	C(29)	H(29A)	105.8
C(30)	C(29)	H(29B)	111.1
C(28)	C(29)	H(29B)	112.3
H(29A)	C(29)	H(29B)	107.7
C(31)	C(30)	C(29)	118(4)

C(31)	C(30)	H(30A)	107.3
C(29)	C(30)	H(30A)	104.7
C(31)	C(30)	H(30B)	108.3
C(29)	C(30)	H(30B)	110.6
H(30A)	C(30)	H(30B)	107.3
C(30)	C(31)	H(31A)	110.1
C(30)	C(31)	H(31B)	109.8
H(31A)	C(31)	H(31B)	109.5
C(30)	C(31)	H(31C)	108.6
H(31A)	C(31)	H(31C)	109.5
H(31B)	C(31)	H(31C)	109.5

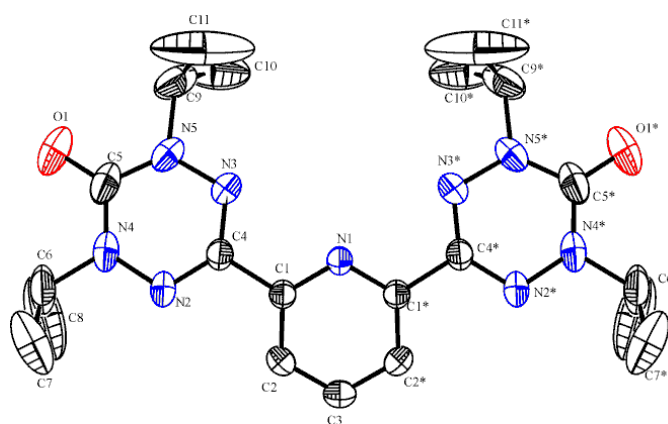


**Figure C-4:** ORTEP view of **2.18**. Thermal ellipsoids displayed at 50% probability level. Hydrogen atoms removed for clarity.

**Table C-4:** Bond lengths (Å) and angles (°) for **2.18**.

C(1)	N(1)	1.3364(17)
C(1)	C(2)	1.391(2)
C(1)	C(4)	1.490(2)
C(2)	C(3)	1.377(2)
C(2)	H(2)	0.9300
C(3)	C(2)#1	1.377(2)
C(3)	H(3)	0.9300
C(4)	N(3)	1.325(2)
C(4)	N(2)	1.331(2)
C(5)	O(1)	1.214(2)
C(5)	N(4)	1.373(3)
C(5)	N(5)	1.374(3)
C(6)	C(8)	1.475(4)
C(6)	N(4)	1.481(3)
C(6)	C(7)	1.484(4)



C(6)	H(6)	0.9800
C(7)	H(7A)	0.9600
C(7)	H(7B)	0.9600
C(7)	H(7C)	0.9600
C(8)	H(8A)	0.9600
C(8)	H(8B)	0.9600
C(8)	H(8C)	0.9600
C(9)	C(11)	1.472(4)
C(9)	C(10)	1.473(4)
C(9)	N(5)	1.479(3)
C(9)	H(9)	0.9800
C(10)	H(10A)	0.9600
C(10)	H(10B)	0.9600
C(10)	H(10C)	0.9600
C(11)	H(11A)	0.9600
C(11)	H(11B)	0.9600
C(11)	H(11C)	0.9600
N(1)	C(1)#1	1.3364(17)
N(2)	N(4)	1.365(2)
N(3)	N(5)	1.3646(19)

N(1)	C(1)	C(2)	122.91(14)
N(1)	C(1)	C(4)	116.26(14)
C(2)	C(1)	C(4)	120.74(13)
C(3)	C(2)	C(1)	118.86(15)
C(3)	C(2)	H(2)	120.6
C(1)	C(2)	H(2)	120.6
C(2)	C(3)	C(2)#1	118.8(2)
C(2)	C(3)	H(3)	120.6
C(2)#1	C(3)	H(3)	120.6
N(3)	C(4)	N(2)	127.13(14)
N(3)	C(4)	C(1)	116.79(13)
N(2)	C(4)	C(1)	115.96(14)
O(1)	C(5)	N(4)	123.4(2)
O(1)	C(5)	N(5)	122.5(2)
N(4)	C(5)	N(5)	114.03(16)
C(8)	C(6)	N(4)	110.3(2)
C(8)	C(6)	C(7)	111.9(3)
N(4)	C(6)	C(7)	110.2(2)
C(8)	C(6)	H(6)	108.1
N(4)	C(6)	H(6)	108.1
C(7)	C(6)	H(6)	108.1
C(6)	C(7)	H(7A)	109.5
C(6)	C(7)	H(7B)	109.5
H(7A)	C(7)	H(7B)	109.5
C(6)	C(7)	H(7C)	109.5

H(7A)	C(7)	H(7C)	109.5
H(7B)	C(7)	H(7C)	109.5
C(6)	C(8)	H(8A)	109.5
C(6)	C(8)	H(8B)	109.5
H(8A)	C(8)	H(8B)	109.5
C(6)	C(8)	H(8C)	109.5
H(8A)	C(8)	H(8C)	109.5
H(8B)	C(8)	H(8C)	109.5
C(11)	C(9)	C(10)	112.5(3)
C(11)	C(9)	N(5)	109.9(2)
C(10)	C(9)	N(5)	111.4(2)
C(11)	C(9)	H(9)	107.6
C(10)	C(9)	H(9)	107.6
N(5)	C(9)	H(9)	107.6
C(9)	C(10)	H(10A)	109.5
C(9)	C(10)	H(10B)	109.5
H(10A)	C(10)	H(10B)	109.5
C(9)	C(10)	H(10C)	109.5
H(10A)	C(10)	H(10C)	109.5
H(10B)	C(10)	H(10C)	109.5
C(9)	C(11)	H(11A)	109.5
C(9)	C(11)	H(11B)	109.5
H(11A)	C(11)	H(11B)	109.5
C(9)	C(11)	H(11C)	109.5
H(11A)	C(11)	H(11C)	109.5
H(11B)	C(11)	H(11C)	109.5
C(1)#1	N(1)	C(1)	117.64(18)
C(4)	N(2)	N(4)	115.06(15)
C(4)	N(3)	N(5)	114.57(14)
N(2)	N(4)	C(5)	124.10(15)
N(2)	N(4)	C(6)	115.57(18)
C(5)	N(4)	C(6)	119.77(17)
N(3)	N(5)	C(5)	124.81(17)
N(3)	N(5)	C(9)	114.79(16)
C(5)	N(5)	C(9)	120.26(17)

---

Symmetry transformations used to generate equivalent atoms: #1 x,-y+1/2,z

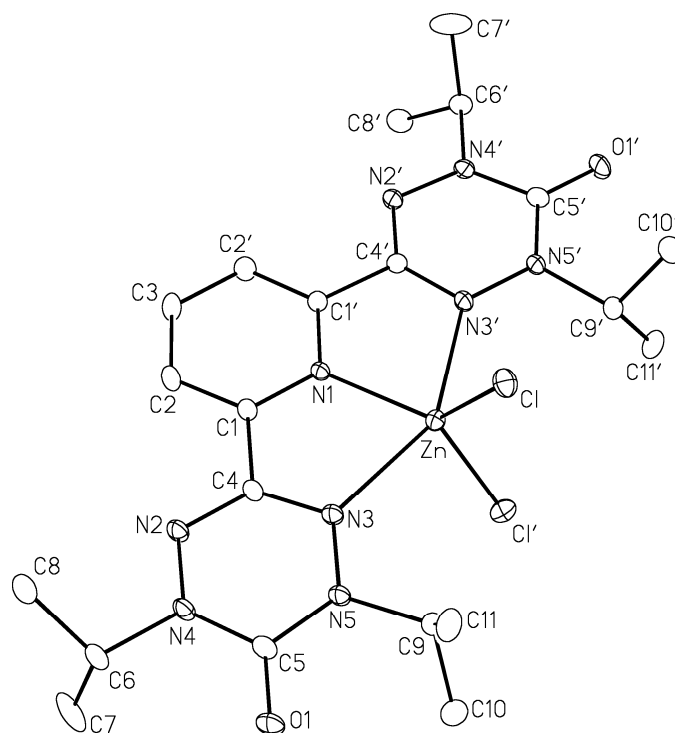


**Figure C-5:** ORTEP view of **2.19**. Thermal ellipsoids displayed at 20% probability level. Hydrogen atoms removed for clarity.

**Table C-5:** Bond lengths (Å) and angles (°) for **2.19**.

---

Zn	Cl	2.2208(6)
Zn	N(1)	2.065(3)
Zn	N(3)	2.3095(19)
O(1)	C(5)	1.209(3)
N(1)	C(1)	1.342(3)
N(2)	N(4)	1.355(3)
N(2)	C(4)	1.327(3)
N(3)	N(5)	1.364(3)
N(3)	C(4)	1.324(3)
N(4)	C(5)	1.382(3)
N(4)	C(6)	1.490(3)
N(5)	C(5)	1.392(3)
N(5)	C(9)	1.484(3)
C(1)	C(2)	1.385(3)
C(1)	C(4)	1.480(3)
C(2)	C(3)	1.382(3)
C(6)	C(7)	1.512(4)
C(6)	C(8)	1.497(4)
C(9)	C(10)	1.514(4)
C(9)	C(11)	1.528(4)

Cl	Zn	Cl'	114.71(4)
Cl	Zn	N(1)	122.645(19)
Cl	Zn	N(3)	98.65(5)
Cl	Zn	N(3')	98.23(5)
Cl'	Zn	N(1)	122.643(19)
Cl'	Zn	N(3)	98.22(5)
Cl'	Zn	N(3')	98.65(5)
N(1)	Zn	N(3)	74.21(5)
N(1)	Zn	N(3')	74.21(5)
N(3)	Zn	N(3')	148.42(10)
Zn	N(1)	C(1)	120.74(14)
Zn	N(1)	C(1')	120.74(14)
C(1)	N(1)	C(1')	118.5(3)
N(4)	N(2)	C(4)	114.4(2)
Zn	N(3)	N(5)	131.23(15)
Zn	N(3)	C(4)	113.14(15)
N(5)	N(3)	C(4)	115.59(19)
N(2)	N(4)	C(5)	124.35(19)
N(2)	N(4)	C(6)	116.0(2)
C(5)	N(4)	C(6)	119.64(19)
N(3)	N(5)	C(5)	122.51(19)
N(3)	N(5)	C(9)	115.74(19)
C(5)	N(5)	C(9)	121.6(2)
N(1)	C(1)	C(2)	122.3(2)
N(1)	C(1)	C(4)	116.0(2)
C(2)	C(1)	C(4)	121.7(2)
C(1)	C(2)	C(3)	118.8(2)
C(2)	C(3)	C(2')	119.2(3)
N(2)	C(4)	N(3)	128.1(2)
N(2)	C(4)	C(1)	116.0(2)
N(3)	C(4)	C(1)	115.9(2)
O(1)	C(5)	N(4)	122.9(2)
O(1)	C(5)	N(5)	122.1(2)
N(4)	C(5)	N(5)	115.0(2)
N(4)	C(6)	C(7)	109.8(2)
N(4)	C(6)	C(8)	110.6(2)
C(7)	C(6)	C(8)	112.6(3)
N(5)	C(9)	C(10)	110.8(2)
N(5)	C(9)	C(11)	110.3(2)
C(10)	C(9)	C(11)	114.1(2)

---

Primed atoms are related to unprimed ones via the crystallographic twofold axis (0, y, 1/4).

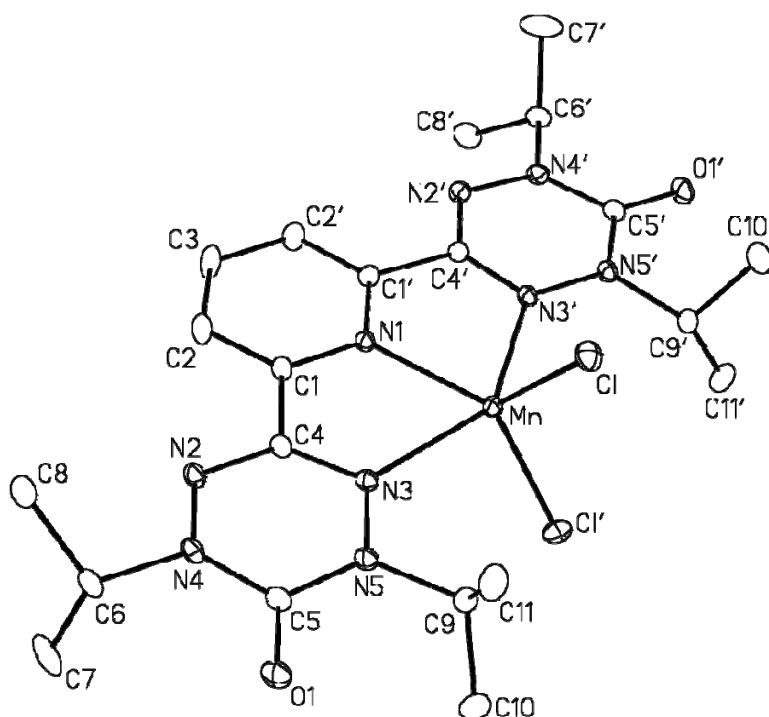


**Figure C-6:** ORTEP view of **2.20**. Thermal ellipsoids displayed at 20% probability level. Hydrogen atoms removed for clarity.

**Table C-6:** Bond lengths (Å) and angles (°) for **2.20**.

---

Mn	Cl	2.3238(4)
Mn	Cl'	2.3238(4)
Mn	N(1)	2.1824(15)
Mn	N(3)	2.3247(11)
Mn	N(3')	2.3247(10)
O(1)	C(5)	1.2118(17)
N(1)	C(1)	1.3443(14)
N(1)	C(1')	1.3442(14)
N(2)	N(4)	1.3512(15)
N(2)	C(4)	1.3215(16)
N(3)	N(5)	1.3663(15)
N(3)	C(4)	1.3344(17)
N(4)	C(5)	1.3824(19)
N(4)	C(6)	1.4893(16)
N(5)	C(5)	1.3892(17)
N(5)	C(9)	1.4875(17)
C(1)	C(2)	1.383(2)

	C(1)	C(4)	1.4793(17)
	C(2)	C(3)	1.3822(18)
	C(2)	C(3')	1.3822(18)
	C(6)	C(7)	1.516(2)
	C(6)	C(8)	1.506(2)
	C(9)	C(10)	1.516(2)
	C(9)	C(11)	1.522(2)
Cl	Mn	Cl'	110.68(2)
Cl	Mn	N(1)	124.662(11)
Cl	Mn	N(3)	100.10(3)
Cl	Mn	N(3')	100.17(3)
Cl'	Mn	N(1)	124.662(11)
Cl'	Mn	N(3)	100.17(3)
Cl'	Mn	N(3')	100.10(3)
N(1)	Mn	N(3)	71.98(3)
N(1)	Mn	N(3')	71.98(3)
N(3)	Mn	N(3')	143.96(6)
Mn	N(1)	C(1)	120.62(8)
Mn	N(1)	C(1')	120.62(8)
C(1)	N(1)	C(1')	118.77(16)
N(4)	N(2)	C(4)	115.24(11)
Mn	N(3)	N(5)	129.40(8)
Mn	N(3)	C(4)	115.52(8)
N(5)	N(3)	C(4)	115.06(11)
N(2)	N(4)	C(5)	123.97(10)
N(2)	N(4)	C(6)	116.18(11)
C(5)	N(4)	C(6)	119.83(11)
N(3)	N(5)	C(5)	122.95(11)
N(3)	N(5)	C(9)	116.09(11)
C(5)	N(5)	C(9)	120.81(11)
N(1)	C(1)	C(2)	122.11(12)
N(1)	C(1)	C(4)	115.50(12)
C(2)	C(1)	C(4)	122.39(12)
C(1)	C(2)	C(3)	118.84(14)
C(2)	C(3)	C(2')	119.3(2)
N(2)	C(4)	N(3)	127.68(12)
N(2)	C(4)	C(1)	115.93(12)
N(3)	C(4)	C(1)	116.39(11)
O(1)	C(5)	N(4)	122.57(12)
O(1)	C(5)	N(5)	122.43(13)
N(4)	C(5)	N(5)	114.99(11)
N(4)	C(6)	C(7)	109.73(12)

N(4)	C(6)	C(8)	110.40(11)
C(7)	C(6)	C(8)	112.95(15)
N(5)	C(9)	C(10)	111.28(13)
N(5)	C(9)	C(11)	111.12(12)
C(10)	C(9)	C(11)	113.90(14)

---

Primed atoms are related to unprimed ones via the crystallographic twofold axis (0, y, 1/4).

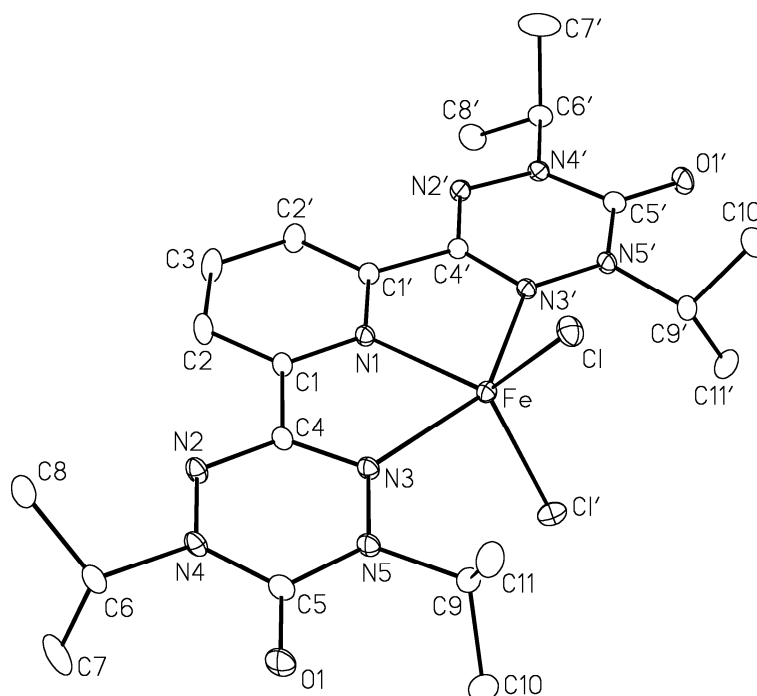


**Figure C-7:** ORTEP view of **2.21**. Thermal ellipsoids displayed at 20% probability level. Hydrogen atoms removed for clarity.

**Table C-7:** Bond lengths (Å) and angles (°) for **2.21**.

---

Fe	Cl	2.2710(5)
Fe	Cl'	2.2710(5)
Fe	N(1)	2.088(2)
Fe	N(3)	2.2772(14)
Fe	N(3')	2.2772(14)
O(1)	C(5)	1.211(2)
N(1)	C(1)	1.344(2)
N(1)	C(1')	1.344(2)
N(2)	N(4)	1.351(2)
N(2)	C(4)	1.325(2)

N(3)	N(5)	1.365(2)
N(3)	C(4)	1.337(2)
N(4)	C(5)	1.384(3)
N(4)	C(6)	1.493(2)
N(5)	C(5)	1.389(2)
N(5)	C(9)	1.485(2)
C(1)	C(2)	1.382(3)
C(1)	C(4)	1.478(2)
C(2)	C(3)	1.384(2)
C(2)	C(3')	1.384(2)
C(6)	C(7)	1.514(3)
C(6)	C(8)	1.503(3)
C(9)	C(10)	1.515(3)
C(9)	C(11)	1.518(3)

Cl	Fe	Cl'	114.48(3)
Cl	Fe	N(1)	122.759(16)
Cl	Fe	N(3)	98.48(4)
Cl	Fe	N(3')	98.25(4)
Cl'	Fe	N(1)	122.759(16)
Cl'	Fe	N(3)	98.25(4)
Cl'	Fe	N(3')	98.48(4)
N(1)	Fe	N(3)	74.41(4)
N(1)	Fe	N(3')	74.41(4)
N(3)	Fe	N(3')	148.81(8)
Fe	N(1)	C(1)	120.47(11)
Fe	N(1)	C(1')	120.47(11)
C(1)	N(1)	C(1')	119.1(2)
N(4)	N(2)	C(4)	115.02(15)
Fe	N(3)	N(5)	131.35(12)
Fe	N(3)	C(4)	113.58(11)
N(5)	N(3)	C(4)	115.03(14)
N(2)	N(4)	C(5)	124.13(14)
N(2)	N(4)	C(6)	116.09(15)
C(5)	N(4)	C(6)	119.77(15)
N(3)	N(5)	C(5)	123.03(15)
N(3)	N(5)	C(9)	116.01(14)
C(5)	N(5)	C(9)	120.86(15)
N(1)	C(1)	C(2)	121.94(17)
N(1)	C(1)	C(4)	115.20(16)
C(2)	C(1)	C(4)	122.86(16)
C(1)	C(2)	C(3)	118.85(19)
C(2)	C(3)	C(2')	119.4(3)



N(2)	C(4)	N(3)	127.74(16)
N(2)	C(4)	C(1)	115.91(16)
N(3)	C(4)	C(1)	116.35(15)
O(1)	C(5)	N(4)	122.62(17)
O(1)	C(5)	N(5)	122.43(19)
N(4)	C(5)	N(5)	114.95(15)
N(4)	C(6)	C(7)	109.73(15)
N(4)	C(6)	C(8)	110.42(15)
C(7)	C(6)	C(8)	112.8(2)
N(5)	C(9)	C(10)	111.00(17)
N(5)	C(9)	C(11)	110.89(16)
C(10)	C(9)	C(11)	114.13(18)

Primed atoms are related to unprimed ones via the crystallographic 2-fold axis ( $1-x, y, 1/2-z$ ).

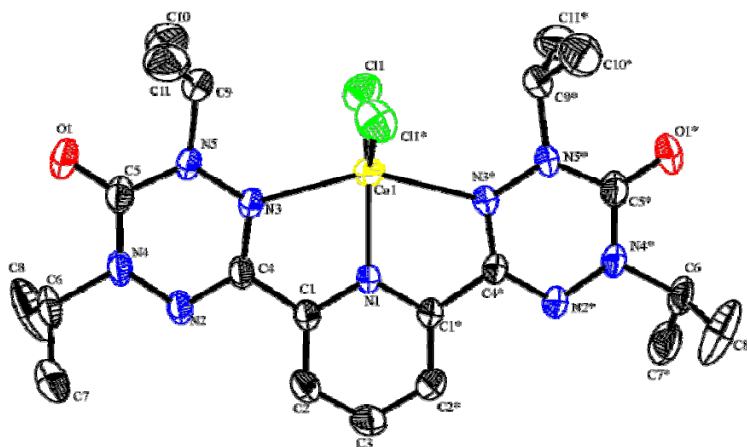


**Figure C-8:** ORTEP view of **2.22**. Thermal ellipsoids displayed at 50% probability level. Hydrogen atoms removed for clarity.

**Table C-8:** Bond lengths (Å) and angles (°) for **2.22**.

C(1)	N(1)	1.3423(19)
C(1)	C(2)	1.376(3)
C(1)	C(4)	1.472(2)
C(2)	C(3)	1.373(3)
C(2)	H(2)	0.9300
C(3)	C(2)#1	1.373(3)
C(3)	H(3)	0.9300
C(4)	N(2)	1.323(2)
C(4)	N(3)	1.327(2)
C(5)	O(1)	1.207(2)

C(5)	N(4)	1.376(3)
C(5)	N(5)	1.389(2)
C(6)	N(4)	1.491(2)
C(6)	C(7)	1.497(3)
C(6)	C(8)	1.502(3)
C(6)	H(6)	0.9800
C(7)	H(7A)	0.9600
C(7)	H(7B)	0.9600
C(7)	H(7C)	0.9600
C(8)	H(8A)	0.9600
C(8)	H(8B)	0.9600
C(8)	H(8C)	0.9600
C(9)	N(5)	1.483(2)
C(9)	C(10)	1.509(3)
C(9)	C(11)	1.514(3)
C(9)	H(9)	0.9800
C(10)	H(10A)	0.9600
C(10)	H(10B)	0.9600
C(10)	H(10C)	0.9600
C(11)	H(11A)	0.9600
C(11)	H(11B)	0.9600
C(11)	H(11C)	0.9600
N(1)	C(1)#1	1.3423(19)
N(1)	Co(1)	2.031(2)
N(2)	N(4)	1.349(2)
N(3)	N(5)	1.363(2)
N(3)	Co(1)	2.2564(14)
Cl(1)	Co(1)	2.2370(5)
Co(1)	Cl(1)#1	2.2370(5)
Co(1)	N(3)#1	2.2564(14)

N(1)	C(1)	C(2)	121.69(17)
N(1)	C(1)	C(4)	115.27(16)
C(2)	C(1)	C(4)	123.03(17)
C(3)	C(2)	C(1)	119.0(2)
C(3)	C(2)	H(2)	120.5
C(1)	C(2)	H(2)	120.5
C(2)#1	C(3)	C(2)	119.6(3)
C(2)#1	C(3)	H(3)	120.2
C(2)	C(3)	H(3)	120.2
N(2)	C(4)	N(3)	127.90(16)
N(2)	C(4)	C(1)	116.05(16)
N(3)	C(4)	C(1)	116.04(15)
O(1)	C(5)	N(4)	122.66(18)
O(1)	C(5)	N(5)	122.30(19)
N(4)	C(5)	N(5)	115.03(15)

N(4)	C(6)	C(7)	110.39(16)
N(4)	C(6)	C(8)	109.59(17)
C(7)	C(6)	C(8)	113.6(2)
N(4)	C(6)	H(6)	107.7
C(7)	C(6)	H(6)	107.7
C(8)	C(6)	H(6)	107.7
C(6)	C(7)	H(7A)	109.5
C(6)	C(7)	H(7B)	109.5
H(7A)	C(7)	H(7B)	109.5
C(6)	C(7)	H(7C)	109.5
H(7A)	C(7)	H(7C)	109.5
H(7B)	C(7)	H(7C)	109.5
C(6)	C(8)	H(8A)	109.5
C(6)	C(8)	H(8B)	109.5
H(8A)	C(8)	H(8B)	109.5
C(6)	C(8)	H(8C)	109.5
H(8A)	C(8)	H(8C)	109.5
H(8B)	C(8)	H(8C)	109.5
N(5)	C(9)	C(10)	110.85(17)
N(5)	C(9)	C(11)	110.72(17)
C(10)	C(9)	C(11)	114.34(19)
N(5)	C(9)	H(9)	106.8
C(10)	C(9)	H(9)	106.8
C(11)	C(9)	H(9)	106.8
C(9)	C(10)	H(10A)	109.5
C(9)	C(10)	H(10B)	109.5
H(10A)	C(10)	H(10B)	109.5
C(9)	C(10)	H(10C)	109.5
H(10A)	C(10)	H(10C)	109.5
H(10B)	C(10)	H(10C)	109.5
C(9)	C(11)	H(11A)	109.5
C(9)	C(11)	H(11B)	109.5
H(11A)	C(11)	H(11B)	109.5
C(9)	C(11)	H(11C)	109.5
H(11A)	C(11)	H(11C)	109.5
H(11B)	C(11)	H(11C)	109.5
C(1)	N(1)	C(1)#1	119.1(2)
C(1)	N(1)	Co(1)	120.45(10)
C(1)#1	N(1)	Co(1)	120.45(10)
C(4)	N(2)	N(4)	114.96(15)
C(4)	N(3)	N(5)	115.03(14)
C(4)	N(3)	Co(1)	112.83(11)
N(5)	N(3)	Co(1)	132.11(11)
N(2)	N(4)	C(5)	124.09(14)
N(2)	N(4)	C(6)	116.09(16)
C(5)	N(4)	C(6)	119.82(15)

N(3)	N(5)	C(5)	122.92(15)
N(3)	N(5)	C(9)	116.08(14)
C(5)	N(5)	C(9)	120.94(15)
N(1)	Co(1)	Cl(1)	123.312(16)
N(1)	Co(1)	Cl(1)#1	123.312(16)
Cl(1)	Co(1)	Cl(1)#1	113.38(3)
N(1)	Co(1)	N(3)	75.40(4)
Cl(1)	Co(1)	N(3)	97.92(4)
Cl(1)#1	Co(1)	N(3)	97.99(4)
N(1)	Co(1)	N(3)#1	75.40(4)
Cl(1)	Co(1)	N(3)#1	97.99(4)
Cl(1)#1	Co(1)	N(3)#1	97.92(4)
N(3)	Co(1)	N(3)#1	150.80(8)

Symmetry transformations used to generate equivalent atoms: #1 -x+1,y,-z+3/2

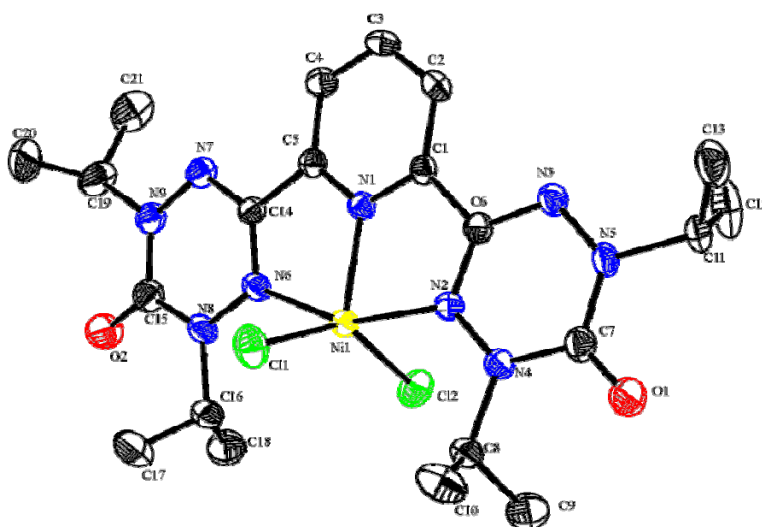


**Figure C-9:** ORTEP view of **2.23**. Thermal ellipsoids displayed at 50% probability level. Hydrogen atoms removed for clarity.

**Table C-9:** Bond lengths (Å) and angles (°) for **2.23**.

C(1)	N(1)	1.336(3)
C(1)	C(2)	1.384(3)
C(1)	C(6)	1.478(3)
C(2)	C(3)	1.392(3)
C(2)	H(2)	0.9500
C(3)	C(4)	1.384(3)
C(3)	H(3)	0.9500
C(4)	C(5)	1.387(3)
C(4)	H(4)	0.9500

C(5)	N(1)	1.339(3)
C(5)	C(14)	1.478(3)
C(6)	N(3)	1.322(3)
C(6)	N(2)	1.336(3)
C(7)	O(1)	1.213(3)
C(7)	N(4)	1.382(3)
C(7)	N(5)	1.393(3)
C(8)	N(4)	1.490(3)
C(8)	C(10)	1.507(4)
C(8)	C(9)	1.513(3)
C(8)	H(8)	1.0000
C(9)	H(9A)	0.9800
C(9)	H(9B)	0.9800
C(9)	H(9C)	0.9800
C(10)	H(10A)	0.9800
C(10)	H(10B)	0.9800
C(10)	H(10C)	0.9800
C(11)	N(5)	1.486(3)
C(11)	C(12)	1.498(4)
C(11)	C(13)	1.500(4)
C(11)	H(11)	1.0000
C(12)	H(12A)	0.9800
C(12)	H(12B)	0.9800
C(12)	H(12C)	0.9800
C(13)	H(13A)	0.9800
C(13)	H(13B)	0.9800
C(13)	H(13C)	0.9800
C(14)	N(7)	1.318(3)
C(14)	N(6)	1.334(3)
C(15)	O(2)	1.210(3)
C(15)	N(8)	1.383(3)
C(15)	N(9)	1.387(3)
C(16)	N(8)	1.488(3)
C(16)	C(18)	1.519(4)
C(16)	C(17)	1.522(4)
C(16)	H(16)	1.0000
C(17)	H(17A)	0.9800
C(17)	H(17B)	0.9800
C(17)	H(17C)	0.9800
C(18)	H(18A)	0.9800
C(18)	H(18B)	0.9800
C(18)	H(18C)	0.9800
C(19)	N(9)	1.487(3)
C(19)	C(21)	1.507(4)
C(19)	C(20)	1.527(5)
C(19)	H(19)	1.0000

C(20)	H(20A)	0.9800
C(20)	H(20B)	0.9800
C(20)	H(20C)	0.9800
C(21)	H(21A)	0.9800
C(21)	H(21B)	0.9800
C(21)	H(21C)	0.9800
N(1)	Ni(1)	1.9728(18)
N(2)	N(4)	1.368(2)
N(2)	Ni(1)	2.1478(19)
N(3)	N(5)	1.359(3)
N(6)	N(8)	1.369(3)
N(6)	Ni(1)	2.1213(19)
N(7)	N(9)	1.357(3)
Cl(1)	Ni(1)	2.2612(7)
Cl(2)	Ni(1)	2.2488(6)

N(1)	C(1)	C(2)	121.8(2)
N(1)	C(1)	C(6)	113.46(19)
C(2)	C(1)	C(6)	124.7(2)
C(1)	C(2)	C(3)	117.6(2)
C(1)	C(2)	H(2)	121.2
C(3)	C(2)	H(2)	121.2
C(4)	C(3)	C(2)	120.6(2)
C(4)	C(3)	H(3)	119.7
C(2)	C(3)	H(3)	119.7
C(3)	C(4)	C(5)	118.2(2)
C(3)	C(4)	H(4)	120.9
C(5)	C(4)	H(4)	120.9
N(1)	C(5)	C(4)	121.1(2)
N(1)	C(5)	C(14)	113.90(19)
C(4)	C(5)	C(14)	125.0(2)
N(3)	C(6)	N(2)	127.3(2)
N(3)	C(6)	C(1)	117.5(2)
N(2)	C(6)	C(1)	115.07(19)
O(1)	C(7)	N(4)	123.0(2)
O(1)	C(7)	N(5)	122.4(2)
N(4)	C(7)	N(5)	114.6(2)
N(4)	C(8)	C(10)	110.6(2)
N(4)	C(8)	C(9)	111.3(2)
C(10)	C(8)	C(9)	113.6(2)
N(4)	C(8)	H(8)	107.0
C(10)	C(8)	H(8)	107.0
C(9)	C(8)	H(8)	107.0
C(8)	C(9)	H(9A)	109.5
C(8)	C(9)	H(9B)	109.5
H(9A)	C(9)	H(9B)	109.5

C(8)	C(9)	H(9C)	109.5
H(9A)	C(9)	H(9C)	109.5
H(9B)	C(9)	H(9C)	109.5
C(8)	C(10)	H(10A)	109.5
C(8)	C(10)	H(10B)	109.5
H(10A)	C(10)	H(10B)	109.5
C(8)	C(10)	H(10C)	109.5
H(10A)	C(10)	H(10C)	109.5
H(10B)	C(10)	H(10C)	109.5
N(5)	C(11)	C(12)	108.9(2)
N(5)	C(11)	C(13)	110.69(19)
C(12)	C(11)	C(13)	114.2(2)
N(5)	C(11)	H(11)	107.6
C(12)	C(11)	H(11)	107.6
C(13)	C(11)	H(11)	107.6
C(11)	C(12)	H(12A)	109.5
C(11)	C(12)	H(12B)	109.5
H(12A)	C(12)	H(12B)	109.5
C(11)	C(12)	H(12C)	109.5
H(12A)	C(12)	H(12C)	109.5
H(12B)	C(12)	H(12C)	109.5
C(11)	C(13)	H(13A)	109.5
C(11)	C(13)	H(13B)	109.5
H(13A)	C(13)	H(13B)	109.5
C(11)	C(13)	H(13C)	109.5
H(13A)	C(13)	H(13C)	109.5
H(13B)	C(13)	H(13C)	109.5
N(7)	C(14)	N(6)	127.9(2)
N(7)	C(14)	C(5)	117.2(2)
N(6)	C(14)	C(5)	114.87(19)
O(2)	C(15)	N(8)	122.9(2)
O(2)	C(15)	N(9)	122.2(2)
N(8)	C(15)	N(9)	114.9(2)
N(8)	C(16)	C(18)	110.8(2)
N(8)	C(16)	C(17)	110.9(2)
C(18)	C(16)	C(17)	114.1(2)
N(8)	C(16)	H(16)	106.9
C(18)	C(16)	H(16)	106.9
C(17)	C(16)	H(16)	106.9
C(16)	C(17)	H(17A)	109.5
C(16)	C(17)	H(17B)	109.5
H(17A)	C(17)	H(17B)	109.5
C(16)	C(17)	H(17C)	109.5
H(17A)	C(17)	H(17C)	109.5
H(17B)	C(17)	H(17C)	109.5
C(16)	C(18)	H(18A)	109.5

C(16)	C(18)	H(18B)	109.5
H(18A)	C(18)	H(18B)	109.5
C(16)	C(18)	H(18C)	109.5
H(18A)	C(18)	H(18C)	109.5
H(18B)	C(18)	H(18C)	109.5
N(9)	C(19)	C(21)	110.7(2)
N(9)	C(19)	C(20)	108.5(3)
C(21)	C(19)	C(20)	112.0(3)
N(9)	C(19)	H(19)	108.5
C(21)	C(19)	H(19)	108.5
C(20)	C(19)	H(19)	108.5
C(19)	C(20)	H(20A)	109.5
C(19)	C(20)	H(20B)	109.5
H(20A)	C(20)	H(20B)	109.5
C(19)	C(20)	H(20C)	109.5
H(20A)	C(20)	H(20C)	109.5
H(20B)	C(20)	H(20C)	109.5
C(19)	C(21)	H(21A)	109.5
C(19)	C(21)	H(21B)	109.5
H(21A)	C(21)	H(21B)	109.5
C(19)	C(21)	H(21C)	109.5
H(21A)	C(21)	H(21C)	109.5
H(21B)	C(21)	H(21C)	109.5
C(1)	N(1)	C(5)	120.62(19)
C(1)	N(1)	Ni(1)	120.19(15)
C(5)	N(1)	Ni(1)	119.18(15)
C(6)	N(2)	N(4)	115.73(18)
C(6)	N(2)	Ni(1)	112.98(14)
N(4)	N(2)	Ni(1)	130.68(14)
C(6)	N(3)	N(5)	114.81(19)
N(2)	N(4)	C(7)	122.84(19)
N(2)	N(4)	C(8)	116.04(18)
C(7)	N(4)	C(8)	121.07(19)
N(3)	N(5)	C(7)	124.13(18)
N(3)	N(5)	C(11)	115.40(18)
C(7)	N(5)	C(11)	120.19(19)
C(14)	N(6)	N(8)	115.46(19)
C(14)	N(6)	Ni(1)	113.59(15)
N(8)	N(6)	Ni(1)	130.64(14)
C(14)	N(7)	N(9)	114.57(19)
N(6)	N(8)	C(15)	122.7(2)
N(6)	N(8)	C(16)	115.92(18)
C(15)	N(8)	C(16)	121.4(2)
N(7)	N(9)	C(15)	124.41(19)
N(7)	N(9)	C(19)	115.89(19)
C(15)	N(9)	C(19)	119.7(2)



N(1)	Ni(1)	N(6)	78.11(7)
N(1)	Ni(1)	N(2)	77.49(7)
N(6)	Ni(1)	N(2)	155.58(8)
N(1)	Ni(1)	Cl(2)	112.68(6)
N(6)	Ni(1)	Cl(2)	96.18(5)
N(2)	Ni(1)	Cl(2)	92.16(5)
N(1)	Ni(1)	Cl(1)	106.85(6)
N(6)	Ni(1)	Cl(1)	93.03(6)
N(2)	Ni(1)	Cl(1)	95.05(5)
Cl(2)	Ni(1)	Cl(1)	140.44(3)

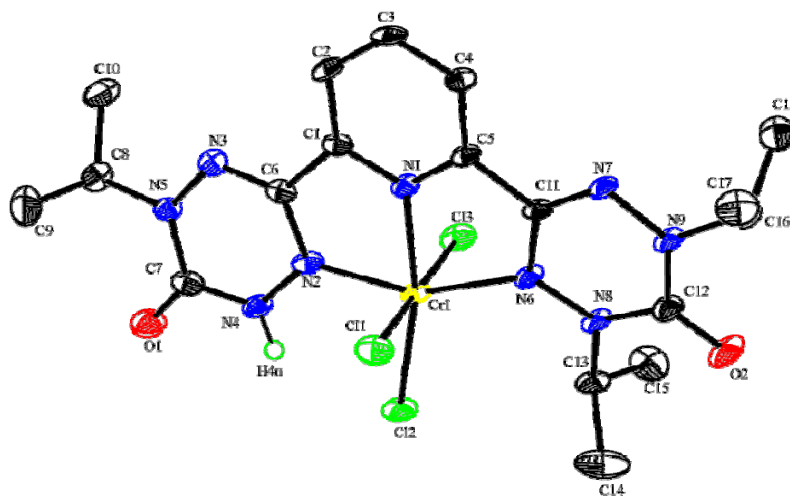


**Figure C-10:** ORTEP view of **2.28b**. Thermal ellipsoids displayed at 50% probability level. Calculated hydrogen atoms removed for clarity.

**Table C-10:** Bond lengths (Å) and angles (°) for **2.28b**.

C(1)	N(1)	1.347(5)
C(1)	C(2)	1.376(6)
C(1)	C(6)	1.471(5)
C(2)	C(3)	1.387(6)
C(2)	H(2)	0.9500
C(3)	C(4)	1.386(6)
C(3)	H(3)	0.9500
C(4)	C(5)	1.384(5)
C(4)	H(4)	0.9500
C(5)	N(1)	1.329(5)
C(5)	C(11)	1.479(5)
C(6)	N(3)	1.313(5)
C(6)	N(2)	1.348(5)

C(7)	O(1)	1.207(5)
C(7)	N(4)	1.360(6)
C(7)	N(5)	1.385(5)
C(8)	N(5)	1.481(5)
C(8)	C(10)	1.500(6)
C(8)	C(9)	1.512(6)
C(8)	H(8)	1.0000
C(9)	H(9A)	0.9800
C(9)	H(9B)	0.9800
C(9)	H(9C)	0.9800
C(10)	H(10A)	0.9800
C(10)	H(10B)	0.9800
C(10)	H(10C)	0.9800
C(11)	N(7)	1.300(5)
C(11)	N(6)	1.356(5)
C(12)	O(2)	1.207(5)
C(12)	N(8)	1.374(5)
C(12)	N(9)	1.378(5)
C(13)	N(8)	1.488(5)
C(13)	C(14)	1.504(6)
C(13)	C(15)	1.520(6)
C(13)	H(13)	1.0000
C(14)	H(14A)	0.9800
C(14)	H(14B)	0.9800
C(14)	H(14C)	0.9800
C(15)	H(15A)	0.9800
C(15)	H(15B)	0.9800
C(15)	H(15C)	0.9800
C(16)	N(9)	1.480(5)
C(16)	C(17)	1.501(6)
C(16)	C(18)	1.505(6)
C(16)	H(16)	1.0000
C(17)	H(17A)	0.9800
C(17)	H(17B)	0.9800
C(17)	H(17C)	0.9800
C(18)	H(18A)	0.9800
C(18)	H(18B)	0.9800
C(18)	H(18C)	0.9800
N(1)	Cr(1)	2.001(3)
N(2)	N(4)	1.351(4)
N(2)	Cr(1)	1.980(3)
N(3)	N(5)	1.354(4)
N(4)	H(4N)	0.83(5)
N(6)	N(8)	1.361(4)
N(6)	Cr(1)	2.093(3)
N(7)	N(9)	1.360(4)

	Cl(1)	Cr(1)	2.2986(13)
	Cl(2)	Cr(1)	2.3274(12)
	Cl(3)	Cr(1)	2.3071(13)
N(1)	C(1)	C(2)	121.0(4)
N(1)	C(1)	C(6)	111.3(3)
C(2)	C(1)	C(6)	127.8(4)
C(1)	C(2)	C(3)	118.2(4)
C(1)	C(2)	H(2)	120.9
C(3)	C(2)	H(2)	120.9
C(4)	C(3)	C(2)	120.7(4)
C(4)	C(3)	H(3)	119.7
C(2)	C(3)	H(3)	119.7
C(5)	C(4)	C(3)	117.7(4)
C(5)	C(4)	H(4)	121.1
C(3)	C(4)	H(4)	121.1
N(1)	C(5)	C(4)	121.6(4)
N(1)	C(5)	C(11)	113.0(3)
C(4)	C(5)	C(11)	125.4(4)
N(3)	C(6)	N(2)	126.0(4)
N(3)	C(6)	C(1)	121.0(4)
N(2)	C(6)	C(1)	113.0(4)
O(1)	C(7)	N(4)	121.8(4)
O(1)	C(7)	N(5)	123.7(4)
N(4)	C(7)	N(5)	114.5(4)
N(5)	C(8)	C(10)	110.7(3)
N(5)	C(8)	C(9)	110.3(4)
C(10)	C(8)	C(9)	113.0(4)
N(5)	C(8)	H(8)	107.6
C(10)	C(8)	H(8)	107.6
C(9)	C(8)	H(8)	107.6
C(8)	C(9)	H(9A)	109.5
C(8)	C(9)	H(9B)	109.5
H(9A)	C(9)	H(9B)	109.5
C(8)	C(9)	H(9C)	109.5
H(9A)	C(9)	H(9C)	109.5
H(9B)	C(9)	H(9C)	109.5
C(8)	C(10)	H(10A)	109.5
C(8)	C(10)	H(10B)	109.5
H(10A)	C(10)	H(10B)	109.5
C(8)	C(10)	H(10C)	109.5
H(10A)	C(10)	H(10C)	109.5
H(10B)	C(10)	H(10C)	109.5
N(7)	C(11)	N(6)	127.2(4)
N(7)	C(11)	C(5)	118.4(3)
N(6)	C(11)	C(5)	114.4(3)

O(2)	C(12)	N(8)	122.9(4)
O(2)	C(12)	N(9)	121.9(4)
N(8)	C(12)	N(9)	115.2(4)
N(8)	C(13)	C(14)	110.7(4)
N(8)	C(13)	C(15)	110.5(3)
C(14)	C(13)	C(15)	114.4(4)
N(8)	C(13)	H(13)	107.0
C(14)	C(13)	H(13)	107.0
C(15)	C(13)	H(13)	107.0
C(13)	C(14)	H(14A)	109.5
C(13)	C(14)	H(14B)	109.5
H(14A)	C(14)	H(14B)	109.5
C(13)	C(14)	H(14C)	109.5
H(14A)	C(14)	H(14C)	109.5
H(14B)	C(14)	H(14C)	109.5
C(13)	C(15)	H(15A)	109.5
C(13)	C(15)	H(15B)	109.5
H(15A)	C(15)	H(15B)	109.5
C(13)	C(15)	H(15C)	109.5
H(15A)	C(15)	H(15C)	109.5
H(15B)	C(15)	H(15C)	109.5
N(9)	C(16)	C(17)	110.3(4)
N(9)	C(16)	C(18)	108.9(3)
C(17)	C(16)	C(18)	113.8(4)
N(9)	C(16)	H(16)	107.9
C(17)	C(16)	H(16)	107.9
C(18)	C(16)	H(16)	107.9
C(16)	C(17)	H(17A)	109.5
C(16)	C(17)	H(17B)	109.5
H(17A)	C(17)	H(17B)	109.5
C(16)	C(17)	H(17C)	109.5
H(17A)	C(17)	H(17C)	109.5
H(17B)	C(17)	H(17C)	109.5
C(16)	C(18)	H(18A)	109.5
C(16)	C(18)	H(18B)	109.5
H(18A)	C(18)	H(18B)	109.5
C(16)	C(18)	H(18C)	109.5
H(18A)	C(18)	H(18C)	109.5
H(18B)	C(18)	H(18C)	109.5
C(5)	N(1)	C(1)	120.8(3)
C(5)	N(1)	Cr(1)	119.9(3)
C(1)	N(1)	Cr(1)	119.3(3)
C(6)	N(2)	N(4)	114.6(3)
C(6)	N(2)	Cr(1)	119.0(3)
N(4)	N(2)	Cr(1)	126.4(3)
C(6)	N(3)	N(5)	116.6(3)

N(2)	N(4)	C(7)	125.1(4)
N(2)	N(4)	H(4N)	110(3)
C(7)	N(4)	H(4N)	124(3)
N(3)	N(5)	C(7)	123.0(3)
N(3)	N(5)	C(8)	118.2(3)
C(7)	N(5)	C(8)	118.7(3)
C(11)	N(6)	N(8)	114.5(3)
C(11)	N(6)	Cr(1)	114.6(3)
N(8)	N(6)	Cr(1)	130.9(2)
C(11)	N(7)	N(9)	115.7(3)
N(6)	N(8)	C(12)	123.4(3)
N(6)	N(8)	C(13)	116.7(3)
C(12)	N(8)	C(13)	119.9(3)
N(7)	N(9)	C(12)	123.6(3)
N(7)	N(9)	C(16)	115.9(3)
C(12)	N(9)	C(16)	120.2(3)
N(2)	Cr(1)	N(1)	77.28(13)
N(2)	Cr(1)	N(6)	154.68(13)
N(1)	Cr(1)	N(6)	77.41(13)
N(2)	Cr(1)	Cl(1)	91.38(10)
N(1)	Cr(1)	Cl(1)	87.47(10)
N(6)	Cr(1)	Cl(1)	88.11(10)
N(2)	Cr(1)	Cl(3)	90.57(10)
N(1)	Cr(1)	Cl(3)	90.62(10)
N(6)	Cr(1)	Cl(3)	89.10(10)
Cl(1)	Cr(1)	Cl(3)	176.91(5)
N(2)	Cr(1)	Cl(2)	90.89(10)
N(1)	Cr(1)	Cl(2)	168.06(10)
N(6)	Cr(1)	Cl(2)	114.43(10)
Cl(1)	Cr(1)	Cl(2)	91.21(5)
Cl(3)	Cr(1)	Cl(2)	91.16(4)

---

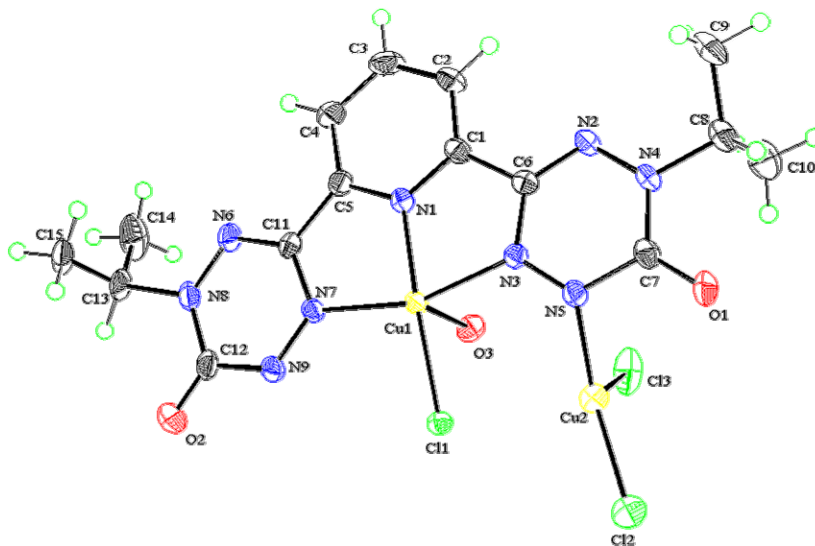


**Figure C-11:** ORTEP view of **2.29**. Thermal ellipsoids displayed at 50% probability level

**Table C-11:** Bond lengths (Å) and angles (°) for **2.29**.

---

C(1)	N(1)	1.336(5)
C(1)	C(2)	1.374(6)
C(1)	C(6)	1.470(6)
C(2)	C(3)	1.384(6)
C(2)	H(2)	0.9500
C(3)	C(4)	1.384(6)
C(3)	H(3)	0.9500
C(4)	C(5)	1.378(6)
C(4)	H(4)	0.9500
C(5)	N(1)	1.333(5)
C(5)	C(11)	1.460(6)
C(6)	N(2)	1.300(5)
C(6)	N(3)	1.370(5)
C(7)	O(1)	1.209(5)
C(7)	N(4)	1.370(5)
C(7)	N(5)	1.418(5)
C(8)	N(4)	1.480(6)
C(8)	C(9)	1.506(7)
C(8)	C(10)	1.507(8)
C(8)	H(8)	1.0000
C(9)	H(9A)	0.9800
C(9)	H(9B)	0.9800
C(9)	H(9C)	0.9800
C(10)	H(10A)	0.9800

C(10)	H(10B)	0.9800
C(10)	H(10C)	0.9800
C(11)	N(6)	1.299(5)
C(11)	N(7)	1.364(5)
C(12)	O(2)	1.197(5)
C(12)	N(8)	1.387(6)
C(12)	N(9)	1.414(6)
C(13)	N(8)	1.488(5)
C(13)	C(14)	1.502(7)
C(13)	C(15)	1.513(6)
C(13)	H(13)	1.0000
C(14)	H(14A)	0.9800
C(14)	H(14B)	0.9800
C(14)	H(14C)	0.9800
C(15)	H(15A)	0.9800
C(15)	H(15B)	0.9800
C(15)	H(15C)	0.9800
N(1)	Cu(1)	1.941(3)
N(2)	N(4)	1.346(5)
N(3)	N(5)	1.323(5)
N(3)	Cu(1)	2.018(3)
N(5)	Cu(2)	1.881(4)
N(6)	N(8)	1.322(5)
N(7)	N(9)	1.292(5)
N(7)	Cu(1)	2.046(3)
O(3)	H(3O)	0.979(10)
O(5)	H(5A)	1.06(6)
Cl(1)	Cu(1)	2.2244(11)
Cl(1)	Cu(2)	2.7068(12)
Cl(2)	Cu(2)	2.1670(14)
Cl(3)	Cu(2)	2.2246(14)

N(1)	C(1)	C(2)	121.0(4)
N(1)	C(1)	C(6)	112.5(4)
C(2)	C(1)	C(6)	126.5(4)
C(1)	C(2)	C(3)	118.1(4)
C(1)	C(2)	H(2)	120.9
C(3)	C(2)	H(2)	120.9
C(2)	C(3)	C(4)	120.6(4)
C(2)	C(3)	H(3)	119.7
C(4)	C(3)	H(3)	119.7
C(5)	C(4)	C(3)	117.9(4)
C(5)	C(4)	H(4)	121.0
C(3)	C(4)	H(4)	121.0
N(1)	C(5)	C(4)	121.1(4)
N(1)	C(5)	C(11)	112.6(4)

C(4)	C(5)	C(11)	126.3(4)
N(2)	C(6)	N(3)	125.6(4)
N(2)	C(6)	C(1)	120.5(4)
N(3)	C(6)	C(1)	113.9(4)
O(1)	C(7)	N(4)	123.5(4)
O(1)	C(7)	N(5)	119.2(4)
N(4)	C(7)	N(5)	117.4(4)
N(4)	C(8)	C(9)	110.6(4)
N(4)	C(8)	C(10)	109.5(4)
C(9)	C(8)	C(10)	113.1(5)
N(4)	C(8)	H(8)	107.8
C(9)	C(8)	H(8)	107.8
C(10)	C(8)	H(8)	107.8
C(8)	C(9)	H(9A)	109.5
C(8)	C(9)	H(9B)	109.5
H(9A)	C(9)	H(9B)	109.5
C(8)	C(9)	H(9C)	109.5
H(9A)	C(9)	H(9C)	109.5
H(9B)	C(9)	H(9C)	109.5
C(8)	C(10)	H(10A)	109.5
C(8)	C(10)	H(10B)	109.5
H(10A)	C(10)	H(10B)	109.5
C(8)	C(10)	H(10C)	109.5
H(10A)	C(10)	H(10C)	109.5
H(10B)	C(10)	H(10C)	109.5
N(6)	C(11)	N(7)	123.9(4)
N(6)	C(11)	C(5)	120.7(4)
N(7)	C(11)	C(5)	115.3(4)
O(2)	C(12)	N(8)	123.4(4)
O(2)	C(12)	N(9)	120.9(4)
N(8)	C(12)	N(9)	115.8(4)
N(8)	C(13)	C(14)	110.0(4)
N(8)	C(13)	C(15)	108.1(4)
C(14)	C(13)	C(15)	113.7(4)
N(8)	C(13)	H(13)	108.3
C(14)	C(13)	H(13)	108.3
C(15)	C(13)	H(13)	108.3
C(13)	C(14)	H(14A)	109.5
C(13)	C(14)	H(14B)	109.5
H(14A)	C(14)	H(14B)	109.5
C(13)	C(14)	H(14C)	109.5
H(14A)	C(14)	H(14C)	109.5
H(14B)	C(14)	H(14C)	109.5
C(13)	C(15)	H(15A)	109.5
C(13)	C(15)	H(15B)	109.5
H(15A)	C(15)	H(15B)	109.5



C(13)	C(15)	H(15C)	109.5
H(15A)	C(15)	H(15C)	109.5
H(15B)	C(15)	H(15C)	109.5
C(5)	N(1)	C(1)	121.3(4)
C(5)	N(1)	Cu(1)	119.4(3)
C(1)	N(1)	Cu(1)	119.2(3)
C(6)	N(2)	N(4)	115.2(3)
N(5)	N(3)	C(6)	119.5(3)
N(5)	N(3)	Cu(1)	125.6(3)
C(6)	N(3)	Cu(1)	114.3(3)
N(2)	N(4)	C(7)	124.0(3)
N(2)	N(4)	C(8)	116.3(4)
C(7)	N(4)	C(8)	119.1(4)
N(3)	N(5)	C(7)	118.2(3)
N(3)	N(5)	Cu(2)	121.8(3)
C(7)	N(5)	Cu(2)	109.6(3)
C(11)	N(6)	N(8)	116.7(4)
N(9)	N(7)	C(11)	120.4(4)
N(9)	N(7)	Cu(1)	126.7(3)
C(11)	N(7)	Cu(1)	113.0(3)
N(6)	N(8)	C(12)	123.7(4)
N(6)	N(8)	C(13)	115.8(4)
C(12)	N(8)	C(13)	120.3(4)
N(7)	N(9)	C(12)	119.4(4)
Cu(1)	Cl(1)	Cu(2)	92.75(4)
N(1)	Cu(1)	N(3)	79.71(14)
N(1)	Cu(1)	N(7)	79.70(14)
N(3)	Cu(1)	N(7)	159.41(14)
N(1)	Cu(1)	Cl(1)	176.70(11)
N(3)	Cu(1)	Cl(1)	97.29(10)
N(7)	Cu(1)	Cl(1)	103.30(10)
N(5)	Cu(2)	Cl(2)	142.94(12)
N(5)	Cu(2)	Cl(3)	94.58(11)
Cl(2)	Cu(2)	Cl(3)	117.67(6)
N(5)	Cu(2)	Cl(1)	89.10(11)
Cl(2)	Cu(2)	Cl(1)	97.02(5)
Cl(3)	Cu(2)	Cl(1)	107.98(4)

---

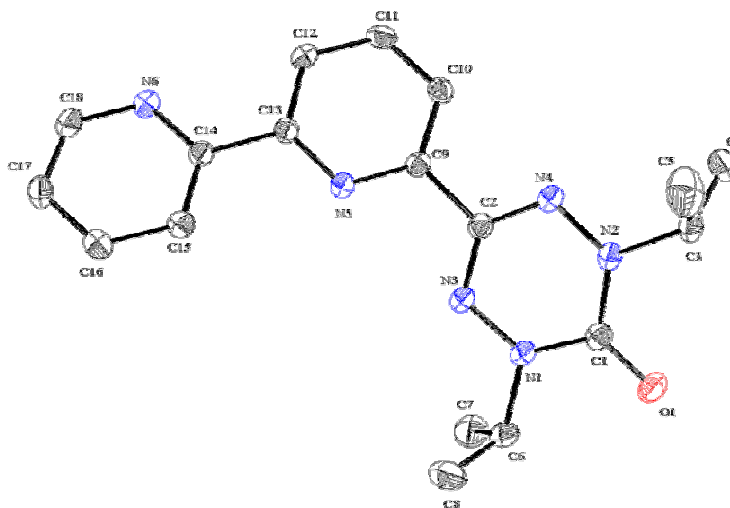


**Figure C-12:** ORTEP view of **3.9**. Thermal ellipsoids displayed at 50% probability level. Hydrogen atoms removed for clarity.

**Table C-12:** Bond lengths (Å) and angles (°) for **3.9**.

---

C(1)	O(1)	1.2174(15)
C(1)	N(2)	1.3779(16)
C(1)	N(1)	1.3791(15)
C(2)	N(4)	1.3237(16)
C(2)	N(3)	1.3278(16)
C(2)	C(9)	1.4892(16)
C(3)	N(2)	1.4785(14)
C(3)	C(5)	1.512(2)
C(3)	C(4)	1.5145(19)
C(3)	H(3)	1.0000
C(4)	H(4A)	0.9800
C(4)	H(4B)	0.9800
C(4)	H(4C)	0.9800
C(5)	H(5A)	0.9800
C(5)	H(5B)	0.9800
C(5)	H(5C)	0.9800
C(6)	N(1)	1.4779(16)
C(6)	C(7)	1.514(2)
C(6)	C(8)	1.518(2)
C(6)	H(6)	1.0000
C(7)	H(7A)	0.9800
C(7)	H(7B)	0.9800
C(7)	H(7C)	0.9800
C(8)	H(8A)	0.9800
C(8)	H(8B)	0.9800

C(8)	H(8C)	0.9800
C(9)	N(5)	1.3358(15)
C(9)	C(10)	1.3938(16)
C(10)	C(11)	1.3822(17)
C(10)	H(10)	0.9500
C(11)	C(12)	1.3783(17)
C(11)	H(11)	0.9500
C(12)	C(13)	1.3930(16)
C(12)	H(12)	0.9500
C(13)	N(5)	1.3407(15)
C(13)	C(14)	1.4844(15)
C(14)	N(6)	1.3415(15)
C(14)	C(15)	1.3884(17)
C(15)	C(16)	1.3855(17)
C(15)	H(15)	0.9500
C(16)	C(17)	1.3813(19)
C(16)	H(16)	0.9500
C(17)	C(18)	1.3826(19)
C(17)	H(17)	0.9500
C(18)	N(6)	1.3346(16)
C(18)	H(18)	0.9500
N(1)	N(3)	1.3674(14)
N(2)	N(4)	1.3613(14)

O(1)	C(1)	N(2)	122.76(11)
O(1)	C(1)	N(1)	123.06(11)
N(2)	C(1)	N(1)	114.18(10)
N(4)	C(2)	N(3)	127.91(11)
N(4)	C(2)	C(9)	114.93(10)
N(3)	C(2)	C(9)	117.14(10)
N(2)	C(3)	C(5)	110.27(11)
N(2)	C(3)	C(4)	109.83(11)
C(5)	C(3)	C(4)	112.68(13)
N(2)	C(3)	H(3)	108.0
C(5)	C(3)	H(3)	108.0
C(4)	C(3)	H(3)	108.0
C(3)	C(4)	H(4A)	109.5
C(3)	C(4)	H(4B)	109.5
H(4A)	C(4)	H(4B)	109.5
C(3)	C(4)	H(4C)	109.5
H(4A)	C(4)	H(4C)	109.5
H(4B)	C(4)	H(4C)	109.5
C(3)	C(5)	H(5A)	109.5
C(3)	C(5)	H(5B)	109.5
H(5A)	C(5)	H(5B)	109.5
C(3)	C(5)	H(5C)	109.5

H(5A)	C(5)	H(5C)	109.5
H(5B)	C(5)	H(5C)	109.5
N(1)	C(6)	C(7)	110.27(11)
N(1)	C(6)	C(8)	109.27(12)
C(7)	C(6)	C(8)	112.66(12)
N(1)	C(6)	H(6)	108.2
C(7)	C(6)	H(6)	108.2
C(8)	C(6)	H(6)	108.2
C(6)	C(7)	H(7A)	109.5
C(6)	C(7)	H(7B)	109.5
H(7A)	C(7)	H(7B)	109.5
C(6)	C(7)	H(7C)	109.5
H(7A)	C(7)	H(7C)	109.5
H(7B)	C(7)	H(7C)	109.5
C(6)	C(8)	H(8A)	109.5
C(6)	C(8)	H(8B)	109.5
H(8A)	C(8)	H(8B)	109.5
C(6)	C(8)	H(8C)	109.5
H(8A)	C(8)	H(8C)	109.5
H(8B)	C(8)	H(8C)	109.5
N(5)	C(9)	C(10)	123.94(11)
N(5)	C(9)	C(2)	116.64(10)
C(10)	C(9)	C(2)	119.42(10)
C(11)	C(10)	C(9)	117.73(11)
C(11)	C(10)	H(10)	121.1
C(9)	C(10)	H(10)	121.1
C(12)	C(11)	C(10)	119.30(11)
C(12)	C(11)	H(11)	120.3
C(10)	C(11)	H(11)	120.3
C(11)	C(12)	C(13)	119.02(11)
C(11)	C(12)	H(12)	120.5
C(13)	C(12)	H(12)	120.5
N(5)	C(13)	C(12)	122.60(10)
N(5)	C(13)	C(14)	117.04(10)
C(12)	C(13)	C(14)	120.36(11)
N(6)	C(14)	C(15)	122.77(11)
N(6)	C(14)	C(13)	116.39(10)
C(15)	C(14)	C(13)	120.83(11)
C(16)	C(15)	C(14)	118.65(12)
C(16)	C(15)	H(15)	120.7
C(14)	C(15)	H(15)	120.7
C(17)	C(16)	C(15)	119.18(12)
C(17)	C(16)	H(16)	120.4
C(15)	C(16)	H(16)	120.4
C(16)	C(17)	C(18)	118.05(12)
C(16)	C(17)	H(17)	121.0

C(18)	C(17)	H(17)	121.0
N(6)	C(18)	C(17)	123.97(12)
N(6)	C(18)	H(18)	118.0
C(17)	C(18)	H(18)	118.0
N(3)	N(1)	C(1)	124.46(10)
N(3)	N(1)	C(6)	115.69(9)
C(1)	N(1)	C(6)	119.76(10)
N(4)	N(2)	C(1)	124.16(9)
N(4)	N(2)	C(3)	115.43(10)
C(1)	N(2)	C(3)	120.40(10)
C(2)	N(3)	N(1)	114.26(10)
C(2)	N(4)	N(2)	114.98(10)
C(9)	N(5)	C(13)	117.37(10)
C(18)	N(6)	C(14)	117.38(11)

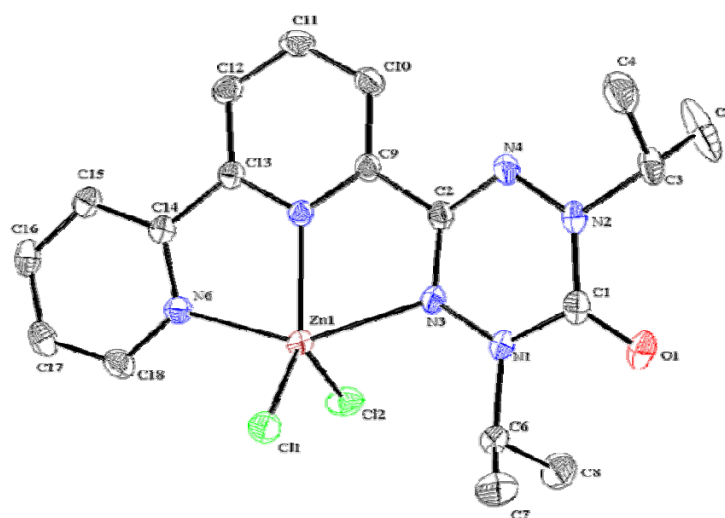


**Figure C-13:** ORTEP view of **3.10**. Thermal ellipsoids displayed at 50% probability level. Hydrogen atoms removed for clarity.

**Table C-13:** Bond lengths (Å) and angles (°) for **3.10**.

C(1)	O(1)	1.2141(19)
C(1)	N(2)	1.382(2)
C(1)	N(1)	1.387(2)
C(2)	N(4)	1.3291(19)
C(2)	N(3)	1.330(2)
C(2)	C(9)	1.481(2)
C(3)	N(2)	1.4918(19)
C(3)	C(4)	1.501(2)

C(3)	C(5)	1.512(3)
C(3)	H(3)	1.0000
C(4)	H(4A)	0.9800
C(4)	H(4B)	0.9800
C(4)	H(4C)	0.9800
C(5)	H(5A)	0.9800
C(5)	H(5B)	0.9800
C(5)	H(5C)	0.9800
C(6)	N(1)	1.488(2)
C(6)	C(8)	1.515(2)
C(6)	C(7)	1.521(3)
C(6)	H(6)	1.0000
C(7)	H(7A)	0.9800
C(7)	H(7B)	0.9800
C(7)	H(7C)	0.9800
C(8)	H(8A)	0.9800
C(8)	H(8B)	0.9800
C(8)	H(8C)	0.9800
C(9)	N(5)	1.3403(19)
C(9)	C(10)	1.388(2)
C(10)	C(11)	1.384(2)
C(10)	H(10)	0.9500
C(11)	C(12)	1.386(2)
C(11)	H(11)	0.9500
C(12)	C(13)	1.388(2)
C(12)	H(12)	0.9500
C(13)	N(5)	1.3509(18)
C(13)	C(14)	1.486(2)
C(14)	N(6)	1.347(2)
C(14)	C(15)	1.390(2)
C(15)	C(16)	1.387(2)
C(15)	H(15)	0.9500
C(16)	C(17)	1.380(2)
C(16)	H(16)	0.9500
C(17)	C(18)	1.389(2)
C(17)	H(17)	0.9500
C(18)	N(6)	1.334(2)
C(18)	H(18)	0.9500
N(1)	N(3)	1.3637(17)
N(2)	N(4)	1.3604(18)
N(3)	Zn(1)	2.3658(12)
N(5)	Zn(1)	2.0910(13)
N(6)	Zn(1)	2.1461(12)
Cl(1)	Zn(1)	2.2532(4)
Cl(2)	Zn(1)	2.2425(4)

O(1)	C(1)	N(2)	122.73(15)
O(1)	C(1)	N(1)	122.37(15)
N(2)	C(1)	N(1)	114.89(13)
N(4)	C(2)	N(3)	127.82(14)
N(4)	C(2)	C(9)	116.19(13)
N(3)	C(2)	C(9)	115.93(13)
N(2)	C(3)	C(4)	110.37(13)
N(2)	C(3)	C(5)	109.78(13)
C(4)	C(3)	C(5)	112.56(17)
N(2)	C(3)	H(3)	108.0
C(4)	C(3)	H(3)	108.0
C(5)	C(3)	H(3)	108.0
C(3)	C(4)	H(4A)	109.5
C(3)	C(4)	H(4B)	109.5
H(4A)	C(4)	H(4B)	109.5
C(3)	C(4)	H(4C)	109.5
H(4A)	C(4)	H(4C)	109.5
H(4B)	C(4)	H(4C)	109.5
C(3)	C(5)	H(5A)	109.5
C(3)	C(5)	H(5B)	109.5
H(5A)	C(5)	H(5B)	109.5
C(3)	C(5)	H(5C)	109.5
H(5A)	C(5)	H(5C)	109.5
H(5B)	C(5)	H(5C)	109.5
N(1)	C(6)	C(8)	110.71(14)
N(1)	C(6)	C(7)	111.25(14)
C(8)	C(6)	C(7)	114.02(15)
N(1)	C(6)	H(6)	106.8
C(8)	C(6)	H(6)	106.8
C(7)	C(6)	H(6)	106.8
C(6)	C(7)	H(7A)	109.5
C(6)	C(7)	H(7B)	109.5
H(7A)	C(7)	H(7B)	109.5
C(6)	C(7)	H(7C)	109.5
H(7A)	C(7)	H(7C)	109.5
H(7B)	C(7)	H(7C)	109.5
C(6)	C(8)	H(8A)	109.5
C(6)	C(8)	H(8B)	109.5
H(8A)	C(8)	H(8B)	109.5
C(6)	C(8)	H(8C)	109.5
H(8A)	C(8)	H(8C)	109.5
H(8B)	C(8)	H(8C)	109.5
N(5)	C(9)	C(10)	122.16(14)
N(5)	C(9)	C(2)	115.21(13)
C(10)	C(9)	C(2)	122.57(14)
C(11)	C(10)	C(9)	118.38(15)

C(11)	C(10)	H(10)	120.8
C(9)	C(10)	H(10)	120.8
C(10)	C(11)	C(12)	119.62(15)
C(10)	C(11)	H(11)	120.2
C(12)	C(11)	H(11)	120.2
C(11)	C(12)	C(13)	119.03(14)
C(11)	C(12)	H(12)	120.5
C(13)	C(12)	H(12)	120.5
N(5)	C(13)	C(12)	121.17(14)
N(5)	C(13)	C(14)	114.96(13)
C(12)	C(13)	C(14)	123.85(13)
N(6)	C(14)	C(15)	121.64(14)
N(6)	C(14)	C(13)	114.80(13)
C(15)	C(14)	C(13)	123.53(14)
C(16)	C(15)	C(14)	118.75(15)
C(16)	C(15)	H(15)	120.6
C(14)	C(15)	H(15)	120.6
C(17)	C(16)	C(15)	119.41(15)
C(17)	C(16)	H(16)	120.3
C(15)	C(16)	H(16)	120.3
C(16)	C(17)	C(18)	118.71(15)
C(16)	C(17)	H(17)	120.6
C(18)	C(17)	H(17)	120.6
N(6)	C(18)	C(17)	122.24(15)
N(6)	C(18)	H(18)	118.9
C(17)	C(18)	H(18)	118.9
N(3)	N(1)	C(1)	123.00(13)
N(3)	N(1)	C(6)	115.80(12)
C(1)	N(1)	C(6)	121.19(13)
N(4)	N(2)	C(1)	124.31(13)
N(4)	N(2)	C(3)	115.55(13)
C(1)	N(2)	C(3)	120.13(13)
C(2)	N(3)	N(1)	115.43(12)
C(2)	N(3)	Zn(1)	113.28(9)
N(1)	N(3)	Zn(1)	131.06(9)
C(2)	N(4)	N(2)	114.41(13)
C(9)	N(5)	C(13)	119.46(13)
C(9)	N(5)	Zn(1)	122.84(10)
C(13)	N(5)	Zn(1)	117.69(10)
C(18)	N(6)	C(14)	119.24(13)
C(18)	N(6)	Zn(1)	124.65(11)
C(14)	N(6)	Zn(1)	116.06(10)
N(5)	Zn(1)	N(6)	76.43(5)
N(5)	Zn(1)	Cl(2)	117.85(3)
N(6)	Zn(1)	Cl(2)	101.25(4)
N(5)	Zn(1)	Cl(1)	123.58(4)



N(6)	Zn(1)	Cl(1)	97.86(4)
Cl(2)	Zn(1)	Cl(1)	118.290(18)
N(5)	Zn(1)	N(3)	72.29(4)
N(6)	Zn(1)	N(3)	148.38(5)
Cl(2)	Zn(1)	N(3)	97.33(3)
Cl(1)	Zn(1)	N(3)	95.51(3)

---

## Appendix D: Raw magnetic data and derivation of magnetic models

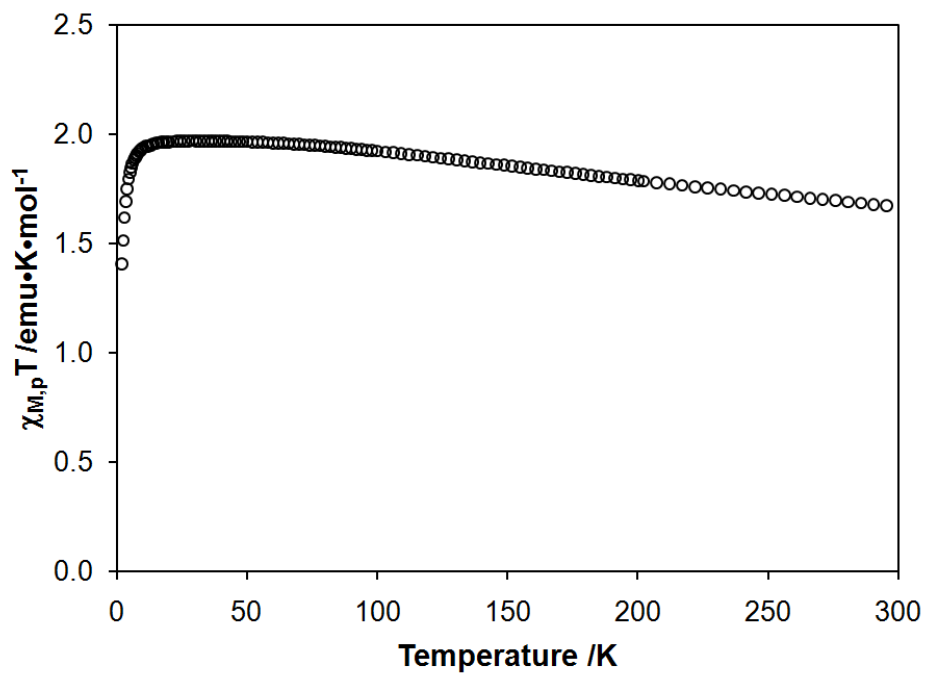


**Figure D-1:** Raw  $\chi T$  vs. T magnetic data for nickel-verdazyl complex **2.14**.

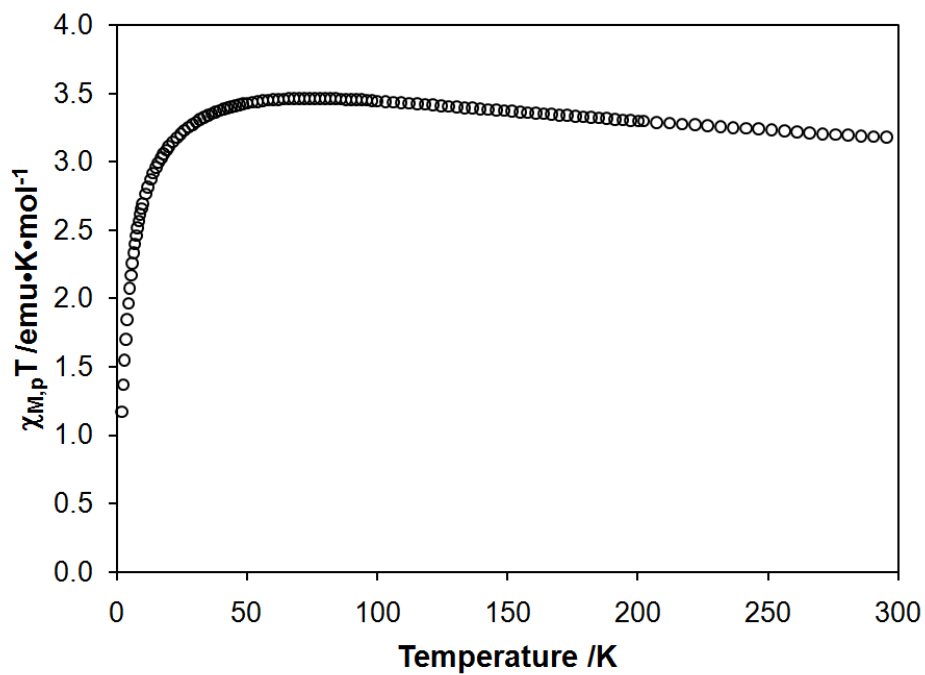


**Figure D-2:** Raw  $\chi T$  vs. T magnetic data for cobalt-verdazyl complex **2.15**.

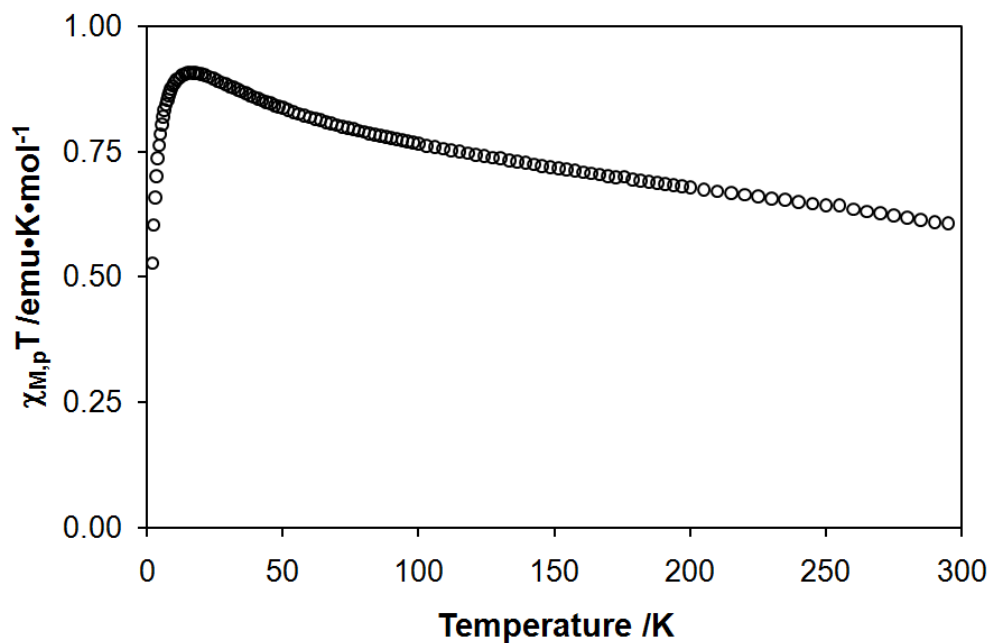


**Figure D-3:** Raw  $\chi T$  vs. T magnetic data for diradical **2.18**.

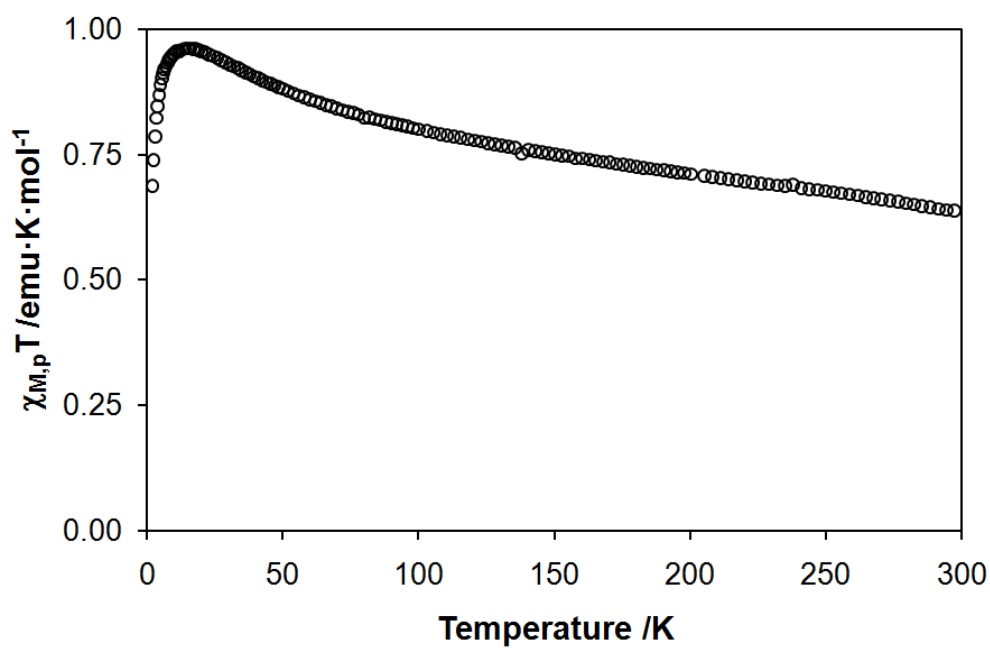


**Figure D-4:** Raw  $\chi T$  vs. T magnetic data for zinc-diradical complex **2.19**.

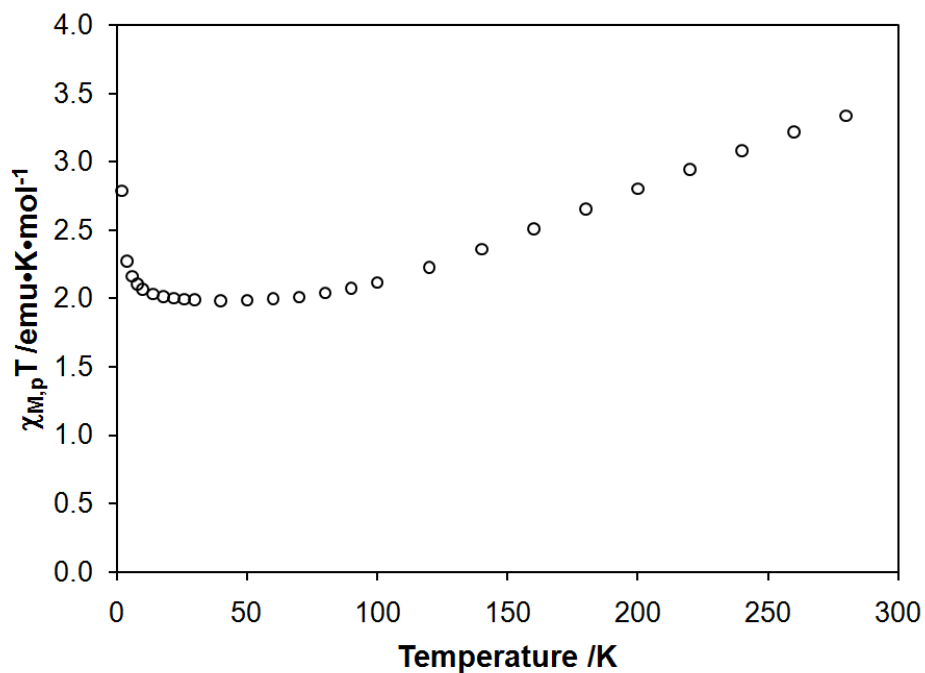


**Figure D-5:** Raw  $\chi T$  vs. T magnetic data for manganese-diradical complex **2.20**.

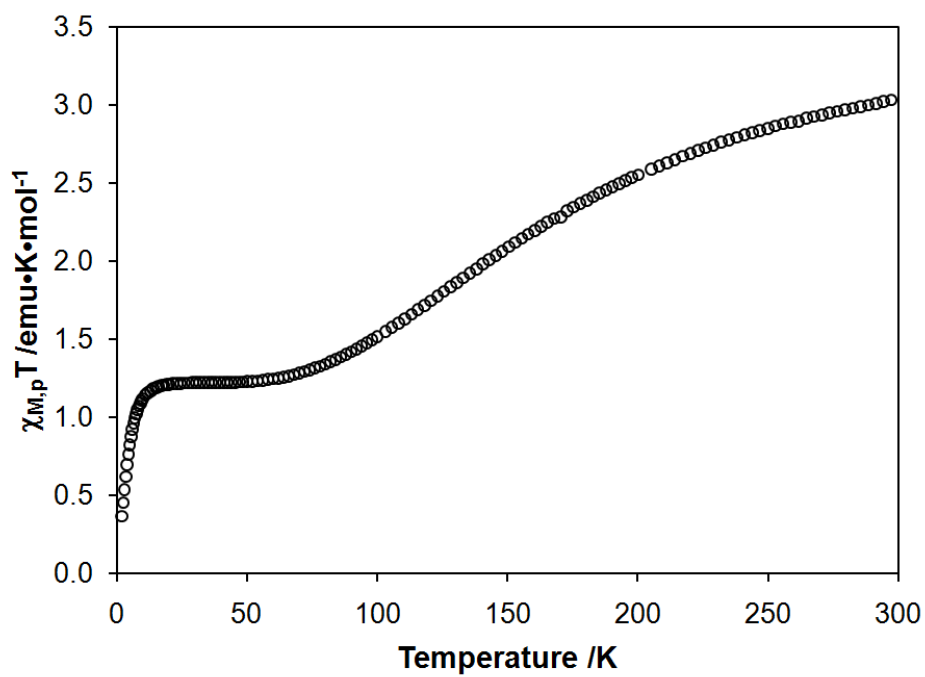


**Figure D-6:** Raw  $\chi T$  vs. T magnetic data for iron-diradical complex **2.21**.

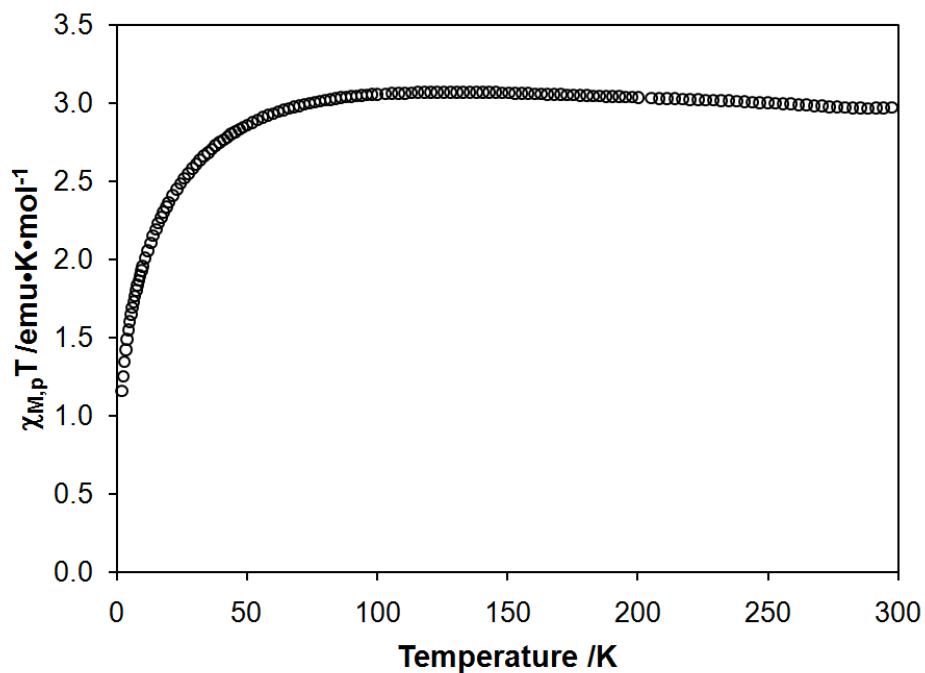


**Figure D-7:** Raw  $\chi T$  vs. T magnetic data for cobalt-diradical complex **2.22**.

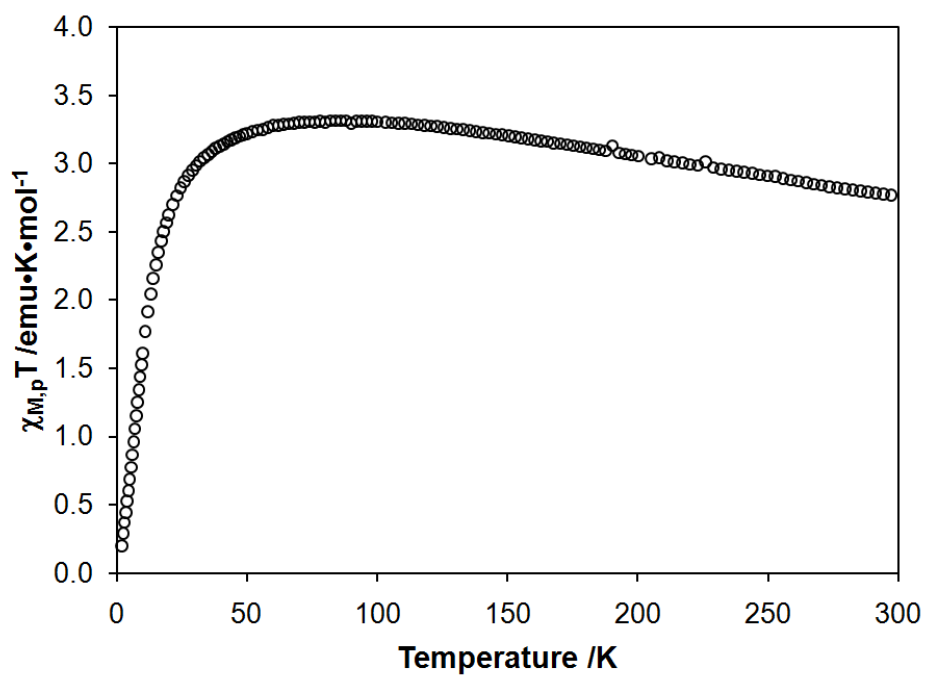


**Figure D-8:** Raw  $\chi T$  vs. T magnetic data for nickel-diradical complex **2.23**.

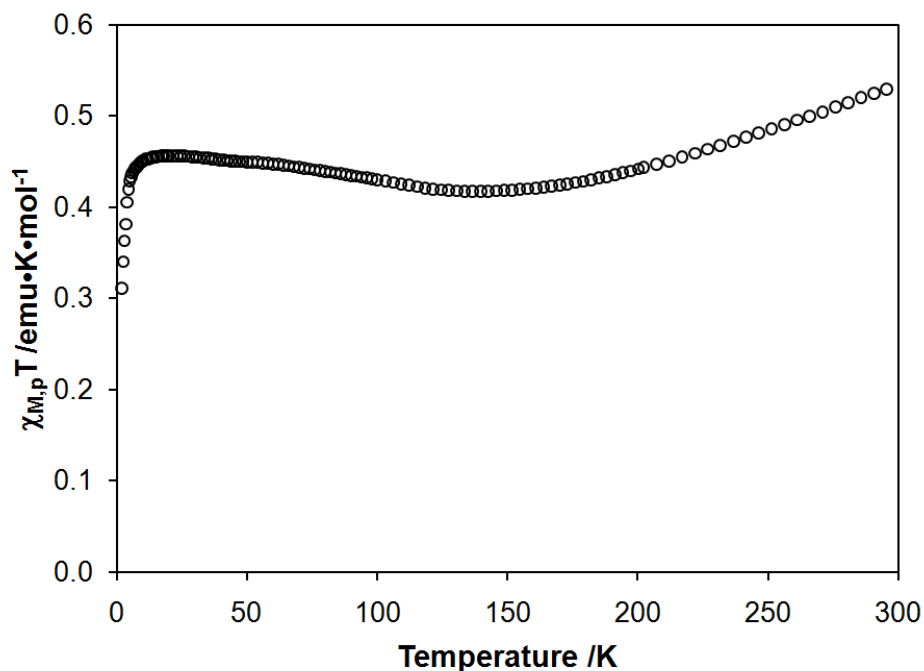


**Figure D-9:** Raw  $\chi T$  vs.  $T$  magnetic data for chromium-diradical complex **2.28b**.

Magnetic data for compounds **2.18** and **2.19** were modelled according to previously described procedures for verdazyl-based diradical compounds.<sup>158</sup> Equations 2.1 (compound **2.14**), 2.2 (compound **2.15**), 2.6 – 2.9 (compounds **2.20** – **2.23**, inclusive) and 2.10 (compound **2.28b**) are based on the derivation of the Van Vleck equation presented by Kahn for multiple spin systems.<sup>277</sup> Equations 2.1 and 2.2 are derived for a simple two-spin system, while equations 2.6 – 2.10 are based on a three-spin triangle.<sup>278</sup> Magnetic data for compounds **2.14**, **2.15**, **2.20** – **2.23** and **2.28b** were simulated by manually plotting the corresponding equations in the desired temperature range using the given parameters (*vide infra*). The best fit was achieved by first visually comparing the model with the data for a range of parameters. The fit was then fine tuned by comparing the goodness of fit factor between the model and the data (see p. 42) resulting from incremental changes in the given parameters.